Design, Synthesis and Biological Evaluation of Novel PBD-Heterocycle Conjugates as Potential Transcription Factor Binding Inhibitors

Rachel Marina Hawkins

Thesis submitted to The School of Pharmacy, University of London in partial fulfilment of the requirements for the degree of Doctor of Philosophy

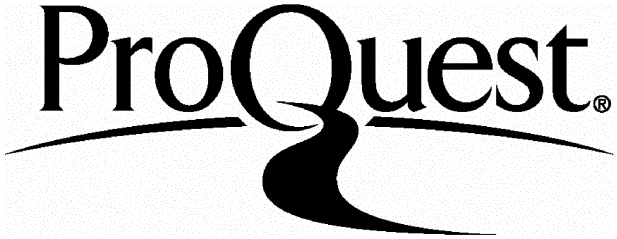

ABSTRACT

Transcription factor binding sites in disease related genes are potential therapeutic targets for small molecules. This research project describes the solution phase chemical synthesis of a small library of PBD-heterocycle conjugates that bind in the minor groove of DNA and inhibit NF-Y binding.

Pyrrolo[2,1-*c*][1,4]benzodiazepines recognise and covalently bind guanine residues in the minor groove of DNA resulting in antitumour and antibiotic activity. In addition, heterocyclic polyamides have exhibited sequence recognition properties via a non-covalent interaction. By varying the heterocycles used different sequences of DNA can be targeted.

Heterocyclic polyamides comprised of two or three heterocycles were assembled in a combinatorial fashion from pyrrole, imidazole and thiazole building blocks. Heterocycles were coupled together using EDCI and DMAP followed by Boc deprotection. Subsequent coupling cycles were repeated depending on the required polyamide length.

The PBD building block synthesis was based on an approach reported by Fukuyama. However, it was discovered that the final step, a saponification, had produced a racemate. The introduction of THP and Alloc protecting groups allowed the successful synthesis of the enantiomerically pure PBD building block. The PBD was coupled to the heterocyclic polyamides and simultaneous Alloc/THP deprotections were performed to yield twenty-one active imine molecules.

Finally, a series of assays were performed on the target compounds in order to assess the effect of different heterocycle combinations on biological activity. The assays investigated sequence recognition properties and DNA binding activity using footprinting and thermal denaturation techniques respectively. Functional assays were carried out to investigate the ability of the compounds to disrupt transcription factor binding. Cytotoxicity data using the K562 cell line and the NCI 60 human tumour cell line panel was also obtained. These assays allowed the molecules to be ranked and lead molecules were identified. A promising molecule, RMH041 (Py-Py-Im-PBD), exhibited impressive DNA binding affinity and the potential to inhibit NF-Y transcription factor binding.

In conclusion, different combinations of heterocycles attached to the PBD unit significantly affect cytotoxicity, DNA binding affinity and the DNA sequence recognised.

ACKNOWLEDGMENTS

Firstly, I would like to thank Professor David Thurston for initiating this project and for his enthusiasm in my work throughout my time at the School of Pharmacy. However, without the supervision of Dr Philip Howard and Dr Geoff Wells, this thesis would never have been written. Over the years, Phil has given invaluable knowledge, time and support, for which I am truly grateful. I would also like to express deepest appreciation for Geoff, whose technical expertise and unending patience guided me through both the practical and theoretical aspects of this project.

I would like to thank the EPSRC and Spirogen Ltd for funding and supporting this research. In particular, Dr. Tom Ellis, and Dr. Chris Martin (Footprinting assay), Ms. Marissa Stephenson (K562 assay), Prof. Terry Jenkins (Thermal denaturation experiments), Dr. Minal Kotecha (EMSA), Dr. Marek Domin (Prep. LCMS), Mr Chi-kit Woo (Dilactam-heterocyclic conjugates) and Mr. Bryan Rees (ISIS).

I am grateful to all members of lab G7, past and present, and other School of Pharmacy friends for making my PhD enjoyable. I am incredibly lucky to have such amazing friends and family who have supported me through this rollercoaster ride. Whether you gave me a roof over my head, danced the night away, distracted me with shopping trips and card games or just listened, I couldn't have done this without you.

Finally, I would like to thank my parents and brother for their never ending love and support. They have always encouraged and believed in me, whatever I have tried to do, on this occasion I've relied on them more than ever.

PLAGIARISM STATEMENT

This thesis describes research conducted in the School of Pharmacy, University of London between 7th May 2002 and 6th May 2005 under the supervision of Professor David Thurston and Dr. Philip Howard.

I certify that the research described is original and that any parts of the work that have been conducted by collaboration are clearly indicated. I also certify that I have written all the text herein and have clearly indicated by suitable citation any part of this dissertation that has already appeared in publication.

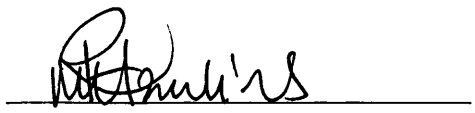

Signature

10th April 2007

Date

TABLE OF CONTENTS

ABBREVIATIONS

Alloc	Allyl Chloroformate
Boc	*N-tert* Butoxycarbonyl
Bp	Base Pair
CBI	Cyclopropylbenzylindole
CR-UK	Cancer Research UK
CSI	Chlorosulphonyl isocyanate
DAIB	Di(acetoxy)iodobenzene
DCM	Dichloromethane
DHP	3, 4-Dihydro-2 H-pyran
DIPEA	Diisopropylethylamine
DMAP	4-Dimethylaminopyridine
DMF	Dimethylformamide
DMSO	Dimethylsulphoxide
DNA	Deoxyribonucleic acid
EDCI	1(-3-Dimethylaminopropyl)-3-ethylcarbodiimide hydrochloride
ES	Electrospray
EtOAc	Ethyl Acetate
EtOH	Ethanol
GI_{50}	50% Growth Inhibition
HCl	Hydrochloric acid
HIV	Human Immunodeficiency Virus
HPLC	High Performance Liquid Chromatography
HRE	Hypoxia Response Element
Im	Imidazole
IR	Infrared
LC_{50}	50% Lethal Concentration
LCMS	Liquid Chromatography Mass Spectrometry
LEF	Lymphoid cell enriched enhancer-binding factor
MeOH	Methanol

MS	Mass Spectrometry
NCI	National Cancer Institute
NF-Y	Nuclear Factor-Y
NMR	Nuclear Magnetic Resonance
PBD	Pyrrolobenzodiazepine
PTSA	*Para*-toluene sulphonic acid
Py	Pyrrole
RNA	Ribonucleic acid
TBP	TATA box binding protein
TEA	Triethylamine
TEMPO	2,2,6,6-Tetramethyl-1-piperidinyloxy (free radical)
TFA	Trifluoroacetic acid
TGI	Total Growth Inhibition
Th	Thiazole
THF	Tetrahydrofuran
THP	Tetrahydropyran
TLC	Thin Layer Chromatography
UV	Ultraviolet
VEGF	Vascular Endothelial Growth Factor

1 INTRODUCTION

In recent years, significant advances have been made in understanding the transformation of a normal cell into a tumour cell. Extensive molecular and cellular studies have revealed that discrepancies in the DNA sequence (i.e. point mutations, deletions, translocations) can affect the biochemical function or expression of specific genes. Consequently, there is considerable interest in the discovery and development of small molecules capable of binding to DNA in a highly sequence selective manner (Wells *et al.,* 2006, Warren *et al.*, 2006, Dervan *et al.,* 2005, Murty and Sugiyama, 2004, Anthony *et al.,* 2004). Such molecules are potentially capable of recognising and binding to specific DNA sequences resulting in the inhibition of oncogene expression which ultimately could control the development of tumour cells. The scope of this gene targeting approach has become increasingly broad as more disease related genes have been identified through the Human Genome Project. It is hoped that the development of selective therapeutic agents that can interact with and down regulate specific genes will eliminate the toxicity associated with more conventional chemotherapy (Thurston, 1999; Browne and Thurlbey, 1996).

1.1 Pyrrolo[2,1-*c*][1,4]benzodiazepines (PBDs)

Pyrrolo[2,1-*c*][1,4]benzodiazepines (PBDs) are examples of molecules that recognise and covalently bind to specific sequences of DNA and the remainder of this chapter will be dedicated to describing this particular family of molecules in more detail.

1.1.1 Naturally occurring PBDs

PBDs, produced by various *Streptomyces* species, have been extensively investigated over the last 40 years, largely due to the antitumour/antibiotic properties associated with this family of molecules. The first PBD to be isolated, anthramycin, was discovered in 1963, and since then several other naturally occurring PBDs (**Figure 1**) have been isolated.

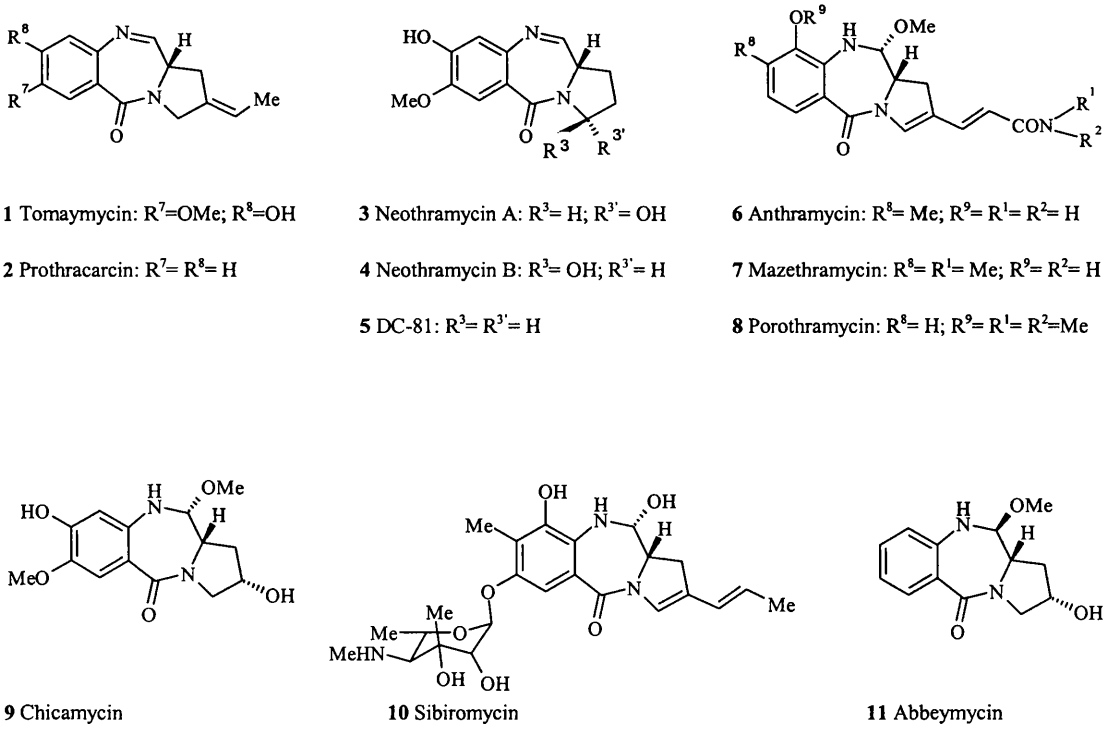

Figure 1. Naturally occurring PBDs.

1.1.2 PBD-DNA interactions

The mechanism by which PBDs interact with DNA has been extensively studied. Kohn and co-workers (Kohn *et al.*, 1974) hypothesised that anthramycin's antitumour antibiotic properties could be attributed to a covalent interaction with DNA. On subjecting the anthramycin-DNA complex to a variety of conditions including

dialysis, gel filtration or treatment with detergent (sodium lauryl sulphate) no dissociation was observed. This finding suggested an irreversible covalent interaction, rather than intercalation or other non covalent binding modes, as non-covalent complexes readily dissociate under these conditions.

Petrusek and co-workers (Petrusek *et al.*, 1981) used radio-labelling techniques to identify which DNA bases the PBD was binding to. More specifically, radio-labelled anthramycin was incubated with poly(dA).poly(dT) and poly(dG).poly(dC) strands. Following denaturation and strand separation the radioactivity of each strand was measured. It was found that anthramycin was exclusively bound to the guanine containing polydeoxynucleotides, confirming an interaction between the PBD and guanine residues.

Experiments to determine which position on the guanine base was interacting with anthramycin were also carried out by Petrusek and colleagues. It was concluded that the N2 position on guanine was implicated in bond formation because covalent DNA-anthramycin interactions were abolished when guanine was replaced with inosine, which lacks the amine group at the 2 position. NMR experiments confirmed the presence of an aminal linkage between the N2 of guanine and the C11 of anthramycin (Graves *et al.*, 1984).

Final confirmation of a covalent interaction between anthramycin and the *exo*cyclic N2 position of guanine was provided when Kopka *et al.* published an X-ray crystal structure of an anthramycin-PBD adduct (Kopka *et al.*, 1994). These adducts have been shown to interfere with the interaction of endonuclease enzymes with DNA

(Puvvada *et al.*, 1993) and to disrupt DNA transcription and RNA synthesis (Puvvada *et al.*, 1997).

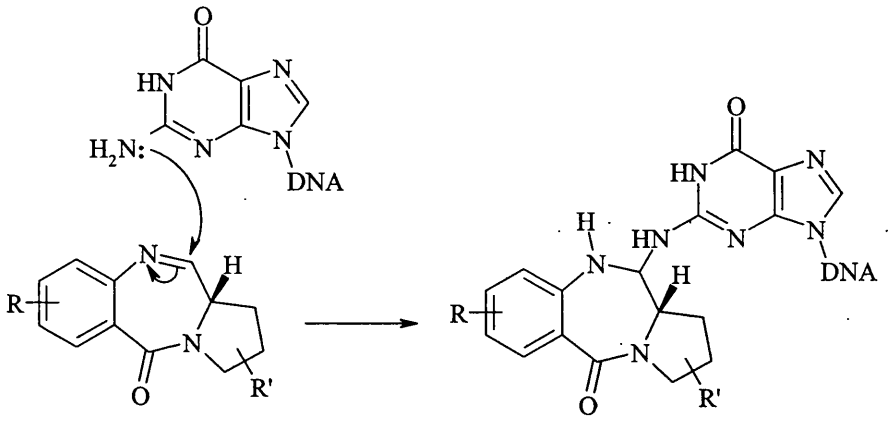

Figure 2. The interaction of a PBD with a guanine base on DNA.

Figure 2 shows a proposed mechanism whereby nucleophilic attack by the *exo*cyclic N2 of a guanine residue at the C11 position of the PBD results in the formation of a covalent aminal linkage (Hertzberg *et al.*, 1986).

Extensive studies involving chemical and enzymatic footprinting, *in vitro* transcription, NMR, fluorescence microscopy and molecular modelling have elucidated the preferred DNA-binding sites of the PBD compounds (Thurston, 1993). In addition to covalently binding to guanine, the compounds form a number of non-covalent interactions with adjacent bases in the DNA minor groove. The overall molecular shape and different ring substituents contribute significantly to these non-covalent interactions. The PBD moiety was found to bind with the C-ring positioned 5' of the alkylated guanine and the A-ring positioned towards 3'. The accepted consensus is that the PBD favours 5'-Pu-G-Pu over 5'-Py-G-Pu or 5'-Pu-G-Py, with

the least preferred site being 5'-Py-G-Py. There is also evidence that a non-covalent interaction with the PBD B-ring favours adenine as the base directly 3' of guanine (**Figure 3**) (Hurley *et al.*, 1988).

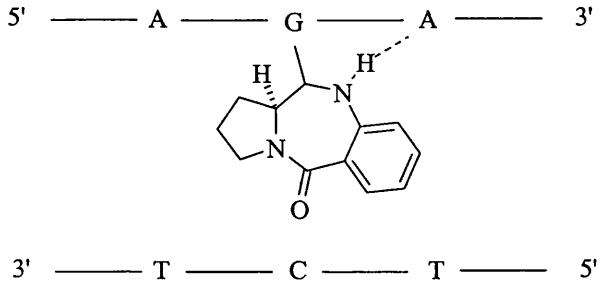

Figure 3. PBD interactions at the preferred binding site of DNA.

1.1.3 Structure activity relationships (SAR) of naturally occurring PBDs

All PBDs comprise of a tricyclic ring system, consisting of an aromatic ring (A), a diazepine ring (B) and a pyrrolo ring (C). The basic ring system with numbering is shown below in **Figure 4**. As can be seen in **Figure 1**, the naturally occurring PBDs differ in the number, type and position of the substituents in both the aromatic A-rings and the pyrrolo C-ring. In addition, the C-ring can either be saturated, *endo*-unsaturated at C2-C3 position or *exo*-unsaturated at C2.

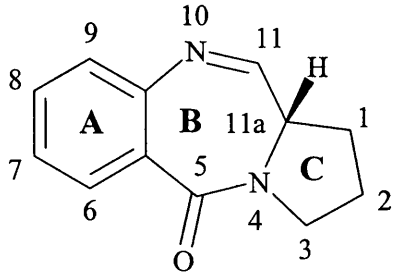

Figure 4. Basic PBD ring system and numbering.

Extensive research has elucidated how the structure of PBDs affects their cytotoxic activity and a summary of the findings is presented below.

1.1.3.1 Substituents on the B-ring

The presence of an electrophilic moiety (imine, carbinolamine, carbinolamine methyl ether) at N10-C11 is essential for biological activity (Hurley *et al.*, 1988). The N10-C11 carbinolamine, imine and carbinolamine methyl ether forms are interconvertible (**Figure 5**) depending on the method of isolation or synthetic work up. The imine form can be isolated by dissolving the PBD in chloroform and evaporating the solvent under vacuum. Replacing chloroform with methanol yields the carbinolamine methyl ether form.

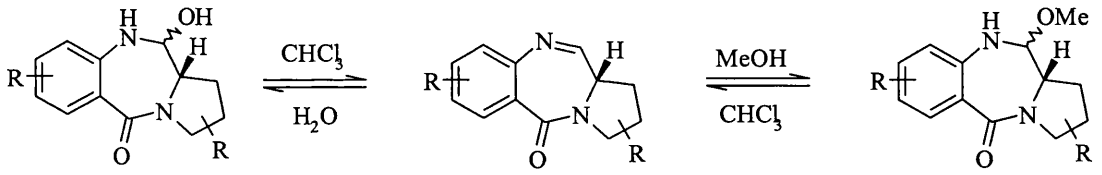

Figure 5. PBD interconvertible forms.

The mechanism by which PBDs exert their biological activity is discussed in Section 1.1.2, however it is important to note that the imine functionality is the active form of the molecule. Therefore, the carbinolamine and methyl ether forms must undergo reversible dehydration to form the imine before bonding to DNA occurs (Hurley, 1977).

1.1.3.2 Stereochemistry at C11a

All naturally occurring PBDs possess (*S*)-stereochemistry at the chiral C11a position. This provides a right handed molecular twist, when viewed from the C-ring toward the A-ring, thus enabling the PBD to attain a snug fit in the minor groove of DNA (Thurston, 1993). A synthetic PBD with the (*R*)-configuration at C11a was shown to be devoid of both DNA binding activity and *in vitro* cytotoxicity (Hurley *et al.*, 1988).

1.1.3.3 Substituents on the C-ring

Thurston and co-workers (Thurston *et al.*, 1999) established that differences in biological activity between the naturally occurring PBDs can be attributed to differences in C-ring structure. The nature of unsaturation present and the type of substituent attached at the C2 position of the PBD is thought to dictate the position of the molecules along the groove of DNA thus influencing potential interactions.

1.1.3.4 Substituents on the A-ring

A-ring substituents are not essential for cytotoxicity, however, electron donating groups at C7, C8 or C9 enhance DNA binding affinity and cytotoxicty. The degree of electrophilicity of the N10-C11 imine functionality, and therefore cytotoxicity, is influenced by the type and position of functional groups on the A-ring. For example, C8 substituents lie along the floor of the DNA minor groove which is in contrast to groups at the C7 position which point out of the minor groove and, therefore, have little steric effect on the DNA interaction. However, these groups do influence the electronic characteristics of the A-ring which affects the electrophilicity of the imine C11 and enhances DNA binding affinity (Guiotto *et al.*, 1998).

1.1.4 Clinical evaluation of PBDs

Unfortunately, the clinical evaluation of a number of naturally occurring PBDs has proved disappointing. More specifically, the clinical potential of anthramycin was impeded by dose-limiting cardiotoxicity (Cargill *et al.*, 1974). It has been proposed that the cardiotoxic side effects are the result of oxidation of the C9 hydroxy group under physiological conditions to form reactive *ortho* quinone imines. These species can stimulate the formation of toxic free radicals which can potentially disrupt sarcosplasmic reticulum function and inhibit myocardial activity *in vitro* (Shaddle *et al.*, 2000). In addition, as electrophiles, the *ortho* quinones can react with cellular nucleophiles (i.e. proteins, DNA, etc...) and cause oxidative stress (Thurston and Hurley, 1983).

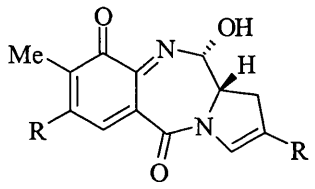

Figure 6. An example of a quinone imine.

Such clinical limitations highlight the need for synthetic analogues that possess antitumour properties without exhibiting dose limiting toxic side effects. One such analogue, SJG-136 (**12**), has been designed and synthesised within the CR-UK Gene Targeting Research Group. SJG-136 is a PBD dimer molecule based on the naturally occurring PBD, tomaymycin, and is currently in phase one clinical trials in the UK and USA. Molecular modelling studies have shown that SJG-136 spans six base pairs and forms interstrand crosslinks (Smellie *et al.*, 2003). Encouragingly, no cardiotoxicity has been observed in preclinical studies conducted by the NCI.

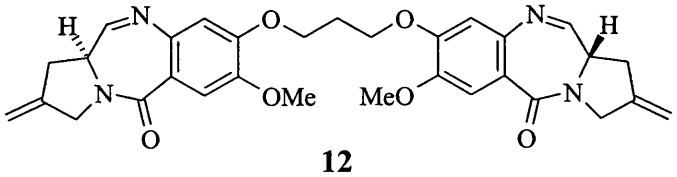

12

Figure 7. Structure of PBD dimer SJG136 (**12**).

1.1.5 Synthesis of PBDs

The chemical synthesis of PBDs is challenging due to the need to incorporate a variety of functional groups. Specifically, the A and C-ring substitution patterns, the N10-C11 imine moiety and the preservation of the required (*S*)-stereochemistry at the C11a position all need to be considered. Several approaches have been employed to synthesise both naturally occurring PBDs and synthetic analogues (Kamal *et al.*, 2002). However, there are limitations and advantages associated with each synthetic approach which need to be taken into account when designing a synthesis for novel PBD target molecules. The most relevant synthetic strategy to this project is the Fukuyama synthesis (Fukuyama *et al.*, 1993), which is briefly discussed below.

1.1.5.1 The Fukuyama Approach

In 1993 Fukuyama and co-workers reported the total synthesis of optically pure porothramycin B. This was achieved by coupling a glutamic acid derivative to 2-nitro-3-methoxybenzoyl chloride (A-ring) followed by C-ring cyclisation. The nitro group was reduced to the corresponding amine, which was subsequently protected using allyl chloroformate. Swern oxidation of the primary alcohol afforded cyclised N10-allyl-carbamate protected carbinolamine (**15**), which was then deprotected to

yield porothramycin B (**16**). The alloc protection, Swern oxidation and imine formation steps are shown in **Scheme 1**.

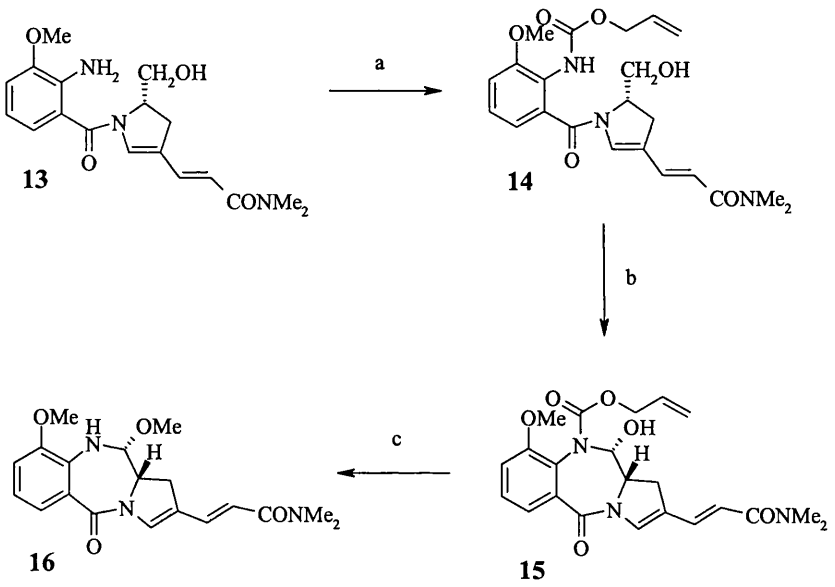

Scheme 1. The final stages steps of Fukuyama's total synthesis of porothramycin B.

a) $ClCO_2CH_2CH{=}CH_2$, Pyr, CH_2Cl_2; b) $(COCl)_2$, DMSO, TEA, CH_2Cl_2; c)i) $(Ph_3P)_4Pd$, pyrrolidine, CH_2Cl_2; ii) MeOH, EtOAc (1:20).

1.2 PBD Dilactams

It has generally been accepted that A and C-ring substituents participate in non-covalent interactions with DNA bases. For example, a PBD dilactam molecule, lacking the N10-C11 imine moiety responsible for covalent binding, has been reported to possess significant *in vivo* antitumour activity in the P388 rat model (Kaneko *et al.*, 1985).

In order to evaluate the non-covalent interactions responsible for the observed biological activity, a series of PBD dilactams, also referred to as PBD-5,11-diones,

has been synthesised by Jones (Jones *et al.*, 1990). Briefly, as shown in **Scheme 2**, 4-benzyloxy-5-methoxy-2-nitrobenzoic acid was coupled to 4-hydroxy-L-proline or L-proline to form the A-C ring coupled product. Subsequent reduction of the nitro amide product effected cyclisation with either removal or retention of the benzyl group depending on the method used. In the final steps, an acylation or carbamoylation, afforded the substituted dilactams. Alternatively, successive oxidation and reduction reactions inverted the stereochemistry at C2 to yield **23** and **24**.

In vitro DNA binding of the dilactam series was evaluated using thermal denaturation and fluorescence quenching studies with calf thymus DNA. Of the compounds tested only the (2*R*)-dihydroxy **20** and (2*R*)-diacetate **25** significantly elevated the melting point of DNA. Similarly, the results of fluorescence studies show that the (*R*)-dihydroxy compound **20** exhibits significant quenching upon incubation with calf thymus DNA. It was concluded that a highly stereospecific reversible interaction occurs between both (*R*)-dihydroxy **20** and (*R*)-diacetate **25** and DNA. In addition, there is a requirement for a hydroxyl functionality at both the C2 and C8 position and (*S*)-stereochemistry at the C2 position, demonstrated by the loss of binding observed with the (*R*)-enantiomer and if either hydroxyl is removed (Jones *et al.*, 1990).

The DNA binding mechanism of dilactams **20** and **25** is clearly different from the imine-containing PBDs, which interact covalently with DNA. As previously stated, the dilactams are incapable of covalent binding as they do not contain the alkylating imine/carbinolamine moiety. However, the observed interaction between DNA and

the dilactams could represent the non-covalent interactions seen between PBDs and DNA.

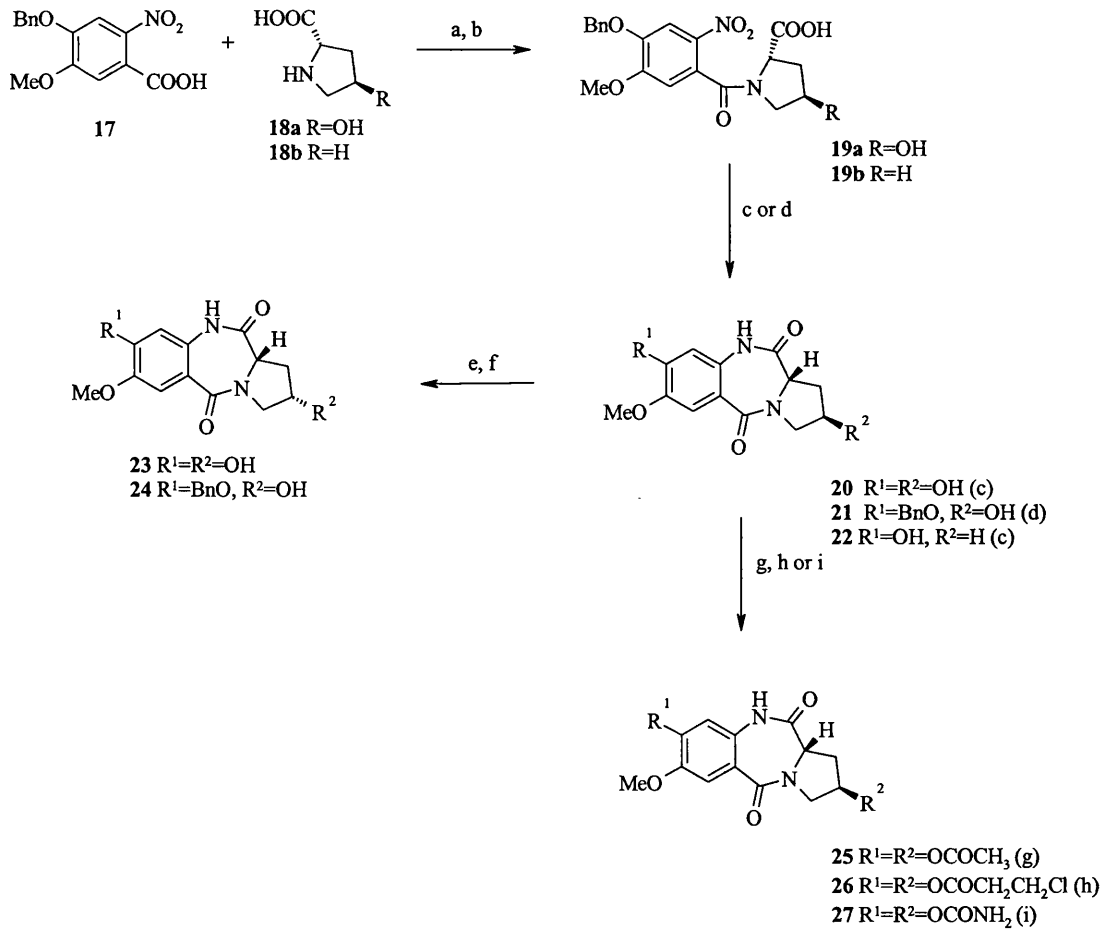

Scheme 2. a) $(COCl)_2$, DMF, toluene; b) Et_3N, H_2O, THF, 0°C; c) H_2, Pd/C, MeOH; d) $SnCl_2.2H_2O$, EtOH; e) CrO_3, H_2SO_4, Me_2CO; f) $NaBH_4$, MeOH; g) Ac_2O, Py; h) $ClCOCH_2CH_2Cl$, $(i\text{-}pr)_2NEt$, DMF; i) CSI, CH_3CN.

2 SEQUENCE RECOGNITION

2.1 Distamycin and netropsin

Low molecular weight ligands have been shown to bind to specific sequences of DNA (Waring, 1981; Hurley, 1989). One set of examples consists of the naturally occurring PBD molecules which have a preference for 5' Pu-G-Pu 3' sequences. However, two non-covalent binding molecules, netropsin (**28**) and distamycin (**29**) were amongst the first compounds found to bind selectively to AT-rich sequences in the minor groove of DNA. Interestingly, it is thought that netropsin and distamycin exert their biological effects in a similar fashion to the PBD molecule, by tightly binding to the DNA double helix and interfering with DNA replication and transcription.

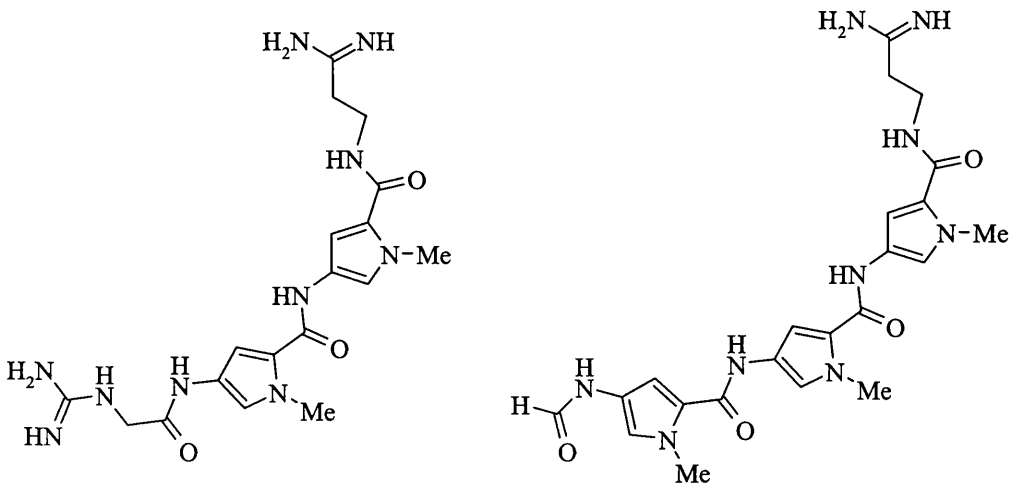

28 **29**

Figure 8. Natural products Netropsin (**28**) and Distamycin (**29**).

X-ray analysis of a netropsin-DNA complex has helped elucidate base pair specific binding. Consequently, it is thought the general binding mechanism by netropsin and

distamycin comprises two main events: 1) the groove binding agent undergoes a hydrophobic transfer from solution into the minor groove. 2) Once in the minor groove molecular interactions including van der Waals forces and hydrogen bond formation can occur (Bailey and Chaires, 1998).

The interaction between netropsin and the AT sequence is stabilised by three main factors: i) hydrogen bonding between the amide NH and the thymine O-2 and adenine N-3 atoms on adjacent base pairs and opposite helix strands; ii) a complementary overall shape, resulting in close ligand-DNA van der Waals contacts and iii) electrostatic interactions between polyanionic DNA and the cationic ligands. Of these factors it is thought that the van der Waals interactions are crucial for sequence recognition (Kopka and Larsen, 1992). Although these molecules make specific hydrogen bond interactions with groups in the DNA minor groove, a large part of their binding energy is derived from hydrophobic interactions (Haq *et al.*, 1997). More specifically, the van der Waals contacts between adenine C-2 hydrogens and CH groups on the pyrrole rings of the drug molecule are responsible for the preferential binding to runs of four or more AT base pairs.

Netropsin does not readily bind to regions of DNA containing G·C base pairs which can be explained by comparing the structure of adenine and guanine. The principal difference between A·T and G·C base pairs in the minor groove is the presence of an exocyclic amine group on the guanine residue. The pyrrole C-H in netropsin sterically clashes with this NH_2 in the DNA minor groove floor preventing netropsin from binding. However, analogues of distamycin, of up to seven pyrroles in length, have been shown to have a greater tolerance for G·C base pairs. This could be the

result of an imperfect fit between the drug and the minor groove of DNA, which is exaggerated with longer analogues, resulting in the drug molecule buckling away from the floor of the minor groove and allowing the intrusion of a guanine NH_2 (Kopka, 1985).

2.2 Lexitropsins

A number of strategies were employed to develop new heterocyclic polyamide agents, the first of which was focused on targeting a longer binding site. This was achieved by synthesising tris, tetra, penta, hexa and hepta *N*-methylpyrrolecarboxamide derivatives of netropsin and distamycin. It was observed that hepta *N*-methylpyrrolecarboxamide did not fit the minor groove of DNA, possibly due to phasing differences between the ligand and DNA base pairs (Youngquist and Dervan, 1985; Dervan, 1986). These differences are caused by pyrrole subunits being slightly longer than one base pair and also more curved than the minor groove and, logically, the more pyrroles that are present the more exaggerated the phasing differences. To restore phasing various linkers have been utilised to join two DNA binding moieties together, thus, resulting in bidentate ligands. A polymethylene tether between two netropsin molecules (**30**) allowed bidentate binding provided that the connector had at least three methylene groups.

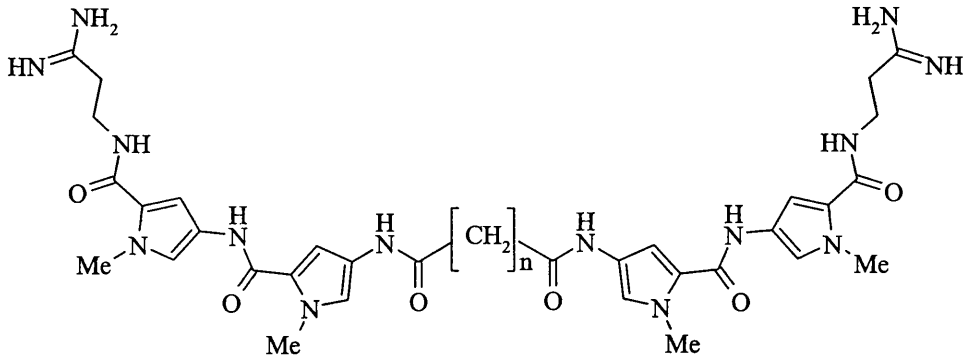

30

Figure 9. Two netropsin molecules joined by a polymethylene linker.

The use of both flexible and rigid linkers (**Figure 10**) allowed ligands to be joined together in a number of different modes (i.e. head to head, head to tail, tail to tail) ensuring that a longer sequence of DNA could be recognised (Kissinger *et al.*, 1990; Rao *et al.*, 1991).

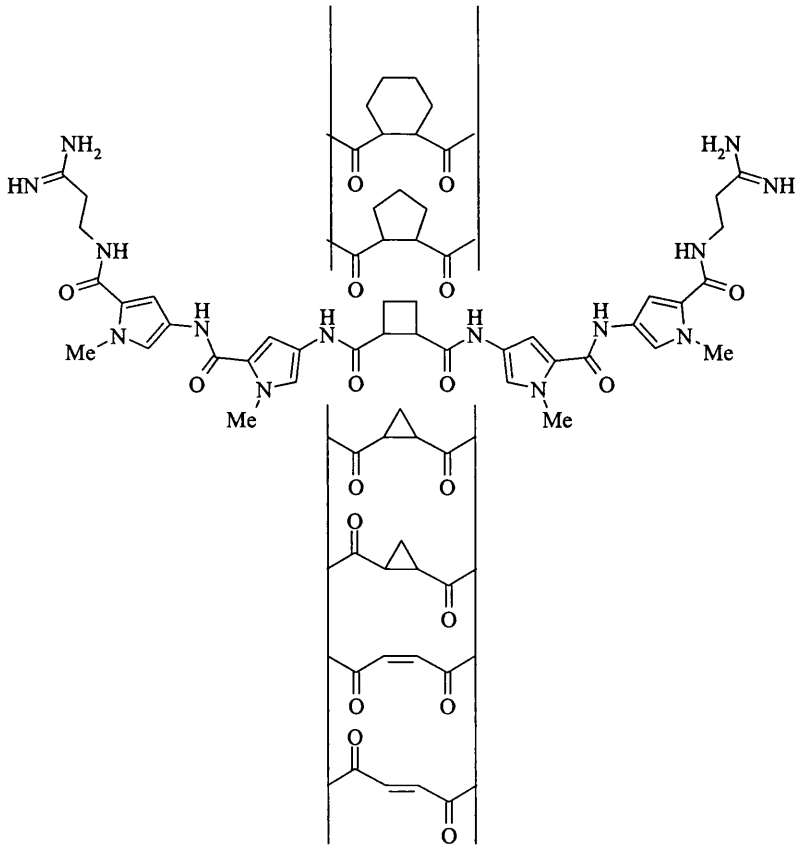

Figure 10. A *bis*(netropsin) molecule with examples of rigid linkers.

It was hypothesised that the substitution of one or more pyrroles by an imidazole could permit the recognition of G·C bases, as replacing the ring CH with a nitrogen atom would provide both space for the NH_2 of guanine and a hydrogen bond acceptor (Kopka, 1985; Goodsell and Dickerson, 1986). Subsequently, Lown and co-workers explored this hypothesis by synthesising several lexitropsin molecules, where the methylpyrroles were replaced with other heterocycles, such as imidazoles, thiazoles, pyrazoles and oxazoles (Lown, 1994). These novel lexitropsin molecules have the ability to bind to sequences containing one or two G·C pairs within an AT sequence. Interestingly, of all the lexitropsins that have been synthesised, it is the imidazole containing molecules that exhibit the most promising binding at GC containing sequences (Lown *et al.* 1986; Krowicki and Lown, 1987; Kissinger *et al.*, 1987; Lee *et al.*, 1988; Lee *et al.*, 1993). It is noteworthy that, despite imidazole units possessing a preference for G·C base pairs, presumably due to hydrogen bonding with the NH_2 of guanine, A·T base pairs can be tolerated due to the lack of steric hindrance. Thiazole lexitropsins have been observed to either accept or avoid a G·C base pair depending on the orientation of the heterocycle with respect to the floor of the minor groove.

More specifically, when the large sulphur atom is facing into the minor groove, no binding to GC sites is observed. Conversely, lexitropsins incorporating sulphur atoms that are directed out of the minor groove (and nitrogen atoms into the groove) prefer binding sites containing G·C base pairs (Rao *et al.*, 1990; Plouvier *et al,* 1991). The potential binding preferences of different heterocycles are set out in **Figure 11** below.

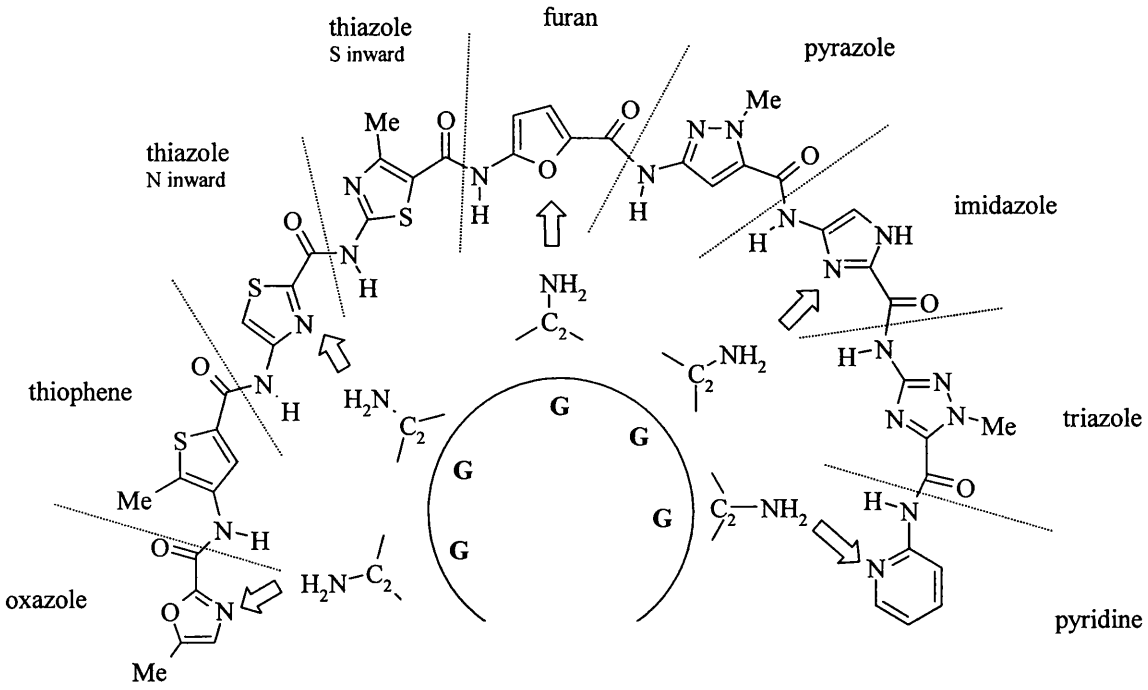

Figure 11. Different heterocycles preferentially binding guanine residues (Origin: Bailly and Chaires, 1998).

The importance of hydrophobic bonding in DNA/lexitropsin complexes has been outlined above. Waigh and co-workers hypothesised that the ability to control lipophilicity would have a significant effect on minor-groove binders. Both distamycin and netropsin possess methyl groups and therefore do not take full advantage of potential hydrobic interactions with the walls of the minor groove, more specifically the methane and methylene groups. A series of dystamcin analogues were synthesised where the methyl groups were replaced with larger alkyl groups to increase contacts with the DNA backbone (James *et al.*, 2004; Anthony *et al.*, 2003). One particular molecule, thiazotropsin A (**Figure 12**), in which one of the *N*-methyl-pyrroles is substituted by an isopropyl-substituted thiazole, has shown improved biological activity. Previously, thiazole molecules have been incorporated into lexitropsins to allow G·C recognition, through positioning the sulphur into the minor groove floor. In the case of thiazotropsin A, the thiazole subunit was designed to

enhance the hydrophobicity of the molecule, rather than affecting steric interactions, by lying at the top of the minor groove. This, in combination with both the adjacent isopropyl group and retention of the hydrogen-bonding capacity, resulted in enhanced affinity and selectivity (Khalaf *et al.*, 2004)

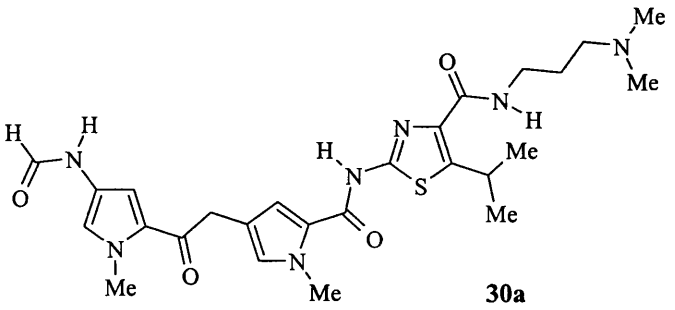

30a

Figure 12. Thiazotropsin A

In brief, the advent of lexitropsin molecules forming a 1:1 complex with DNA in the minor groove, has enabled G·C base pairs within binding sites to be tolerated. However, such molecules are not regarded as being G·C specific and, furthermore, lexitropsins exhibit reduced overall DNA binding affinity when compared to the parent natural products. This lack of G·C specificity was initially thought to be due to differences in molecular electrostatic potential between AT and GC base pair regions, with the strongly negative potential of the AT rich regions preferring the positively charged groups of the ligand (Lown, 1994; Pullman and Pullman, 1981). However this theory seems unlikely as both neutral and positively charged lexitropsins have exhibited the same interaction with AT rich sequences (Zhang *et al*, 1993). It is now thought that the lack of G·C specificity is attributable to the minor groove being wider in G/C regions, resulting in a greater distance between the drug and the walls of the minor groove, thus weakening crucial van der Waals contacts (Urbach and Dervan, 2001).

2.3 Binding stoichiometry

In 1992 Wemmer and co-workers used NMR studies to investigate the binding of distamycin-A to DNA (Fagan and Wemmer, 1992; Pelton and Wemmer, 1990). Initially the structure of the minor groove binding site was found to match the shape and width of the drug molecule, suggesting a 1:1 drug-DNA complex. However, at higher concentrations of distamycin-A, two drug molecules were observed to bind side-by-side in an anti-parallel head to tail orientation at the AT rich sequence. Each distamycin molecule forms hydrogen bonds to one strand of DNA and van der Waals interactions with each other and the walls of the minor groove. It was thought that the minor groove of DNA could expand slightly to accommodate ligands binding in a 2:1 mode, which has since been confirmed by crystal structure analysis (Chen *et al.*, 1994).

Figure 13. Binding of distamycin to DNA. On the left, distamycin is bound to a DNA dodecanucleotide in the 1:1 binding mode. On the right, two distamycin molecules are bound to a DNA octamer in the 2:1 binding mode. (Origin: Goodsell, 2001).

The ability of distamycin-type molecules to form a 2:1 complex with DNA combined with the synthesis of lexitropsins has led to enhanced sequence specificity and binding affinity. In the 1:1 binding mode, lexitropsins contact the centre of each base pair allowing GC base pairs to be discriminated from AT base pairs. However, pyrrole lexitropsins recognise both A·T and T·A with imidazole lexitropsins recognising both G·C and C·G, resulting in only partial base specificity. However, the 2:1 binding mode allows each individual base to be recognised as a result of each heterocycle being in contact with a single base.

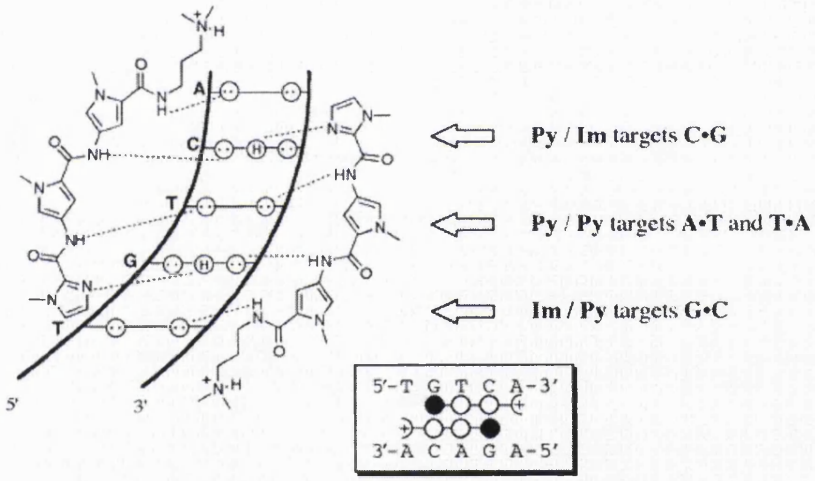

Figure 14. Model for anti-parallel dimer Im-Py-Py binding 5'-TGTCA-3'. The unsymmetrical pair Im-Py distinguishes GC from CG and both AT and TA. (Origin: Dervan, 2001).

Dervan and co-workers used lexitropsin consisting of two pyrroles and an imidazole to formulate the base pair specificity rules that govern sequence recognition in the 2:1 binding mode. It was observed that pairs of Im/Py (where Im and Py are imidazole and pyrrole subunits, respectively) recognised G·C and Py/Im recognised C·G with neither combination recognising A·T or T·A (Wade *et al.,* 1992). The Py/Py pair did, however, recognise but not distinguish between T·A or A·T (**Figure 14**). NMR

studies conducted by Wemmer and co-workers in 1992 confirmed the $(Im\text{-}Py\text{-}Py)_2$-DNA model and supported the rules of base pair recognition by lexitropsins in the 2:1 complex (Mrksich *et al.*, 1992; Wade *et al.*, 1993).

2.4 Hairpin Polyamides

One limitation when using lexitropsins to target a specific sequence is the molecule's ability to form both 2:1 and 1:1 complexes with DNA which can result in ambiguous recognition. This problem was overcome by covalently linking two lexitropsin molecules together via an appropriate linker to form a hairpin, thus forcing the ligand to bind DNA as a 2:1 complex. As a result, such hairpin molecules possess the potential for enhanced sequence specificity but also the ability to span more base pairs in a predictable way (Mrksic *et al.*, 1994).

Dervan and co-workers have synthesised a number of polyamide hairpins that are comprised of three main types of building block: imidazoles, pyrroles and hydroxypyrroles (discussed below). Base pair recognition is achieved by linking the heterocycles in an anti-parallel pairing strategy with a γ-aminobutyric acid linker to connect the subunits in a carboxy to amino direction to form a "hairpin motif". Hydroxypyrrole subunits weakly favour binding to thymine and therefore, replacement of a pyrrole with a bulkier 3-hydroxypyrrole unit has allowed the discrimination between A·T and T·A base pairs. It was originally thought that the preference for thymine arises due to hydrogen bonding between 3-hydroxy and carboxyamido groups to the O-2 of a thymine residue (Trauger *et al.*, 1996), this theory has since been confirmed by a high resolution X-ray structure (White *et al.*, 1999; Bremer *et al.*, 2000). This discovery completed the four base pair code with the

antiparallel pairing sequences being C·G (Py/Im), G·C (Im/Py), T·A (Hp/Py) and A·T (Py/Hp) (Kielkopf *et al.*, 1998; White *et al.*, 1998). Registry between the hairpin heterocycles and DNA base pairs can be maintained by addition of paired β-alanine or γ-aminobutyric acid residues which restore the curvature of the molecule. This enables recognition of larger binding sites through better alignment with the DNA helix (Trauger *et al.*, 1996; Swalley *et al.*, 1997; Trauger *et al.*, 1998).

More recently Dervan and collaborators (Weyermann and Dervan, 2002) have reported the synthesis of a head to head linked hairpin polyamide dimer that can recognise a ten base pair sequence. It was found that a head to head combination with a C_4 linker (**31**) had the most favourable DNA binding properties with regard to specificity and affinity. None of the dimers investigated could bind to sequences longer than 10 bp with reasonable selectivity. A possible explanation for this could be that linker lengths C_3-C_6 are insufficient to span this site. For specific 11 bp sites to be recognised rigid linkers need to be investigated.

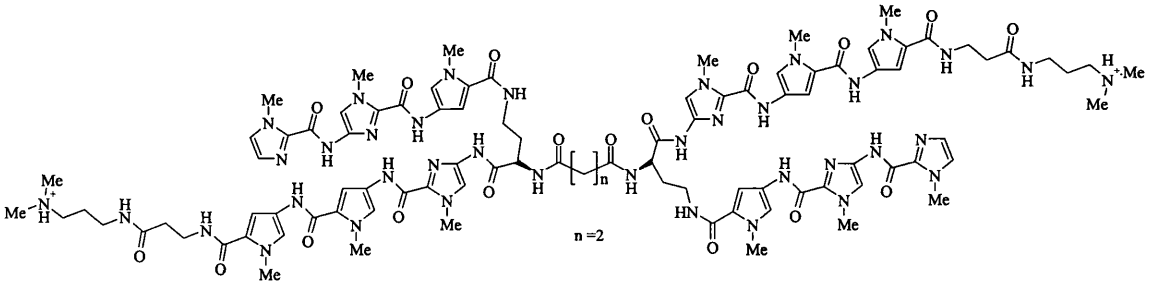

31

Figure 15. Head to head linked polyamide hairpin.

Work has also progressed towards the synthesis of turn to tail linked polyamides (Kers and Dervan, 2002). It is known that the success of tandem polyamides depends on the linker length between the two individual hairpins. While researching this

problem, Kers and Dervan decided to study two variables of the DNA-tandem polyamide complex. Firstly increasing the length of the amino acid linker by incremental steps of one methylene unit and secondly variation of the binding site from 10-11 bp by insertion of one bp at the linker position. Two series of polyamides were synthesised, either containing an aliphatic amino acid linker (**Figure 16**), or a short amino acid linker together with an unpaired imidazole.

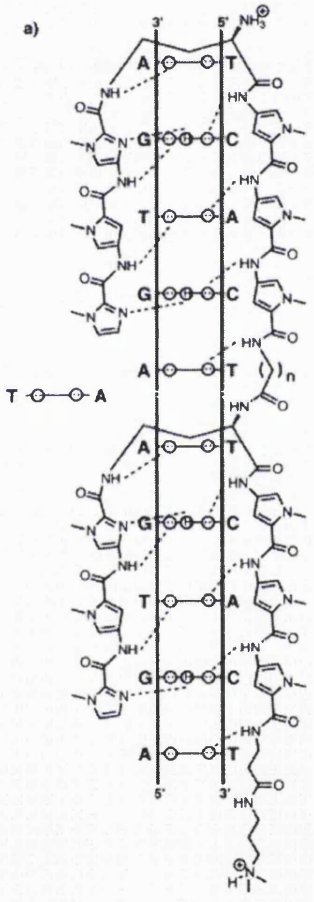

Figure 16. Representation of the polyamide/DNA complex formed between tandem polyamides and the 10 (or 11) bp match site 5'-AGTGA(T)AGTGA-3'. Circles containing an H represent lone pairs of N3 of purines and O2 of pyrimidines. Circles containing an H represent the N2 hydrogen of Guanine. Putative hydrogen bonds are illustrated by dotted lines. (Origin: Kers and Dervan, 2002).

The molecules were investigated using DNase I footprinting titration. The studies showed that 5-aminovaleric acid or 2-(2-aminoethoxy)acetic acid, connecting two six ring hairpin polyamides could target a 10 bp binding site. An 11 bp binding site can

be targeted but with a low selectivity over the 10 bp binding site using 5-aminovaleric acid with an unpaired imidazole unit.

Despite the success of the hairpin polyamides with respect to their interaction with double stranded DNA, these molecules have limitations. Firstly there are potential water solubility problems with molecules of this size. Secondly molecules of this type are less likely to penetrate the nuclear membrane within most cellular environments. Studies performed by Belitsky (Belitsky *et al.*, 2002) revealed that in the majority of live cells, polyamide-bodipy conjugates (bodipy FL being a fluorophore) are localised within the cytoplasm and not the nucleus of cells. However, more recent investigations suggest that the dye identity significantly influences nuclear uptake, such that dye-conjugates cannot be used a cellular penetration prediction for unlabelled analogues. To illustrate this, Dervan and co-workers synthesised a polyamide-fluorescein conjugate which targeted the hypoxia response element (HRE) and inhibited vascular endothelial growth factor (VEGF) expression in HeLa cells. Inhibition of VEGF expression is a marker for effective nuclear localisation of HRE-targeted polyamides. For comparative purposes a small library of non-fluorescent HRE-targeted polyamides was synthesised. Members of this library bind the HRE with affinities comparable or superior to the fluorescein-labelled analogues (Nickols *et al.*, 2007).

2.5 Polyamide conjugates

In light of the problems associated with solubility, cellular penetration and the fact that neither distamycin nor netropsin has significant antitumour activity, the conjugation of a cytotoxic moiety to the polyamide has proved popular. Several functional groups with a range of biological properties have been conjugated to netropsin, distamycin and lexitropsins. In hairpin type molecules this can be achieved by replacing the conventional γ-aminobutyric acid linker with analogues equipped with other functional groups. Several examples of polyamide conjugates are discussed below.

2.5.1 Linkage to DNA alkylating agents

It is well known that most alkylating agents react with purine residues of DNA via an electrophilic attack mechanism. More specifically, chlorambucil and cisplatin react with the N-7 position of guanine residues in the major groove of DNA (Hansen and Hurley, 1996; Tomasz, 1994) whereas duocarmycin A and CC-1065 are minor groove, adenine specific alkylators (Hurley and Draves, 1993; Boger and Johnson, 1996). However, it was hoped that the conjugation of alkylating agents with a DNA reading element (i.e. a lexitropsin or polyamide hairpin molecule) would modify the alkylation pattern of such an agent allowing it to be targeted to a specific site. This would overcome both the issues of negligible antitumour properties associated with the polyamides and displacement by transcription machinery as the molecules would be covalently bound to the appropriate site on DNA.

The first alkylator-lexitropsin hybrids to be synthesised were netropsin and distamycin analogues equipped with *N*-chloracetyl and *N*-bromoacetyl substituents (Arcamore *et al.*, 1989). One example, *N*-bromoacetyldistamycin (**32**) reacts with a single adenine in the sequence 5'-GTTTA·5'-TA*AAC within a 167 bp restriction fragment (Baker and Dervan, 1989). The alkylating benzoyl or benzyl mustard moieties have also been coupled to lexitropsins (Lee *et al.*,1993; Wyatt *et al.*, 1997, Ciucci *et al.*,1996). Furthermore, bis(mustard) crosslinked lexitropsins have been synthesised (Chen *et al.*, 1995) which exploit the antiparallel side-side motif. Interestingly, distamycin analogues conjugated to *N*-chloroacetyl, *N*-bromoacetyl, benzoyl or benzyl mustards exhibit no detectable guanine N-7 interactions but instead, almost exclusive *adenine alkylation in the minor groove of DNA*. This observation provides important information regarding which subunit directs the conjugate to the preferred binding site. It would appear that the minor groove binding preferences displayed by lexitropsins override that of the mustard moiety, which would otherwise alkylate the N-7 position of guanine in the major groove. The most notable example of this type of molecule is *bis*(2-chloroethyl)aminobenzoyl derivative of distamycin. This molecule, also referred to as tallimustine (**33**), alkylates the 3' purine residue within the sequence 5'-TTTTGPu-3' and exhibits significant anti-cancer activity due to its interaction with DNA.

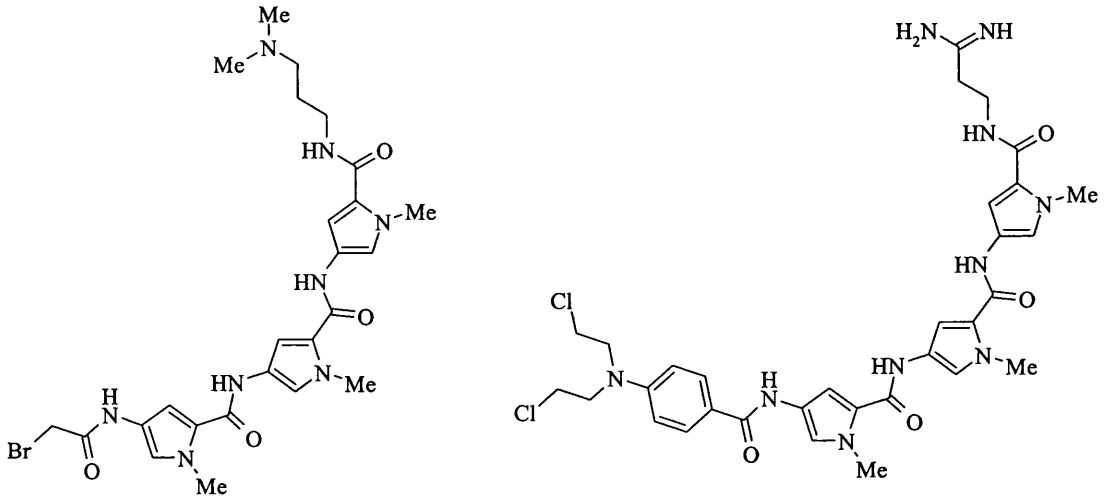

32 **33**

Figure 17. *N*-bromoacetyldistamycin (**32**) and tallimustine (**33**).

Lown and co-workers have designed and synthesised a series of lexitropsin cyclopropylpyrroloindole (CPI) hybrids (Wang *et al.*, 1996) which form stable adducts in the minor groove of DNA (Fregeau *et al.*, 1995). Similarly, Dervan took the approach one step further to create hairpin polyamide-*seco*-CBI conjugates. The criteria for the design of these molecules stipulated that the reactive moiety must specifically alkylate in the minor groove proximal to the hairpin polyamide target site. The pharmacophore found in (+)-CC-1065 and duocarmycins was an ideal candidate for these molecule types (Chang and Dervan, 2000). As expected, the conjugates were shown to efficiently and selectively alkylate a single adenine adjacent to a polyamide match site.

The PBD, another DNA alkylating moiety, has also been coupled to lexitropsin type molecules and is of particular relevance to this work. It will be discussed in more detail in Section 2.6.

2.5.2 Linkages to polyamines

Bruice and colleagues substituted the *N*-methyl group on the central heterocycle unit of distamycin with a branched polyamine to give a tren-microgonotropen (**34**) (He *et al.*, 1993; He *et al.*, 1994). The polyamine can act as a hook appendage to increase affinity for DNA via interaction with the phosphodiester backbone or with the major groove of DNA (Blaskó *et al.*, 1994). It has been shown (Satz and Bruice, 2002) that utilising the versatility of these molecules can increase the base pair specificity. The solid phase synthesis of a microgonotropen resulted in a compound able to distinguish nine base pair AT rich binding sites from sites possessing less than nine contiguous AT base pairs, and molecular modelling of this compound suggested that the molecule adopts a "spiral-like" conformation which fits almost a full turn of the DNA helix.

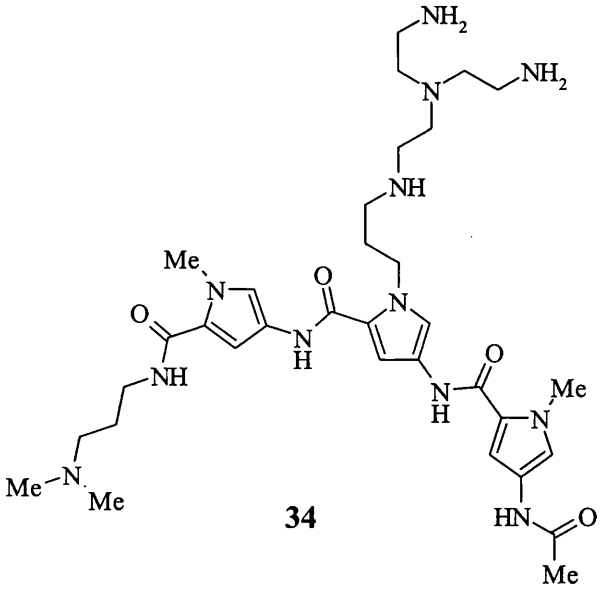

34

Figure 18. Example of a tren-microgonotropen.

2.6 Polyamide PBD conjugates

Lown and co-workers have synthesised a set of PBD-lexitropsin conjugates comprising imidazole and pyrrole subunits (Damayanthi *et al.*, 1999). The PBD moiety was coupled to pyrrole (n = 1-3) subunit via a propyl linker. Interestingly, the *N*-(dimethylamino)propyl tail differs from the natural products, distamycin and netropsin, which possess an amidinoalkyl terminus. The PBD-lexitropsin compounds **35, 36** and **37** (**Figure 19**) were a mixture of both the N10-C11 imine and the carbinolamine methyl ether forms with an overall yield of 28-30%. Unfortunately, it was not possible to separate the imine and the carbinolamine methyl ether forms due to poor solubility associated with these conjugates. In addition, a set of three imidazole (**38, 39, 40**) and two imidazole and pyrrole (**41, 42**) containing analogues were synthesised (Kumar and Lown, 2003; Kumar *et al.*, 2002) with overall yields ranging between 35-40%. Once again, an equal mixture of the imine and carbinolamine methyl ether was observed and poor solubility hindered separation.

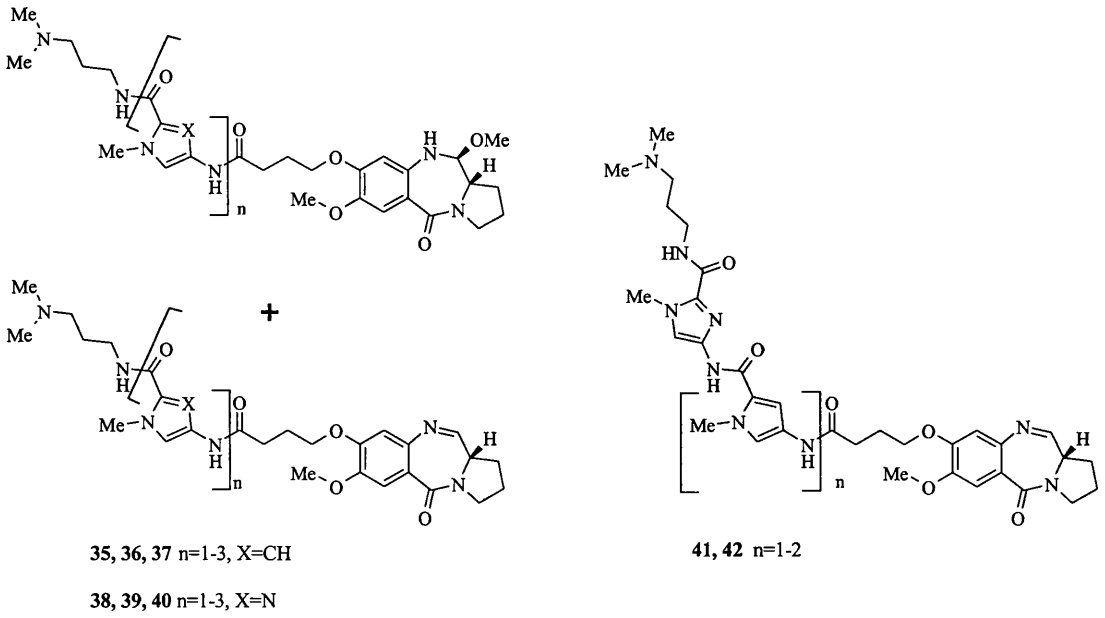

Figure 19. PBD-polyamide conjugates reported by Lown.

Biological evaluation in the NCI 60 cell-line panel allowed cytotoxicity profiles for each compound to be obtained. Compounds **36** and **37** exhibited modest cytotoxicity with average LC_{50} values ranging from 7.5-86.5 μM for **36** (n = 2) to 0.9-93 μM for **37** (n = 3). Compounds **38, 39, 40, 41** and **42** were not significantly active against the 60 cell-line panel with mean GI_{50}, TGI and LC_{50} values in the range of 16.22-95.50 μM. No DNA binding or sequence selectivity data for these molecules has been reported.

Similarly, a set of PBD-distamycin and related analogues **43, 44, 45** and **46** has been synthesised by Baraldi and co-workers (**Figure 20**) (Baraldi *et al.*, 1998). Baraldi has utilised a three carbon linker, rather than the four carbon linker favoured by Lown, and has retained the amidine terminus of the natural products. Unfortunately, NCI data is not reported to allow direct comparison of these two sets of molecules. However, cytotoxicity evaluations of these molecules in both K562 and Jurkat human tumour cell lines suggested that increasing the length of the polyamide subunit leads to an increase in cytotoxicty, where only molecules **45** and **46** were more potent than the PBD and heterocyclic subunits on their own.

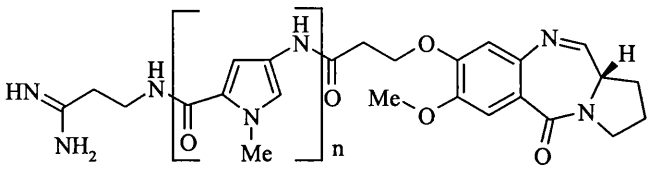

43, 44, 45, 46 n=1-4

Figure 20. PBD-polypyrrole conjugates reported by Baraldi.

More recently, Lown and co-workers have reported a set of sixteen PBD-polyamide conjugates containing pyrrole and imidazole subunits but with ring glycosylated heterocycles (**47-54**) in order to enhance water solubility (**Figure 21**). The hydroxyl group of the glycosyl moiety was acetylated for eight of the molecules, for the remaining eight the acetyl group was removed. All sixteen molecules contain either one or two glycosyl groups but otherwise were directly comparable to the first generation of conjugates (**35-42**) synthesised by Lown. However, decreased cytotoxicity was observed for all the glycosylated molecules in the series, either acetylated or not.

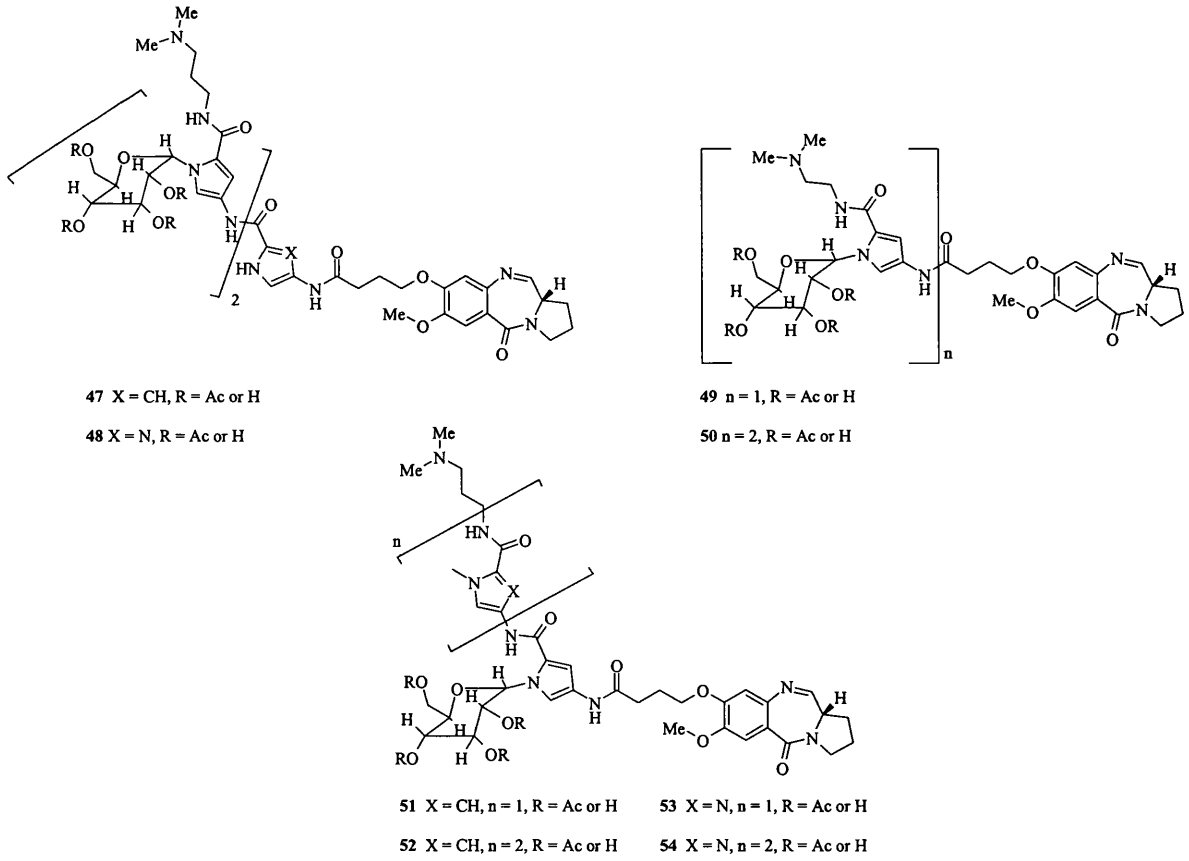

Figure 21. Glycosylated polyamide-PBD conjugates reported by Lown.

Recently, PBD-heterocyclic conjugates have been investigated further by Wells and co-workers (Wells *et al.*, 2006). An increasing number (n = 1-6) of pyrrole subunits were attached to a PBD unit in order to identify the optimal polyamide length for increased binding affinity. The series of molecules (**55-60, Figure 21**) possessed a methyl ester tail which differs from the previously reported amidine and dimethyl-propyl termini. A synthetic advantage of incorporating a methyl ester tail is that the pure N10-C11 imine molecules can be isolated. Molecular modelling of the series predicted that a four-carbon methylene linker between the PBD and first heterocycle is preferred, ensuring the conjugates maintain a more isohelical structure and therefore have a better fit in the minor groove. The four carbon linker has been utilised by Lown but is in contrast to the three carbon linker used in Baraldi's set of molecules.

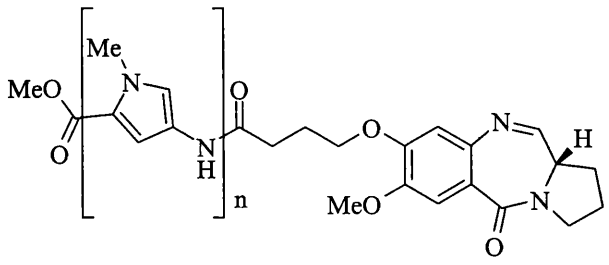

55 - 60 n = 1-6

Figure 22. PBD-polypyrrole conjugates reported by Wells.

The series of molecules **55-60** have exhibited higher cytotoxicity values in NCI 60 cell-line panel than either the Lown or Baraldi conjugates with LC_{50} values ranging from 1.07-11.5 μM. This could be the result of increased cellular/nuclear penetration by the compounds containing a methyl ester terminus. Thermal denaturation studies demonstrated the compounds impressive ability to stabilise the DNA helix by between 8.1-21.2 °C at 18 hours incubation when compared with double stranded

DNA alone. The tri-pyrrole PBD conjugate (**57**) produced a ΔT_m value of 21.2 °C which is higher than that recorded for SJG-136, a covalent, interstrand crosslinking PBD dimer (20.5 °C at 18h). Furthermore, the ΔT_m value for **57** (n = 3) is 50-times greater than the PBD unit alone and 5-fold greater than the tri-pyrrole unit alone.

DNA footprinting and *in vitro* transcription studies performed on this set of molecules confirm that the conjugates appear to interact with DNA in a synergistic manner with respect to the PBD and polypyrroles alone, where the target sequence was found to be a run of A/T base pairs (polyamide component) adjacent to a PBD binding site.

3 TARGETING DNA WITH LOW MOLECULAR WEIGHT SEQUENCE SELECTIVE MOLECULES

For many years DNA has been the traditional target for chemotherapeutic intervention in human cancers (Henderson and Hurley, 1995). However, classical alkylators target DNA *in toto*, exerting their effects on all rapidly dividing cells. Recent advances in molecular biology have lead to a more sophisticated understanding of cancer. In particular, many signalling pathways critical to cancer cells have been elucidated. These pathways consist of networks of regulatory proteins; however all of the proteins are the product of transcription/translation from a DNA template. Sequence selective DNA binders offer the prospect of targeting oncogenic signalling pathways at their genetic roots.

The first step in the expression of a gene is the transcription of DNA to generate messenger RNA (mRNA), which is subsequently translated to a protein. Each region of the DNA helix that produces a functional RNA molecule constitutes a gene. mRNA is synthesised by RNA polymerases that are directed by specific sequences on the DNA template. The amount of RNA transcribed from a particular region of DNA is controlled by regulatory proteins that bind to specific sites on DNA close to the coding sequence of a gene; this ensures that the gene is transcribed at the proper time in the appropriate cell type. More specifically, the transcription of particular genes is enhanced or inhibited by regulatory proteins, known as transcriptional activators or repressors which respond to cellular and environmental cues (Ansari, 2001). However, mutations, deletions and translocations within DNA can effect either

expression or biological function of specific genes. In the context of cancer, the most frequently mutated genes are proto-oncogenes and tumour suppressor genes.

Molecular biologists have identified a large number of changes in DNA sequences that promote the transformation of a normal cell into a malignant one. With this in mind, a drug capable of recognising and binding to specific sequences of DNA has the potential to inhibit the expression of certain oncogenes and consequently inhibit the development of tumour cells. Currently, the development of such a drug is limited by the difficulty in discriminating between different genes, resulting in binding to both the genomes of normal and cancer cells. For example, a molecule with a site selectivity of three base pairs can only distinguish between one in thirty two random sequences, which in the human genome (*circa* three billion bases in length) equates to approximately 100,000,000 unique binding sites (Dervan, 1986). Therefore specificity for longer sequences, approximately 16-18 bases long, is statistically required in order to target a unique DNA sequence or to down-regulate transcription of a specific gene.

The different regions of DNA that are potential targets for therapeutic intervention are summarised below:

3.1 Coding region of DNA

Eukaryotic genes contain coding regions of DNA which dictate the sequence of amino acids required to form a particular protein. More specifically, a unique combination of three base pairs (a codon) specifies an amino acid. In order for the protein to be synthesised, the entire length of the gene, including introns and exons, is transcribed

into a large RNA molecule. The coding region, therefore, presents itself as an important target for DNA binding drugs; however there are several disadvantages associated with this approach. For instance, the inhibition of transcription by interactions between DNA and non-covalent molecules, such as the hairpin polyamides, may be difficult to achieve due to the transcription machinery potentially dislodging the polyamide molecule. A means of overcoming this problem is to utilise an alkylating moiety, which would form an irreversible covalent bond with DNA and prevent the transcription of the gene in question.

Sugiyama and co-workers demonstrated that alkylation of the template strand in the coding region of DNA by Py-Im polyamide-cyclopropylpyrroloindole (CPI) conjugate resulted in the production of truncated mRNA, effectively inhibiting transcription *in vitro* (Oyoshi *et al.*, 2003). More recently, the same research group reported successful gene silencing using a CBI-polyamide conjugate to selectively alkylate target sequences within the coding region of DNA (Shinohara *et al.*, 2006). Fluorescent microscopy and quantification of green fluorescent protein (GFP) mRNA using real-time PCR confirmed that gene silencing was caused by sequence-specific alkylation of the coding region of the GFP gene. However, the results were limited to exogenous DNA alkylation due to the conjugates only spanning 6 base pairs. In order for this type of molecule to have any therapeutic use, longer molecules which can recognise extended DNA sequences would have to be synthesised.

As carcinogenesis arises from mutations in the coding region of a gene it is a logical necessity to know the exact sequence generated by the mutation in order to design a drug capable of binding to that particular site and inhibit transcription. In addition,

mutations vary between individuals; therefore targeting the mutated region for a particular patient would involve genetic profiling and individually designed drugs. Secondly, using alkylating molecules to target the coding region can eventually result in truncated proteins which could have aberrant biological functions that potentially trigger other signalling cascades involved in cancer or other gene-based diseases.

3.2 Promoters

Eukaryotic transcription is initiated by RNA polymerase II, which recognises specific sequences in the genome, a start site and a termination site, which characterise a protein-coding unit. The promoter region is located approximately 30-100 bp upstream (5') of the start site, RNA polymerase binds to this region before initiating transcription. However, eukaryotic RNA polymerase enzymes alone cannot initiate transcription *in vitro*, requiring the involvement of additional proteins, the general transcription factors (GTFs). The GTFs assemble as a complex on the DNA at the promoter in order to recruit the RNA polymerase II to this site.

The core promoter region is comprised of three distinct motifs, namely, the TATA box (a short sequence of DNA primarily composed of T and A nucleotides), the Initiator (INR) and the Downstream Promoter Element (DPE). The TATA box is bound by the TATA box-binding protein (TBP). In addition, the other two elements, INR and DPE bind proteins that are found in a complex with the TBP. These proteins, known as TBP Associated Factors (TAFs), deliver the TBP to a given promoter through recognition of the DPE. Together the TBP and TAFs are known as TFIID (TF stands for transcription factor and II refers to RNA polymerase II). The binding of this complex to DNA recruits several other general transcription factors,

namely, TFIIA, TFIIB, TFIIE and TFIIH, which allow stable protein/DNA interactions, entry and disengagement of RNA polymerase II. In the presence of the four ribonucleoside triphosphates the fully assembled complex is capable of initiating RNA synthesis from specific start sites, which are typically located 25 to 30 nucleotides downstream of the TATA box.

However, it is the specific transcription factors that initiate transcription in particular genes rather than the general transcription factors which are required for global transcription of most eukaryotic genes.

3.2.1 Transcription factor binding sites within the promoter

Many general and specific transcription factors occupy pivotal positions in the regulation of gene expression, where cell signalling pathways intersect with the transcriptional machinery. A high proportion of protein-coding genes within the human genome represent transcription factors, where 1850 genes out of 13,500 whose molecular function was assigned, are classified as transcription factors (Venter *et al.*, 2001). In light of this, transcription factors should present an important target for therapeutic intervention at the signalling/transcription interface using sequence selective DNA binding molecules.

Many transcription factors exert their function by binding to specific sites on DNA, either within the promoter region or at distant sequences that enhance or attenuate the initiation of transcription by RNA polymerase II (Hurst, 1996; Patiglou *et al.*, 1997), the latter case is discussed in Section 3.2.2.

Currently, the most popular method for investigating transcription factor interactions with specific binding sites is the electrophoretic mobility shift assay (EMSA) (Sun and Hurley, 1995; Dickinson *et al.*, 1998; Chiang *et al.*,2000) in which protein-DNA complexes migrate as discrete bands, distinct from free DNA. This approach has also been exploited to elucidate the effect of DNA binding drugs on transcription factor interactions with specific binding sites. DNAse I footprinting is another widely-used method of investigating the effects of DNA binding drugs on transcription factor/DNA interactions, where transcription factor and drug molecule binding sites can be identified as regions (footprints) protected from DNase I cleavage enzymes.

Dervan and co-workers reported the use of EMSA assays to demonstrate targeting of the Ets transcription factor binding site (EBS) of the HER2/neu promoter using Py-Im polyamides. This particular target was of interest as the HER2/neu oncogene (a tyrosine kinase enzyme) is amplified and up-regulated in 25-30% of human cancers. A number of polyamide molecules were synthesised to target the EBS and adjacent upstream or downstream flanking sequences which are specific to this promoter. The Ets proteins bind in both the major and minor grooves of DNA, a GGAA sequence is recognised in the major groove, however, binding also occurs in the minor groove immediately flanking GGAA. Quantitative DNase I footprinting analysis revealed that the polyamides bound with high affinity to their target sites. In addition, it was observed by EMSA that one polyamide inhibited protein-DNA complex formation with an IC_{50} value of 2.2 nM in comparison to 500 nM for distamycin. *In vitro* transcription assays were also conducted in order to evaluate the biological effect of the polyamide interaction with the Ets DNA complex formation, where it was observed that the synthetic polyamides were significantly more potent inhibitors of

HER2/neu promoter driven transcription than distamycin (Chiang *et al.*, 2000). It was concluded that the non-covalent binding of the rationally designed polyamide in the 3'-flanking region was sufficient to inhibit protein-DNA interaction at the HER2/neu promoter.

The ability of minor groove binding molecules to have an impact on proteins that bind in the major groove is of great importance in the potential therapeutic use of polyamides. The majority of gene regulation is controlled by interactions within the major groove of DNA and the discovery that polyamide molecules can influence major groove interactions significantly increases the number of potential targets.

3.2.2 Targeting repressor/enhancer binding sites

Regulatory elements are gene-specific sequences that are located upstream of the core promoter and control the rate of transcription initiation. They include both upstream activation sequences (UAS) and upstream repression sequences (URS) which serve as binding sites for enhancers and repressors of transcription respectively. In response to various signals the appropriate transcriptional activator or repressor binds to its cognate DNA site to up-regulate or down-regulate the expression of the targeted set of genes, respectively.

Dervan and co-workers reported the use of hairpin polyamides to block HIV replication by targeting regulatory sequences in the HIV-1 enhancer (Dickinson *et al.*, 1998). The compounds were directed to sequences that directly flank or partially overlap the DNA-recognition element so that ligands might act selectively on the HIV enhancer without affecting the transcription of cellular genes. Using two different

polyamide sequences two minor groove binding proteins i) TBP, which binds to the TATA box in the HIV-1 promoter, and ii) LEF-1 a lymphoid cell-enriched enhancer binding factor were targeted. The polyamides competed with the endogenous transcription factors and successfully inhibited HIV-1 transcription *in vivo*. The individual polyamides only modestly reduced virus replication in peripheral blood mononuclear cells, however, when given in combination the polyamides were found to dramatically affect viral replication. Encouragingly, the effects seen were not the result of interactions with other host cell proteins as transcription of T-cell surface receptors CD4 and CD8 was unaffected, as was the expression of other cellular genes involved in T-cell activation. However, the inhibition observed cannot definitely be attributed to binding of the ligand at the target site due to the potential for such molecules (spanning 6-7 bp) to recognise multiple binding sites in the viral genome.

3.2.3 Targeting the CCAAT-box

The CCAAT-box is present in approximately 30% of eukaryotic promoters (Bucher, 1990) and has been found to play an important role in transcriptional activation, especially in TATA-less promoters, where an intact CCAAT is an essential requirement. In higher eukaryotes, CCAAT-box containing promoters are found in genes with a variety of functions i.e. developmental control and tissue specific genes, housekeeping and inducible genes and genes that regulate the cell cycle. Interestingly, the promoters of cell cycle regulating genes usually contain more than one CCAAT-box situated close to, and sometimes overlapping, the start site. One protein that binds to the CCAAT-box is Nuclear Factor Y (NF-Y) which is also referred to as the CCAAT binding protein (CBF). NF-Y is a ubiquitous transcription factor comprised of three subunits, NF-YA, NF-YB and NF-YC (**Figure 22**) which

are all required for DNA binding. Initially, the NF-YB and NF-YC subunits form a dimer, which offers a complex surface for NF-YA association. The resulting trimer binds to DNA with high affinity and specificity, for most sites *Kd* is between 10^{-10} and 10^{-11}, which is higher than for most other transcription factors (Kim and Sheffrey, 1990; Bi *et al.*, 1997).

DNA topoisomerase II (topo II), a nuclear enzyme which alters the topology of DNA, is essential for several nuclear processes. Two isoforms of the enzyme exist, Topo IIα and Topo IIβ and their activities and expression differ greatly. Topo IIα is believed to play a vital role in mitosis (Kimura *et al.*, 1994; Grue *et al.*, 1998). The Topo IIα promoter is regulated very tightly through NF-Y interactions with five inverted CCAAT boxes (ICBs).

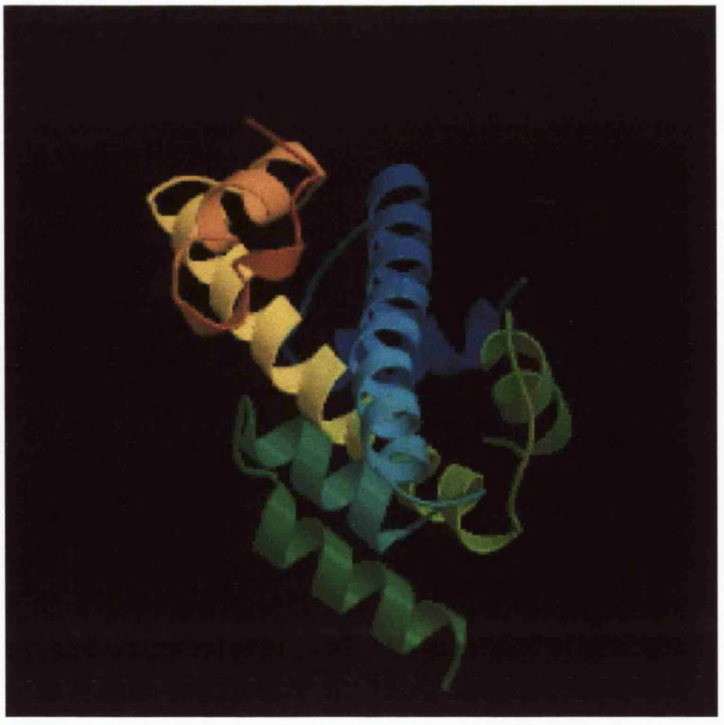

Figure 23. Structure of NF-Y subunits.

Binding of NF-Y to ICB2 in confluent cancer cells represses the expression of the Topo IIα gene, which has been shown to contribute to resistance to Topo II poisons such as etoposide (Baraldi *et al.,* 2000). Inhibition of NF-Y binding to the CCAAT-box by anti-cancer drugs has been reported, examples include Genistein, ET743 and HMN-154 (Zhou and Lee, 1998; Bonfanti *et al.*, 1999; Tanaka *et al.*, 1999). An alternative approach is to target the CCAAT-box sites using sequence specific DNA binding drugs, which, given the high affinity and specificity with which NF-Y binds to the CCAAT-box, could be problematic if using non-covalent ligands. A solution would be to use a polyamide-alkylator conjugate which could not be displaced by the endogenous transcription factor. In addition, targeting the sequences flanking the CCAAT box would lead to an increased selectivity which is crucial given that the CCAAT box is present in 30% of eukaryotic genes.

4 AIMS

The aim of this project was to synthesise, characterise and evaluate a small library of heterocycle-PBD conjugates for biological evaluation.

4.1 Design and synthesis

As discussed previously there is considerable interest in the regulation of transcription by polyamide molecules. It has been reported that sequence selectivity is dependent on the type of heterocycle used and its position within the polyamide chain. In addition, PBDs possess intrinsic antitumour activity and bind covalently to DNA in the minor groove.

Wells and co-workers within the CR-UK Gene Targeted Drug Design research group have synthesised a small set of PBD-polyamide conjugates (1-6 pyrroles). These molecules have generated significant biological interest, particularly the 2 and 3 pyrrole-PBD conjugates, in footprinting, thermal denaturation and transcription stop assays.

It was therefore decided to extend the study by preparing a focused library of PBD-heterocycle polyamides based on the template provided by the 2 and 3 pyrrole PBD conjugates. Two sets were selected, the first containing pyrroles and imidazoles in all possible dimeric and trimeric combinations. In a second set the imidazoles were replaced by thiazoles, thus allowing the two sets to be directly compared.

In addition, the heterocyclic polyamides were coupled to a dilactam capping unit to allow the influence of covalent (PBD) and non-covalent binding (dilactam) to be assessed.

On completion of the chemical synthesis of both the PBD-heterocycle conjugates and the dilactam-heterocycle conjugates, the aim was to assess their activity in a range of biological assays. Such assays would provide data on cytotoxic activity, as well as affinity and selectivity for DNA sequences.

Imidazole Series	Thiazole Series
Py-Im-PBD	Py-Th-PBD
Im-Py-PBD	Th-Py-PBD
Im-Im-PBD	Th-Th-PBD
Py-Py-Im-PBD	Py-Py-Th-PBD
Py-Im-Py-PBD	Py-Th-Py-PBD
Py-Im-Im-PBD	Py-Th-Th-PBD
Im-Im-Py-PBD	Th-Th-Py-PBD
Im-Py-Py-PBD	Th-Py-Py-PBD
Im-Py-Im-PBD	Th-Py-Th-PBD
Im-Im-Im-PBD	Th-Th-Th-PBD
Py-Py-PBD	Py-Py-Py-PBD

Table 1. Target compounds. Py = pyrrole, Im = imidazole, Th = thiazole.

5 CHEMICAL RESULTS AND DISCUSSION

The target molecule synthesis was divided into three distinct stages. Namely, the preparation of the PBD and heterocyclic building blocks, subunit coupling and deprotection to form the final molecules.

5.1 Synthesis of PBD acid building block

The PBD polyamide conjugate would be prepared in a convergent fashion, i.e. joining a PBD capping unit to the appropriate heterocyclic polyamide towards the end of the synthetic route. The PBD imines are relatively sensitive moieties and are usually unmasked in the final step of a PBD synthesis. For this reason it would be prudent to mask the N10-C11 moiety during the coupling to the polyamide component.

The Fukuyama approach (Fukuyama *et al.*, 1993) to PBD synthesis is ideally suited to the synthesis of PBD capping units, as N10 protection is integral to the synthetic strategy. The PBD precursor can be coupled to the polyamide subunit with the N10-C11 moiety safely protected.

Commercially available vanillin (**61**) and methyl-4-bromobutyrate were coupled together under mild, basic conditions to incorporate the butanoic acid side chain in 94% yield. Subsequent nitration of the aldehyde **62** using nitric acid (70%) provided the nitroaldehyde **63** in 84% yield. ^{1}H NMR analysis confirmed product formation by changes in the aromatic region of the spectrum and gain of triplet signals corresponding to the butanoic side chain.

Oxidation of the aldehyde with potassium permanganate furnished the acid **64** in 63% yield. Activation of the acid using oxalyl chloride followed by coupling to the commercially available *S*-pyrrolidinemethanol formed the A-C ring coupled product **65** (96%). Mass spectral analysis revealed a signal at 397 m/z (M+1) and NMR studies indicated signals corresponding to both A and C ring characteristics.

The next step was the reduction of the aromatic nitro group, prior to Boc protection. This was partially achieved with hydrogen (30 psi) and a 5 % palladium on charcoal catalyst. However, the reaction failed to go to completion, with only a small amount of the starting material being consumed, probably due to poisoning of the catalyst. Due to a temporary lack of fresh palladium on charcoal, an alternative Raney Nickel reduction was performed. This particular method had also been previously employed within the research group, resulting in high yields of product. TLC revealed the presence of some impurities which were removed by flash chromatography to furnish the aniline **66** in 68% yield.

The next step in the synthetic route involved protection of the N10 amino group using Boc anhydride. The choice of protecting group deviates from the approach reported by Fukuyama wherein the N10 amine functional group was protected as the allyl carbamate (Alloc). However, Alloc deprotection involves a palladium catalyst which is usually removed by column chromatography. In order to avoid this time consuming step the Boc protecting group was chosen. Boc deprotection is achieved by treatment with TFA, followed by an aqueous work up, using 1M HCl and 1M $NaHCO_3$. The purity of the Boc-protected product is usually sufficient to avoid column chromatography.

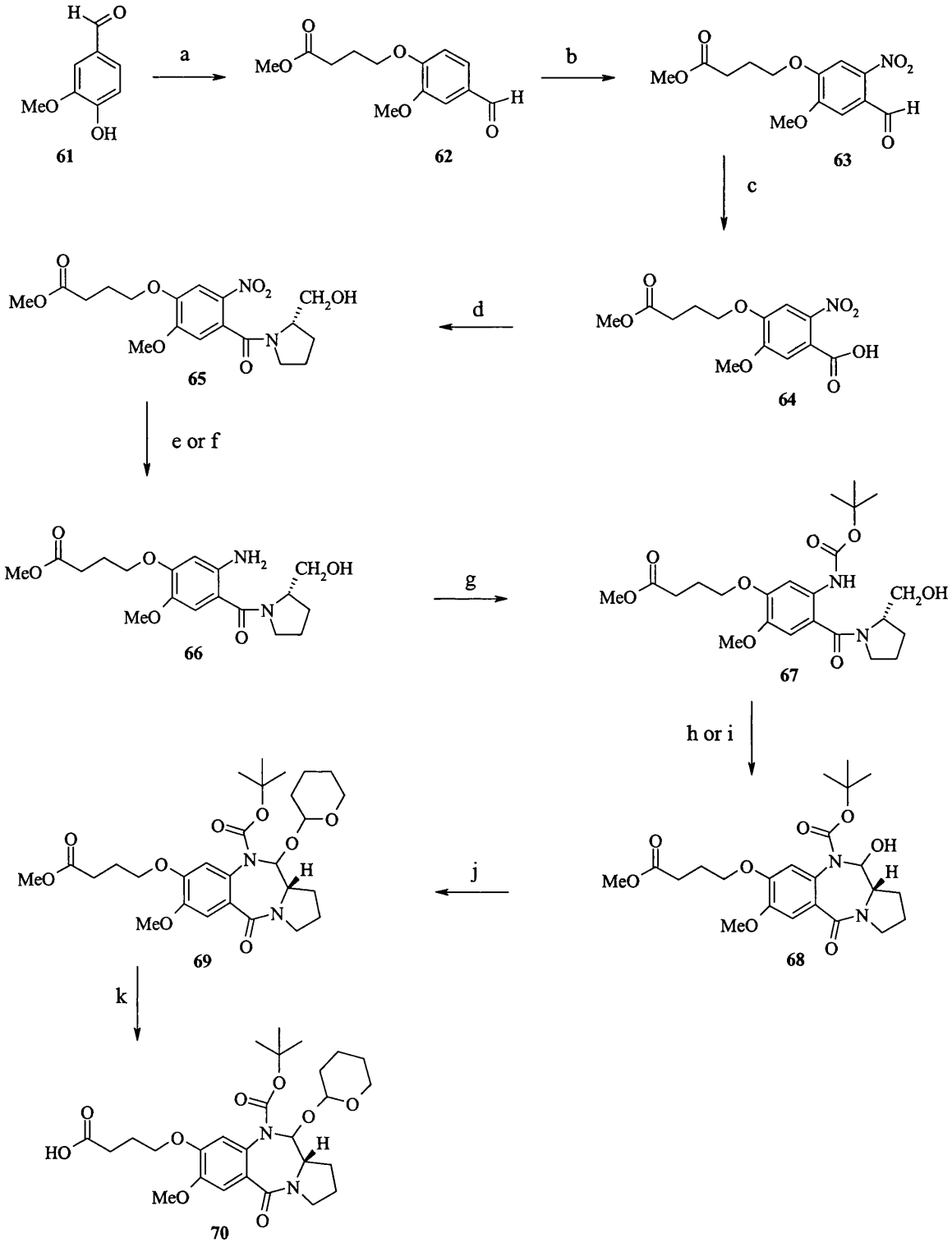

Scheme 3. a) DMF, K_2CO_3, methyl-4-bromobutyrate, 94%; b) HNO_3, Ac_2O, 0 °C, 84%; c) $KMnO_4$, H_2O, Me_2CO, 63%; d) DCM, $(COCl)_2$, *S*-pyrrolidinemethanol, TEA, 96%; e) H_2, Pd/C, EtOH; f) Raney Ni, hydrazine hydrate, MeOH, 68%; g) BOC_2O, THF, reflux, 75% h) $(COCl)_2$, DMSO, DIPEA, DCM, 80%; i) DAIB, TEMPO, DCM, 66%; j) DHP, PTSA, EtOAc, 100%; k) NaOH, MeOH, H_2O, 98%.

The Boc-protected methyl ester **67** was successfully synthesised in a 75% yield as confirmed by the presence of a single NMR peak, with an integral of nine, at 1.40 ppm.

The penultimate step of the synthesis involved a spontaneous oxidation/ring closure to form the protected carbinolamine. This was achieved by oxidation of the Boc-protected methyl ester under Swern conditions. Monitoring the reaction by TLC revealed an impurity, most probably the result of over oxidation to the undesired dilactam. This impurity was removed using flash column chromatography to afford the PBD methyl ester **68** in an 80% yield.

In order to avoid the malodorous by-products of the Swern reaction, a second oxidation method was employed. This method involved treating the methyl ester intermediate with di(acetoxy)iodobenzene (DAIB) and a catalytic amount of 2,2,6,6-tetramethyl-1-piperidinyloxy free radical (TEMPO) (De Mico *et al.*, 1997) to furnish a brown foam in 66% yield. Several factors make the DAIB/TEMPO reaction preferable to the Swern oxidation, despite the observed decrease in yield. Unlike the Swern reaction, chromatographic purification of the product was not required with this oxidation method as no over oxidation to the dilactam was observed. In addition, anhydrous conditions are not required for the TEMPO/DAIB reaction facilitating monitoring of the reaction's progress.

The final step involved the saponification of the methyl ester to form the desired acid. Treatment of the ring closed Boc protected carbinolamine with 1M sodium hydroxide solution yielded the target molecule as a colourless foam in 98% yield. However the

optical rotation was found to be zero indicating a racemic mixture, where both the *R* and *S* enantiomers at C11a are present in equal concentration. This was highly undesirable as only the *(S)*-configuration provides the appropriate three dimensional shape for isohelicity with the minor groove of DNA. Racemisation at the C11a position reduces both DNA binding affinity and biological activity. A PBD with the *(R)*-configuration was devoid of *in vitro* cytotoxicity and DNA binding affinity (Thurston, 1993).

5.1.1 Overcoming racemisation at the C11a position of PBD acid

Racemisation at the C11a position of the PBD acid is thought to have occurred during the final step of the synthetic route. The saponification reaction involves the use of 1M sodium hydroxide, a strong base. It is thought the B ring of the PBD was opened as a result of an initial nucleophilic attack by the hydroxide ion on the C11 hydroxyl group. The proposed mechanism by which racemisation at the C11a position occurred can be seen in **Figure 24.**

On studying this mechanism it is clear that the C11 position needs to be protected in order to avoid racemisation. Several protecting groups were investigated by another member of the research group (Tiberghien, A. unpublished results) with the conclusion that a THP group was most favourable. Incorporation of a THP protecting group at the C11 position preserved the (*S*)-stereochemistry, thus abolishing racemisation. In addition, both the Boc group and the THP group could be removed simultaneously under the same acidic conditions. The only disadvantage with the addition of a THP protecting group is the incorporation of another chiral centre, making it difficult to assess the optical purity of C11 during the synthesis. However,

Boc and THP deprotection, followed by re-esterification allowed chiral column HPLC analysis to be carried out. Only one peak was present, confirming that only the (*S*)-enantiomer was present.

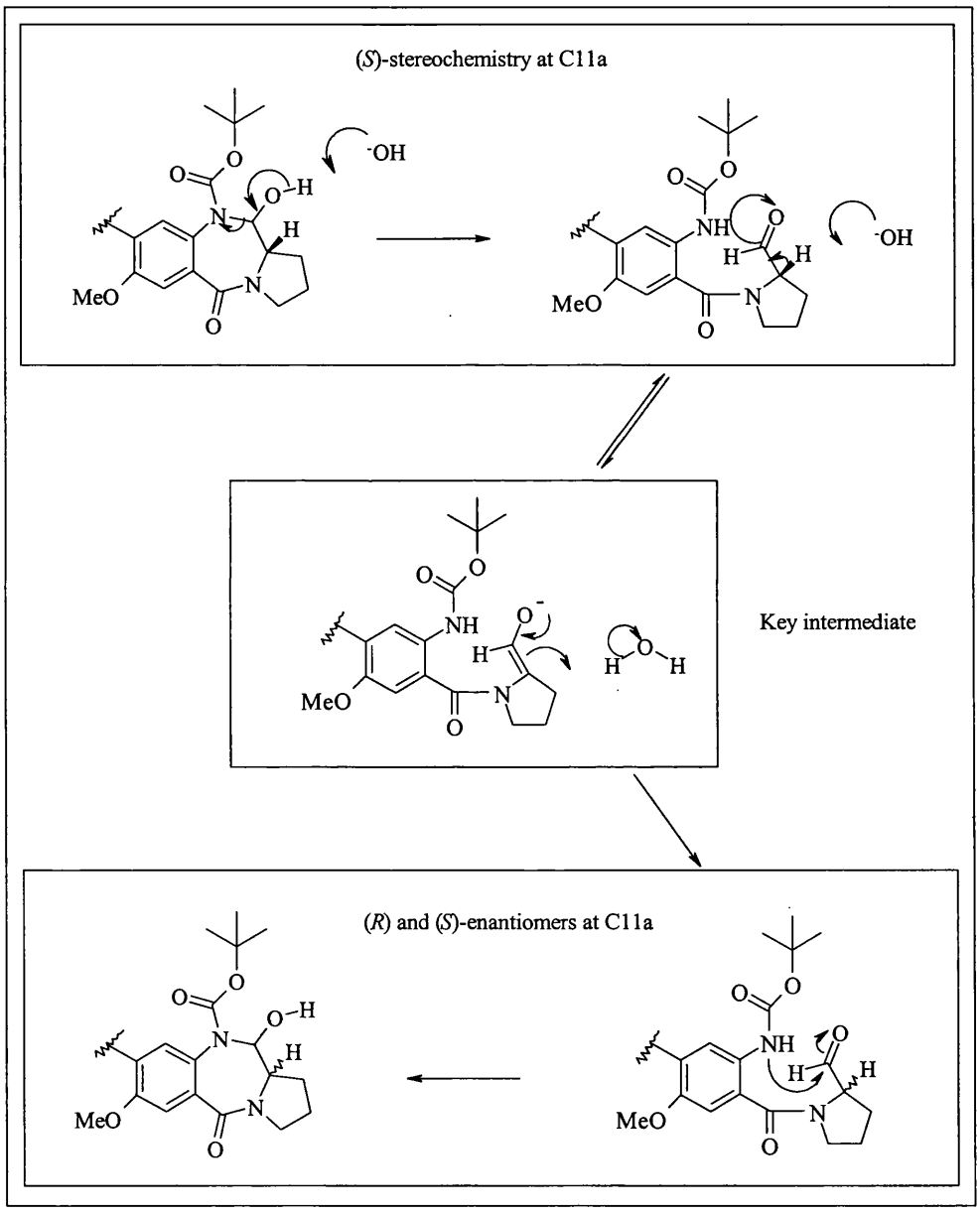

Figure 24. Proposed mechanism for racemisation of the PBD acid building block.

Tercel *et al.* have also observed racemisation at the C11a position of a synthetic PBD following a basic hydrolysis reaction (Tercel *et al.*, 2003). Consequently, the ester

group was protected with a trichloroethyl (TCE) group which can be easily converted to the acid using Zn powder in acetic acid, thus avoiding basic cleavage conditions. This strategy was not directly transferable to the synthesis of the PBD acid, as Tercel *et al.* employed an alloc protecting group at the N10 position. This contrasts with the work described here, where a Boc protecting group was utilised for reasons previously stated. In addition, intermediate **68** was readily available, reducing the number of synthetic steps needed to produce the PBD capping unit.

The tetrahydropyran (THP) protecting group was introduced using 3, 4-dihydro-2 H-pyran (DHP) and a catalytic amount of 4-toluenesulfonic acid to give **69** in 100% yield. The Boc-THP protected methyl-ester compound was a mixture of diastereomers due to the mixed stereochemistry at the pyran C-2 position of the THP group, however, saponification gave the desired acid **70** (98%) in chirally pure form at the C11a position which was confirm by chiral column liquid chromatography. Structural confirmation was achieved using NMR studies and mass spectral analysis, which revealed a signal at 535 with 100% relative intensity.

Due to difficulties associated with removal of the Boc and THP groups (Section 5.6.1) the PBD capping unit synthesis was repeated with the Boc protection step being replaced with the introduction of an Alloc group.

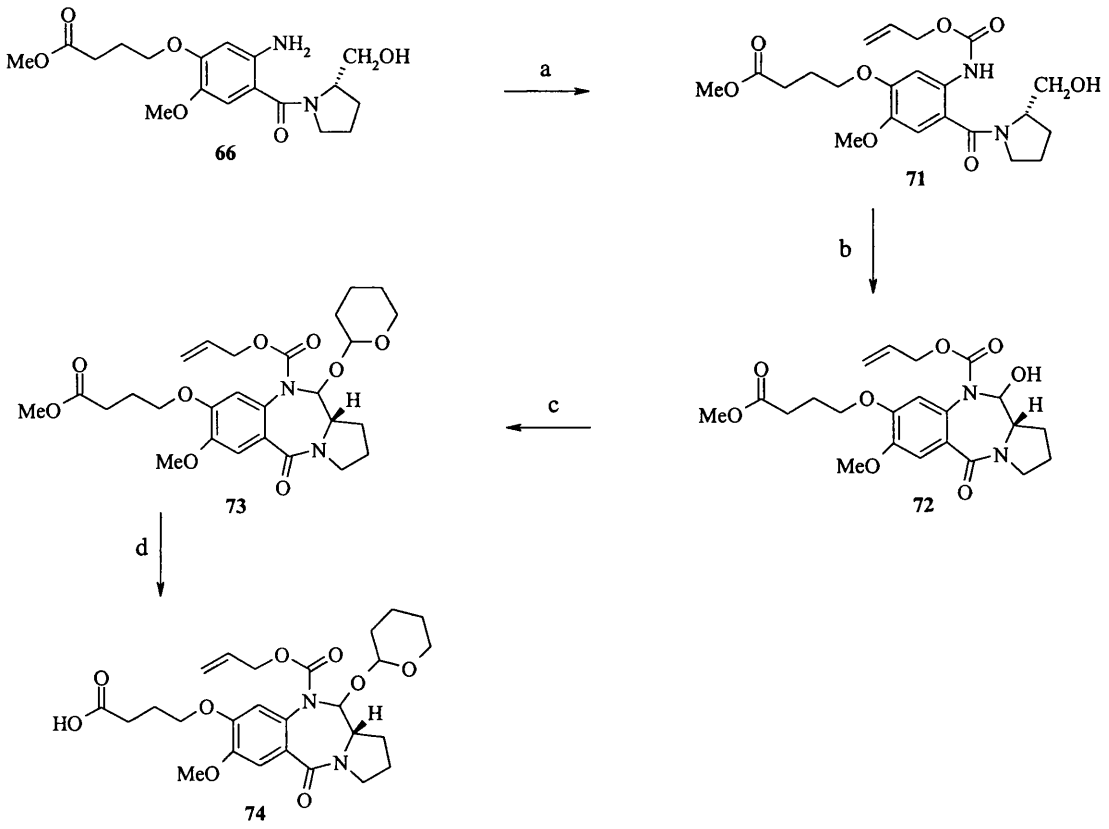

Scheme 4. a) Alloc-Cl, CH_2Cl_2, 95%; b) DAIB, TEMPO, DCM, 62%; c DHP, PTSA, EtOAc, 100%; d) NaOH, MeOH, H_2O, 96%.

The methyl-ester amine intermediate was treated with allyl chloroformate to yield the Alloc protected product **71** in 95% yield. Encouragingly, ^{1}H NMR and ^{13}C NMR spectroscopy revealed the presence of characteristic signals associated with the Alloc protecting group. The ring closed molecule **72** was obtained on addition of DAIB and a catalytic amount of TEMPO to furnish a brown foam in 62% yield. The final steps involved incorporation of the THP protecting group and ester hydrolysis to form the desired acid (**74**) in 100% and 96% yields respectively. The ^{1}H NMR and ^{13}C NMR spectra obtained for the final PBD capping unit were identical to those of the literature compound, thus confirming successful synthesis.

5.2 Synthesis of the dilactam building block

The dilactam building block was synthesised to allow direct comparison of non-covalently interacting heterocyclic conjugates with the alkylating PBD-polyamide library.

The first three steps (introducing the carboxyl sidechain) of the dilactam synthesis were identical to the PBD acid synthesis discussed earlier. The B-ring cyclisation step is based on the synthesis reported by Jones (Jones *et al.*, 1990). Therefore, the intermediate **64** was the starting material for the dilactam synthesis.

The acid **64** was activated using oxalyl chloride and treated with the commercially available proline methyl ester to form the A and C ring skeleton **75** as a yellow oil in 96% yield. Mass spectral analysis revealed the presence of a molecular ion (M+1) at 425, which corresponds to expected molecular weight of **75**.

The next step was the reduction of the nitro group via palladium on charcoal-catalysed hydrogenation. In contrast to the previous N10 protected carbinolamine synthesis, TLC revealed complete consumption of starting material. It was anticipated that the reduction of the nitro group would bring about a spontaneous ring closure. However, the appearance of a polar fluorescent spot by TLC suggested the presence of an amine group. Therefore, the reaction product was treated with a catalytic amount of conc. HCl to yield the desired ring closed product **76** as a red/brown oil in 42% yield. ^{1}H NMR studies confirmed the successful synthesis of the ring closed product on the disappearance of the C-ring methyl ester signal.

The final step involved a saponification reaction to convert the methyl ester to the required acid group. The methyl ester **76** was treated with sodium hydroxide solution to afford the acid **77** as a white foam in 58% yield. ^{1}H NMR confirmed the successful synthesis of the dilactam building block **77**, however, once again the optical rotation was also found to be zero, indicating racemisation at the C11a position.

An acid hydrolysis was utilised as the final step, replacing the strongly basic saponification thought to cause racemisation at the C11a position. The ring closed methyl ester **76** was treated with HCl, however no conversion to the acid **78** was observed.

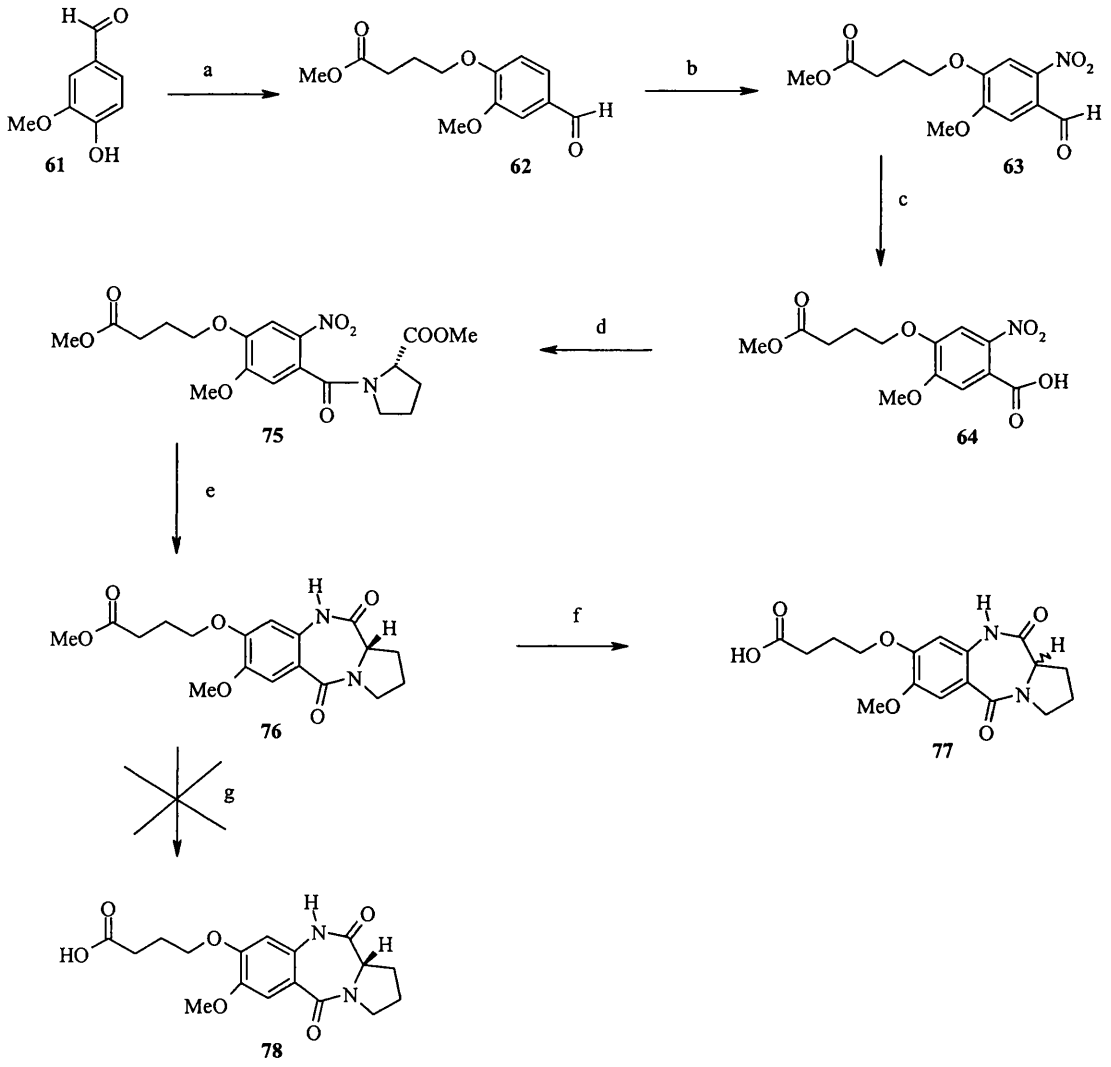

Scheme 5. a) DMF, K_2CO_3, methyl-4-bromobutyrate, 94%; b) HNO_3, Ac_2O, 0 °C, 84%; c) $KMnO_4$, H_2O, $MeCO_2$, 74%; d) DCM, $(COCl)_2$, proline methyl ester, TEA, 96%; e) H_2, Pd/C, EtOH, 42%; f) NaOH, H_2O, MeOH, 58%; g) HCl, H_2O, THF.

5.2.1 Overcoming racemisation of the dilactam

As with the PBD acid building block, it was hypothesised that racemisation at the C11a position of the dilactam occurred during the saponification step. The proposed mechanism is shown in **Figure 25**.

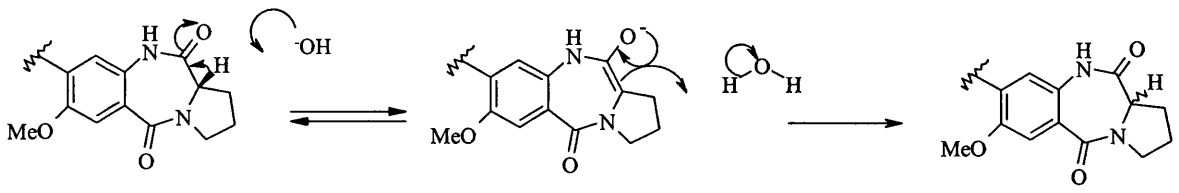

Figure 25. Proposed mechanism for the racemisation of the dilactam building block

It is important to synthesise the dilactam with only the (*S*)-configuration for reasons that have been previously discussed. Unfortunately the addition of a protecting group at the C11 position is not applicable to a dilactam PBD synthesis.

A new synthetic route (**Scheme 6**) was designed to avoid racemisation at the C11a position based on the approach reported by Jones *et al.* Another member of the research group successfully synthesised the enantiomerically pure dilactam building block using this new strategy. The unsuccessful strategy described in **Scheme 5** differs greatly from the synthesis shown below. Briefly, a benzyl protected A-ring **79** was coupled to proline methyl ester to form the A-C product **80**. Subsequent reduction using hydrogen (30 psi) and palladium on charcoal, provided the ring closed dilactam **81**. The 4-bromobutyric acid benzyl ester was then coupled to the dilactam core under mildly basic conditions. Finally, reduction yielded the enantiomerically pure dilactam building block (**83**).

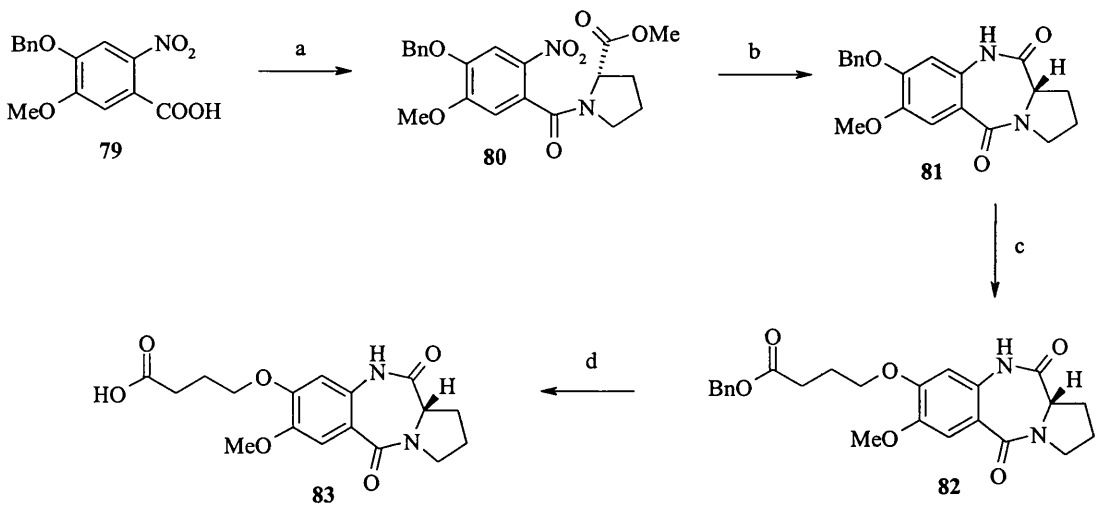

Scheme 6. a) i) $(COCl)_2$, DMF, DCM; ii) L-proline methyl ester hydrochloride, Et_3N, DCM, -30°C, 70%; b) Pd/C, H_2, EtOH; c) K_2CO_3, 4-bromobutyric acid benzyl ester, DMF, 71%; d) Pd/C, H_2, EtOAc, 99%.

Unfortunately time constraints did not allow the synthesis of the dilactam via the revised approach, however, a series of dilactam-heterocycle conjugates were prepared by Mr Chi-kit Woo (Spirogen). Biological testing on this set of molecules was conducted allowing the influence of covalent (PBD) and non-covalent binding (dilactam) to be assessed.

5.3 Synthesis of heterocyclic building blocks

The heterocyclic amino esters and the Boc-protected heterocyclic acids (**Figure 26**) were prepared as previously reported (Swalley *et al.*, 1996; Boger *et al.*, 2000).

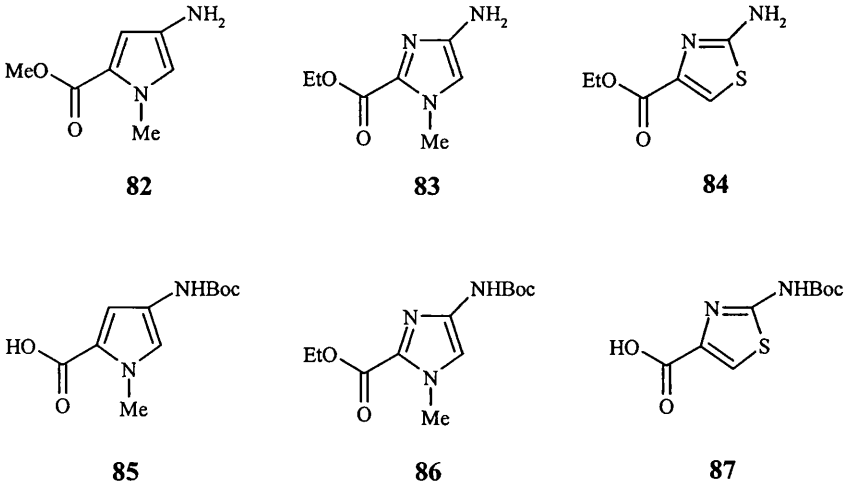

Figure 26. Heterocyclic building blocks, Pyrrole (**84** and **87**) Imidazole (**85** and **88**) and Thiazole (**86** and **89**).

5.4 Amide coupling reactions

Two solution phase strategies were investigated in order to couple the heterocyclic building blocks together via an amide linkage. Distamycin A has previously been synthesised by coupling *N*-methyl-4-nitropyrrole-2-carboxylic acid chlorides to a 4-amino-pyrrole, followed by reduction of the nitro group prior to subsequent coupling reactions (Lown and Krowicki, 1985).

As a proof of principle study, two of the target molecules, Py-Py-Py and Im-Py-Py were selected to be synthesised via this nitro reduction approach. **Scheme 7** presents the proposed synthetic strategy for the preparation of these two target molecules, however, to avoid repetition only the pyrrole trimer route is shown. The initial building blocks were coupled in DMF to form the imidazole-pyrrole and the pyrrole dimer molecules in 53% and 68% yields respectively. Reduction of the nitro-ester compound using a Parr hydrogenator (40 Psi) and palladium on charcoal catalyst formed the amine compounds. The pyrrole acid building block was subsequently coupled to the amine to yield both the Im-Py-Py and pyrrole trimer molecule. Unfortunately, no trimer product was retrieved from the initial attempts, although repetition of the final coupling step using the pyrrole dimer resulted in the formation of the pyrrole trimer in modest yield (39%).

The low yields obtained and reaction failures were possibly due to long hydrogenation reaction times (60 h) which allowed the degradation of the amine. Replacement of ethyl acetate with DMF resulted in shorter reaction times but decreased amine purity. In

addition, it was decided that this approach was not applicable for the thiazole containing compounds as trace amounts of sulphur are known to poison the palladium catalyst.

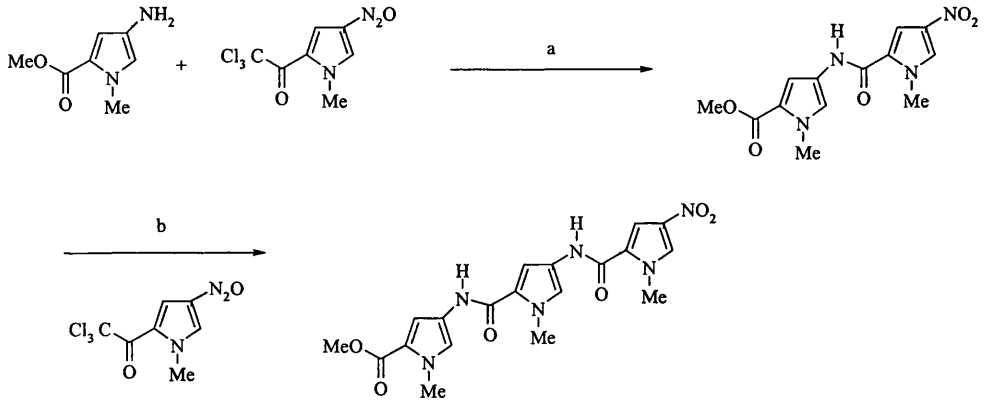

Scheme 7. a) DMF, 53%; b)i) H_2, Pd/C, EtOH. ii) DMF

An alternative coupling method was successfully employed (Boger *et al.*, 2000). This strategy involved the use of 1(-3-dimethylaminopropyl)-3-ethylcarbodiimide hydrochloride (EDCI) and 4-dimethylaminopyridine (DMAP) as coupling reagents (**Scheme 8**) followed by a work-up involving simple liquid/liquid extraction to furnish the product.

Coupling of the amino ester building block to the Boc-protected acid gave the *N*-Boc heterocyclic dimer. Boc deprotection, using 4M HCl in dioxane, furnished the amine which was subsequently coupled to Boc-protected acid to yield the Boc-protected trimer (**Table 2).**

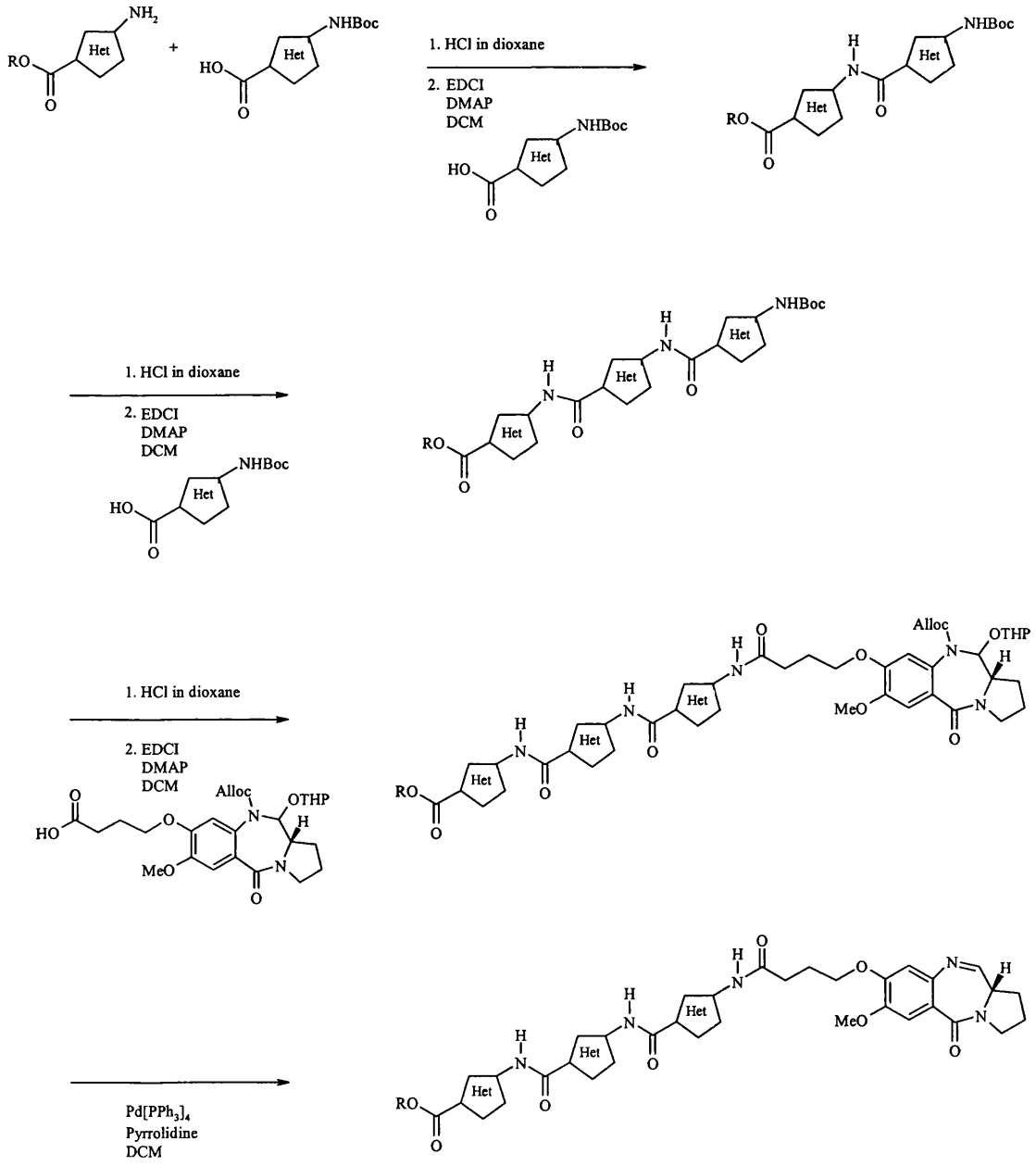

Scheme 8. General EDCI/DMAP coupling approach where Het = Pyrrole, Thiazole, Imidazole.

Reaction	Product Structure	Time (h)	Yield (%)	Comments
Py + Py	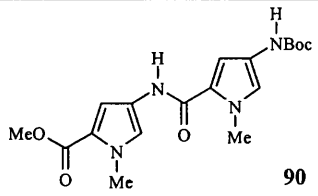 **90**	18	99	
Py + Im	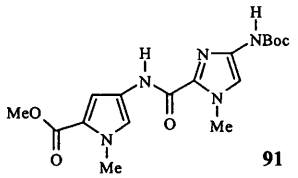 **91**	48	76	Purified by column chromatography (Chloroform: 100)
Py + Th	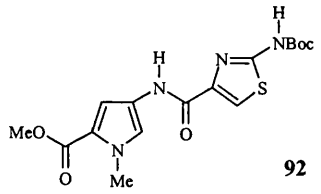 **92**	120	77	
Im + Py	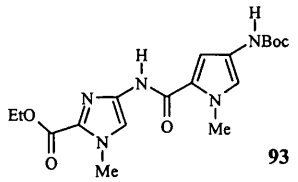 **93**	60	95	Purified using column chromatography (EtOAc: Hexane, 70:30)
Im + Im	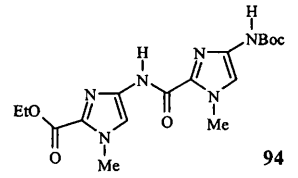 **94**	168	43	Purified using column chromatography (EtOAc: Hexane, 70:30)
Th + Py	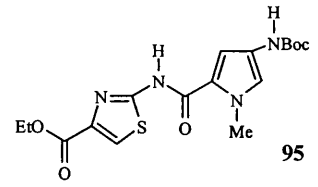 **95**	168	70	
Th + Th	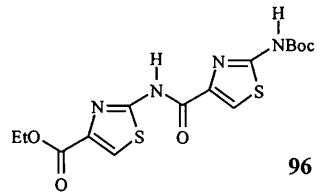 **96**	192	71	

Reaction	Product Structure	Time (h)	Yield (%)	Comments
Py-Py + Py	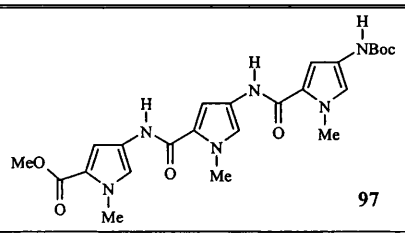 **97**	24	65	
Py-Py + Im	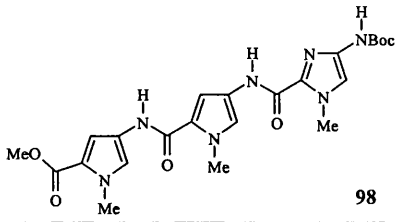 **98**	120	99	Purified using column chromatography (DCM: MeOH, 97:3)
Py-Im + Im	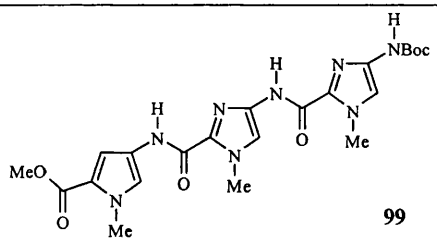 **99**	168	57	Purified using column chromatography (DCM: MeOH, 98:2)
Im-Py + Py	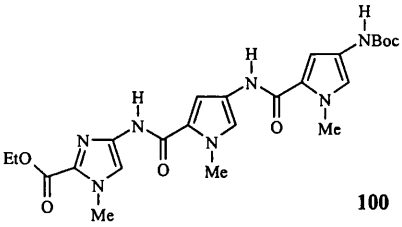 **100**	18	91	
Im-Py + Im	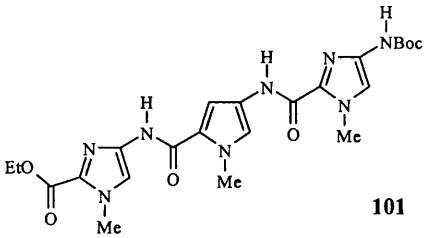 **101**	18	84	Purified using column chromatography (DCM: MeOH, 97:3)
Im-Im + Im	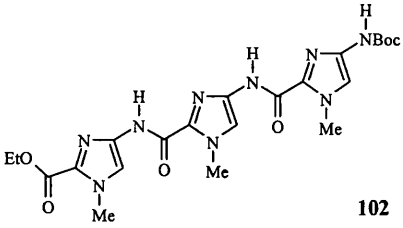 **102**	192	48	Purified using column chromatography (DCM: MeOH, 98:2)

Reaction	Product Structure	Time (h)	Yield (%)	Comments
Py-Im + Py	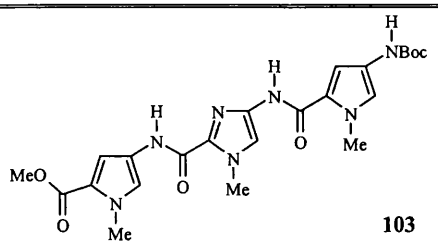 **103**	168	73	Purified using column chromatography (DCM: MeOH, 97:3)
Py-Th + Th	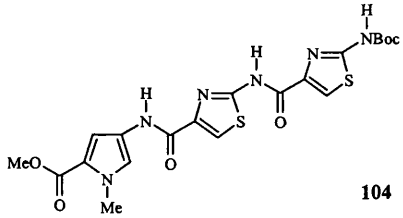 **104**	264	48	Purified using chromatography (DCM:MeOH, 98:2).
Th-Py + Py	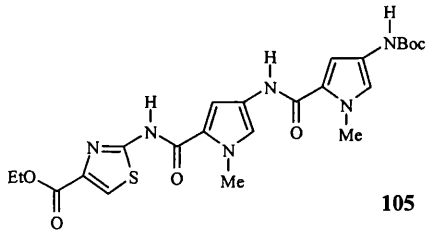 **105**	48	80	Purified using column chromatography (DCM: MeOH, 98:2)
Th-Py + Th	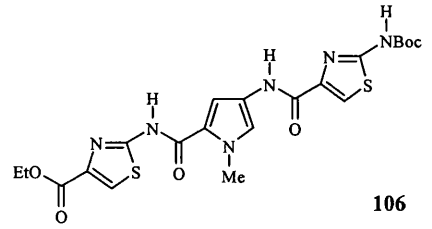 **106**	18	86	Purified using column chromatography (DCM: MeOH, 97:3)
Th-Th + Th	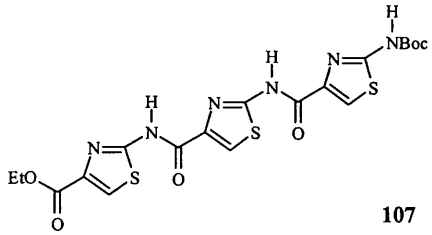 **107**	264	52	Purified using column chromatography (DCM: MeOH, 97:3)
Py-Th + Py	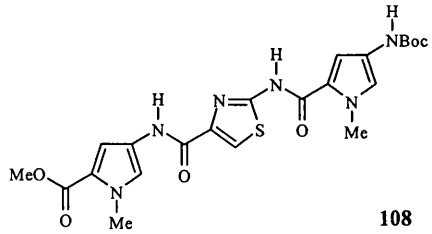 **108**	240	56	Purified using chromatography (DCM:MeOH, 98:2)

Reaction	Product Structure	Time (h)	Yield (%)	Comments
Py-Py + Th	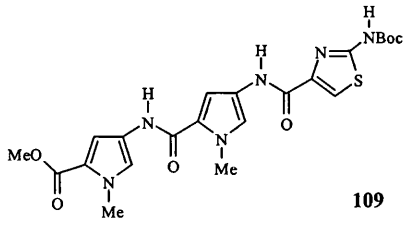 **109**	120	76	Purified using column chromatography (DCM: MeOH, 98:2)
Im-Im + Py	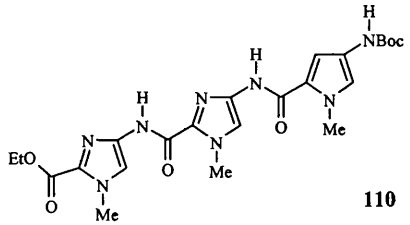 **110**	192	32	Purified using column chromatography (DCM: MeOH, 97:3)
Th-Th + Py	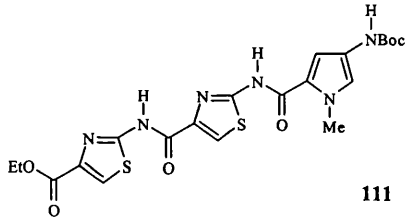 **111**	264	57	Purified using column chromatography (DCM: MeOH, 97:3)

Table 2. Heterocyclic subunit reaction times, product yields and associated comments.

5.4.1 Heterocyclic coupling reactions

All the PBD-heterocycle conjugates were prepared via EDCI/DMAP mediated coupling reactions (**Scheme 8**), however, some modifications were made depending on the type of heterocycle used.

In general, the coupling reactions proved more complicated than was originally anticipated. Overall, it was difficult to monitor the progress of the coupling reactions as TLC proved inconclusive. This was partially overcome by carrying out a small scale work up to eliminate a proportion of the starting materials and coupling reagents, allowing a clearer evaluation of the reaction's progress. However, on many occasions

NMR analysis revealed the product to be a mixture of starting material and desired compound due to the reaction having not gone to completion. The acquisition of analytical LCMS equipment allowed real time monitoring of the coupling reactions leading to higher yields and greater product purity.

The initial coupling reactions were carried out using 1.2 and 1.5 equivalents of DMAP and EDCI respectively. However, Boger reported higher yields by doubling the amount of coupling reagents used for small scale coupling reactions. This modification was applied to subsequent coupling reactions with success, for example, the product yield for the trimer Th-Py-Py increased from 62% to 80%.

The EDCI/DMAP coupling approach had been successfully applied when synthesising only pyrrole containing heterocycle-PBD conjugates (Wells *et. al.*, 2006). However, several problems were encountered when imidazole and thiazole building blocks were incorporated, which are summarised below.

5.4.2 Imidazole coupling reactions

The conventional work-up for EDCI/DMAP coupling reactions involves acid and basic washes in order to remove excess coupling reagents and unreacted starting material. Initial coupling reactions, incorporating an imidazole heterocycle, resulted in very poor yields. It was determined that the imidazole containing product was protonated during the acid wash steps and was subsequently extracted into the aqueous layer. In order to overcome this problem the acid was replaced with deionised water resulting in good

product yields. However, the crude product frequently required purifying by column chromatography in order to remove impurities.

5.4.3 Thiazole coupling reactions

Reaction times

Observed reactions times were approximately doubled when coupling a heterocycle to a thiazole amine compared with a pyrrole amine. The first attempt to couple a pyrrole acid to a thiazole amine building block resulted in a 24% yield with a reaction time of 60 h. This reaction was repeated, higher equivalents of the coupling reagents were used and the reaction time was increased to 168 h, which resulted in a significantly higher product yield (70%). However, increased reaction times delayed synthetic progress and also increased the possibility of degradation of the starting materials and product when using a thiazole compared with the pyrrole or imidazole heterocycles. As a result, lower product yields were tolerated when coupling thiazole containing molecules.

Work up

The work-up employed by Wells and co-workers (Wells *et. al.*, 2006) to synthesise pyrrole containing polyamides involved the use of a strong acid (1N HCl) wash. In light of the problems experienced with the imidazole containing molecules a modification to the work up was made, whereby HCl was replaced with a weaker acid (citric acid) for the washing steps. However, the addition of citric acid occasionally resulted in the formation of emulsions, making it difficult to extract the product In particular, this occurred twice when coupling the Boc-protected pyrrole building block to a thiazole-pyrrole dimer. In the first instance addition of brine was sufficient to separate the organic and aqueous

layers. However, on the second occasion, this proved unsuccessful and the solution had to be filtered through celite in order to progress with the extraction.

Solubility

It was observed that Boc-deprotection of the thiazole prior to coupling reactions was frequently unsuccessful. Due to monitoring problems (see Section 5.4.1) this was only detected after the coupling step when characterisation of the product revealed incomplete deprotection. It was known that the thiazole containing compounds were less soluble compared with the imidazole/pyrrole containing molecules leading to the possibility that the thiazole compounds were not completely in solution when using HCl in dioxane. It was observed that a precipitate was present following addition of HCl in dioxane but rapid formation of the salt could also account for this. As a result, the Boc-protected starting material was dissolved in THF prior to addition of HCl in dioxane to ensure all the starting material was in solution. This approach was applied to all subsequent heterocycle Boc-deprotection reactions resulting in increased product purity, with less Boc-protected starting material being present.

Although use of THF generally resulted in complete Boc-deprotection there were some instances where the starting material was insoluble in THF and a completely different Boc-deprotection procedure had to be employed. In particular, a solution of DCM:TFA:water (50:47.5:2.5) was successfully utilised to deprotect the heterocyclic dimers to achieve the synthesis of the following molecules: Py-Th-Th, Th-Th-Th, Py-Th-Py, and Th-Th-Py. For these molecules the subsequent coupling reaction was carried out in DMF in order to avoid further insolubility problems.

5.5 Coupling PBD building block to heterocycle subunit

The protected PBD-heterocycle conjugates (**Table 3**) were prepared by Boc deprotection of the intermediate dimers/trimers followed by EDCI/DMAP mediated coupling of the resulting amino ester heterocyclic subunit and the PBD capping unit in yields ranging between 34 and 95 %.

Reaction	Product Structure	Yield (%)
Py-Py-PBD	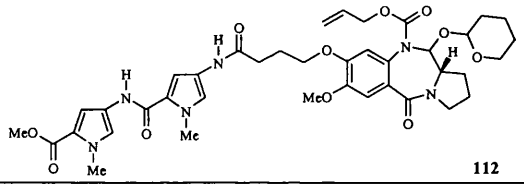 **112**	93
Py-Im-PBD	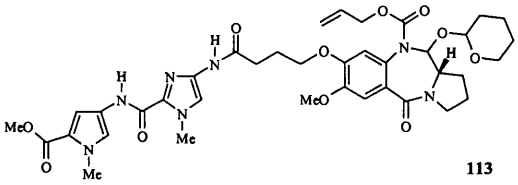 **113**	72
Py-Th-PBD	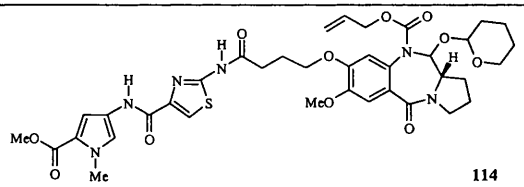 **114**	66
Im-Py-PBD	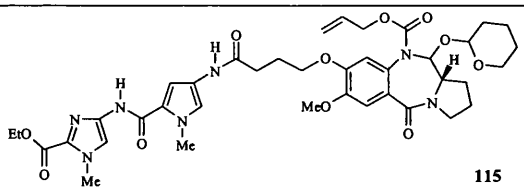 **115**	84
Im-Im-PBD	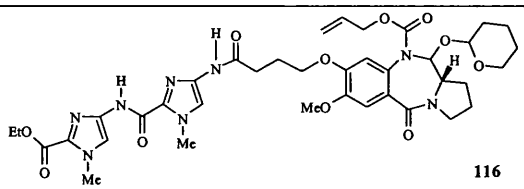 **116**	34

Reaction	Product Structure	Yield (%)
Th-Py-PBD	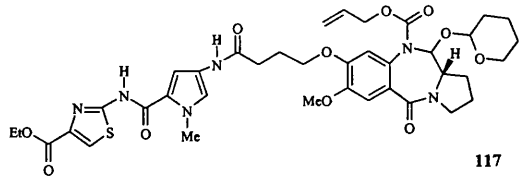 117	90
Th-Th-PBD	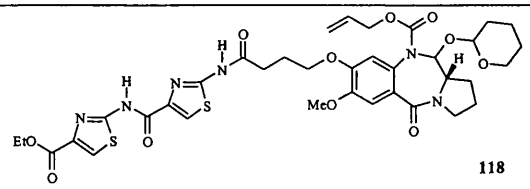 118	34
Py-Py-Py-PBD	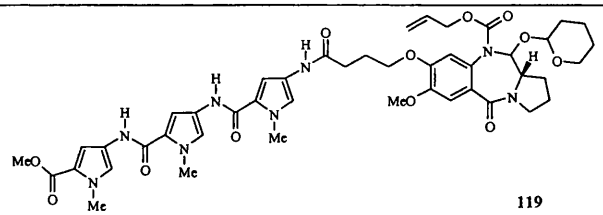 119	65
Py-Py-Im-PBD	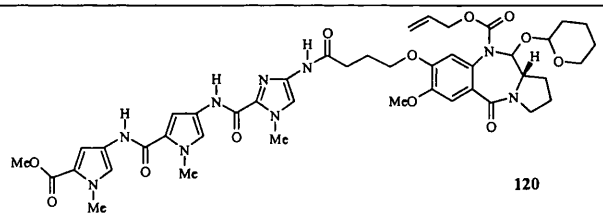 120	86
Py-Im-Im-PBD	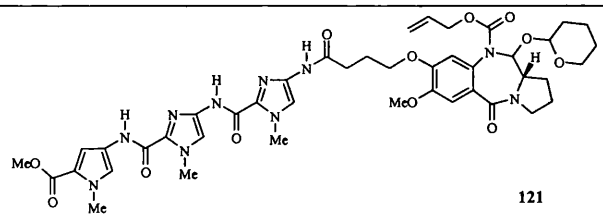 121	94
Im-Py-Py-PBD	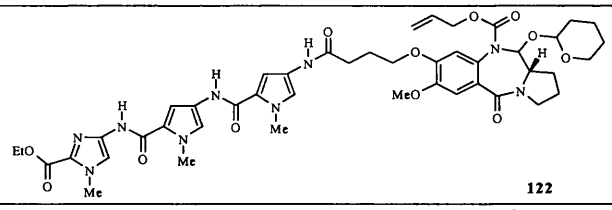 122	95
Im-Py-Im-PBD	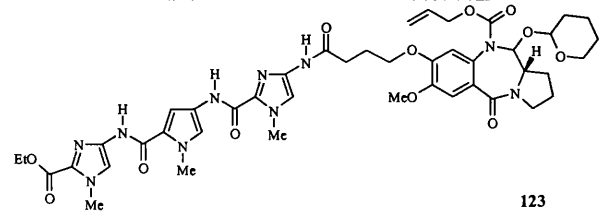 123	72

Reaction	Product Structure	Yield (%)
Im-Im-Im-PBD	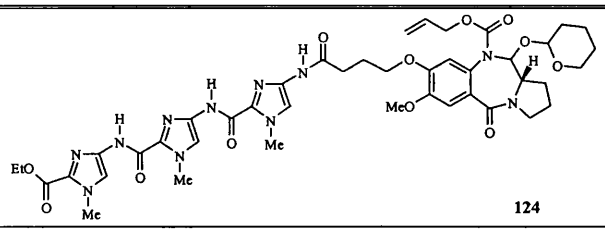 124	78
Py-Im-Py-PBD	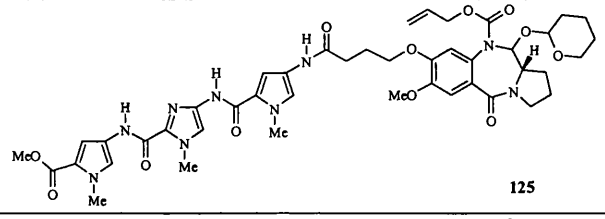 125	95
Py-Th-Th-PBD	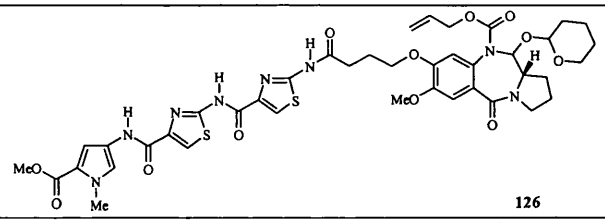 126	48
Th-Py-Py-PBD	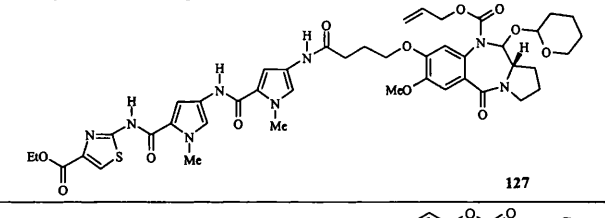 127	77
Th-Py-Th-PBD	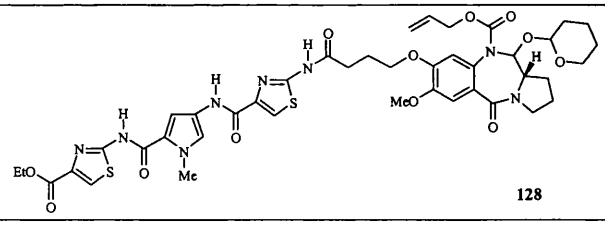 128	84
Th-Th-Th-PBD	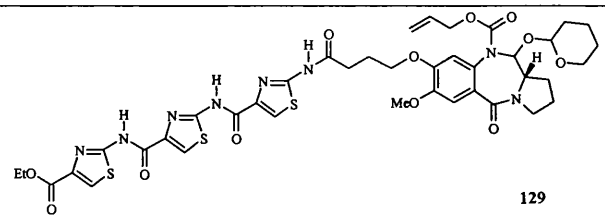 129	73
Py-Th-Py-PBD	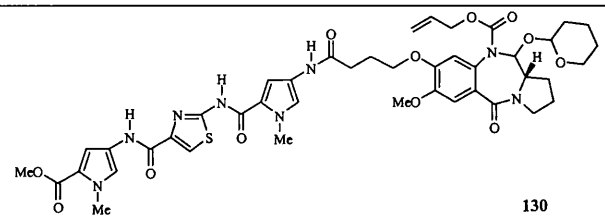 130	75

Reaction	Product Structure	Yield (%)
Py-Py-Th-PBD	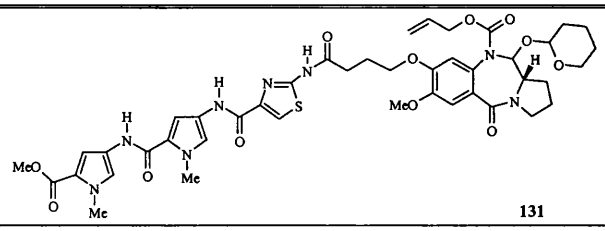 131	68
Im-Im-Py-PBD	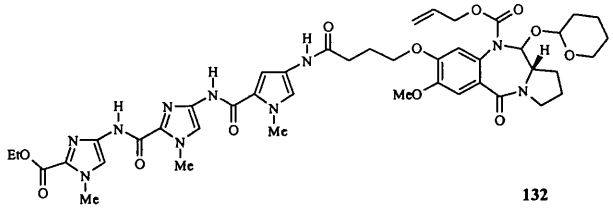 132	86
Th-Th-Py-PBD	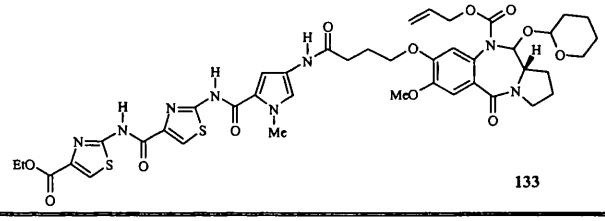 133	91

Table 3. Protected PBD-heterocycle conjugate yields.

In general, decreased product yields were observed when coupling the PBD to a thiazole amine, for reasons stated earlier. The PBD capping unit is a sensitive moiety and excessive reaction times could have lead to degradation. Interestingly, the highest yields were achieved when coupling the PBD to a pyrrole amine, in the shortest reaction times.

Characterisation

The intermediate products of each synthetic step were characterised using NMR and, where available, LCMS analysis. The success of product formation was confirmed by the presence of amide NMR peaks and a single LCMS peak corresponding to the correct molecular weight.

5.6 Deprotection to form final compounds

5.6.1 Boc and THP deprotection

The Boc-THP-PBD acid was coupled (EDCI/DMAP) to one heterocyclic subunit (Py-Th-Py-PBD) and a proof of principle deprotection was carried out under acidic conditions. It was hoped that both the THP and Boc protecting groups would be removed simultaneously to form the imine target molecule. However, LCMS analysis revealed two product peaks in a 3:1 ratio, with molecular weights corresponding to a THP protected target molecule and the imine final compound, respectively. Interestingly, NMR analysis revealed the presence of the imine moiety suggesting that the THP group had migrated from the original C11 position. It is possible that under acidic conditions the THP group acted as an electrophile, attacking the pyrrole ring.

Given that the majority of the target molecules contain pyrrole units it was decided that an alternative PBD protecting group should be employed in order to avoid THP group migration. The Alloc protecting group has frequently been used to protect the N10 position of PBDs and acidic conditions are not required for removal. Therefore, as previously described, an Alloc-THP-PBD capping unit was synthesised and coupled to the heterocyclic subunits.

5.6.2 Alloc and THP deprotection

All the PBD-hetrocycle conjugates underwent N10-Alloc-deprotection using palladium *tetrakis*[triphenylphosphine] and pyrrolidine which also resulted in concerted removal of the C11-O-THP protecting group. Analytical LCMS of the reaction mixture confirmed complete deprotection to yield the imine. No work up was required as preparatory LCMS was immediately utilised to give the pure imines in 6-40% yield (**Table 4**).

Reaction	Product Structure	Yield (%)	Comments
Py-Py-PBD	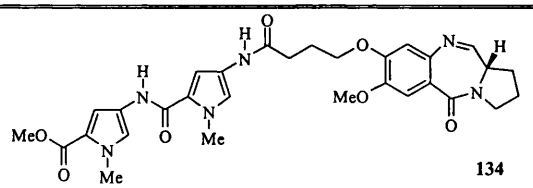 **134**	35	
Py-Im-PBD	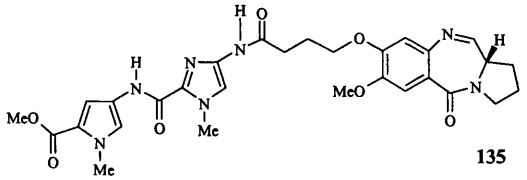 **135**	25	
Py-Th-PBD	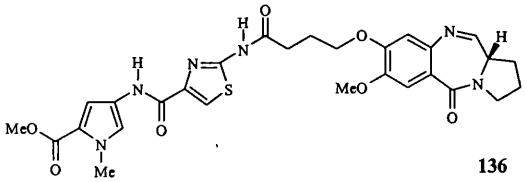 **136**	8	
Im-Py-PBD	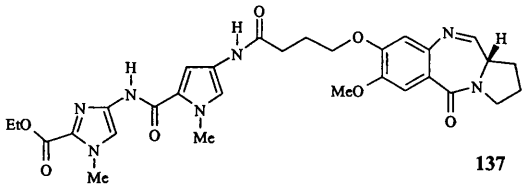 **137**	26	
Im-Im-PBD	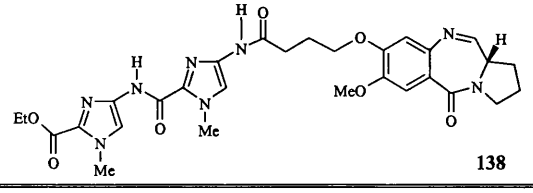 **138**	90	Purified by column chromatography DCM:MeOH, 96:4

Reaction	Product Structure	Yield (%)	Comments
Th-Py-PBD	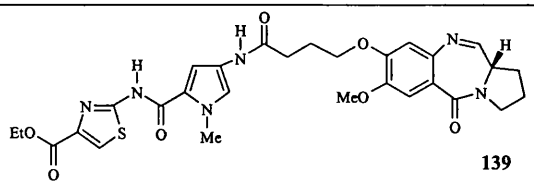 139	15	
Th-Th-PBD	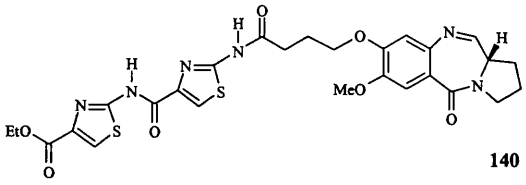 140	40	
Py-Py-Py-PBD	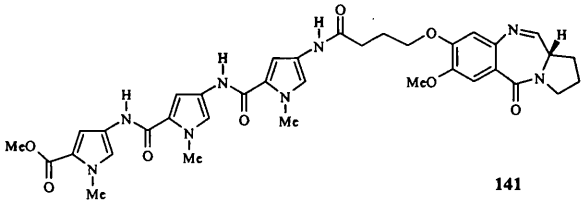 141	26	
Py-Py-Im-PBD	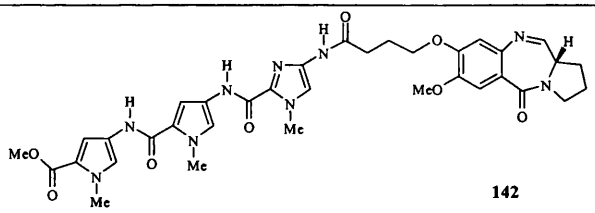 142	29	
Py-Im-Im-PBD	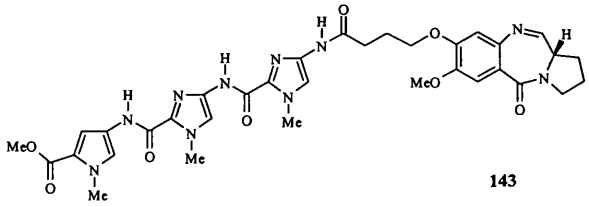 143	28	
Im-Py-Py-PBD	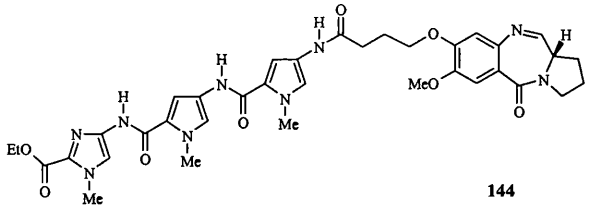 144	17	

Reaction	Product Structure	Yield (%)	Comments
Im-Py-Im-PBD	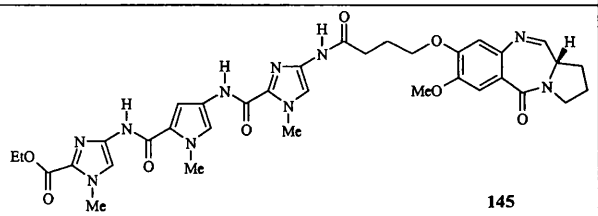 145	27	
Im-Im-Im-PBD	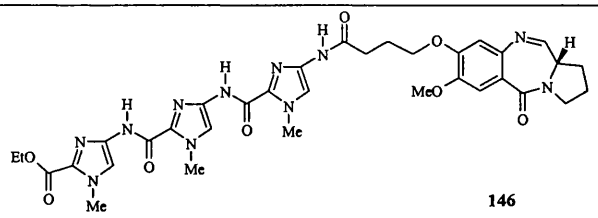 146	22	
Py-Im-Py-PBD	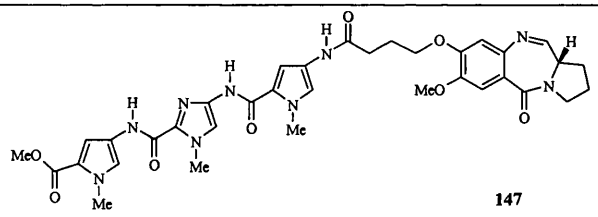 147	16	
Py-Th-Th-PBD	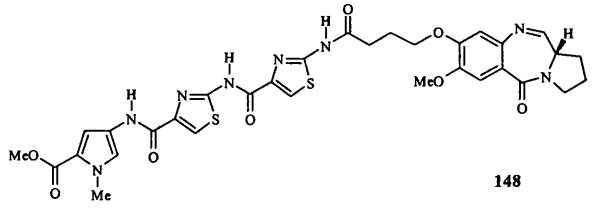 148	0	Unsuccessful Alloc/THP deprotection. No final product retrieved
Th-Py-Py-PBD	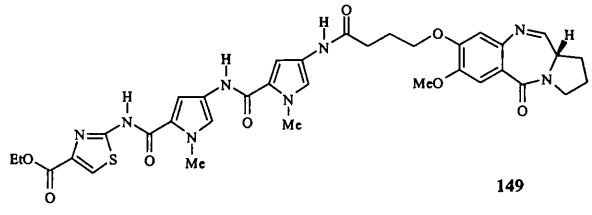 149	6	
Th-Py-Th-PBD	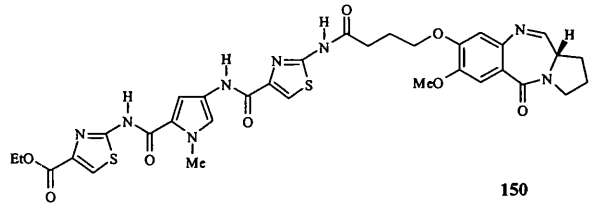 150	8	

Reaction	Product Structure	Yield (%)	Comments
Th-Th-Th-PBD	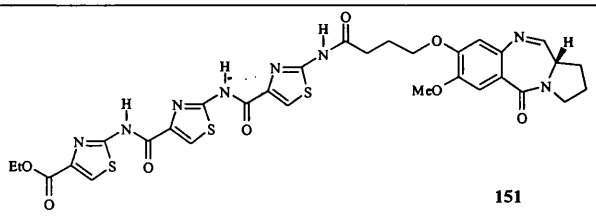 151	12	
Py-Th-Py-PBD	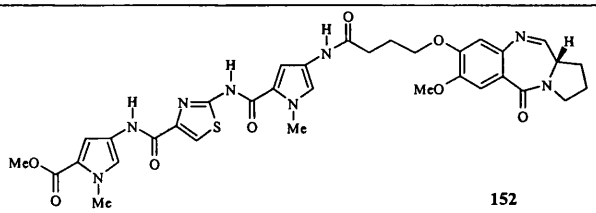 152	35	
Py-Py-Th-PBD	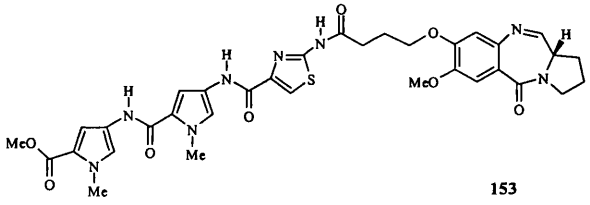 153	37	
Im-Im-Py-PBD	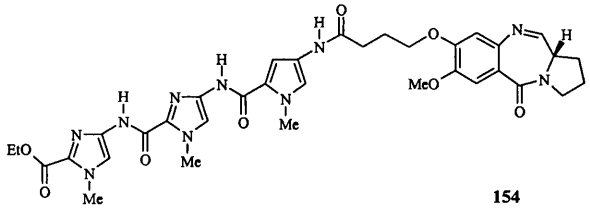 154	14	
Th-Th-Py-PBD	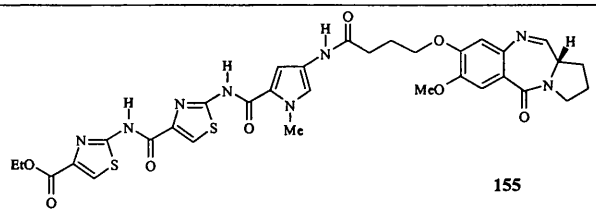 155	8	

Table 4. Final step PBD-heterocycle conjugate product yields and associated comments.

Significant losses were experienced in the preparatory mass directed HPLC process, resulting in very low yields. This was a result of only the pure fractions being freeze-dried to ensure high purity of the final molecules. Only a small amount of the protected PBD-imidazole dimer was available for deprotection so the final product was purified using column chromatography in order to enable an increased product recovery. The Im-Im-PBD imine was recovered in a 90% yield, which is significantly higher than the yields reported above. On reflection, it may have been more productive to have purified all the compounds by column chromatography, however this is laborious and time consuming when compared with the high throughput HPLC purification. At this stage of the project it was important to complete the deprotection steps promptly in order to explore the biological activity of the PBD-heterocycle conjugates and if this data proved interesting then the synthetic approach could be modified to improve efficiency.

No product was recovered by preparatory HPLC of the Py-Th-Th-PBD compound. The protected molecule was treated with palladium *tetrakis*[triphenylphosphine]/ pyrrolidine and the reaction time was increased from 1 h to 3 h, after which, LCMS analysis revealed a very small product peak. Attempts to isolate the final product using mass directed preparatory HPLC were unsuccessful. Resynthesis of this conjugate was attempted in order to complete the library, however the solubility and deprotection difficulties associated with thiazole containing molecules, described in Section 5.4.3, and time constraints prevented this and no final product was obtained.

Characterisation

The final products were characterised using NMR, high resolution mass spectrometry and LCMS analysis using four different systems. The success of product formation was confirmed by the presence of imine NMR peaks and the absence of signals associated with Alloc or THP protecting groups. Single LCMS peaks (indicating high purity) corresponding to the correct molecular weight were obtained for each target compound using a combination of solvent systems and columns. Final confirmation was achieved using high resolution mass spectrometry where the correct molecular weight was determined for all the final compounds.

6 BIOLOGICAL RESULTS AND DISCUSSION

The library of PBD-heterocycle conjugates were submitted for cytotoxicity analysis in both the K562 human leukaemia cell line and the 60 cell-line NCI panel. In addition, further *in vitro* assays to assess DNA binding affinity, sequence selectivity and potential to disrupt NF-Y transcription factor binding were also conducted. Experimental details for the biological assays undertaken are described in the experimental section 8.

6.1 K562 Cytotoxicity Results

Studies using human chronic myeloid leukaemia (K562) cells were conducted by Ms Marissa Stephenson (Spirogen) in order to assess the cytotoxic potential of the PBD-heterocycle conjugates (**Table 4**). The test molecules were incubated with K562 cells for 96 h. Although the primary purpose of the study was to investigate the ability of the PBD-heterocycle conjugate to inhibit transcription factor binding it should not be forgotten that the PBD moiety is intrinsically cytotoxic. It was therefore of interest to determine whether the presence of the heterocyclic unit modulated the cytotoxicity of the PBD. As well as being interesting data in its own right this information would be extremely useful when designing future *in vitro* and *in vivo* experiments.

Compound	Identity	IC_{50} (nM)
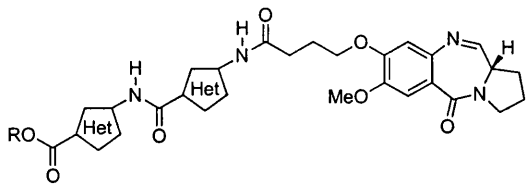 PBD dimer conjugates		
RMH031	Py-Py-PBD	2.3
RMH037	Im-Py-PBD	50.0
RMH067	Im-Im-PBD	85.2
RMH071	Th-Th-PBD	263.3
RMH033	Py-Im-PBD	710.3
RMH035	Th-Py-PBD	> 1 mM
RMH073	Py-Th-PBD	Undetermined
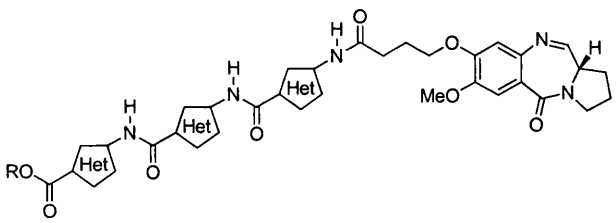 PBD trimer conjugates		
RMH047	Py-Th-Py-PBD	1.9
RMH063	Th-Py-Py-PBD	7.1
RMH065	Th-Th-Py-PBD	10.5
RMH061	Th-Py-Th-PBD	10.6
RMH043	Py-Py-Th-PBD	17.0
RMH049	Py-Im-Im-PBD	26.7
RMH055	Im-Py-Im-PBD	34.0
RMH045	Py-Im-Py-PBD	46.0
RMH057	Im-Py-Py-PBD	47.5

Compound	Identity	IC_{50} (nM)
RMH053	Im-Im-Py-PBD	57.8
RMH051	Im-Im-Im-PBD	234.8
RMH059	Th-Th-Th-PBD	683.7
RMH041	Py-Py-Im-PBD	Undetermined
RMH039	Py-Py-Py-PBD	Undetermined

Table 5. IC_{50} values obtained in the K562 cell-line for the PBD-heterocycle conjugates.

The tabulated data shows that all the PBD-heterocyclic molecules tested are very potent cytotoxic agents with the exception of RMH035, which was subsequently found to have degraded. In addition, an IC_{50} value could not be obtained for RMH041, RMH039 and RMH073 although this phenomenon has previously been observed in this particular assay when testing molecules that were found to be highly potent cytotoxic agents in the NCI 60 cell line panel.

On comparison of the IC_{50} values for the presented PBD-heterocycle conjugates with both the previously tested PBD and heterocyclic subunits on their own, an important observation can be made. The IC_{50} for the PBD capping unit is 0.526 μM which is considerably less cytotoxic than that of most of the PBD-heterocyclic conjugates, indicating that the incorporation of the polyamide subunit greatly increases the potency of the molecule. This is a particularly interesting observation given the SAR of PBDs. Firstly, it is the N10-C11 imine moiety of the PBD that is responsible for the covalent linkage with DNA. As previously discussed the heterocyclic subunit binds to DNA via

non-covalent interactions. Secondly, the PBD capping unit lacks the C-ring substituents usually responsible for potentiating cytotoxic activity.

As the PBD subunit remains constant throughout the sets of conjugates, the enhanced potency observed can only be attributed to the addition of the heterocyclic portion of the molecule. However, the tri-pyrrole polyamide subunit by itself is not particularly cytotoxic with an IC_{50} value of >10 μM, which suggests that the increase in cytotoxicity observed is a result of the PBD being coupled to the polyamide subunit. This would be consistent with the polyamide unit contributing additional hydrogen bonding, Van der Waals and hydrophobic interactions, thus improving the DNA binding ability of the conjugate as a whole.

However, there does not appear to be a clear correlation between cytotoxic activity and the identity of the individual heterocycles in the heterocyclic portion of the conjugate. Generally, molecules which contain only thiazole or imidazole heterocycles are substantially less active than the pyrrole containing members of the library. Unfortunately, the data for the trimer conjugates does not allow an assessment of whether the replacement of a pyrrole with a thiazole or an imidazole affects the cytotoxic activity. However, by comparing RMH031 and RMH037, two dimer PBD conjugates, it can be seen that substituting a pyrrole with an imidazole considerably affects the potency with IC_{50} values of 2.3 nM and 50.0 nM respectively.

The most potent conjugate (for which an IC_{50} value could be obtained) is RMH047, a thiazole containing molecule with an IC_{50} values of 1.9 nM. Interestingly, the next most

potent molecule of the library is a PBD dimer conjugate, RMH031, with an IC_{50} value of 2.3 nM, although on the whole the PBD trimer conjugates are more cytotoxic than the dimer molecules. This trend could be attributed to the opportunity for increased hydrogen bonding and hydrophobic interactions between the longer polyamides and DNA.

Interestingly, it can be observed that for the PBD trimer conjugates presented in **Table 5**, the molecules containing thiazoles are more cytotoxic than the imidazole equivalents, although this trend does not appear within the PBD dimer conjugates.

In addition, the slight differences in IC_{50} values for the PBD-polyamides suggest that cytotoxicity is also dependent on the type and number of heterocycles present. This could possibly be explained by differences in the shape of the conjugates with the most potent molecules possessing a more complementary fit with the DNA. It is significant that the most potent PBD-heterocycle molecules are as active as SJG-136, a known cross-linking agent. This observation might be construed as circumstantial evidence of some PBD-polyamide conjugates adopting a 2:1 binding mode with regard to the DNA duplex. The least active molecules are those which are not predicted to overlap, only binding DNA in a 1:1 fashion.

In conclusion, the addition of the heterocyclic subunit to the PBD potentiates cytotoxicity as evaluated using the K562 cell line, however the significance of the heterocyclic composition and mechanism by which this occurs remains to be determined.

6.2 NCI Cytotoxicity Results

All the PBD-heterocycle conjugates were evaluated using an *in vitro* cytotoxicity screen developed by the National Cancer Institute (NCI). The compounds were screened against a panel of 60 human tumour cell lines and a comprehensive graphical report of the data generated was obtained. More specifically, a dose response curve was created for each cell line by plotting the calculated percentage growth against the $\log_{10}$ of the corresponding concentration. The principle parameters measured are GI_{50}, TGI and LC_{50}, which represent the concentrations at which the percentage growth is 50, 0 and -50 respectively. In addition, mean graphs are compiled which allow visual representation of potential selectivity in specific cell lines or sub-panels. Horizontal bars to the right represent increased sensitivity of the cell line to the compound compared to average sensitivity of all cell lines examined. Horizontal bars to the left indicate decreased sensitivity of the cell line to the compound under investigation.

Compound	Identity	GI_{50} (nM)	TGI (nM)	LC_{50} (nM)
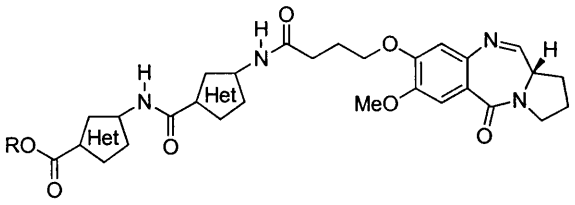 PBD dimer conjugates				
RMH073	Py-Th-PBD	3.1	96.0	9100.0
RMH031	Py-Py-PBD	11.0	120.0	10000.0
RMH035	Th-Py-PBD	14.8	363.0	19100.0
RMH067	Im-Im-PBD	35.5	933.0	13500.0
RMH071	Th-Th-PBD	70.8	813.0	12300.0
RMH037	Im-Py-PBD	100.0	1445.0	32400.0
RMH033	Py-Im-PBD	691.8	4898.0	19500.0
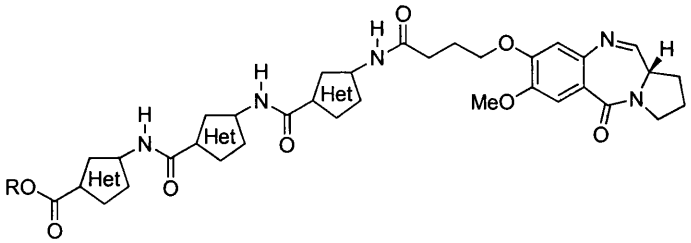 PBD trimer conjugates and control molecules				
RMH041	Py-Py-Im-PBD	1.3	24.0	2300.0
RMH043	Py-Py-Th-PBD	1.4	30.0	4400.0
RMH061	Th-Py-Th-PBD	1.7	28.0	2600.0
RMH047	Py-Th-Py-PBD	2.8	50.0	9100.0
RMH063	Th-Py-Py-PBD	2.9	28.0	8900.0
RMH045	Py-Im-Py-PBD	3.0	20.0	6600.0
RMH057	Im-Py-Py-PBD	3.8	37.0	6800.0
RMH049	Py-Im-Im-PBD	3.8	37.0	6800.0
RMH055	Im-Py-Im-PBD	4.2	141.0	12300.0

Compound	Identity	GI_{50} (nM)	TGI (nM)	LC_{50} (nM)
SJG-136	PBD dimer	7.4	87100.0	562.0
RMH053	Im-Im-Py-PBD	13.5	275.0	9500.0
RMH039	Py-Py-Py-PBD	15.0	32.0	1100.0
RMH051	Im-Im-Im-PBD	87.1	1288.0	15400.0
RMH059	Th-Th-Th-PBD	281.8	2042.0	15800.0
PBD unit	Methyl-ester imine PBD	1740.0	11800.0	46800.0
Py-Py-Py	Pyrrole trimer	16600.0	44700.0	85100.0
CKW230	Py-Py-Py-dilactam	49000.0	>50000.0	>50000.0
RMH065	Th-Th-Py-PBD	Undetermined	Undetermined	Undetermined

Table 6. NCI 60 cell-line panel mean GI_{50}, TGI, and LC_{50} values for the PBD-heterocycle conjugates, SJG-136 and control molecules.

The tabulated data broadly reflects the cytotoxicity data obtained in the K562 assay where all of the PBD-heterocyclic molecules tested are very potent cytotoxic agents. Interestingly, GI_{50} values were obtained for RMH041 and RMH073 which are 1.3 and 3.1 nM respectively. This observation identifies RMH041 (Py-Py-Im-PBD) and RMH073 (Py-Th-PBD) as the most potent trimer and dimer conjugate molecules respectively in the series.

Again, comparison of the GI_{50} values for the presented PBD-heterocycle conjugates with both the previously tested PBD and heterocyclic subunits on their own (**Table 6**), indicates that the combination of the polyamide subunit and PBD greatly increases the potency of the molecule. In addition, the majority of trimer-PBD conjugates are more potent that SJG-136, the PBD dimer molecule (GI_{50}= 7.4 nM).

As observed in the K562 assay there does not appear to be a clear correlation between cytotoxic activity and the identity of the individual heterocycles in the heterocyclic portion of the conjugate. However, for the PBD-trimer conjugates, it is clear that the molecules that contain one imidazole or thiazole are more potent than the conjugates consisting of only pyrroles or more than one imidazole/thiazole. In addition, the trimer and dimer conjugates that include a thiazole have lower GI_{50} values than the imidazole containing analogues, with the exception of RMH041 (Py-Py-Im-PBD).

Comparison of the dose response curves for all 60 cell lines allows the PBD-heterocycle conjugates to be divided into two distinct categories based on the shape of the curve. The curves for most cytotoxic molecules are flat in contrast to curves derived from the less potent conjugates which are sigmoidal in shape. Examples of this observation are presented in **Figures 27** and **28**. The occurrence of a flat dose response curve may indicate that the compound is acting as a cytostatic as opposed to a cytotoxic agent.

The mean graphs demonstrating selectivity in specific cell lines or sub-panels for each of the heterocyclic conjugates can be found in the Appendix section.

6.2.1 Comparison of K562 and NCI data.

The IC_{50} values obtained in the K562 assay were statistically compared with the NCI average GI_{50} values using Pearsons correlation co-efficient. Encouragingly, the two sets of cytotoxicity data are positively correlated, where $r = 0.89$.

National Cancer Institute Developmental Therapeutics Program Dose Response Curves	NSC : D736537 / 1	SSPL : 0CCJ	EXP. ID : 0508NS15
	Report Date : October 04, 2005	Test Date : August 15, 2005	

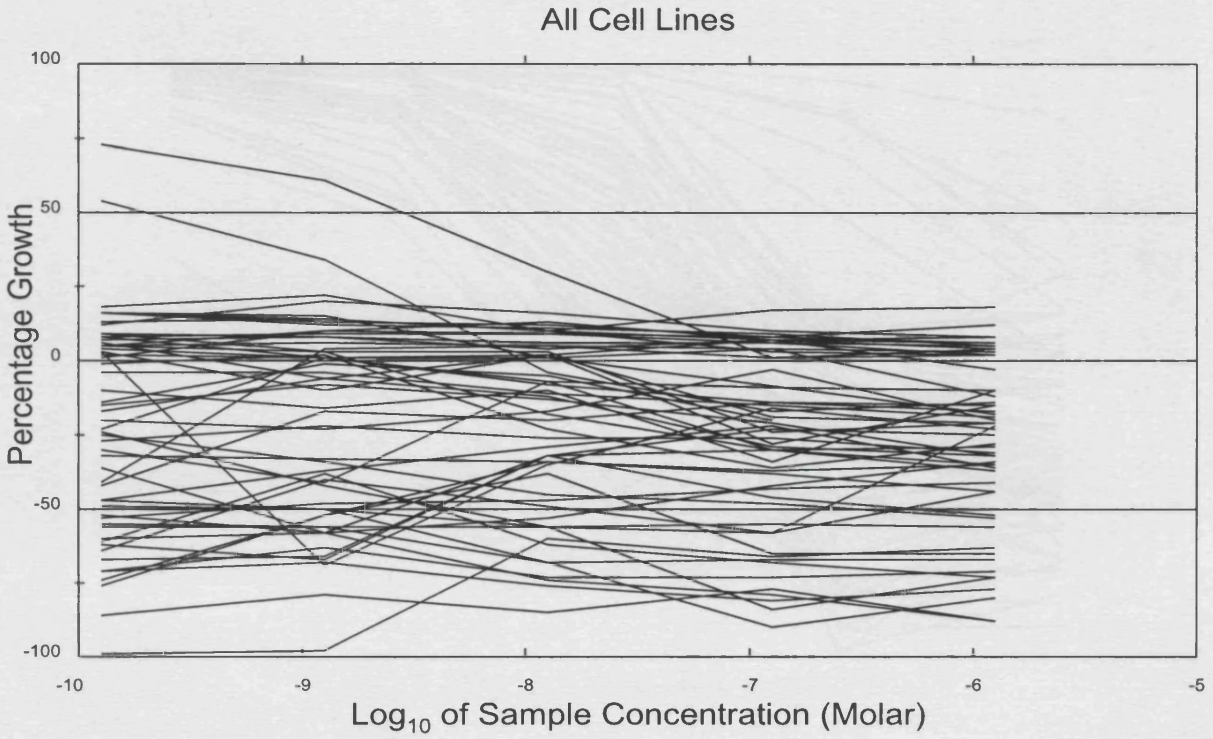

Figure 27. 60 Cell-line profile for Py-Py-Im-PBD (Flat curve).

National Cancer Institute Developmental Therapeutics Program Dose Response Curves	NSC : D736547 / 1	SSPL : 0CCJ	EXP. ID : 0508NS15
	Report Date : October 04, 2005	Test Date : August 15, 2005	

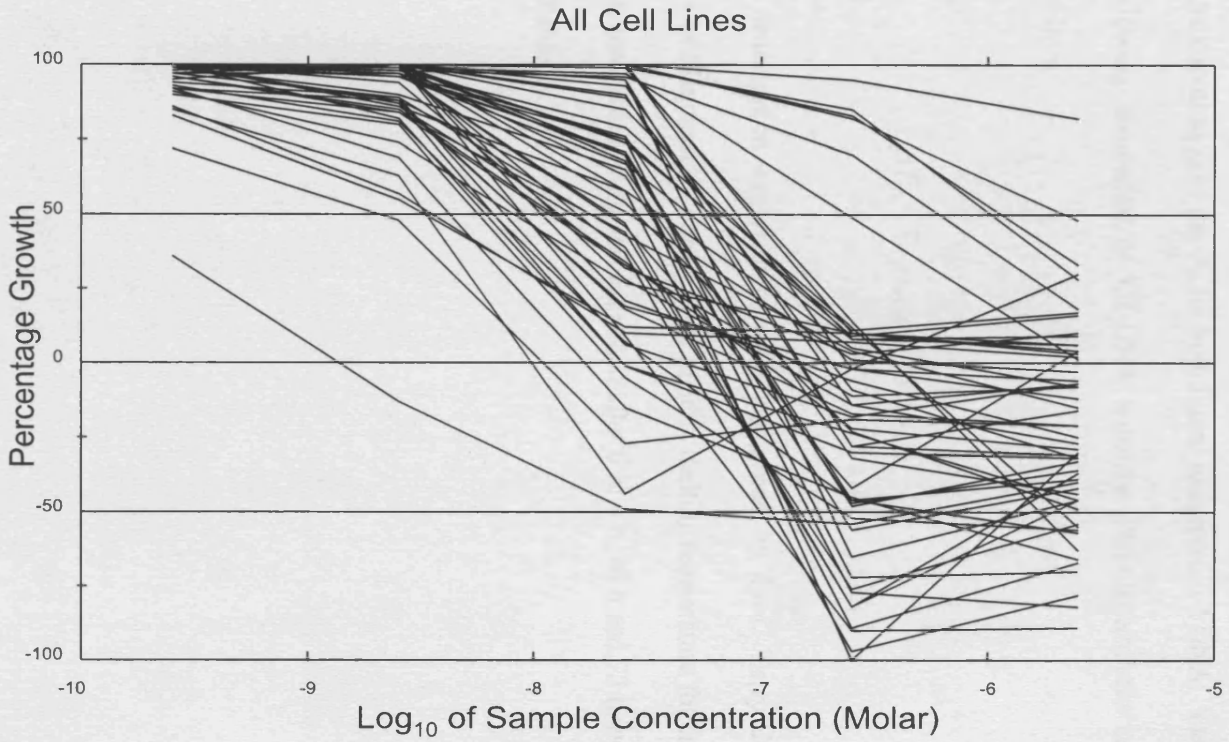

Figure 28. 60 Cell-line profile for Th-Th-Th-PBD (Sigmoidal curve).

6.3 DNA binding affinity

Thermal denaturation studies using calf thymus (CT) DNA were undertaken to investigate the DNA binding affinity of each PBD-heterocycle conjugate. Thermal denaturation temperatures (T_m) were determined from optical absorbance versus temperature curves to give the T_m for both ligand and untreated DNA. The change in T_m (ΔT_m) following incubation of CT-DNA with the PBD-heterocycle conjugates was calculated from:

$$\Delta T_m = T_{m\,(\text{DNA-drug})} - T_{m\,(\text{DNA})}$$

Thermal denaturation experiments were performed by Prof. Terry Jenkins at the University of Manchester. The increase in helix melting temperature for each member of the PBD-heterocycle library was examined after 0 h, 4 h, 18 h and 72 h incubation times at 37°C (**Table 7**).

Compound	Identity	Induced ΔT_m (°C) after incubation at 37 ± 0.1 °C for			
		0 h [c]	4 h	18 h	72 h
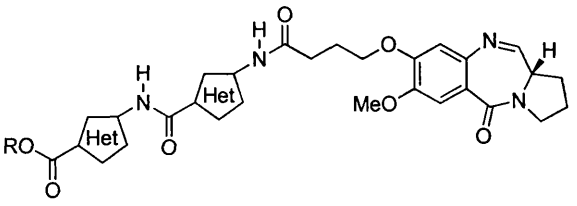 PBD dimer conjugates					
RMH073	Py-Th-PBD	14.5	15.2	15.8	16.1
RMH031	Py-Py-PBD	13.7	14.5	15.1	15.3
RMH067	Im-Im-PBD	10.3	10.9	11.4	11.4
RMH037	Im-Py-PBD	10.0	10.7	11.2	11.3
RMH035	Th-Py-PBD	9.3	9.6	10.2	10.5
RMH071	Th-Th-PBD	7.7	8.0	8.3	8.4
RMH033	Py-Im-PBD	2.8	3.0	3.1	3.2
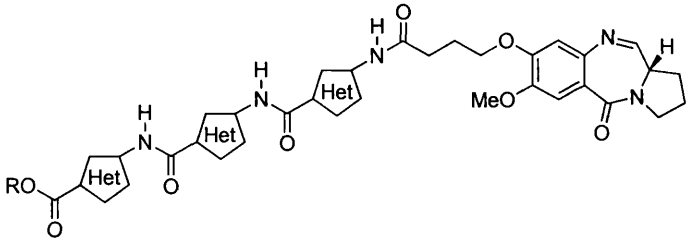 PBD trimer conjugates					
RMH041	Py-Py-Im-PBD	19.1	19.8	21.1	21.6
RMH047	Py-Th-Py-PBD	18.5	19.9	20.7	20.9
RMH039	Py-Py-Py-PBD	17.0	18.7	20.2	20.9
RMH057	Im-Py-Py-PBD	16.8	17.6	18.7	18.8
RMH063	Th-Py-Py-PBD	16.8	17.7	18.6	18.8

Compound	Identity	Induced ΔT_m (°C) After incubation at 37 ± 0.1 °C for			
		0 h [c]	4 h	18 h	72 h
RMH043	Py-Py-Th-PBD	16.4	17.4	18.2	18.5
RMH045	Py-Im-Py-PBD	15.5	16.0	16.9	17.2
RMH055	Im-Py-Im-PBD	14.9	15.7	16.2	16.4
RMH049	Py-Im-Im-PBD	14.3	15.0	15.4	15.6
RMH053	Im-Im-Py-PBD	13.9	14.8	15.2	15.5
RMH051	Im-Im-Im-PBD	11.0	11.7	12.0	12.1
RMH059	Th-Th-Th-PBD	10.0	10.7	10.9	11.0
RMH065	Th-Th-Py-PBD	7.5	8.0	8.4	8.4
RMH061	Th-Py-Th-PBD	6.4	6.8	7.1	7.3

Table 7. Effect of PBD-heterocycle conjugates on the thermal denaturation of calf thymus DNA [ab].

[a] For CT-DNA at pH 7.00 ± 0.01, ΔT_m = 67.82 ± 0.07 °C (mean from >90 experiments). All ΔT_m values are ± 0.1–0.2 °C.

[b] For a fixed 1:10 molar ratio of [ligand]/[DNA]. DNA concentration = 50 μM(bp) and ligand concentration = 5 μM, in aqueous sodium phosphate buffer [10 mM sodium phosphate + 1 mM EDTA, pH 7.00 ± 0.01].

[c] 0 h values shown actually reflect some 30 min heating within the spectrophotometer used for the T_m analysis. This is unavoidable and cannot be circumvented in temperature scan-based assays.

The tabulated data shows that all the novel PBD-heterocycle conjugates increase the thermal stability of the DNA duplex. More specifically, the tripeptide containing molecules exhibit higher affinity for DNA than the dipeptide conjugates. This trend could be attributed to the opportunity for additional interactions between the longer polyamides and DNA, resulting in elevated DNA melting temperatures.

Thermal denaturation studies have previously been conducted on GWL78-2 and GWL79-1, synthesised by Dr G. Wells (Wells *et al.*, 2006), which are structurally identical to RMH031 and RMH039, respectively. The ΔT_m values for GWL78-2 of 13.9, 15.0 and 15.6 °C (for 0, 4 and 18 hours incubation) compare well with the ΔT_m values recorded for RMH031 (13.7, 14.5 and 15.1 °C for 0, 4 and 18 hours). The same can be concluded for GWL79-1 and RMH039 with ΔT_m values of 17.3, 19.6 and 21.2 °C and 17.0, 18.7 and 20.2 for 0, 4 and 18 hours, respectively.

As expected, all the PBD-heterocyclic compounds show the characteristic kinetic effect of a PBD upon incubation with the DNA, as the induced ΔT_m shifts increase with time to a maximal value. More interestingly, it would appear that most of the induced effect appears within a short time period, suggesting that the polyamide chain is an effective and rapid delivery vehicle to the minor groove for the alkylating PBD subunit.

Previously, thermal denaturation studies have been conducted on the control PBD imine capping unit, which gave ΔT_m values of 0.2, 0.3 and 0.4 °C (at 0, 4 and 18 hours). This small increase over time indicates that the heterocyclic polyamide moiety is essential for the significantly elevated DNA melting temperatures seen in **Table 7**, suggesting that the heterocycles are interacting in the minor groove of DNA and enhancing DNA stabilisation.

RMH041 (Py-Py-Im-PBD) has a higher affinity for DNA than the parent tri-pyrrole molecule (RMH039) with ΔT_m values of 19.1, 19.8 and 21.1 °C compared with 17.0, 18.7

and 20.2 °C for 0, 4 and 18 hours respectively. In addition, RMH041 stabilises DNA more effectively than SJG-136, a PBD based sequence selective interstrand crosslinking agent that has one of the highest ΔT_m values reported (16.1, 18.2 and 20.5 °C), at the same 1:10 molar ratio of [ligand]/[DNA] (**Table 8**). Therefore, it is possible that some of the PBD-heterocycle conjugates are binding in a 2:1 fashion, effectively stabilising the duplex DNA by acting in a similar way to crosslinking agents.

Compound	Identity	Induced ΔT_m (°C) After incubation at 37 ± 0.1 °C for		
		0 h	4 h	18 h
RMH041	Py-Py-Im-PBD	19.1	19.8	21.1
RMH039	Py-Py-Py-PBD	17.0	18.7	20.2
SJG136	PBD dimer	16.1	18.2	20.5

Table 8. Comparison of ΔT_m values for selected PBD-heterocycle conjugates with SJG-136.

Replacing pyrrole units with imidazole and thiazole heterocycles has a number of effects on the ΔT_m values depending on their position in the polyamide chain and the number present. For the dimer conjugates, the introduction of an imidazole has a small detrimental effect upon binding affinity, with the exception of RMH033, which has a significantly lower ΔT_m than all the other members of the library. Subsequent HPLC studies showed this molecule to have degraded since initial characterisation which accounts for the disappointing results observed here. The incorporation of an imidazole molecule at the PBD end of the trimer heterocyclic chain slightly increases DNA binding affinity. Interestingly, the inclusion of a single imidazole in either of the other two

possible positions has little effect on binding affinity whereas two or more imidazole units result in a progressive loss of binding to the CT-DNA. It may be significant that imidazoles should not favour the 2:1 binding mode which would account for lower ΔT_m values.

In the dimer conjugate series, the effect of a thiazole is dependant on its position in the chain. This phenomenon is best demonstrated on comparison of the ΔT_m values for Py-Th-PBD (14.5, 15.2, 15.8 and 16.1 °C for 0, 4, 18 and 72 h) with Th-Py-PBD (9.3, 9.6, 10.2 and 10.5 °C for 0, 4, 18 and 72 h). By positioning the thiazole molecule next to the PBD moiety the duplex DNA is stabilised by over 5 °C. In addition, Th-Th-PBD reduces DNA binding by approximately 45% compared to Py-Py-PBD.

The incorporation of one thiazole in the trimer conjugates is well tolerated as demonstrated by Py-Th-Py-PBD exhibiting the second highest DNA binding affinity for the entire library of both dimer and trimer heterocyclic conjugates. Again, the inclusion of two or three thiazoles results in a markedly reduced affinity for duplex DNA.

One disadvantage associated with using calf thymus DNA for thermal denaturation studies is the sheer quantity of base pairs that are available for binding. In addition, the exact base pair sequence is rarely known. As such, an increase in ΔT_m could be attributed to several drug molecules binding at several sites and stabilising the DNA helix to a greater degree than a molecule which has a high specificity and only binds to one site. Therefore, the molecules exhibiting the highest ΔT_m value could be interpreted as being

the least specific, rather than possessing the highest binding affinity. If this was the case it would be logical to expect the molecules which could theoretically bind to the most sites (i.e. molecules consisting only of imidazoles or thiazoles which can tolerate all base pairs) to exhibit the highest ΔT_m values. However, the data in **Table 7** shows that both Th-Th-Thy-PBD and Im-Im-Im-PBD stabilised the DNA helix by only 12.0 °C and 10.9 °C respectively, which is considerably lower than Py-Py-Im-PBD (ΔT_m = 21.1 °C). It would be necessary to carry out further investigations using shorter oligomers of known length and sequence to confirm that the ΔT_m values displayed in **Table 7** are a measure of DNA binding affinity rather than lack of specificity.

Table 9 shows that there is a modest preference for A/T-rich tracts compared to G/C regions for the dipeptide series, but this effect is reduced or abolished for the tripeptide ligands. There is no obvious pattern of A/T versus G/C stabilisation for the various heterocyclic substitutions from this assay, as the overall effects are only modest.

In conclusion, the PBD-heterocycle conjugates are high affinity ligands for heterosequence natural DNA. The polyamide chain length and composition has a strong effect on binding affinity, with the most effective molecule stabilising DNA better than known crosslinkers, i.e. SJG-136.

6.3.1 Comparison of K562 data and ΔT_m values

The IC_{50} values obtained in the K562 assay were statistically compared with the ΔT_m values using Pearsons correlation co-efficient. It was found that no correlation existed (r = -0.39) between potency and DNA affinity for this set of compounds. This observation contrasts the popular theory that potency is related to the molecules ability to bind DNA with high affinity. However, this statistical analysis could be limited as it is comparing the behaviour of the compound on isolated DNA versus a whole cell. Alternatively, the lack of correlation could support the hypothesis that the results of CT DNA thermal denaturation studies do not measure binding affinity but lack of specificity, as previously discussed.

Compound	Identity	Induced T_m shift (°C)[a]			AT/GC
		$\Delta T_m^{0.2}$	$\Delta T_m^{0.5}$	$\Delta T_m^{0.8}$	ratio[b]
PBD-dimer conjugates					
RMH031	Py-Py-PBD	14.5	13.7	11.9	1.2
RMH033	Py-Im-PBD	2.7	2.8	2.9	1.0
RMH037	Im-Py-PBD	10.8	10.0	8.1	1.3
RMH067	Im-Im-PBD	10.7	10.3	8.7	1.2
RMH073	Py-Th-PBD	14.4	14.5	13.5	1.1
RMH035	Th-Py-PBD	9.9	9.3	7.5	1.3
RMH071	Th-Th-PBD	8.3	7.7	6.2	1.3
PBD-trimer conjugates					
RMH039	Py-Py-Py-PBD	16.3	17.0	17.9	0.9
RMH041	Py-Py-Im-PBD	18.2	19.1	19.2	0.9
RMH045	Py-Im-Py-PBD	14.9	15.5	15.2	1.0
RMH057	Im-Py-Py-PBD	17.5	16.8	15.2	1.1
RMH049	Py-Im-Im-PBD	13.7	14.3	13.9	1.0
RMH055	Im-Py-Im-PBD	14.8	14.9	13.9	1.1
RMH053	Im-Im-Py-PBD	14.2	13.9	12.7	1.1
RMH051	Im-Im-Im-PBD	11.1	11.0	10.0	1.1
RMH043	Py-Py-Th-PBD	15.7	16.4	17.0	0.9
RMH047	Py-Th-Py-PBD	18.4	18.5	17.9	1.0
RMH063	Th-Py-Py-PBD	17.2	16.8	15.6	1.1
RMH061	Th-Py-Th-PBD	6.3	6.4	6.3	1.0
RMH065	Th-Th-Py-PBD	7.2	7.5	7.7	0.9
RMH059	Th-Th-Th-PBD	9.9	10.0	9.1	1.1

Table 9. Differential effects of C8-functionalised PBDs on the A/T-rich and G/C-rich domains of the melting curve for calf thymus DNA

[a]Ligand-induced alteration in T_m compared to the native drug-free calf thymus DNA, determined at 20%, 50% and 80% progress through the duplex melting curve. A fixed [ligand]/[DNA(bp)] ratio of 5 μM:50 μM was used, without incubation treatment at 37 °C.

[b]Values of $\Delta T_m^{0.2}/\Delta T_m^{0.8}$ >1.0 indicate AT-preferential binding behaviour, whereas ratios <1.0 indicate a binding preference for GC-rich portions of the host DNA duplex.

6.4 DNA SEQUENCE SELECTIVITY

DNase I footprinting was used to identify the affinity and sequence selectivity of DNA-binding by the PBD-polyamide conjugates. DNase I footprinting is a highly sensitive assay capable of yielding information on the sequence selectivity and affinity of DNA binding molecules. Graphical analysis of DNase I footprinting gels, using differential cleavage plot and score graphs can identify and assess high-affinity binding sites from the electrophoresis data. The footprinting assay was conducted with the assistance of Dr. Tom Ellis (Spirogen).

The standard footprinting approach involves radiolabelling the DNA to allow visualisation of the DNA fragmentation on exposure of the gel to X-ray film. However, a new approach has been developed where radiolabels are replaced with IR dyes and the gel is visualised through detection of the dyes using a diode laser. One advantage of the IR approach is that 700 bp of DNA can be analysed compared with approximately 100-200 base pairs using the standard method.

The PBD-heterocycle conjugates were footprinted against 700 bp of the human Topo-IIa promoter, which is known to include five ICBs, which as previously discussed are potential targets for therapeutic intervention.

The PBD-heterocycle conjugates were used to validate the IR footprinting assay and analysis methods were developed using the data obtained. Unfortunately, some problems, such as the presence of artifactual footprints, have been discovered using this method, therefore, the data cannot be reliably analysed fully.

As such, the generated footprinting data was used as an initial screen to determine which molecules should be selected for testing in the NF-Y functional assay (EMSA). More specifically, the ability of the conjugates to bind at ICB 1 and 2 sites was of particular interest.

All members of the PBD-heterocycle library were prepared at a range of concentrations and incubated overnight with the DNA fragment prior to DNase I cleavage.

6.4.1 PBD-diheterocycle conjugates

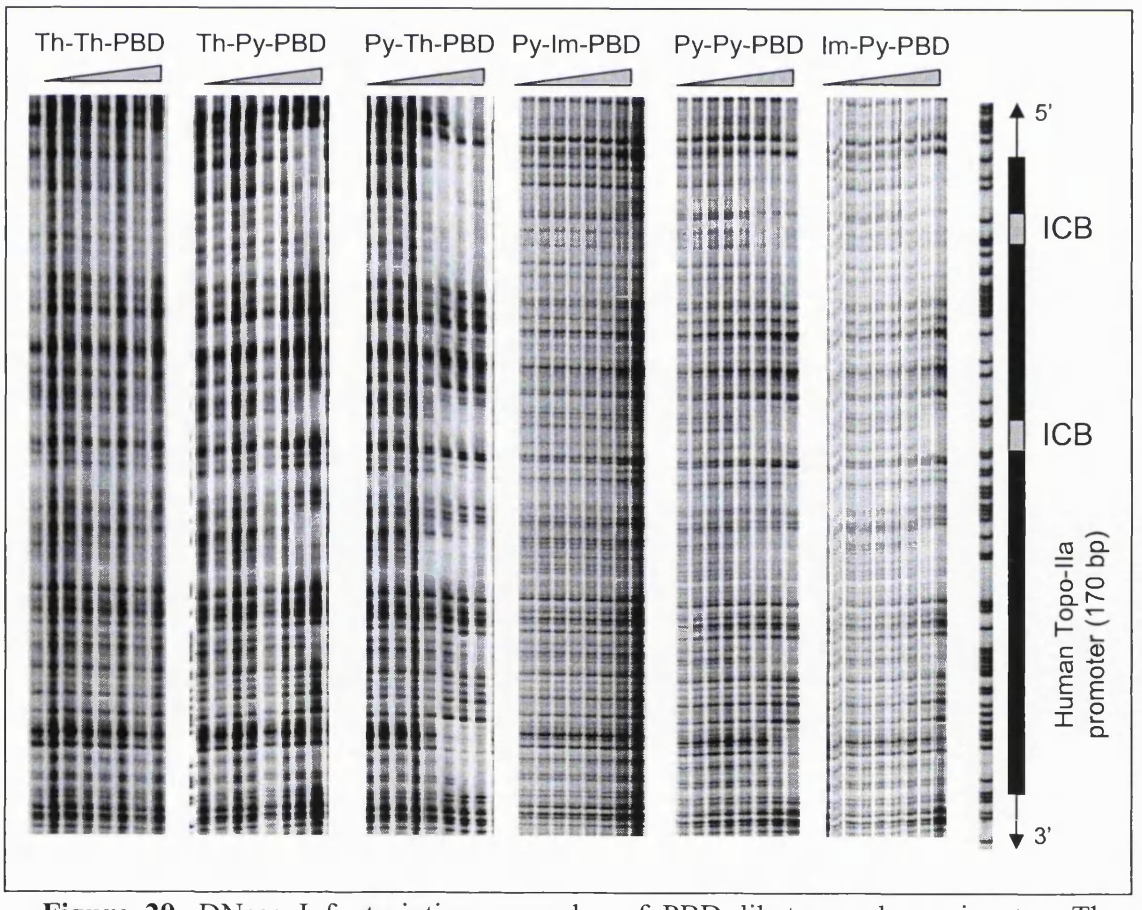

Figure 29. DNase I footprinting examples of PBD-diheterocycle conjugates. The results from 170 bp of the human Topo-IIa promoter are shown. Eight lanes were used to assess each conjugate, with concentrations increasing left to right (0, 1.6, 8, 40, 200, 1000, 5000 and 25000 nM in each case). Marker lanes allow sequence identification. Py = pyrrole, Im = imidazole, Th= thiazole.

The footprinting results indicate that for diheterocycle conjugates the incorporation of an imidazole or a thiazole does affect both DNA-binding affinity and sequence-selectivity. For example, at the ICB1 site DNA-binding is first seen at higher concentrations for the imidazole-containing conjugates compared with Py-Py-PBD and pyrrole and thiazole containing conjugates (at 5000 nM and 1000 nM respectively).

The conjugate Py-Th-PBD binds to the ICB2 site at lower concentrations than the Py-Py-PBD compound (200 nM and 1000 nM respectively). In addition to this, differences in sequence-selectivity due to incorporation of imidazoles and thiazoles are clearly observable. These differences are identifiable as variation in the footprinting pattern across the entire region, and are particularly noticeable towards the bottom of **Figure 29**.

6.4.2 PBD-triheterocycle conjugates

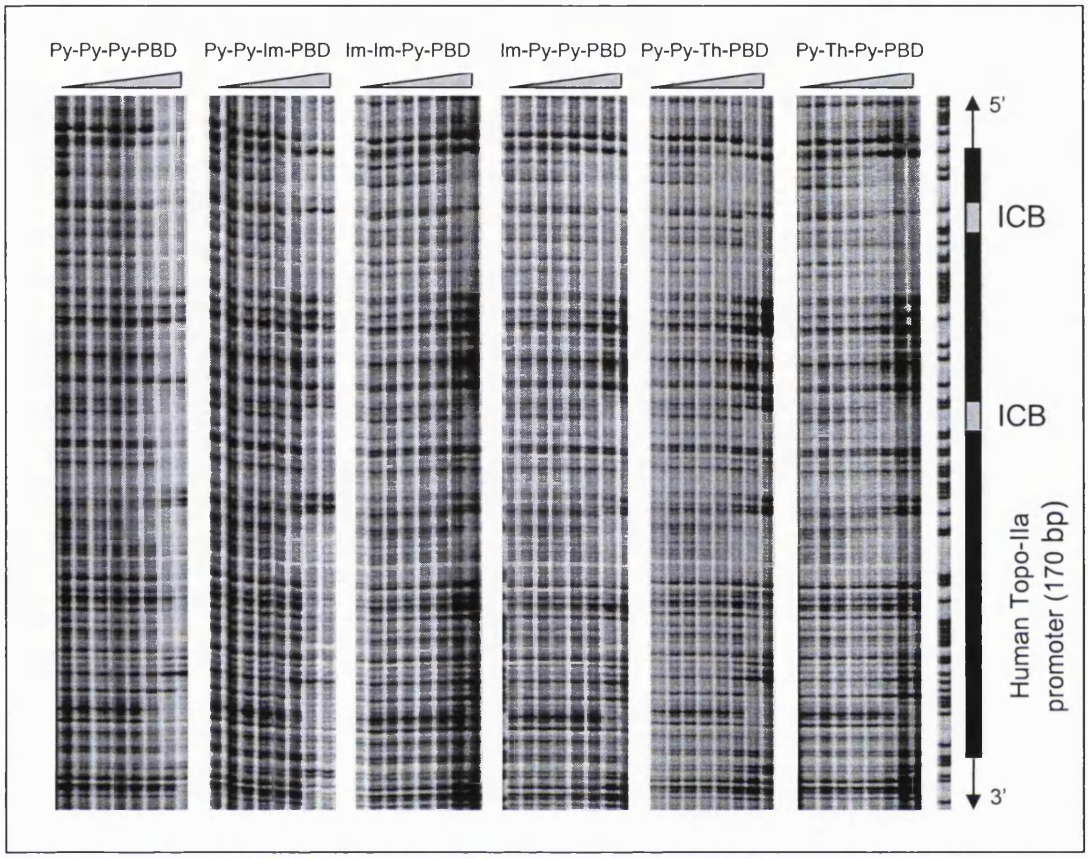

Figure 30. DNase I footprinting examples of PBD-triheterocycle conjugates. The results from 170 bp of the human Topo-IIa promoter are shown. Eight lanes were used to assess each conjugate, with concentrations increasing left to right (0, 1.6, 8, 40, 200, 1000, 5000 and 25000 nM in each case). Marker lanes allow sequence identification. Py = pyrrole, Im = imidazole, Th = thiazole).

The footprinting results for triheterocycle conjugates confirm that the incorporation of heterocycles other than pyrrole affects both DNA-binding affinity and sequence-selectivity, as expected. As in **Figure 29**, differences in sequence-selectivity are clearly observed as variation in the footprinting pattern across the entire region, and once more this is particularly noticeable at sequences towards the bottom (3') end of the gel image. Variation in DNA-binding affinities is also identifiable and, as in **Figure 29**, a sequence just upstream (5') of ICB2 best illustrates this. Binding is seen at this sequence at 1.6 nM for the Py-Py-Py-PBD conjugate, but the concentration

required to footprint this sequence with the other conjugates analysed varies between 200 and 5000 nM.

6.4.3 PBD-heterocycle conjugate binding at ICB1 and ICB2

Compound	Identity	Concentration (μM) at which DNA binding is observed	
		ICB1	ICB2
RMH031	Py-Py-PBD	1	1
RMH033	Py-Im-PBD	> 25	> 25
RMH037	Im-Py-PBD	5	5
RMH067	Im-Im-PBD	25	5
RMH073	Py-Th-PBD	0.2	0.2
RMH035	Th-Py-PBD	> 25	1
RMH071	Th-Th-PBD	> 25	> 25
RMH039	Py-Py-Py-PBD	1	5
RMH041	Py-Py-Im-PBD	5	1
RMH045	Py-Im-Py-PBD	1	5
RMH049	Py-Im-Im-PBD	> 25	> 25
RMH057	Im-Py-Py-PBD	5	5
RMH055	Im-Py-Im-PBD	> 25	1
RMH053	Im-Im-Py-PBD	25	25
RMH051	Im-Im-Im-PBD	> 25	> 25
RMH043	Py-Py-Th-PBD	5	5
RMH047	Py-Th-Py-PBD	5	1
RMH065	Th-Th-Py-PBD	> 25	> 25
RMH061	Th-Py-Th-PBD	> 25	> 25
RMH063	Th-Py-Py-PBD	5	5
RMH059	Th-Th-Th-PBD	> 25	> 25

Table 10. The concentration of each PBD-heterocycle conjugate at which footprints are observed at ICB 1 and ICB 2.

The tabulated data shows the concentration of each PBD-heterocycle conjugate at which footprints at ICB 1 and 2 are observed. The compounds with the highest affinity for the two ICB sites were selected to be tested in the functional EMSA assay. In addition to selecting the molecules with the greatest potential to inhibit NF-Y binding, two molecules, RMH051 and RMH059, which were not expected to bind to the ICB sites, were also selected.

6.5 NF-Y GEL SHIFT ASSAY

The gel shift assay or EMSA investigates the ability of the polyamide conjugate to inhibit the NF-Y transcription factor from binding to the ICBs. This is of particular importance as in a cell the polyamide conjugate would have to compete with the endogenous transcription factor in order to inhibit transcription. It is therefore necessary for the polyamide-PBD conjugate to have an equal or greater affinity for the DNA sequence than the transcription factor, for any inhibitory effects to be observed. As NF-Y binds to the ICB sites with high affinity and specificity, this could prove challenging.

Eight members of the PBD-heterocycle conjugate library were selected for evaluation in the NF-Y gel shift assay. Compounds that had the potential to disrupt NF-Y transcription factor binding were identified by footprinting studies, as previously discussed in Section 6.4. Six of the eight chosen molecules were observed to bind at the inverted CCAAT box (ICBs) sites on topoisomerase IIα promoter with reasonably high affinity. Of the remaining compounds, only one footprinted at the highest concentration (25 μM) and the other did not bind to any DNA sequence.

The assay was performed on ICB1 and ICB2 sequences (shown below).

ICB1 5' CAGGGATTGGCTGGT 3'

ICB2 5' CTACGATTGGTTCTT 3'

6.5.1 ICB1

Four molecules were tested in the EMSA gel shift assay at ICB1, the results of which are shown below (**Figure 31** and **Table 11**).

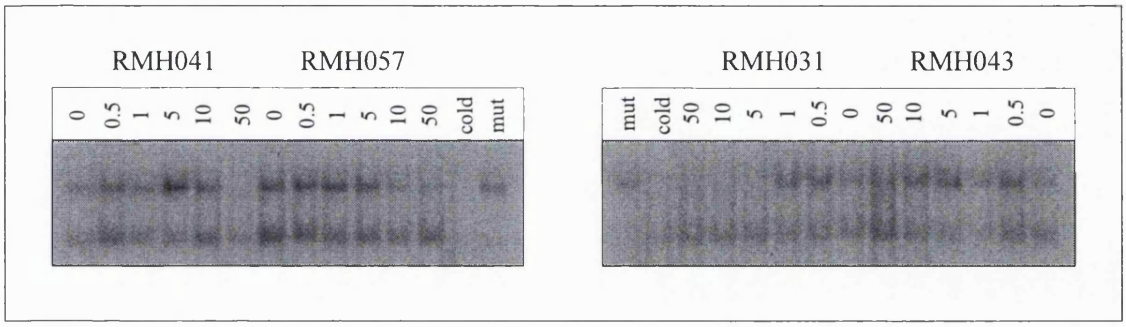

Figure 31. Gel pictures for RMH031, RMH043, RMH041 and RMH057 at the concentrations (μM) shown at ICB1.

Compound	Identity	Lowest concentration at which NF-Y binding inhibition was observed (μM)
RMH031	Py-Py-PBD	5
RMH041	Py-Py-Im-PBD	50
RMH043	Py-Py-Th-PBD	50
RMH057	Im-Py-Py-PBD	>50

Table 11. Effect of PBD-heterocycle conjugates on NF-Y transcription factor binding at ICB1.

Of the four molecules tested at ICB1, the pyrrole dimer RMH031 inhibited NF-Y binding at the lowest concentration (5 μM). Moreover, RMH057 did not inhibit NF-Y binding at the concentrations used.

6.5.2 ICB2

All eight of the selected molecules were screened to assess their potential to inhibit NF-Y binding at ICB2, the results of which are shown below (**Figure 32** and **Table 12**).

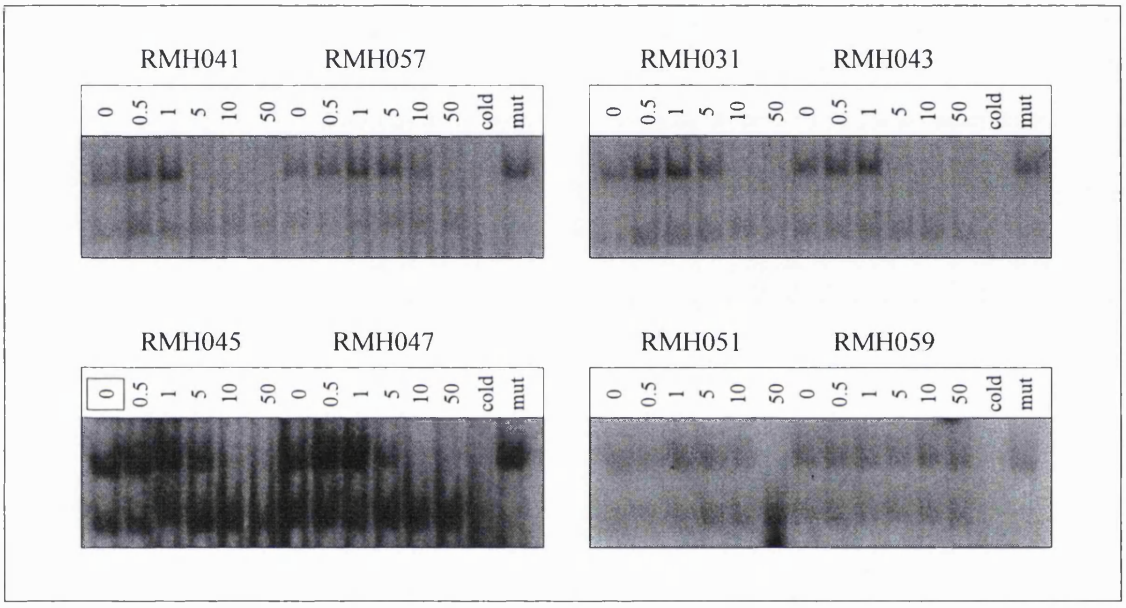

Figure 32. Gel pictures for RMH031, RMH043, RMH041, RMH057, RMH045, RMH047, RMH051 and RMH059 at the concentrations (μM) shown at ICB2.

Again, the pyrrole dimer molecule (RMH031) inhibited NF-Y binding at the lowest concentration (5 μM). Interestingly, RMH041 also inhibited NF-Y binding at ICB2 at 5 μM, a concentration ten-fold lower than that required to inhibit ICB1, demonstrating that RMH041 has a greater affinity for ICB2 than ICB1.

Similarly, a five-fold difference in the concentration of RMH043 necessary to inhibit NF-Y binding was observed between ICB1 and ICB2, 50 μM and 10 μM respectively. In addition, no inhibition was observed at ICB1 using RMH057, which

is in contrast to ICB2, where the transcription factor was inhibited from binding at a concentration of 50 μM.

Compound	Identity	Lowest concentration at which NF-Y binding inhibition was observed (μM)
RMH041	Py-Py-Im-PBD	5
RMH031	Py-Py-PBD	5
RMH043	Py-Py-Th-PBD	10
RMH04	Py-Th-Py-PBD	10
RMH04	Py-Im-Py-PBD	10
RMH057	Im-Py-Py-PBD	50
RMH051	Im-Im-Im-PBD	50
RMH059	Th-Th-Th-PBD	>50

Table 12. Effect of PBD-heterocycle conjugates on NF-Y transcription factor binding at ICB2.

The two molecules, RMH045 and RMH047 are structurally different from each other because of the presence of an imidazole or a thiazole in the middle position within the trimer. The concentration at which inhibition was observed at ICB2 for these two molecules was the same, 10 μM.

RMH051 and RMH059 were not expected to inhibit NF-Y binding based on the footprinting data. The tri-thiazole-PBD conjugate (RMH059) did not inhibit NF-Y binding at ICB2 at the highest concentration tested; however, the tri-imidazole-PBD conjugate (RMH051) did inhibit binding at 25 μM.

The differences observed in the conjugates ability to inhibit NF-Y binding at ICB1 and ICB2 can only be attributed to the difference in the flanking sequences either side of the ICB. Interestingly, more PBD binding sites (guanine residues) are present in ICB1 sequence which should offer increased potential drug-DNA interactions. It is possible that the decreased number of PBD binding sites within ICB2 forces the polyamide-PBD conjugates to bind to a particular position which is more favourable to inhibit NF-Y binding, as transcription factor binding was inhibited at the same or lower concentrations at ICB2 for all the molecules tested.

Unfortunately, no obvious trends can be observed with relation to binding affinity for thiazole-containing molecules compared with imidazole-containing conjugates. In addition, no correlation exists between position of imidazoles/thiazoles within the trimer subunit and binding affinity. This is disappointing, as it is clear that changing the order and composition of the trimer subunit has an effect on ability to inhibit NF-Y binding.

In conclusion, the gel shift assay has assessed the functional potential of the PBD-heterocycle conjugates and allowed lead molecules to be identified. The results shown in **Table 11** and **12** suggest that both RMH031 and RMH041 are capable of inhibiting NF-Y binding at low concentrations as predicted by the footprinting studies. Interestingly, all the PBD-heterocycle conjugates had a higher affinity for ICB2. In addition, RMH041 inhibited NF-Y binding at ICB2 at a lower concentration than ICB1 and as a result could be considered to be more selective for the ICB2 sequence.

7 CONCLUSIONS AND FUTURE WORK

7.1 Conclusions

A library of PBD-heterocyclic conjugates, consisting of pyrrole, thiazole and imidazole heterocycles, was successfully prepared using a solution phase EDCI/DMAP coupling strategy.

The PBD acid building block was synthesised using an approach based on the latter steps of the total synthesis of porothramycin B reported by Fukuyama. Unfortunately, initial efforts to synthesise the PBD acid resulted in a racemate. The presence of both enantiomers was discovered by optical rotation measurements and was later confirmed by chiral HPLC. However, the addition of a THP group at the C11 position, the penultimate step in the synthesis, preserved the essential (*S*)-stereochemistry.

Amide coupling reactions using EDCI/DMAP afforded the heterocycle trimer and dimer subunits which were subsequently coupled to the Alloc-protected PBD building block. Increased product yields were observed as a result of modifications made to the synthetic strategy. More specifically, the use of different extraction methods, higher equivalents of coupling reagents and improved reaction monitoring increased the coupling reaction efficiency.

Mass directed preparatory HPLC furnished the active PBD-heterocyclic conjugates in high purity following the final Alloc deprotection step. Low final product yields (6-40 %) were obtained when purifying using preparatory LCMS compared with flash column chromatography (90%).

Unfortunately one member of the PBD-heterocycle library, Py-Th-Th-PBD was not synthesised due to the failure of the final deprotection step. Efforts to resynthesise this molecule were reluctantly abandoned due to solubility problems and time constraints.

Biological evaluation of the library of PBD-heterocycle conjugates yielded some interesting observations. Initial cytotoxicity data, in both the K562 assay and NCI 60 cell line panel, revealed the conjugates to be potent cytotoxic agents. The most potent molecule was RMH041, an imidazole containing trimer conjugate, with a GI_{50} value of 1.3 nM. Interestingly, coupling a PBD to a heterocyclic subunit potentiated the activity of the molecule as the conjugate was significantly more cytotoxic than the subunits on their own.

Thermal denaturation studies were performed on the final products to investigate DNA binding affinity. Many molecules exhibited high affinity for DNA resulting in elevated DNA melting temperatures. For example, RMH041 stabilised the DNA helix by 21.1°C which is higher than the ΔT_m value obtained by SJG-136 (20.5°C), a known interstrand crosslinking agent. This may indicate that some molecules bind to DNA in a 2:1 mode and function as pseudo crosslinking agents.

DNAse I footprinting allowed the identification of the conjugates that bound with the highest affinity to the ICB sites in the human Topo II α promoter and therefore could potentially inhibit transcription factor binding. Eight PBD-heterocycle conjugates were tested in the functional NF-Y gel shift assay and inhibition of NF-Y was seen at concentrations of between 5 and 50 μM at ICB 1 and 2.

Overall, a promising lead molecule, RMH041 (Py-Py-Im-PBD) was identified, which exhibited impressive DNA binding affinity and the potential to inhibit transcription.

7.2 Future work

Due to the promising biological results observed for this set of PBD-heterocycle conjugates, a number of research avenues could be explored further. Firstly, it would be interesting to conduct further radiolabelled footprinting studies to enable comprehensive analysis of the effect of different heterocycles on DNA sequence selectivity and affinity. Different DNA sequences could be used which correspond to the predicted preferred sequence for each of the PBD-heterocyclic conjugates

In addition, activity in whole cell systems should be explored. A chromosomal histone immuno precipitation (CHIP) assay would determine whether the PBD-heterocycle conjugates can inhibit NF-Y transcription in the presence of other cellular proteins.

The library of molecules could be tested against a variety of interesting targets. A modified ELISA assay could be utilised for this purpose and has the advantage of being relatively high throughput.

An important area requiring further investigation is the binding mode which the PBD-heterocycle conjugates adopt with DNA. NMR experiments or MS analysis may determine whether the activity of the more potent molecules is linked to binding stoichiometry, i.e. 2:1 or 1:1.

8 EXPERIMENTAL

^{1}H-NMR spectra were acquired using a Bruker Advance 400 spectrometer at 400 MHz. Coupling constants are quoted in Hertz (Hz). Chemical shifts are reported in parts per million (ppm) downfield from tetramethylsilane. Spin multiplicities are described as a s (singlet), br s (broad singlet), d (doublet), dd (doublet of doublets), t (triplet), q (quartet), p (pentuplet), and m (multiplet).

LC-MS analysis method 1 was performed using a Luna 3μ C8(2) column with a flow rate of 1.5 mL/min and a linear gradient solvent system going from 95:5 solvent A:B at time 0 to 5:95 A:B at 4 minutes after sample injection then maintained at 5:95 until 7 minutes. LCMS analysis method 2 was performed using a Luna 3μ C8(2) column with a flow rate of 1.5 mL/min and a linear gradient solvent system going from 95:5 solvent A:B at time 0 to 5:95 A:B at 3 minutes after sample injection then maintained at 5:95 until 5 minutes. Solvent A is 0.1% formic acid in water, solvent B is 0.1% formic acid in acetonitrile. The electrospray mass spectrometer was operated in switching mode to obtain both positive and negative ion spectra.

LCMS analysis method 3 and 4 were performed using a Phenomenex Luna 5μ C18(2) 250 x 4.6 mm column and a Phenomenex Gemini 5μ C18 100 x 4.6 mm column, respectively. The solvent composition was the same for both columns: (A) water and 0.1% formic acid and (B) acetonitrile and 0.1% formic acid. The solvent was delivered at a flow rate of 1.5 mL/min using gradient elution:

Time (min)	Flow (mL/min)	A (%)	B (%)
Initial	1.5	95	5
18.0	1.5	5	95
22.0	1.5	5	95
23.0	1.5	95	5
30.0	1.5	95	5

The HPLC system consisted of: a Waters 2767 sample manager fitted with a 20 μL loop, a Waters 2996 PDA and a Waters micromass ZQ mass spectrometer. The ZQ was operated using electrospray ionisation, scanning from 100-1500 Da in positive ion mode. All injections were 20 μL with the flow being split approx. 10 times, ensuring that only 150 μL was entering the electrospray source.

Flash chromatography was performed using Merck Kieselgel 60 F254 silica gel. Extraction and chromatography solvents were bought and used without further purification from Fisher Scientific, UK. All chemicals were purchased from Sigma-Aldrich, Lancaster or BDH.

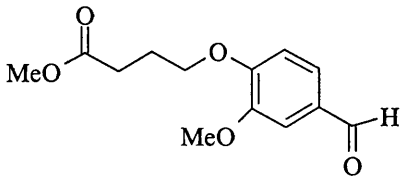

4-(4-Formyl-2-methoxyphenoxy)butanoic acid methyl ester (62)

A slurry of vanillin (38 g, 0.251 mol), methyl-4-bromobutyrate (50 g, 34.2 mL, 1.05 equiv.) and K_2CO_3 (54 g, 1.5 equiv.) in DMF (200 mL) was stirred at room temperature overnight (16 h). Water (1 L) was then added whilst stirring and the precipitate was collected by vacuum filtration, washed with water and dried to yield a white solid, (59.5 g, 94%). ^{1}H-NMR ($CDCl_3$) (400 MHz) δ 9.82 (s, 1H, formyl-H) 7.45 (m, 2H, H-3,5) 6.96 (d, 1H, J = 8.1 Hz, H-6) 4.14 (t, 2H, J = 6.3 Hz, side chain H-1) 3.90 (s, 3H, OCH_3) 3.70 (s, 3H, side chain CO_2CH_3) 2.56 (t, 2H, J = 7.2 Hz, side chain H-3) 2.21 (p, 2H, J = 6.7 Hz, side chain H-2); ^{13}C-NMR ($CDCl_3$) (100MHz) δ 190.9, 173.4, 153.8, 149.9, 130.1, 126.8, 111.5, 109.2, 67.8, 56.0, 51.7, 30.3, 24.2; MS *m/z* (ES^+) (relative intensity) 253 (M+1).

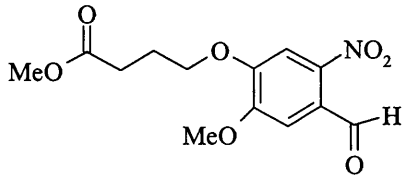

4-(4-Formyl-2-methoxy-5-nitrophenoxy)butanoic acid methyl ester (63)

A solution of the aldehyde (59.5 g, 0.236 mol) in acetic anhydride (200 mL) was added slowly to a mixture of 70% HNO_3 (900 mL) and acetic anhydride (200 mL) at 0 °C. The mixture was allowed to stir at 0 °C for 2.5 h. The solution was then poured on to ice in a 5 L flask and the volume adjusted to 5 L with ice and water. The resulting light-sensitive pale-yellow precipitate was immediately collected by vacuum filtration, washed with cold water and dried to yield the product (59.09 g, 84%) . ^{1}H-NMR (d_6-DMSO) (400 MHz) δ 10.21 (s, 1H, formyl-H) 7.72 (s, 1H, H-6) 7.4 (s, 1H, H-3) 4.23 (t, 2H, J = 6.2 Hz, side chain H-1) 3.98

(s, 3H, OCH_3) 3.56 (s, 3H, side chain CO_2CH_3) 2.54 (t, 2H, J = 7.1 Hz, side chain H-3) 2.12 (p, 2H, J = 6.3 Hz, side chain H-2); ^{13}C-NMR (DMSO) (100MHz) δ 188.5, 172.8, 152.7, 151.0, 143.5, 124.7, 110.1, 108.2, 68.4, 56.4, 51.3, 29.7, 23.8; MS *m/z* (FAB) (relative intensity) 298 (M+1).

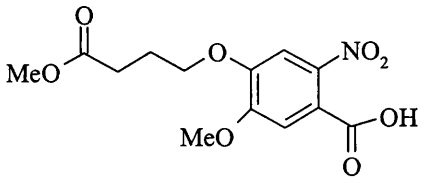

5-Methoxy-4-(3-methoxycarbonylpropoxy)-2-nitrobenzoic acid (64)

A hot solution of 10 % $KMnO_4$ (50 g in 500 mL of water) was added over 10 mins to a solution of nitrobenzaldehyde **61** (59.09 g, 0.189 mol) in acetone (450 mL), resulting in a vigorous reflux. The reaction mixture was allowed to stir for 1 h, over which time the exotherm subsided, followed by vacuum filtration through a pad of celite. The filter pad was washed with hot water (1 L) and treated with sodium bisulphite in 1 M HCl (80 g, 500 mL). The filtrated was diluted with water (3 L) and acidified to pH 1 with conc. HCl. The resulting precipitate was collected by vacuum filtration and dried *in vacuo* to afford 39.07 g of product (63%). ^{1}H-NMR (d_6-DMSO) (400 MHz) δ 7.58 (s, 1H, H-3) 7.29 (s, 1H, H-6) 4.12 (t, 2H, J = 5.7 Hz, side chain H-1) 3.91 (s, 3H, OCH_3) 3.62 (s, 3H, side chain OCH_3) 2.43 (t, 2H, J = 7.0 Hz, side chain H-3) 2.06 (p, 2H, J = 6.3 Hz, side chain H-2); ^{13}C-NMR (DMSO-d_6) (100MHz) δ 172.8, 166.0, 151.8, 149.2, 141.3, 121.1, 111.3, 107.9, 68.1, 56.4, 51.3, 29.7, 23.8; MS *m/z* (ES^-) (relative intensity) 312 (M-1).

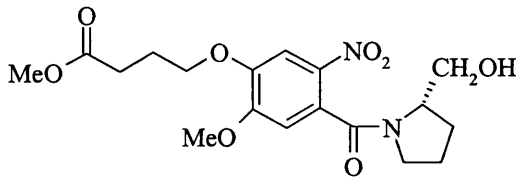

4-[4-((2*S*)-2-Hydroxymethylpyrrolidine-1-carbonyl)-2-methoxy-5-nitrophenoxy] butanoic acid methyl ester (65)

Oxalyl chloride (11.86 mL, 1.1 equiv.) and a catalytic amount of DMF (2 drops) were added to a suspension of nitrobenzoic acid (38.7 g, 0.124 mol) in anhydrous DCM (300 mL) and the reaction was allowed to stir overnight. The resulting acid chloride was added dropwise over 6 h to a solution of *S*-pyrrolidinemethanol (13.39 mL, 1.1 equiv.) and TEA (38 mL, 2.2 equiv.) in anhydrous DCM (200 mL) under an atmosphere of nitrogen maintaining the temperature at -30°C throughout. The reaction mixture was allowed to reach room temperature and stir overnight. The resulting solution was washed with 1M HCl (2 × 200 mL), twice with water, then once with brine. Drying with $MgSO_4$ and concentration *in vacuo* gave the product as a pale yellow foam (49.5 g, 96%). ^{1}H-NMR ($CDCl_3$) (400 MHz) δ 7.70 (s, 1H, H-9) 6.80 (s, 1H, H-6) 4.40 (m, 1H, CH_2*OH*) 4.15 (t, 2H, *J* = 6.2 Hz, side chain H-1) 3.95 (s, 3H, OCH_3) 3.95-3.73 (m, 2H, H-3) 3.69 (s, 3H, OCH_3) 3.15 (t, 2H, *J* = 6.7 Hz, C*H*$_2$-OH) 2.56 (t, 2H, *J* = 7.1 Hz, side chain H-3) 2.20 (m, 2H, side chain H-2) 1.90-1.70 (m, 4H, H-1,H-2); ^{13}C-NMR ($CDCl_3$) (100MHz) δ 173.2, 154.8, 148.4, 109.2, 108.4, 68.4, 66.1, 61.5, 56.7, 51.7, 49.5, 30.3, 28.4, 24.4, 24.2; $[\alpha]^{24}_D$ = -84° (*c* = 1, $CHCl_3$); MS *m/z* (ES^+) (relative intensity) 397 (M+1).

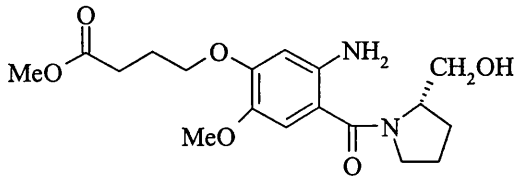

4-[5-Amino-4-((2*S*)-2-hydroxymethyl-pyrrolidine-1-carbonyl)-2-methoxy-phenoxy]-butyric acid methyl ester (66)

A slurry of 10% Pd/C (1 g) in EtOAc was added to a solution of nitro-compound **65** (10 g, 25 mmol) in EtOH (120 mL) and hydrogenated in a Parr hydrogenated at 40 psi until no further H_2 uptake was observed. The reaction mixture was filtered through celite and the solvent removed *in vacuo*. The resulting amine (8.97 g, 97%) was used directly in the next step.

Raney Nickel method

Hydrazine (6.43 mL in 70 mL MeOH) was slowly added dropwise to a solution of nitro-compound **65** (49.55 g, 0.125 mol) over Raney nickel (5.4 g) at reflux. After addition the reaction mixture was allowed to cool to room temperature. The Raney nickel was then decanted and the solution filtered through celite, care was taken not to allow the raney nickel to dry. The resulting solution was concentrated *in vacuo* and purified using column chromatography (EtOAc:Hexane; 70:30) to yield the amine product (31.11 g, 68%) which was used directly in the next step.

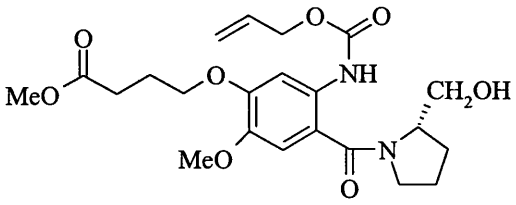

4-[5-Allyloxycarbonylamino-4-((2*S*)-2-hydroxymethylpyrrolidine-1-carbonyl)-2-methoxyphenoxy]butanoic acid methyl ester (71)

A solution of allyl chloroformate (5.0 mL, 1 equiv.) in anhydrous DCM (50 mL) was added dropwise to a solution of amine **66** (17.32 g, 0.047 mol) and anhydrous pyridine (7.64 mL, 0.095 mol) in dry DCM (50 mL) at 0 °C. The resulting solution was allowed to stir overnight at room temperature. The mixture was then washed with cold 1M HCl (100 ml), water (100 mL), saturated aqueous $NaHCO_3$ (100 mL), and then brine (100 mL). The organic solution was then dried ($MgSO_4$), and the solvent was removed *in vacuo* to yield the product as a brown foam (20.32 g, 95%). ^{1}H-NMR ($CDCl_3$) (400 MHz) δ 8.78 (bs, 1H, NH) 7.75 (s, 1H, H-9), 6.82 (s, 1H, H-6) 5.97 (m, 1H, allyl H-2) 5.38-5.34 (dd, 1H, J = 1.5, 17.2 Hz, allyl H-3) 5.27-5.24 (dd, 1H, J = 1.3, 10.4 Hz, allyl H-3) 4.63 (m, 2H, allyl H-1) 4.40 (bs, 2H, CH_2-OH) 4.11 (t, 2H, J = 6.3 Hz, side chain H-1) 3.82 (s, 4H, OCH_3, OH) 3.69 (m, 4H, OCH_3, H-11a) 3.61-3.49 (m, 2H, H-3) 2.54 (t, 2H, J = 7.4 Hz, side chain H-3) 2.18 (p, 2H, J = 6.7 Hz, side chain H-2) 1.92-1.70 (m, 4H, H-1, H-2); ^{13}C-NMR ($CDCl_3$) δ (100MHz) 173.4,170.9, 153.6, 150.5, 144.0, 132.5, 132.0, 118.1, 115.4, 111.6, 105.6, 67.7, 66.6, 65.8, 61.1, 60.4, 56.6, 51.7, 30.5, 28.3, 25.1, 24.3;$[\alpha]^{26}_D$ = -67° (c = 0.45, $CHCl_3$); MS *m/z* (FAB$^+$) 451 (M+1). LCMS (method 1) rt = 2.90 min; *m/z* (ES$^+$) 451 (M+1).

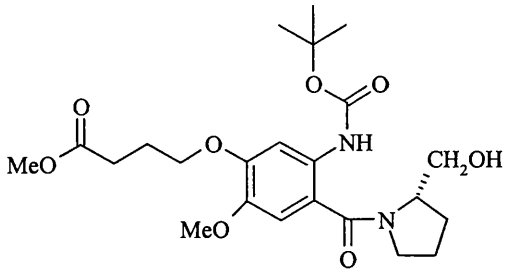

4-[5-tert-Butoxycarbonylamino-4-(2-hyrodoxy-pyrrolidine-1-carbonyl)-2-methoxy-phenoxy]-butyric acid methyl ester (67)

A solution of di-tert-butyl dicarbonate (5.88 g, 1.1 equiv.) in THF (100 mL) was added to amine **66** (8.97 g, 0.0245 mol) and heated under reflux overnight. The THF was then removed *in vacuo* and the residue dissolved in EtOAc (50 mL). The resulting solution was washed with water (2 x 100 mL) and brine (2 x 100 mL) and dried over $MgSO_4$. Concentration *in vacuo* yielded the product as a brown oil (8.58 g, 75%). ^{1}H-NMR ($CDCl_3$) (400 MHz) δ 8.38 (br s, 1H, N-H) 7.75 (s, 1H, H-9) 6.79 (s, 1H, H-6) 4.56-4.18 (m, 2H, side chain H-1) 4.10 (t, 2H, J = 6.15 Hz, -CH_2-OH) 3.80 (m, 4H, O-CH_3, OH) 3.68 (m, 4H, O-CH_3, H-3) 3.62-3.37 (m, 2H, H-3, H-11a) 2.53 (t, 2H, J = 7.37 Hz, side chain H-3) 2.16 (m, 2H, side chain H-2) 1.97-1.59 (m, 4H, H-1, H-2) 1.40 (s, 9H, Boc-H); ^{13}C-NMR ($CDCl_3$) (100MHz) δ 173.5,171.1, 153.1, 150.6, 146.7, 143.8, 132.5, 111.9, 105.8, 85.2, 80.3,67.7,61.1, 60.4, 56.8, 51.6, 30.6, 28.4, 27.4, 24.5; $[\alpha]^{23}_D$ = -65° (c = 0.17, $CHCl_3$); MS m/z (ES^+) 467 (M+1).

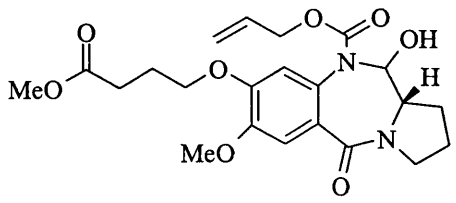

(11a*S*) 11-Hydroxy-7-methoxy-8-(3-methoxycarbonylpropoxy)-5-oxo-2,3,11,11a-tetrahydro-1*H*,5*H*-pyrrolo[2,1-*c*][1,4]benzodiazepine-10-carboxylic acid allyl ester (72)

TEMPO (7.04 g, 0.1 equiv.) was added to a solution of Alloc-protected compound **71** (20.32 g, 0.0451 mol) and DAIB (17.43 g, 1.1 equiv.) in DCM (200 mL) and allowed to stir overnight at room temperature. The reaction mixture was washed with sodium metabisulphite (2 x 150 mL), $NaHCO_3$ (2 x 150 mL) and brine (2 x 150 mL) and dried over $MgSO_4$. The solvent was removed *in vacuo* to yield a brown oil (12.52g, 62%). ^{1}H-NMR ($CDCl_3$) (400 MHz) δ 7.22 (s, 1H, H-9) 6.67 (s, 1H, H-6) 5.75 (m, 1H, allyl H-2) 5.65 (m, 1H, H-11) 5.13 (d, 2H, J = 12.9 Hz, allyl H-3) 4.69-4.40 (m, 2H, allyl H-1) 4.11 (m, 2H, side chain H-1) 3.95 (m, 4H, OCH_3, OH) 3.67 (m, 4H, OCH_3, H-3) 3.58-3.45 (m, 2H, H-3,11a) 2.52 (t, 2H, J = 7.2 Hz, side chain H-3) 2.19-1.96 (m, 6H, side chain H-2, H-1,2); ^{13}C-NMR ($CDCl_3$) (100MHz) δ 173.4, 167.0, 156.0, 149.9, 148.7, 131.8, 128.3, 125.9, 118.1, 113.9, 110.7, 86.0, 67.9, 66.8, 60.4, 59.9, 56.1, 51.7, 46.4, 30.3, 28.7, 24.2, 23.1, 21.1; $[\alpha]^{26}_D$ = +112 ° (c = 0.6, $CHCl_3$); MS *m/z* (ES^+) 449 (M+1). LCMS (method 1) rt = 2.56 min; *m/z* (ES^+) 448 (M+1).

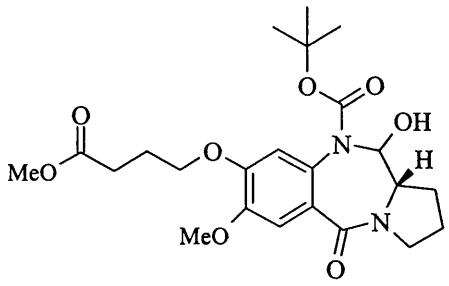

(11a*S*) 11-Hydroxy-7-methoxy-8-(3-methoxycarbonyl-propoxy)-5-oxo-2,3,11,11a-tetrahydro-1*H*,5*H*-pyrrolo[2,1-*c*][1,4]benzodiazepine-10-carboxylic acid tert-butyl ester (68)

Oxalyl chloride (9.0 mL, 1.8 equiv.) in anhydrous DCM (150 mL) was cooled to –40 °C and a solution of anhydrous DMSO (12 mL, 3.6 equiv.) in anhydrous DCM (150 mL) was added dropwise over 1.5 h, maintaining the temperature below –37 °C. A transient white suspension was formed which then redissolved. The crude Boc-protected amine (25.0 g, 53.6 mmol) in anhydrous DCM (225 mL) was added dropwise over 2 h maintaining the temperature below –37 °C. The mixture was stirred at -40 °C for a further 1 h. A solution of DIPEA (32.0 mL, 4.3 equiv.) in anhydrous DCM (75 mL) was added dropwise over 30 mins and the reaction was allowed to warm to room temperature. The mixture was extracted with a concentrated aqueous solution of citric acid (300 mL). (pH 2 - 3 after extraction). The organic phase was washed with water (2 × 400 mL) and brine (300 mL), then dried ($MgSO_4$). Solvent removal *in vacuo* gave a paste; column chromatography (EtOAc:hexane, 60:40) yielded the product (19.95 g, 80%).

The Boc-protected amine (8.58 g, 0.018 mol) was added to a solution of DAIB (6.52 g, 1.1 equiv.) in DCM (100 mL). The resulting solution was treated with TEMPO (0.287 g, 0.1 equiv.) and allowed to stir overnight at room temperature. The mixture was washed with sodium metabisulphite (2 x 75 mL), $NaHCO_3$ (2 x 75 mL) and brine (2 x 75 mL) and dried over $MgSO_4$. The solvent was removed *in vacuo* to yield a brown oil (5.62g, 66%).^{1}H-NMR

($CDCl_3$) (400 MHz) δ 7.13 (s, 1H, H-9) 6.01 (s, 1H, H-6) 4.97 (m, 1H, H-11) 3.94 (m, 2H, side chain H-1) 3.73-3.70 (m, 4H, OCH_3, OH) 3.69-3.67 (m, 4H, OCH_3, H-3) 3.41-3.30 (m, 2H, H-3,11a) 2.25 (t, 2H, J = 7.2 Hz, side chain H-3) 2.10-1.58 (m, 6H, side chain H-2, H-1,2) 1.40 (9H, s, Boc-H); ^{13}C-NMR ($CDCl_3$) (100MHz) δ 172.0, 171.0, 169.7, 146.2, 135.9, 134.9, 114.0, 110.9, 98.8, 84.2, 72.9, 72.0, 60.4, 56.3, 50.4, 43.7, 29.6, 29.0, 25.7, 20.8, 19.0, 17.9; $[\alpha]^{24}_D$ = +108 ° (c = 0.15, $CHCl_3$); MS m/z (ES^+) 465 (M+1).

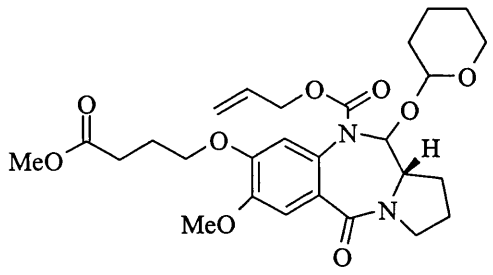

(11a*S*)-7-Methoxy-8-(3-methoxycarbonylpropoxy)-5-oxo-11-(tetrahydropyran-2-yloxy)-2,3,11,11a-tetrahydro-1*H*,5*H*-pyrrolo[2,1-*c*][1,4]benzodiazepine-10-carboxylic acid allyl ester (73)

4-toluenesulfonic acid (catalytic quantity, 0.050 g) was added to a solution of dihydropyran (16.3 mL, 10 equiv.) in EtOAc (30 mL) and stirred for 10 min. The carbinolamine **72** (8.0 g, 0.0172 mol) was then added in one portion and the mixture was stirred for 2 h. The solution was diluted with EtOAc (100 mL) and washed with saturated aqueous $NaHCO_3$ (100 mL), followed by brine (100 mL). The organic layer was dried ($MgSO_4$), and the solvents were removed under vacuum to yield the product as a brown oil (9.54 g, 100%) ^{1}H-NMR ($CDCl_3$) (400 MHz) mixture of diastereoisomers δ 7.21-7.19 (m, 1H, H-9) 6.88-6.58 (m, 1H, H-6) 5.88-5.70 (m, 2H, allyl H-2, H-11) 5.13-5.02 (m, 2H, allyl H-3) 4.95-4.81 (m, 1H, pyran H-2) 4.70-4.35 (m, 2H, allyl H-1) 4.10-3.99 (m, 2H, side chain H-1) 3.97-3.82 (m, 4H, OCH_3, H11a) 3.73-3.62 (m, 4H, OCH_3, H-3) 3.60-3.40 (m, 3H, pyran H-6, H-3) 2.55-2.48 (m, 2H, side chain H-3) 2.20-1.68 (m, 6H, side chain H-2, H-1,2) 1.64-1.49 (m, 6H, pyran H-3,4,5);

^{13}C-NMR ($CDCl_3$) (100MHz) δ 173.4, 167.1, 149.5, 132.0, 114.3, 100.0, 98.2, 94.5, 91.6, 68.2, 67.3, 66.2, 64.0, 63.5, 63.4, 62.8, 56.1, 51.6, 51.5, 46.3, 46.3, 31.1, 30.8, 30.7, 30.3, 30.2, 29.0, 25.4, 25.3, 25.2, 24.2, 20.0, 19.9, 19.6; MS *m/z* (ES^+) (relative intensity) 533 (M+1). LCMS (method 1) rt = 3.48 min; *m/z* (ES^+) 533 (M+1).

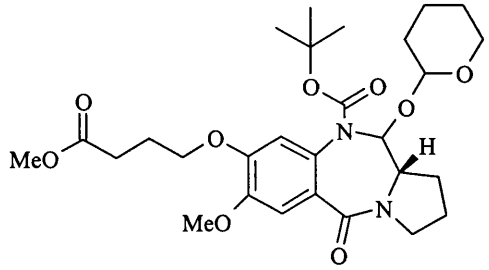

(11a*S*)-7-Methoxy-8-(3-carboxylpropoxy)-5-oxo-11-(tetrahydropyran-2-yloxy)-2,3,11,11a-tetrahydro-1*H*,5*H*-pyrrolo[2,1-*c*][1,4]benzodiazepine-10-carboxylic acid tert-butyl ester (69)

4-toluenesulfonic acid (catalytic quantity, 0.020 g) was added to a solution of dihydropyran (4.1 mL, 10 equiv.) in EtOAc (35 mL) and stirred for 10 min. The carbinolamine **68** (2.0 g, 4.62 mmol) was then added in one portion and the mixture was stirred for 2 h. The solution was diluted with EtOAc (50 mL) and washed with saturated aqueous $NaHCO_3$ (50 mL), followed by brine (50 mL). The organic layer was dried ($MgSO_4$), and the solvents were removed under vacuum to yield the product as a brown oil (2.48 g, 100%).^{1}H-NMR ($CDCl_3$) (400 MHz) mixture of diastereoisomers δ 7.13-7.09 (m, 1H, H-9) 6.01-5.89 (m, 1H, H-6),5.12-5.08 (m, 1H, pyran H-2) 4.68-4.65(m, 1H, H-11) 3.95-3.87 (m, 2H, side chain H-1) 3.78-3.69 (m, 4H, OCH_3, H11a) 3.66-3.60 (m, 4H, OCH_3, H-3) 3.55-3.36 (m, 3H, pyran H-6, H-3) 2.27-2.24 (m, 2H, side chain H-3) 2.12-1.72 (m, 6H, side chain H-2, H-1,2) 1.69-1.57 (m, 6H, pyran H-3,4,5) 1.42 (s, 9H, Boc-H); ^{13}C-NMR ($CDCl_3$) (100MHz) δ 172.3, 171.1, 169.9, 146.5, 135.8, 134.5, 114.3, 110.9, 98.8, 96.1, 81.8, 72.6, 72.0, 63.6, 58.5, 56.3, 50.3,

43.7, 33.1, 29.5, 29.0, 28.1, 25.6, 20.8, 19.3, 19.0, 17.8; MS *m/z* (ES^+) (relative intensity) 548 (M+1).

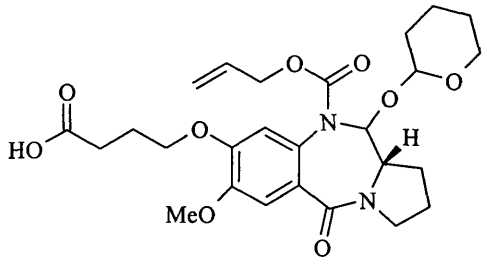

(11a*S*)-8-(3-Carboxypropoxy)-7-methoxy-5-oxo-11-(tetrahydropyran-2-yloxy)-2,3,11,11a-tetrahydro-1*H*,5*H*-pyrrolo[2,1-*c*][1,4]benzodiazepine-10-carboxylic acid allyl ester (74)

A solution of sodium hydroxide (1.51 g, 0.378 mol) in water (30 mL) was added to the protected carbinolamine **73** (10.05 g, 0.189 mol) in MeOH (100 mL) and stirred at 70 °C for 15 min. The solvent was removed *in vacuo* and water (60 mL) was added. The aqueous solution was allowed to return to room temperature and the pH was adjusted to <4 by addition of a 5 % aqueous citric acid solution. The precipitate was extracted with EtOAc (150 mL). The organic layer was washed with brine (50 mL) and dried ($MgSO_4$). The solvent was removed under vacuum, then Et_2O (70 mL) was added to the residue and removed *in vacuo* to yield the product as an off-white foam (9.4 g, 96%). ^{1}H-NMR (d_6-DMSO) (400 MHz) mixture of diastereoisomers δ 7.11-7.08 (m, 1H, H-9) 6.90-6.85 (m, 1H, H-6) 5.85-5.68 (m, 2H, allyl H-2, H-11) 5.47-4.89 (m, 3H, allyl H-3, pyran H-2) 4.71-4.28 (m, 2H, allyl H-1) 4.11-3.93 (m, 2H, side chain H-1) 3.93-3.76 (m, 4H, OCH_3, H-11a) 3.61-3.45 (m, 2H, H-3) 3.44-3.21 (m, 2H, pyran H-6) 2.47-2.33 (m, 2H, side chain H-3) 2.22-1.76 (m, 6H, side chain H-2, H-1,2) 1.76-1.29 (m, 6H, pyran H-3,4,5); ^{13}C-NMR (d_6-DMSO) (100MHz) δ 174.1, 173.9, 171.6, 166.4, 165.9, 149.4, 148.3, 148.1, 132.6, 116.5, 114.3, 110.8, 110.5, 99.0, 67.5, 67.4, 65.7, 65.5, 62.7, 59.8, 55.7, 45.6, 30.7, 30.3, 30.0, 29.7, 28.4, 28.2, 24.9, 24.7, 23.9,

23.8, 22.7, 22.6; MS *m/z* (ES^+) (relative intensity) 519 (M+1). LCMS (method 1) rt = 2.95 min; *m/z* (ES^+) 519 (M+1).

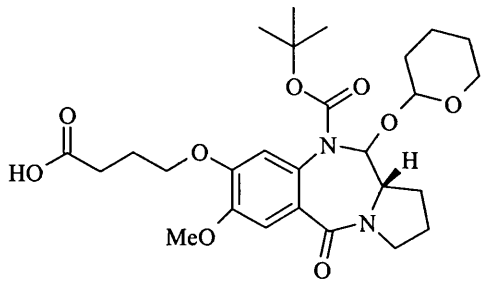

(11a*S*)-8-(3-Carboxypropoxy)-7-methoxy-5-oxo-11-(tetrahydropyran-2-yloxy)-2,3,11,11a-tetrahydro-1*H*,5*H*-pyrrolo[2,1-*c*][1,4]benzodiazepine-10-carboxylic acid tert-butyl ester (70)

A solution of sodium hydroxide (0.41 g, 10.21 mmol) in water (8 mL) was added to the protected carbinolamine **69** (2.797 g, 5.103 mmol) in MeOH (30 mL) and stirred at 70 °C for 15 min. The reaction mixture was concentrated *in vacuo* and water (10 mL) was added. The aqueous solution was allowed to return to room temperature and the pH was adjusted to <4 by addition of a 5 % aqueous citric acid solution. The precipitate was extracted with EtOAc (50 mL) and the organic layer was washed with brine (30 mL) and dried over $MgSO_4$. The solvent was removed under vacuum, then Et_2O (50 mL) was added to the residue and removed *in vacuo* to yield a white foam (2.67 g, 98%). ^{1}H-NMR ($CDCl_3$) (400 MHz) mixture of diastereoisomers δ 7.11-7.07 (m, 1H, H-9) 6.05-5.95 (m, 1H, H-6) 5.10-5.06(m, 1H, pyran H-2) 4.68-4.66 (m, 1H, H-11) 3.94-3.89 (m, 2H, side chain H-1) 3.78-3.70 (m, 1H, H11a) 3.68-3.61 (m, 4H, OCH_3, H-3) 3.56-3.36 (m, 3H, pyran H-6, H-3) 2.25-2.22 (m, 2H, side chain H-3) 2.12-1.72 (m, 6H, side chain H-2, H-1,2) 1.68-1.57 (m, 6H, pyran H-3,4,5) 1.45 (9H, s, Boc-H); ^{13}C-NMR ($CDCl_3$) (100MHz) δ 177.1, 171.0, 169.7, 146.2, 135.9, 114.0, 110.9, 98.8, 96.1, 81.8, 72.9, 72.0, 63.6, 58.5, 56.3, 43.7, 33.1, 32.2, 29.0, 28.2, 25.4, 20.8, 19.3, 19.0, 17.9; MS (ES^+) *m/z* (relative intensity) 535 (M+1). LCMS (method 1) rt = 3.22 min; *m/z* (ES^+) 535 (M+1).

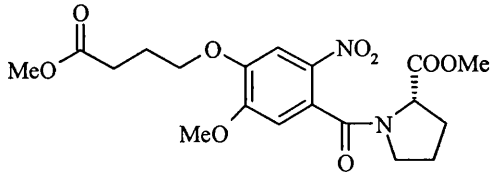

4-{2-Methoxy-4-[2-(1-methoxy-vinyl)-pyrrolidine-1-carbonyl]-5-nitro-phenoxy}-butyric acid (75)

Oxalyl chloride (1.8 mL, 1.1 equiv.) and a catalytic amount of DMF (2 drops) were added to a suspension of nitrobenzoic acid (6 g, 0.019 mol) in anhydrous DCM (60 mL) and the reaction was allowed to stir overnight. The resulting acid chloride was added dropwise over 3 h to a solution of proline methyl ester (3.5 g, 1.1 equiv.) and TEA (6 mL, 2.2 equiv.) in anhydrous DCM (60 mL) under an atmosphere of nitrogen maintaining the temperature at -30°C throughout. The reaction mixture was allowed to reach room temperature and stir overnight. The resulting solution was washed with 10% citric acid (2 × 200 mL), twice with water, then once with brine. Drying with $MgSO_4$ and concentration *in vacuo* gave the product as a yellow foam (7.78 g, 96%). ^{1}H-NMR ($CDCl_3$) (400 MHz) δ 7.70 (s, 1H, H-6) 6.80 (s, 1H, H-3),4.40 (m, 1H, H-2) 4.15 (t, 2H, J = 6.2 Hz, side chain H-1) 3.95 (s, 3H, OCH_3) 3.95-3.73 (m, 2H, H-5) 3.69 (s, 6H, OCH_3) 2.56 (t, 2H, J = 7.1 Hz, side chain H-3) 2.20 (m, 3H, side chain H-2, H-3) 1.90-1.70 (m, 3H, H-3,4); ^{13}C-NMR (d_6-DMSO) (100MHz) δ 172.0, 169.7, 153.6, 146.4, 139.8, 122.2, 114.1, 110.1, 72.0, 58.7, 56.3, 50.4, 43.1, 29.6, 25.7, 22.8, 20.2; MS *m/z* (ES^+) (relative intensity) 425 (M+1)

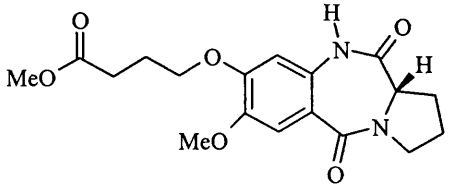

4-(7-Methoxy-5,11-dioxo-2,3,5,10,11,11a-hexahydro-1*H*- pyrrolo[2,1-*c*][1,4]benzo diazepin-8-yloxy)-butyric acid methyl ester (76)

A slurry of 10% Pd/C (0.15 g) in EtOAc was added to a solution of nitro-compound **75** (1.5 g, 3.35 mmol) in EtOH (60 mL) and hydrogenated in a Parr hydrogenated at 40 psi until no further H_2 uptake was observed (5 h). The reaction mixture was filtered through celite and the solvent removed *in vacuo*. The resulting residue was suspended in THF (1ml), treated with 1M HCl (10 mL) and allowed to stir overnight at room temperature. The reaction mixture was diluted with DCM (10 mL) and washed with water (2 x 10 mL) and brine (2 x 10 mL) then dried over $MgSO_4$. Concentration *in vacuo* yielded the ring closed product as a brown oil (0.534 mg, 42%). ^{1}H-NMR (d_6-DMSO) (400 MHz) δ 10.18 (s, 1H, N-H) 7.27 (s, 1H, H-9) 7.19 (s, 1H, H-6) 3.95-3.89 (m, 3H, side chain H-1, H-11a) 3.73 (s, 3H, OCH_3) 3.68-3.59 (m, 4H, OCH_3, H-3) 3.41-3.38 (m, 1H, H-3) 2.27 (t, 2H, J = 7.2 Hz, side chain H-3) 2.09 -1.60 (m, 6H, side chain H-2, H-1,2); ^{13}C-NMR (d_6-DMSO) (100MHz) δ 172.0, 169.9, 145.6, 143.1, 132.2, 119.0, 113.4, 106.9, 96.1, 72.1, 59.5, 56.5, 50.4, 42.7, 29.6, 25.7, 23.5, 19.8; MS (ES^+) *m/z* (relative intensity) 365 (M+1).

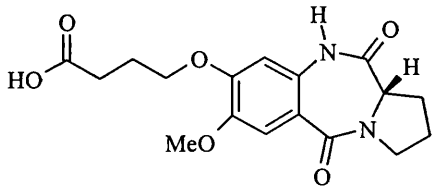

7-Methoxy-8-(4-oxo-pentyloxy)-1,2,3,11a-tetrahydro-10*H*-pyrrolo[2,1-*c*][1,4]benzodiazepine-5,11-dione (77)

A solution of sodium hydroxide (0.58 g, 2 equiv.) in water (10 mL) was added to the dilactam **76** (2.6 g, 7.19 mmol) in MeOH (10 mL) and stirred at 60 °C for 25 min. The reaction mixture was concentrated *in vacuo* and water (10 mL) was added. The aqueous solution was allowed to return to room temperature and the pH was adjusted to <4 by addition of a 5 % aqueous citric acid solution. The product precipitated on addition of EtOAc (20 mL) and was collected by filtration and dried to yield a white solid. The filtrate was washed with brine (30 mL), dried over $MgSO_4$ and concentrated *in vacuo* to yield a white foam (1.47 g, 58%). Racemate: ^{1}H-NMR (d_6-DMSO) (400 MHz) δ 10.18 (s, 1H, N-H) 7.27 (s, 1H, H-9) 7.19 (s, 1H, H-6) 3.95-3.89 (m, 3H, side chain H-1, H-11a) 3.73 (s, 3H, OCH_3) 3.65-3.60 (m, 1H, H-3) 3.41-3.38 (m, 1H, H-3) 2.27 (t, 2H, J = 7.2 Hz, side chain H-3) 2.09 -1.60 (m, 6H, side chain H-2, H-1,2); ^{13}C-NMR (d_6-DMSO) (100MHz) δ 175.3, 172.0, 169.7, 145.6, 143.1, 132.2, 119.0, 113.4, 106.9, 72.1, 59.5, 56.3, 42.7, 32.1, 25.4, 23.6, 19.8; $[\alpha]^{25}_D = 0$ ° (c = 0.5, $CHCl_3$); MS (ES^+) *m/z* (relative intensity) 350 (M+1).

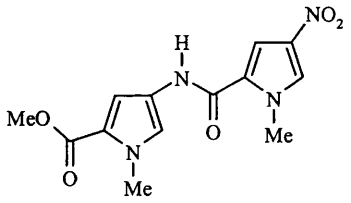

1-Methyl-4-[(1-methyl-4-nitro-1*H*-pyrrole-2-carbonyl)-amino]-1*H*-pyrrole-2-carboxylic acid methyl ester

The pyrrole amine (1 g, 5.25 mmol) and the nitro-pyrrole acid chloride (1.41 g, 5.25 mmol) were dissolved in anhydrous DMF (5 mL) and allowed to stir for 48 h at room temperature. A precipitate was formed and collected by filtration. The solid was resuspended in EtOAc and concentrated *in vacuo* to yield the product as a yellow foam (1.082 g, 68%).^{1}H-NMR (d_6-DMSO) (400 MHz) δ 10.25 (s, 1H, N-H) 8.17 (s, 1H, Py-H) 7.55 (s, 1H, Py-H) 7.45 (s, 1H, Py-H) 6.89 (s, 1H, Py-H) 3.95 (s, 3H, N-CH_3) 3.85 (s, 3H, N-CH_3) 3.74 (s, 3H, O-CH_3).

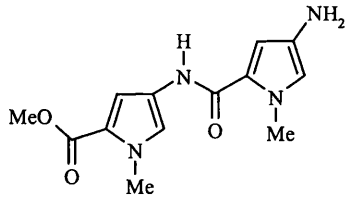

4-[(4-Amino-1-methyl-1*H*-pyrrole-2-carbonyl)-amino]-1-methyl-1*H*-pyrrole-2-carboxylic acid methyl ester

A slurry of 10% Pd/C (0.04 g) in EtOAc was added to a solution of the nitro-compound (0.20 g, 0.653 mmol) in EtOH (100 mL) and hydrogenated in a Parr hydrogenated at 40 psi until no further H_2 uptake was observed (48 h). The reaction mixture was filtered through celite and the solvent removed *in vacuo*. The resulting amine was used directly in the next step.

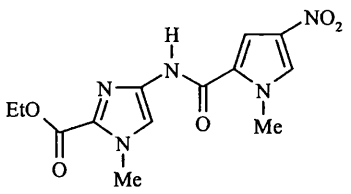

1-Methyl-4-[(1-methyl-4-nitro-1*H*-pyrrole-2-carbonyl)-amino]-1*H*-imidazole-2-carboxylic acid ethyl ester

The imidazole amine (1 g, 5.9 mmol) and the nitro-pyrrole acid chloride (1.6 g, 5.9 mmol) were dissolved in anhydrous DMF (5 mL) and allowed to stir for 48 h at room temperature. A precipitate was formed and collected by filtration. The solid was resuspended in EtOAc and concentrated *in vacuo* to yield the product as a yellow foam (1.003 g, 53%). ^{1}H-NMR (d_6-DMSO) (400 MHz) δ 11.19 (s, 1H, N-H) 8.21 (s, 1H, Im-H) 7.75 (s, 1H, Py-H) 7.62 (s, 1H, Py-H) 4.27 (q, 2H, J = 7.2 Hz, OC*H*$_2$CH$_3$) 3.95 (s, 3H, N-CH$_3$) 3.94 (s, 3H, N-CH$_3$) 1.28 (t, 3H, J = 7.2 Hz, OCH$_2$C*H*$_3$).

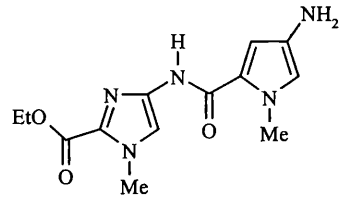

4-[(4-Amino-1-methyl-1*H*-pyrrole-2-carbonyl)-amino]-1-methyl-1*H*-imidazole-2-carboxylic acid ethyl ester

A slurry of 10% Pd/C (0.04 g) in EtOAc was added to a solution of the nitro-compound (0.20 g, 0.653 mmol) in EtOH (100 mL) and hydrogenated in a Parr hydrogenated at 40 psi until no further H_2 uptake was observed (60 h). The reaction mixture was filtered through celite and the solvent removed *in vacuo*. The resulting amine was used directly in the next step.

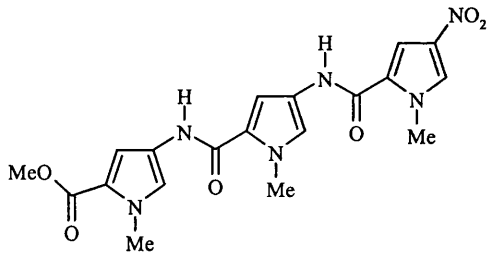

1-Methyl-4-({1-methyl-4-[(1-methyl-4-nitro-1*H*-pyrrole-2-carbonyl)-amino]-1*H*-pyrrole-2-carbonyl}-amino)-1*H*-pyrrole-2-carboxylic acid methyl ester

The pyrrole amine dimer (0.2 g, 0.724 mmol) and the nitro-pyrrole acid chloride (0.177 g, 0.724 mmol) were dissolved in anhydrous DMF (5 mL) and allowed to stir for 96 h at room temperature. The resulting precipitate was collected by vacuum filtration, resuspended in EtOAc and concentrated *in vacuo* to yield the product as a yellow foam (0.121 g, 39%).^{1}H-NMR (d_6-DMSO) (400 MHz) δ 10.25 (s, 1H, N-H) 9.98 (s, 1H, N-H) 8.19 (s, 1H, Py-H) 7.58 (s, 1H, Py-H) 7.45 (s, 1H, Py-H) 7.30 (s, 1H, Py-H) 7.09 (s, 1H, Py-H) 6.89 (s, 1H, Py-H) 3.98 (s, 3H, N-CH_3) 3.86 (s, 3H, N-CH_3) 3.85 (s, 3H, N-CH_3) 3.71 (s, 3H, O-CH_3).

General procedure A: Coupling imidazole containing molecules

EDCI (2 equiv.) and DMAP (2.5 equiv.) were added to a solution of amine and acid components in dry DMF or DCM (5 mL). The reaction mixture was allowed to stir for X hours. The resulting solution was diluted with DCM (40 mL) and washed with deionised water (3 x 30 mL) then sat. $NaHCO_3$ solution (3 x 30 mL). The organic layer was dried over $MgSO_4$ and concentrated *in vacuo* to give the product.

General procedure B: Coupling thiazole containing molecules

EDCI (2 equiv.) and DMAP (2.5 equiv.) were added to a solution of amine and acid components in dry DMF or DCM (5 mL). The reaction mixture was allowed to stir for X hours. The resulting solution was diluted with DCM (40 mL) and washed with 10% citric acid solution (3 x 30 mL) then sat. $NaHCO_3$ solution (3 x 30 mL). The organic layer was dried over $MgSO_4$ and concentrated *in vacuo* to give the product.

General procedure C: Boc deprotection (4M HCl in dioxane):

The Boc protected amine was treated with 4M HCl in dioxane (5 mL). The reaction mixture was allowed to stir for 30 mins during which time a precipitate formed. The solvent was removed *in vacuo* and the remaining residue was dried under vacuum.

General procedure D: Boc deprotection (95% TFA):

The Boc protected amine was treated with 95% aqueous TFA (5 mL) and allowed to stir for 30 mins. The solvent was removed *in vacuo* and the residue was dried under vacuum.

General procedure E: Alloc deprotection

Palladium *tetrakis*[triphenylphosphine] (0.05 equiv.) was added to a solution of the Alloc-THP-PBD-heterocycle conjugate and pyrrolidine (1.1 equiv.) in dry DCM (5 mL). The reaction mixture was allowed to stir at room temperature for 1 hour. The solvent was removed *in vacuo* and the product was purified using a preparative HPLC coupled to a mass directed fraction collector. Pure fractions were combined and lyophilised to yield the solid product.

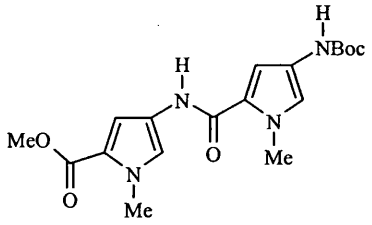

4-[(4-*tert*-Butoxycarbonylamino-1-methyl-1*H*-pyrrole-2-carbonyl)amino}-1-methyl-1*H*-pyrrole-2-carboxylic acid methyl ester (90)

A solution of the pyrrole amine (0.5 g, 2.74 mmol) and the Boc-protected pyrrole acid (0.658 g, 2.74 mmol) in anhydrous DCM (5 mL) was treated with EDCI (0.630 g, 1.2 equiv.) and DMAP (0.502 g, 1.5equiv.) then stirred over night at room temperature. The reaction mixture was diluted with EtOAc (50 mL) and washed with 10 % HCl solution (3 × 50 mL) and saturated $NaHCO_3$ solution (3 × 50 mL), dried ($MgSO_4$) and concentrated *in vacuo* to give an off white foam (1.02 g, 99%). ^{1}H-NMR (d_6-DMSO) (400 MHz) δ 9.86 (s, 1H, N-H) 9.12 (s, 1H, Boc-N-H) 7.45 (s, 1H, Py-H) 6.89 (s, 2H, Py-H) 6.83 (s, 1H, Py-H) 3.83 (s, 3H, N-CH_3) 3.79 (s, 3H, N-CH_3) 3.73 (s, 3H, O-CH_3) 1.45 (s, 9H, Boc-H); LCMS (method 1) rt = 3.43 min; *m/z* (ES+) 378 (M+1).

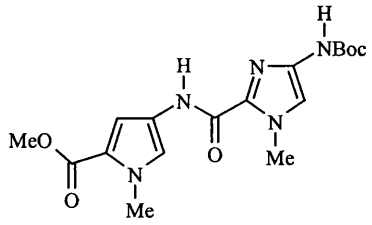

4-[(4-*tert*-Butoxycarbonylamino-1-methyl-1*H*-imidazole-2-carbonyl)-amino]-1-methyl-1*H*-pyrrole-2-carboxylic acid methyl ester (91)

A solution of the pyrrole amine (0.100 g, 0.525 mmol) and the Boc protected imidazole acid (0.127 g, 0.525 mmol) in dry DCM (5 mL) was treated with EDCI and DMAP according to general procedure A (48 h). The product was purified using column chromatography (Chloroform, 100%) to yield a brown foam (0.151 g, 76%). ^{1}H-NMR (d_6-DMSO) (400 MHz)

δ 10.15 (s, 1H, N-H) 9.32 (s, 1H, Boc-N-H) 7.58 (s, 1H, Im-H) 7.25 (s, 1H, Py-H) 7.06 (s, 1H, Py-H) 3.98 (s, 3H, N-CH_3) 3.91 (s, 3H, N-CH_3) 3.77 (s, 3H, O-CH_3) 1.45 (s, 9H, Boc-H); LCMS (method 1) rt = 3.43 min; *m/z* (ES+) 378 (M+1).

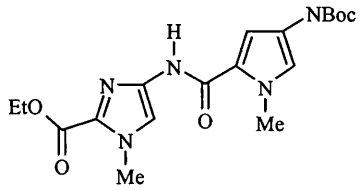

4-[(4-*tert*-Butoxycarbonylamino-1-methyl-1*H*-pyrrole-2-carbonyl)-amino]-1-methyl-1*H*-imidazole-2-carboxylic acid ethyl ester (93)

The imidazole amine (0.500 g, 2.95 mmol) and the Boc protected pyrrole acid (0.710 g, 2.95 mmol) were dissolved in dry DMF (5 mL) and coupled according to general procedure A (60 h). The product was purified using column chromatography (EtOAc:Hexane, 70:30) to yield an orange foam (1.163 g, 95%). ^{1}H-NMR (d_6-DMSO) (400 MHz) δ 10.64 (s, 1H, N-H) 7.64 (s, 1H, Im-H) 6.98 (s, 1H, Py-H) 6.93 (d, 1H, J = 1.2 Hz, Py-H) 4.27 (q, 2H, J = 7.1 Hz, OCH_2CH$_3$) 3.93 (s, 3H, N-CH_3) 3.81 (s, 3H, N-CH_3) 1.45 (s, 9H, Boc-H) 1.30 (t, 3H, J = 7.1 Hz, OCH$_2$CH_3); LCMS (method 2) rt = 1.77 min; *m/z* (ES+) 392 (M+1).

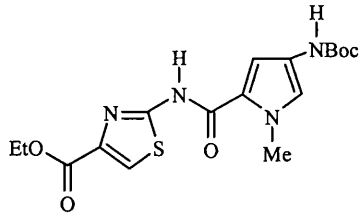

2-[(4-*tert*-Butoxycarbonylamino-1-methyl-1*H*-pyrrole-2-carbonyl)-amino]-thiazole-4-carboxylic acid ethyl ester (95)

The thiazole amine (0.500 g, 1.98 mmol) and the Boc protected pyrrole acid (0.470 g, 1.98 mmol) were dissolved in dry DMF (5 mL) and coupled according to general procedure B (168 h). This yielded the product as a cream foam (0.546 g, 70%). ^{1}H-NMR (d_6-DMSO) (400

MHz) δ 12.52 (s, 1H, N-H) 9.17 (s, 1H, Boc-N-H) 8.02 (s, 1H, Thz-H) 7.20 (s, 1H, Py-H) 7.14 (s, 1H, Py-H) 4.28 (q, 2H, J = 7.1 Hz, OCH_2CH$_3$) 3.85 (s, 3H, N-CH$_3$) 1.45 (s, 9H, Boc-H) 1.30 (t, 3H, J = 7.1 Hz, OCH$_2$CH_3); LCMS (method 1) rt = 3.62 min; *m/z* (ES+) 395 (M+1).

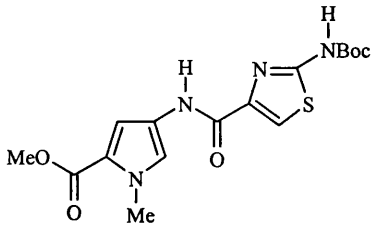

4-[(2-*tert*-Butoxycarbonylamino-thiazole-4-carbonyl)-amino]-1-methyl-1*H*-pyrrole-2-carboxylic acid methyl ester (92)

The pyrrole amine (0.500 g, 2.74 mmol) and the Boc protected thiazole acid (0.668 g, 2.74 mmol) were dissolved in dry DMF (5 mL) and the reaction was performed as described in general procedure B (120 h). This solution was treated with EDCI (1.5 equiv.) and DMAP (1.2 equiv.). The product was an off-white foam (0.797 g, 77%). ^{1}H-NMR (d_6-DMSO) (400 MHz) δ 12.36 (s, 1H, N-H) 9.82 (s, 1H, Boc-N-H) 7.81 (s, 1H, Thz-H) 7.50 (s, 1H, Py-H) 7.01 (s, 1H, Py-H) 3.89 (s, 3H, N-CH$_3$) 3.74 (s, 3H, O-CH$_3$) 1.45 (s, 9H, Boc-H); LCMS (method 1) rt = 3.30 min; *m/z* (ES+) 381 (M+1).

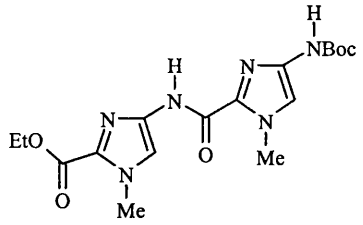

4-[(4-*tert*-Butoxycarbonylamino-1-methyl-1*H*-imidazole-2-carbonyl)-amino]-1-methyl-1*H*-imidazole-2-carboxylic acid ethyl ester (94)

The imidazole amine (0.500 g, 2.96 mmol) and the Boc protected imidazole acid (0.714 g, 2.96 mmol) were dissolved in dry DMF (5 mL). The reaction was performed as described in general procedure A (168 h), using EDCI (1.5 equiv.) and DMAP (1.2 equiv.). Concentration *in vacuo* yielded a foam, 0.825 g, which was purified using column chromatography (silica gel, eluted with EtOAc 70%, Hexane 30%) to give a yellow foam (0.506 g, 43%). ^{1}H-NMR (d_6-DMSO) (400 MHz) δ 9.68 (s, 1H, N-H) 9.62 (s, 1H, N-H) 7.66 (s, 1H, Im-H) 7.28 (s, 1H, Im-H) 4.28 (q, 1H, J = 7.1 Hz, OCH_2CH$_3$) 3.94 (s, 6H, N-CH$_3$) 1.46 (s, 9H, Boc-H) 1.30 (t, 3H, J = 7.1 Hz, OCH$_2$CH_3); LCMS (method 2) rt = 1.77 min; *m/z* (ES+) 393 (M+1).

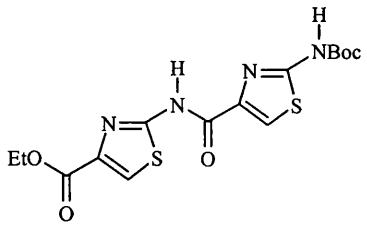

2-[(2-*tert*-Butoxycarbonylamino-thiazole-4-carbonyl)-amino]-thiazole-4-carboxylic acid ethyl ester (96)

The thiazole amine (0.500 g, 1.98 mmol) and the Boc protected thiazole acid (0.483 g, 1.98 mmol) were dissolved in dry DMF. The reaction was performed as described in general procedure B (192 h), using EDCI (1.5 equiv.) and DMAP (1.2 equiv.). This yielded a yellow foam 0.562 g (71%). ^{1}H-NMR (d_6-DMSO) (400 MHz) δ 12.36 (m, 1H, N-H) 11.83 (s, 1H, N-H) 8.29 (s, 1H, Thz-H) 8.10 (s, 1H, Thz-H) 4.29 (q, 2H, J = 7.1 Hz, OCH_2CH$_3$) 1.50 (s,

9H, Boc-H) 1.30 (t, 3H, J = 7.1 Hz, OCH_2CH_3); LCMS (method 1) rt = 3.70 min; *m/z* (ES+) 399 (M+1).

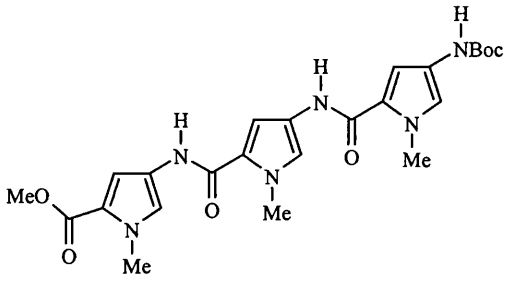

4-({4-[(4-*tert*-Butoxycarbonylamino-1-methyl-1*H*-pyrrole-2-carbonyl)-amino]-1-methyl-1*H*-pyrrole-2-carbonyl}-amino)-1-methyl-1*H*-pyrrole-2-carboxylic acid methyl ester (97)

The Boc pyrrole dimer (0.200 g, 0.532 mmol) was deprotected using 4M HCl in dioxane as described in general procedure C. The resulting residue was dissolved in anhydrous DCM (5 mL) and the Boc-pyrrole acid (0.128 g, 0.532 mmol) was added followed by EDCI (0.153 g, 1.5 equiv) and DMAP (0.078 g, 1.2 equiv). The reaction mixture was stirred at room temperature for 24 h then diluted with EtOAc (50 mL) and washed with 1M HCl solution (3 × 50 mL), saturated $NaHCO_3$ solution (3 × 50 mL), and dried over $MgSO_4$. Concentration *in vacuo* yielded a brown foam (0.172 g. 65%). ^{1}H-NMR (d_6-DMSO) δ 9.90 (1H, s, NH), 9.86 (1H, s, NH), 9.13 (1H, s, Boc-NH), 7.46 (1H, d, J = 1.9 Hz, Py-H), 7.21 (1H, d, J = 1.7 Hz, Py-H), 7.06 (1H, d, J = 1.7 Hz, Py-H), 6.91 (1H, s, Py-H), 6.90 (1H, s, Py-H), 6.85 (1H, s, Py-H), 3.84 (6H, s, NCH_3), 3.81 (3H, s, NCH_3), 3.74 (3H, s, OCH_3), 1.46 (9H, s, Boc-H). LCMS (method 1) rt = 2.98 min; *m/z* (ES+) 499 (M+1).

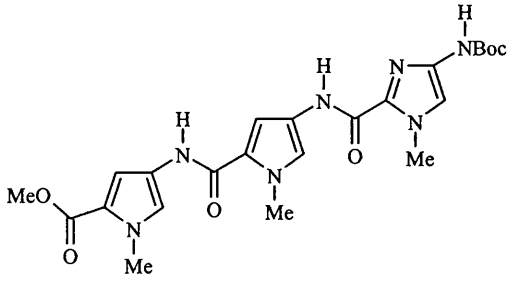

4-({4-[(4-*tert*-Butoxycarbonylamino-1-methyl-1*H*-imidazole-2-carbonyl)-amino]-1-methyl-1*H*-pyrrole-2-carbonyl}-amino)-1-methyl-1*H*-pyrrole-2-carboxylic acid methyl ester (98)

The Boc pyrrole dimer (0.400 g, 1.06 mmol) was deprotected using 4M HCl in dioxane as described in general procedure C. The resulting residue was dissolved in dry DCM (5 mL) and the Boc protected imidazole acid (0.256 g, 1.06 mmol) was added and coupled as described in general procedure A (120 h). The product was purified using column chromatography (DCM:MeOH, 97:3) to yield a brown foam (0.527 g,99%). ^{1}H-NMR (d_6-DMSO) (400 MHz) δ 9.98 (s, 1H, N-H) 9.94 (s, 1H, N-H) 9.36 (s, 1H, N-H) 7.47 (d, 1H, J = 1.9 Hz, Py-H) 7.27 (d, 1H, J = 1.9 Hz, Py-H) 7.22 (s, 1H, Im-H) 7.16 (d, 1H, J = 1.8 Hz, Py-H) 6.90 (d, 1H, J = 2.0 Hz, Py-H) 3.94 (s, 3H, N-CH_3) 3.84 (s, 3H, N-CH_3) 3.84 (s, 3H, N-CH_3) 3.74 (s, 3H, O-CH_3) 1.45 (s, 9H, Boc-H); LCMS (method 2) rt = 1.90 min; *m/z* (ES+) 500 (M+1).

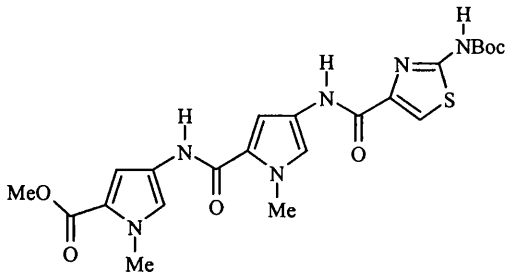

4-({4-[(2-*tert*-Butoxycarbonylamino-thiazole-2-carbonyl)-amino]-1-methyl-1*H*-pyrrole-2-carbonyl}-amino)-1-methyl-1*H*-pyrrole-2-carboxylic acid methyl ester (109)

The Boc pyrrole dimer (0.300 g, 0.80 mmol) was deprotected using 4M HCl in dioxane as described in general procedure C. The resulting residue was dissolved in dry DCM (5 mL) and the Boc protected thiazole acid (0.195 g, 0.80 mmol) was added and coupled as described in general procedure B (120 h). The product was purified using column chromatography (DCM:MeOH, 98:2) to yield a brown foam (0.368 g, 76%). ^{1}H-NMR (d_6-DMSO) (400 MHz) δ 11.66 (s, 1H, N-H) 9.95 (s, 1H, N-H) 9.73 (s, 1H, N-H) 7.82 (s, 1H, Thz-H) 7.47 (s, 1H, Py-H) 7.30 (s, 1H, Py-H) 7.08 (s, 1H, Py-H) 6.90 (d, 1H, J = 1.4 Hz, Py-H) 3.85 (s, 3H, N-CH_3) 3.84 (s, 3H, N-CH_3) 3.74 (s, 3H, O-CH_3) 1.50 (s, 9H, Boc-H); LCMS (method 1) rt = 3.35 min; *m/z* (ES+) 502 (M+1).

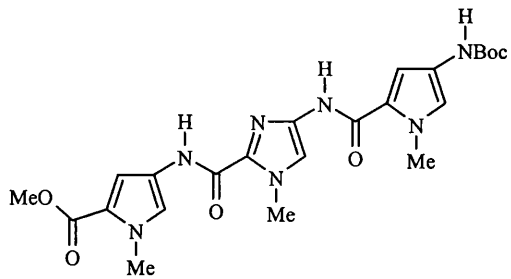

4-({4-[(4-*tert*-Butoxycarbonylamino-1-methyl-1*H*-pyrrole-2-carbonyl)-amino]-1-methyl-1*H*-imidazole-2-carbonyl}-amino)-1-methyl-1*H*-pyrrole-2-carboxylic acid methyl ester (103)

The Boc pyrrole-imidazole dimer (0.263 g, 0.70 mmol) was deprotected using 4M HCl in dioxane as described in general procedure C. The resulting residue was dissolved in dry DMF

(5 mL) and the Boc protected pyrrole acid (0.169 g, 0.70 mmol) was added and coupled as described in general procedure A (168 h). The product was purified using column chromatography (DCM:MeOH, 97:3) to yield an orange foam (0.256 g, 73%). ^{1}H-NMR (d_6-DMSO) (400 MHz) δ 1H-NMR (400 MHz) 10.15 (s, 1H, N-H) 10.08 (s, 1H, N-H) 9.09 (s, 1H, N-H) 7.52 (d, 1H, J = 1.5 Hz, Py-H) 7.20 (s, 1H, Im-H) 7.01 (d, 1H, J = 1.8 Hz, Py-H) 6.99 (d, 1H, J = 1.8 Hz, Py-H) 6.89 (d, 1H, J = 1.9 Hz, Py-H) 3.97 (s, 1H, N-CH_3) 3.93 (s, 1H, N-CH_3) 3.84 (s, 1H, N-CH_3) 3.73 (s, 3H, O-CH_3) 1.45 (s, 9H, Boc-H); LCMS (method 2) rt = 1.87 min; *m/z* (ES+) 500 (M+1).

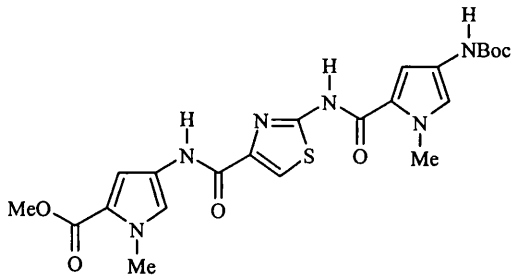

4-({2-[(4-*tert*-Butoxycarbonylamino-1-methyl-1*H*-pyrrole-2-carbonyl)-amino]-thiazole-4-carbonyl}-amino)-1-methyl-1*H*-pyrrole-2-carboxylic acid methyl ester (108)

The Boc pyrrole-thiazole dimer (0.399 g, 1.07 mmol) was deprotected using 4M HCl in dioxane as described in general procedure C. The resulting residue was dissolved in dry DMF (5 mL) and the Boc protected pyrrole acid (0.258 g, 1.07 mmol) was added and coupled as described in general procedure B (240 h) This yielded a brown foam 0.367 g, which was purified by column chromatography (silica gel, eluted with DCM 98%, MeOH 2%) (0.303 g, 56%). ^{1}H-NMR (d_6-DMSO) (400 MHz) δ 9.92 (s, 1H, N-H) 9.82 (s, 1H, N-H) 9.19 (s, 1H, N-H) 7.82 (s, 1H, Thz-H) 7.49 (d, 1H, J = 1.8 Hz, Py-H) 7.27 (m, 1H, Py-H) 7.05 (s, 1H, Py-H) 7.00 (d, 1H, J = 1.9 Hz, Py-H) 3.86 (s, 3H, N-CH_3) 3.83 (s, 3H, N-CH_3) 3.73 (s, 3H, O-CH_3) 1.46 (s, 9H, Boc-H); MS *m/z* (ES+) 503 (M+1).

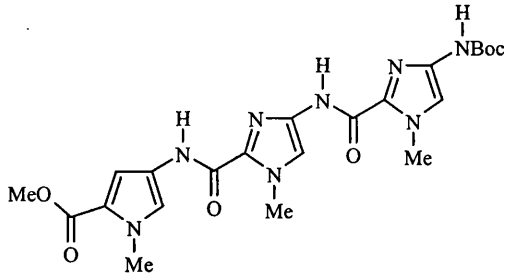

4-({4-[(4-*tert*-Butoxycarbonylamino-1-methyl-1*H*-imidazole-2-carbonyl)-amino]-1-methyl-1*H*-imidazole-2-carbonyl}-amino)-1-methyl-1*H*-pyrrole-2-carboxylic acid methyl ester (99)

The Boc pyrrole-imidazole dimer (0.263 g, 0.70 mmol) was deprotected using 4M HCl in dioxane as described in general procedure C. The resulting residue was dissolved in dry DMF (5 mL) and the Boc protected imidazole acid (0.169 g, 0.70 mmol) was added and coupled as described in general procedure A (168 h). The product was purified by column chromatography (DCM:MeOH, 98:2) to give a brown foam (0.303 g, 57%). ^{1}H-NMR (d_6-DMSO) (400 MHz) δ 10.55 (s, 1H, N-H) 9.62 (s, 1H, N-H) 9.25 (s, 1H, N-H) 7.56 (s, 1H, Im-H) 7.51 (s, 1H, Py-H) 7.28 (s, 1H, Im-H) 7.03 (s, 1H, Py-H) 4.00 (s, 3H, N-CH_3) 3.97 (s, 3H, N-CH_3) 3.84 (s, 3H, N-CH_3) 3.74 (s, 1H, O-CH_3) 1.45 (s, 9H, Boc-H); LCMS (method 1) rt = 3.58 min; *m/z* (ES+) 501 (M+1).

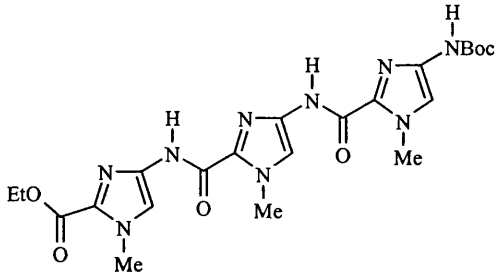

4-({4-[(4-*tert*-Butoxycarbonylamino-1-methyl-1*H*-imidazole-2-carbonyl)-amino]-1-methyl-1*H*-imidazole-2-carbonyl}-amino)-1-methyl-1*H*-imidazole-2-carboxylic acid ethyl ester (102)

The Boc imidazole dimer (0.253 g, 0.65 mmol) was deprotected using 4M HCl in dioxane as described in general procedure C. The resulting residue was dissolved in dry DMF (5 mL) and the Boc protected imidazole acid (0.150 g, 0.65 mmol) was added. The resulting solution was treated with EDCI (1.5 equiv.) and DMAP (2 equiv.) and coupled as described in general procedure A (192 h). The product was purified using column chromatography (DCM:MeOH, 98:2) to yield a brown foam (0.160 g, 48%). ^{1}H-NMR (d_6-DMSO) (400 MHz) δ 10.22 (s, 1H, N-H) 9.64 (s, 1H, N-H) 9.43 (s, 1H, N-H) 7.69 (s, 1H, Im-H) 7.62 (s, 1H, Im-H) 7.28 (s, 1H, Im-H) 4.30 (q, 2H, J = 7.0 Hz, OCH_2CH$_3$) 4.00 (s, 3H, N-CH$_3$) 3.97 (s, 3H, N-CH$_3$) 3.95 (s, 3H, N-CH$_3$) 1.46 (s, 9H, Boc-H) 1.31 (t, 1H, J = 7.1 Hz, OCH$_2$CH_3); LCMS (method 1) rt = 3.45 min; *m/z* (ES+) 516 (M+1).

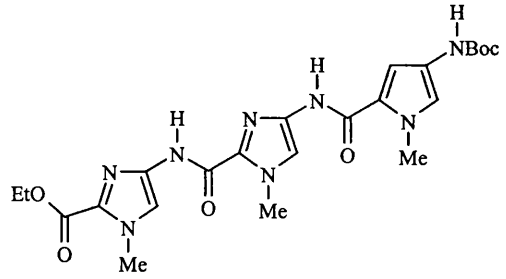

4-({4-[(4-*tert*-Butoxycarbonylamino-1-methyl-1*H*-pyrrole-2-carbonyl)-amino]-1-methyl-1*H*-imidazole-2-carbonyl}-amino)-1-methyl-1*H*-imidazole-2-carboxylic acid ethyl ester (110)

The Boc imidazole dimer (0.253 g, 0.65 mmol) was deprotected using 4M HCl in dioxane as described in general procedure C. The resulting residue was dissolved in dry DMF (5 mL) and the Boc protected pyrrole acid (0.156 g, 0.65 mmol) was added. The resulting solution was treated with EDCI (1.5 equiv.) and DMAP (2 equiv.) and coupled as described in general procedure A (192 h). The product was purified using column chromatography (DCM:MeOH, 97:3) to yield a brown foam (0.109 g, 32%). ^{1}H-NMR (d_6-DMSO) (400 MHz) δ 10.34 (s, 1H, N-H) 9.75 (s, 1H, N-H) 9.09 (s, 1H, N-H) 7.67 (s, 1H, Im-H) 7.59 (s, 1H, Im-H) 6.99 (s, 1H, Py-H) 6.91 (s, 1H, Py-H) 4.29 (dd, 2H, J = 7.0 Hz, J = 14.0 Hz, OCH_2CH$_3$) 3.98 (s, 3H, N-CH$_3$) 3.95 (s, 3H, N-CH$_3$) 3.82 (s, 3H, O-CH$_3$) 1.45 (s, 9H, Boc-H) 1.31 (t, 3H, J = 7.0 Hz, OCH$_2$CH_3); LCMS (method 2) rt = 1.87 min; *m/z* (ES+) 515 (M+1).

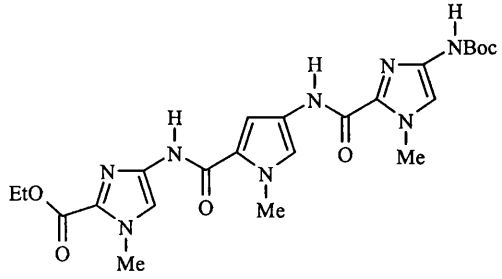

4-({4-[(4-*tert*-Butoxycarbonylamino-1-methyl-1*H*-pyrrole-2-carbonyl)-amino]-1-methyl-1*H*-pyrrole-2-carbonyl}-amino)-1-methyl-1*H*-imidazole-2-carboxylic acid ethyl ester (101)

The Boc imidazole-pyrrole dimer (0.200 g, 0.51 mmol) was deprotected using 4M HCl in dioxane as described in general procedure C. The resulting residue was dissolved in dry DMF (5 mL) and the Boc protected imidazole acid (0.123 g, 0.51 mmol) was added and coupled as described in general procedure A (18 h). The product was purified using column chromatography (DCM:MeOH, 97:3) to yield a brown foam (0.220 g, 84%). ^{1}H-NMR (d_6-DMSO) (400 MHz) δ 10.70 (s, 1H, N-H) 9.77 (s, 1H, N-H) 9.39 (s, 1H, N-H) 7.95 (s, 1H, Im-H) 7.67 (s, 1H, Im-H) 7.39 (d, 1H, J = 1.8 Hz, Py-H) 7.19 (d, 1H, J = 1.9 Hz, Py-H) 4.28 (q, 2H, J = 7.1 Hz, OCH_2CH$_3$) 3.94 (s, 6H, N-CH$_3$) 3.86 (s, 3H, N-CH$_3$) 1.46 (s, 9H, Boc-H) 1.30 (t, 1H, J = 7.1 Hz, OCH$_2$CH_3); LCMS (method 2) rt = 1.83 min; *m/z* (ES+) 515 (M+1).

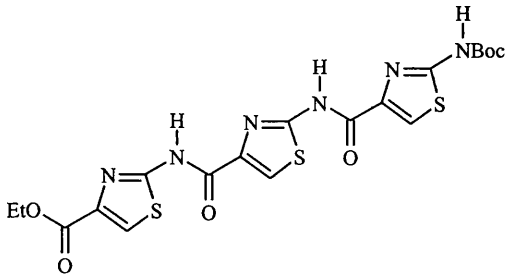

2-({2-[(2-*tert*-Butoxycarbonylamino-thiazole-4-carbonyl)-amino]-thiazole-4-carbonyl}-amino)-thiazole-4-carboxylic acid ethyl ester(107)

The Boc thiazole dimer (0.281 g, 0.71 mmol) was deprotected using 95% TFA as described in general procedure D. The resulting residue was dissolved in dry DMF (5 mL) and the Boc

protected thiazole acid (0.172 g, 0.71 mmol) was added and coupled as described in general procedure B (264 h). The product was purified using column chromatography (DCM:MeOH, 97:3) to yield a yellow foam (0.193 g, 52%). ^{1}H-NMR (d_6-DMSO) (400 MHz) 12.50 (s, 1H, N-H) 12.40 (s, 1H, N-H) 11.86 (s, 1H, N-H) 8.32 (s, 1H, Thz-H) 8.10 (s, 1H, Thz-H) 8.04 (s, 1H, Thz-H) 4.29 (q, 2H, J = 7.0 Hz, OCH_2CH$_3$) 1.47 (s, 9H, Boc-H) 1.30 (t, 3H, J = 7.1 Hz, OCH$_2$CH_3); LCMS (method 1) rt = 3.88 min; *m/z* (ES+) 525 (M+1).

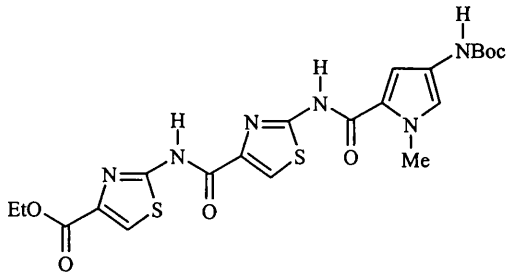

2-({2-[(4-*tert*-Butoxycarbonylamino-1-methyl-1*H*-pyrrole-2-carbonyl)-amino]-thiazole-4-carbonyl}-amino)-thiazole-4-carboxylic acid ethyl ester (111)

The Boc thiazole dimer (0.281 g, 0.71 mmol) was deprotected using 95% TFA as described in general procedure D. The resulting residue was dissolved in dry DMF (5 mL) and the Boc protected pyrrole acid (0.170 g, 0.71 mmol) was added and coupled as described in general procedure B (264 h). The product was purified using column chromatography (DCM:MeOH, 97:3) to yield a yellow foam (0.210 g, 57%). ^{1}H-NMR (d_6-DMSO) (400 MHz) 12.50 (s, 1H, N-H) 12.40 (s, 1H, N-H) 9.19 (s, 1H, N-H) 8.35 (s, 1H, Thz-H) 8.08 (s, 1H, Thz-H) 7.71 (s, 1H, Py-H) 7.27 (s, 1H, Py-H) 4.29 (q, 2H, J=7.0 Hz, OCH_2CH$_3$) 3.87 (s, 3H, N-CH$_3$) 1.46 (s, 9H, Boc-H) 1.30 (t, 3H, J=7.1 Hz, OCH$_2$CH_3); LCMS (method 1) rt = 3.57 min; *m/z* (ES-) 519 (M-1).

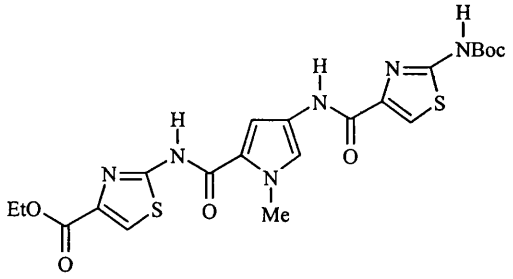

2-({4-[(2-*tert*-Butoxycarbonylamino-thiazole-4-carbonyl)-amino]-1-methyl-1*H*-pyrrole-2-carbonyl}-amino)-thiazole-4-carboxylic acid ethyl ester (106)

The Boc thiazole-pyrrole dimer (0.250 g, 0.64 mmol) was deprotected using 4M HCl in dioxane as described in general procedure C. The resulting residue was dissolved in dry DMF (5 mL) and the Boc protected thiazole acid (0.155 g, 0.64 mmol) was added and coupled as described in general procedure B (18 h). The product was purified using column chromatography (DCM:MeOH, 97:3) to yield a yellow foam (0.282 g, 86%). ^{1}H-NMR (d_6-DMSO) (400 MHz) δ 11.63 (s, 1H, N-H) 11.10 (s, 1H, N-H) 9.68 (s, 1H, N-H) 8.04 (s, 1H, Thz-H) 7.84 (s, 1H, Thz-H) 7.55 (d, 1H, J = 1.5 Hz, Py-H) 7.41 (d, 1H, J = 1.3 Hz, Py-H) 4.29 (q, 2H, J = 7.1 Hz, OC*H*$_2$CH$_3$) 3.92 (s, 3H, N-CH$_3$) 1.51 (s, 9H, Boc-H) 1.31 (t, 3H, J = 7.1 Hz, OCH$_2$C*H*$_3$); LCMS (method 1) rt = 3.05 min; *m/z* (ES+) 521 (M+1).

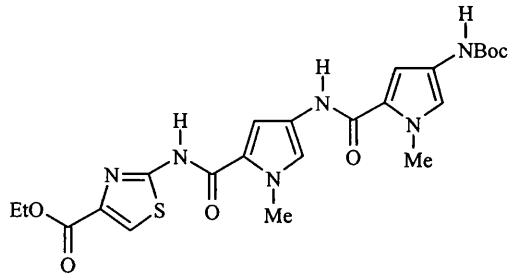

2-({4-[(4-*tert*-Butoxycarbonylamino-1-methyl-1*H*-pyrrole-2-carbonyl)-amino]-1-methyl-1*H*-pyrrole-2-carbonyl}-amino)-thiazole-4-carboxylic acid ethyl ester (105)

The Boc thiazole-pyrrole dimer (0.200 g, 0.51 mmol) was deprotected using 4M HCl in dioxane as described in general procedure C. The resulting residue was dissolved in dry DCM (5 mL) and the Boc protected pyrrole acid (0.122 g, 0.51 mmol) was added and coupled

as described in general procedure B (48 h). The product was purified using column chromatography (DCM:MeOH, 98:2) to yield an off-white foam (0.210 g, 80%). ^{1}H-NMR (d_6-DMSO) (400 MHz) δ 9.93 (s, 2H, N-H) 9.08 (s, 1H, N-H) 8.03 (s, 1H, Thz-H) 7.47 (s, 1H, Py-H) 7.37 (s, 1H, Py-H) 6.90 (s, 1H, Py-H) 6.86 (s, 1HPy-H) 4.29 (q, 2H, J = 7.1 Hz, OCH_2CH$_3$) 3.89 (s, 3H, N-CH$_3$) 3.81 (s, 3H, N-CH$_3$) 1.46 (s, 9H, Boc-H) 1.31 (t, 3H, J = 7.1 Hz, OCH$_2$CH_3); LCMS (method 1) rt = 3.65 min; *m/z* (ES+) 516 (M+1).

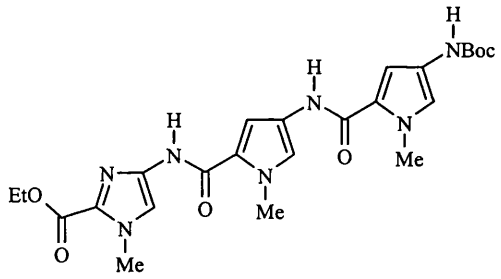

4-({4-[(4-*tert*-Butoxycarbonylamino-1-methyl-1*H*-pyrrole-2-carbonyl)-amino]-1-methyl-1*H*-pyrrole-2-carbonyl}-amino)-1-methyl-1*H*-imidazole-2-carboxylic acid ethyl ester (100)

The Boc imidazole-pyrrole dimer (0.200 g, 0.51 mmol) was deprotected using 4M HCl in dioxane as described in general procedure C. The resulting residue was dissolved in dry DMF (5 mL) and the Boc protected pyrrole acid (0.123 g, 0.51 mmol) was added and coupled as described in general procedure A (18 h). This yielded the product as an orange foam (0.240 g, 91%). ^{1}H-NMR (d_6-DMSO) (400 MHz) δ 10.71 (s, 1H, N-H) 9.86 (s, 1H, N-H) 9.08 (s, 1H, N-H) 7.95 (s, 1H, Im-H) 7.67 (s, 1H, Py-H) 7.33 (d, 1H, J = 1.8 Hz, Py-H) 7.10 (d, 1H, J = 1.8 Hz, Py-H) 6.89 (s, 1H, Py-H) 4.28 (q, 2H, J = 7.1 Hz, OCH_2CH$_3$) 3.94 (s, 3H, N-CH$_3$) 3.85 (s, 1H, N-CH$_3$) 3.80 (s, 1H, N-CH$_3$) 1.46 (s, 9H, Boc-H) 1.30 (t, 3H, J = 7.1 Hz, OCH$_2$CH_3); LCMS (method 1) rt = 2.02 min; *m/z* (ES+) 517 (M+1).

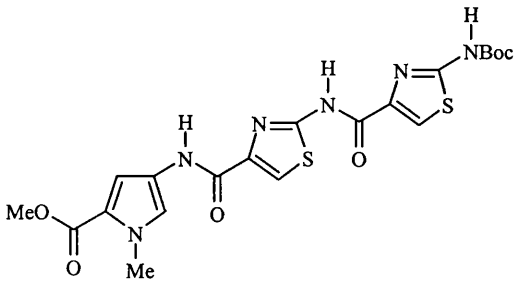

4-({2-[(4-*tert*-Butoxycarbonylamino-thiazole-4-carbonyl)-amino]-thiazole-4-carbonyl}-amino)-1-methyl-1*H*-pyrrole-2-carboxylic acid methyl ester (104)

The Boc pyrrole-thiazole dimer (0.399g, 1.074 mmol) was deprotected using 4M HCl in dioxane as described in general procedure C. The resulting residue was dissolved in dry DMF (5 mL) and the Boc protected thiazole acid (0.262 g, 1.074 mmol) was added and coupled as described in general procedure B (264 h). The product was purified using column chromatography (DCM:MeOH, 98:2) to yield a yellow foam (0.261 g, 48%).^{1}H-NMR (d_6-DMSO) (400 MHz) δ 11.60 (s, 1H, N-H) 11.12 (s, 1H, N-H) 10.27 (s, 1H, N-H) 8.22 (s, 1H, Thz-H) 7.89 (s, 1H, Thz-H) 7.49 (d, 1H, J = 1.8 Hz, Py-H) 7.00 (d, 1H, J = 1.9 Hz, Py-H) 3.86 (s, 3H, N-CH_3) 3.73 (s, 3H, O-CH_3) 1.46 (s, 9H, Boc-H); LCMS (method 1) rt = 3.59 min; *m/z* (ES+) 507 (M+1).

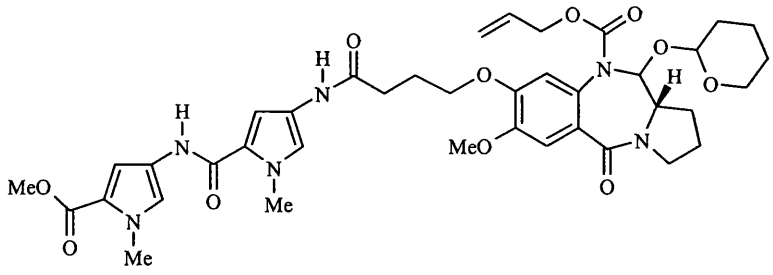

(11aS)-8-{3-[2-(5-methoxycarbonyl-1-methyl-1*H*-pyrrol-3-ylcarbamoyl)-1-methyl-1*H*-pyrrol-3-ylcarbamoyl]-propoxy}-7-methoxy-5-oxo-11-(tetrahydropyran-2-yloxy)-2,3,11,11a-tetrahydro-1*H*,5*H*-pyrrolo[2,1-*c*][1,4]benzodiazepine-10-carboxylic acid allyl ester (112)

The Boc pyrrole-pyrrole dimer (0.100 g, 0.266 mmol) was deprotected using 4M HCl in dioxane as described in general procedure C. The resulting residue was dissolved in dry DCM (5 mL) and the Alloc-THP-PBD acid (0.138 g, 0.266 mmol), EDCI (0.102 g, 2 equiv.) and DMAP (0.081 g, 2.5 equiv.) were added. The reaction mixture was stirred at room temperature for 48 h then diluted with EtOAc (50 mL) and washed with 1M HCl solution (3 × 50 mL), saturated $NaHCO_3$ solution (3 × 50 mL), and dried over $MgSO_4$. Concentration *in vacuo* yielded a brown foam (0.164 g. 79%). LCMS (method 1) rt = 3.42 min; *m/z* (ES^+) 777 (M+1).

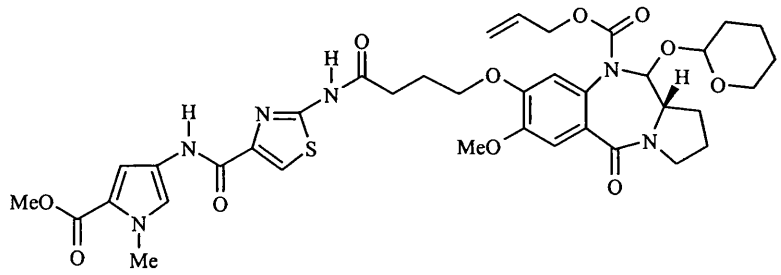

(11aS)-8-{3-[4-(5-methoxycarbonyl-1-methyl-1*H*-pyrrol-3-ylcarbamoyl)-thiazol-2-ylcarbamoyl]-propoxy}-7-methoxy-5-oxo-11-(tetrahydropyran-2-yloxy)-2,3,11,11a-tetrahydro-1*H*,5*H*-pyrrolo[2,1-*c*][1,4]benzodiazepine-10-carboxylic acid allyl ester (114)

The Boc pyrrole-thiazole dimer (0.150 g, 0.40 mmol) was deprotected using 4M HCl in dioxane as described in general procedure C. The resulting residue was dissolved in dry DCM (5 mL) and the Alloc-THP-PBD acid (0.205 g, 0.40 mmol) was added and coupled as described in general procedure B to yield a yellow foam (0.208 g, 66%). LCMS (method 1) rt = 3.35 min; *m/z* (ES+) 781 (M+1).

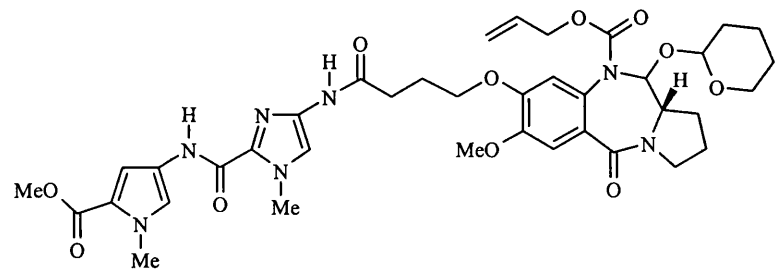

(11aS)-8-{3-[2-(5-methoxycarbonyl-1-methyl-1*H*-pyrrol-3-ylcarbamoyl)-1-methyl-1*H*-imidazol-4-ylcarbamoyl]-propoxy}-7-methoxy-5-oxo-11-(tetrahydropyran-2-yloxy)-2,3,11,11a-tetrahydro-1*H*,5*H*-pyrrolo[2,1-*c*][1,4]benzodiazepine-10-carboxylic acid allyl ester (113)

The Boc pyrrole-imidazole dimer (0.100 g, 0.27 mmol) was deprotected using 4M HCl in dioxane as described in general procedure C. The resulting residue was dissolved in dry DCM (5 mL) and the Alloc-THP-PBD acid (0.137 g, 0.27 mmol) was added and coupled as

described in general procedure B to yield a brown foam (0.151 g, 72%). LCMS (method 1) rt = 3.47 min; *m/z* (ES+) 778 (M+1).

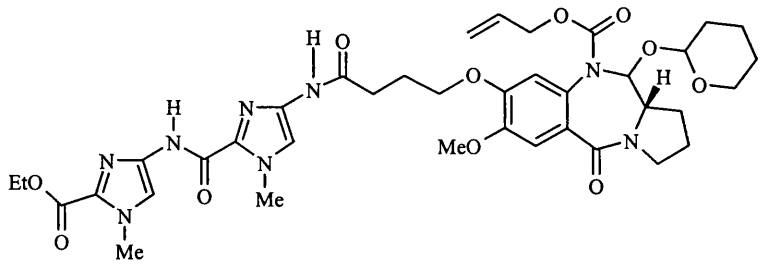

(11aS)-8-{3-[2-(2-Ethoxycarbonyl-1-methyl-1H-imidazol-4-ylcarbamoyl)-1-methyl-1*H*-imidazol-4-ylcarbamoyl]-propoxy}-7-methoxy-5-oxo-11-(tetrahydropyran-2-yloxy)-2,3,11,11a-tetrahydro-1*H*,5*H*-pyrrolo[2,1-*c*][1,4]benzodiazepine-10-carboxylic acid allyl ester (116)

The Boc imidazole dimer (0.130 g, 0.33 mmol) was deprotected using 4M HCl in dioxane as described in general procedure C. The resulting residue was dissolved in dry DCM (5 mL) and the Alloc-THP-PBD acid (0.172 g, 0.33 mmol) was added and coupled as described in general procedure A to yield a brown foam (0.090 g, 34%). LCMS (method 1) rt = 3.38 min; *m/z* (ES+) 793 (M+1).

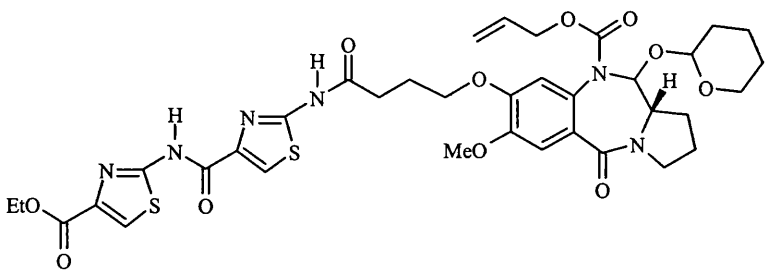

(11aS)-8-{3-[4-(4-Ethoxycarbonyl-thiazol-2-ylcarbamoyl)-thiazol-2-ylcarbamoyl]-propoxy}-7-methoxy-5-oxo-11-(tetrahydropyran-2-yloxy)-2,3,11,11a-tetrahydro-1*H*,5*H*-pyrrolo[2,1-*c*][1,4]benzodiazepine-10-carboxylic acid allyl ester (118)

The Boc thiazole dimer (0.156 g, 0.39 mmol) was deprotected using 95% TFA as described in general procedure D. The resulting residue was dissolved in dry DCM (5 mL) and the Alloc-THP-PBD acid (0.202 g, 0.39 mmol) was added and coupled as described in general procedure B to yield a yellow foam (0.102 g, 34%). LCMS (method 1) rt = 3.58 min; *m/z* (ES+) 799 (M+1).

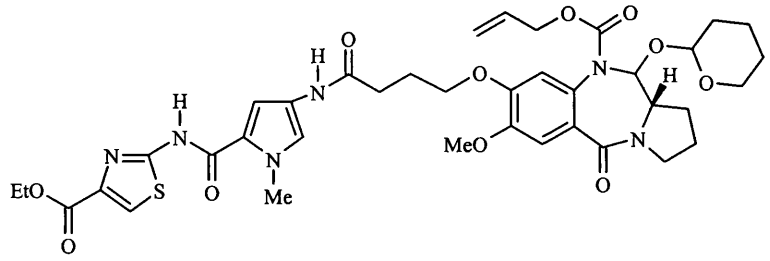

(11aS)-8-{3-[5-(4-Ethoxycarbonyl-thiazol-2-ylcarbamoyl)-1-methyl-1*H*-pyrrol-3-ylcarbamoyl]-propoxy}-7-methoxy-5-oxo-11-(tetrahydropyran-2-yloxy)-2,3,11,11a-tetrahydro-1*H*,5*H*-pyrrolo[2,1-*c*][1,4]benzodiazepine-10-carboxylic acid allyl ester (117)

The Boc pyrrole-thiazole dimer (0.150 g, 0.38 mmol) was deprotected using 4M HCl in dioxane as described in general procedure C. The resulting residue was dissolved in dry DCM (5 mL) and the Alloc-THP-PBD acid (0.197 g, 0.38 mmol) was added and coupled as

described in general procedure B to yield a yellow foam (0.274 g, 90%). LCMS (method 1) rt = 3.45 min; *m/z* (ES+) 795 (M+1).

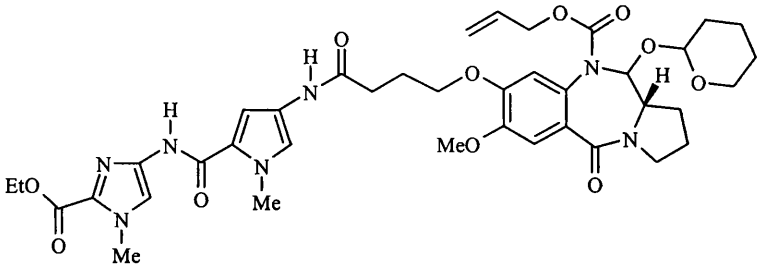

(11aS)-8-{3-[5-(2-Ethoxycarbonyl-1-methyl-1H-imidazol-4-ylcarbamoyl)-1-methyl-1*H*-pyrrol-3-ylcarbamoyl]-propoxy}-7-methoxy-5-oxo-11-(tetrahydropyran-2-yloxy)-2,3,11,11a-tetrahydro-1*H*,5*H*-pyrrolo[2,1-*c*][1,4]benzodiazepine-10-carboxylic acid allyl ester (115)

The Boc imidazole-pyrrole dimer (0.130 g, 0.33 mmol) was deprotected using 4M HCl in dioxane as described in general procedure C. The resulting residue was dissolved in dry DCM (5 mL) and the Alloc-THP-PBD acid (0.172 g, 0.33 mmol) was added and coupled as described in general procedure B to yield a brown foam (0.220 g, 84%). LCMS (method 1) rt = 3.33 min; *m/z* (ES+) 792 (M+1).

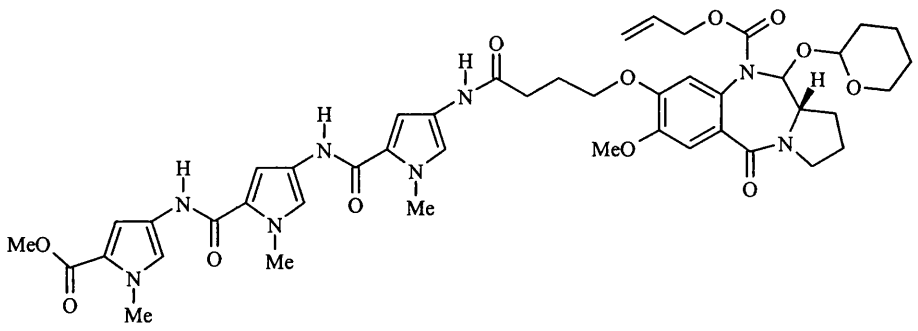

(11aS)-8-(3-{2-[5-(5-methoxycarbonyl-1-methyl-1*H*-pyrrol-3-ylcarbamoyl)-1-methyl-1*H*-pyrrol-3-ylcarbamoyl]-1-methyl-1*H*-pyrrol-3-ylcarbamoyl}-propoxy)-7-methoxy-5-oxo-11-(tetrahydropyran-2-yloxy)-2,3,11,11a-tetrahydro-1*H*,5*H*-pyrrolo[2,1-*c*][1,4]benzo diazepine-10-carboxylic acid allyl ester (119)

The Boc pyrrole-pyrrole-imidazole trimer (0.100 g, 0.201 mmol) was deprotected using 4M HCl in dioxane as described in general procedure C. The resulting residue was dissolved in dry DCM (5 mL) and the Alloc-THP-PBD acid (0.104 g, 0.201 mmol), EDCI (0.077 g, 2 equiv.) and DMAP (0.061 g, 2.5 equiv.) were added. The reaction mixture was stirred for 40 h at room temperature then diluted with EtOAc (50 mL) and washed with 1M HCl solution (3 × 50 mL), saturated $NaHCO_3$ solution (3 × 50 mL), and dried over $MgSO_4$. Concentration *in vacuo* yielded a brown foam (0.173 g. 96%). LCMS (method 1) rt = 3.47 min; *m/z* (ES+) 899 (M+1).

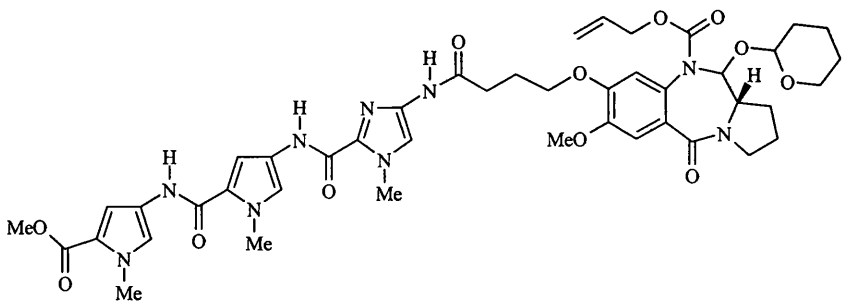

(11aS)-8-(3-{2-[5-(5-methoxycarbonyl-1-methyl-1*H*-pyrrol-3-ylcarbamoyl)-1-methyl-1*H*-pyrrol-3-ylcarbamoyl]-1-methyl-1*H*-imidazol-4-ylcarbamoyl}-propoxy)-7-methoxy-5-oxo-11-(tetrahydropyran-2-yloxy)-2,3,11,11a-tetrahydro-1*H*,5*H*-pyrrolo[2,1-*c*][1,4]benzo diazepine-10-carboxylic acid allyl ester (120)

The Boc pyrrole-pyrrole-imidazole trimer (0.250 g, 0.50 mmol) was deprotected using 4M HCl in dioxane as described in general procedure C. The resulting residue was dissolved in dry DCM (5 mL) and the Alloc-THP-PBD acid (0.259 g, 0.50 mmol) was added and coupled as described in general procedure A to yield a brown foam (0.385 g, 86%). LCMS (method 1) rt = 3.33 min; *m/z* (ES+) 900 (M+1).

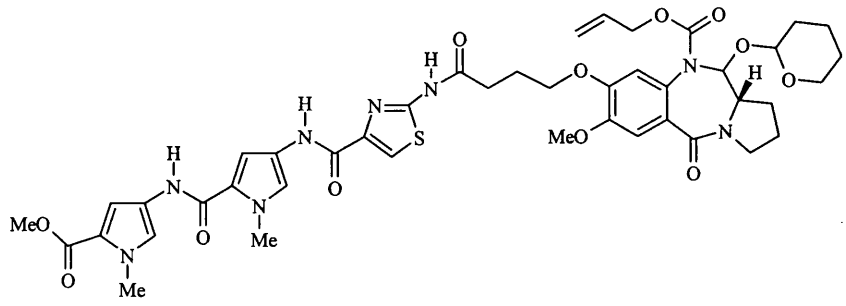

(11aS)-8-(3-{4-[5-(5-methoxycarbonyl-1-methyl-1*H*-pyrrol-3-ylcarbamoyl)-1-methyl-1*H*-pyrrol-3-ylcarbamoyl]-thiazol-2-ylcarbamoyl}-propoxy)-7-methoxy-5-oxo-11-(tetrahydropyran-2-yloxy)-2,3,11,11a-tetrahydro-1*H*,5*H*-pyrrolo[2,1-*c*][1,4]benzo diazepine-10-carboxylic acid allyl ester (131)

The Boc pyrrole-pyrrole-thiazole trimer (0.200 g, 0.40 mmol) was deprotected using 4M HCl in dioxane as described in general procedure C. The resulting residue was dissolved in dry

DCM (5 mL) and the Alloc-THP-PBD acid (0.206 g, 0.40 mmol) was added and coupled as described in general procedure B to yield a yellow foam (0.142 g ,68%). LCMS (method 2) rt = 2.00 min; *m/z* (ES+) 521 (M+1).

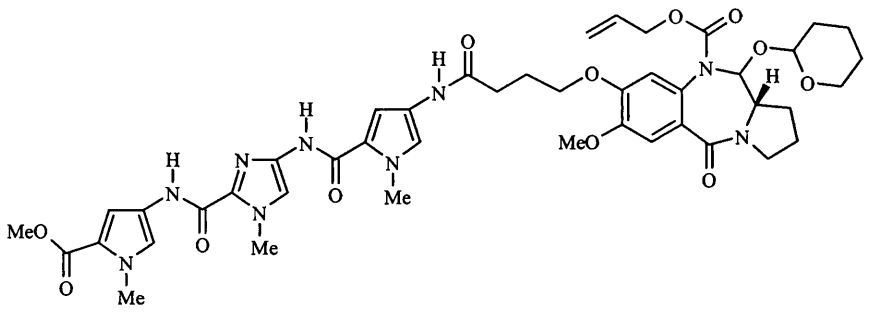

(11aS)-8-(3-{5-[2-(5-methoxycarbonyl-1-methyl-1*H*-pyrrol-3-ylcarbamoyl)-1-methyl-1*H*-imidazol-4-ylcarbamoyl]-1-methyl-1*H*-pyrrol-3-ylcarbamoyl}-propoxy)-7-methoxy-5-oxo-11-(tetrahydropyran-2-yloxy)-2,3,11,11a-tetrahydro-1*H*,5*H*-pyrrolo[2,1-*c*][1,4]benzodiazepine-10-carboxylic acid allyl ester (125)

The Boc pyrrole-imidazole-pyrrole trimer (0.163 g, 0.33 mmol) was deprotected using 4M HCl in dioxane as described in general procedure C. The resulting residue was dissolved in dry DCM (5 mL) and the Alloc-THP-PBD acid (0.169 g, 0.33 mmol) was added and coupled as described in general procedure A to yield a brown foam (0.283 g, 95%). LCMS (method 1) rt = 3.47 min; *m/z* (ES+) 900 (M+1).

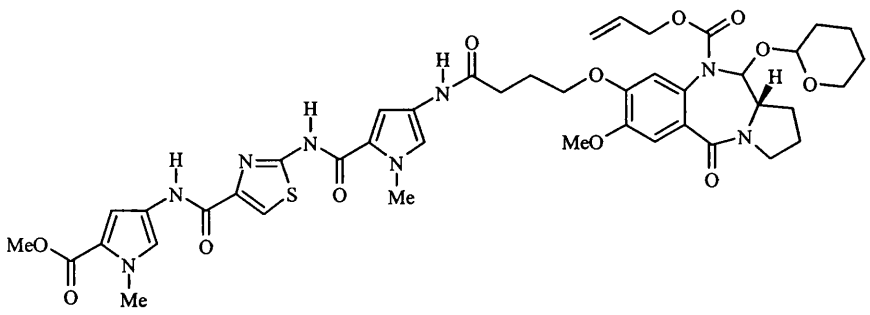

(11aS)-8-(3-{5-[4-(5-methoxycarbonyl-1-methyl-1*H*-pyrrol-3-ylcarbamoyl)-thiazol-2-ylcarbamoyl]-1-methyl-1*H*-pyrrol-3-ylcarbamoyl}-propoxy)-7-methoxy-5-oxo-11-(tetrahydropyran-2-yloxy)-2,3,11,11a-tetrahydro-1*H*,5*H*-pyrrolo[2,1-*c*][1,4]benzo diazepine-10-carboxylic acid allyl ester (130)

The Boc pyrrole-thiazole-pyrrole trimer (0.103 g, 0.20 mmol) was deprotected using 4M HCl in dioxane as described in general procedure C. The resulting residue was dissolved in dry DCM (5 mL) and the Alloc-THP-PBD acid (0.100 g, 0.20 mmol) was added and coupled as described in general procedure B to yield a yellow foam (0.135 g, 75%). LCMS (method 1) rt = 3.55 min; *m/z* (ES+) 903 (M+1).

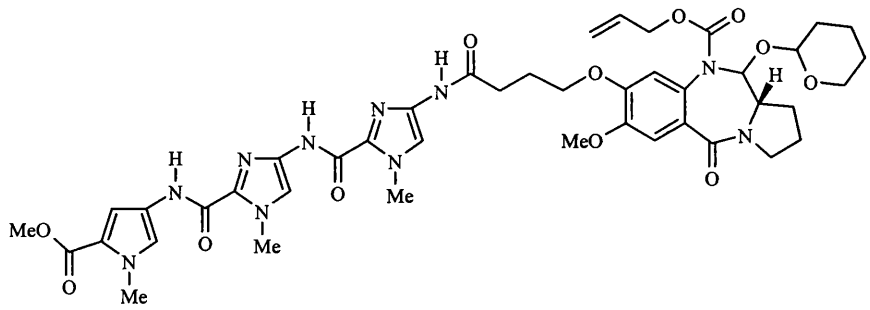

(11aS)-8-(3-{2-[2-(5-methoxycarbonyl-1-methyl-1*H*-pyrrol-3-ylcarbamoyl)-1-methyl-1*H*-imidazol-4-ylcarbamoyl]-1-methyl-1*H*-imidazol-4-ylcarbamoyl}-propoxy)-7-methoxy-5-oxo-11-(tetrahydropyran-2-yloxy)-2,3,11,11a-tetrahydro-1*H*,5*H*-pyrrolo[2,1-*c*][1,4]benzo diazepine-10-carboxylic acid allyl ester (121)

The Boc pyrrole-imidazole-imidazole trimer (0.060 g, 0.12 mmol) was deprotected using 4M HCl in dioxane as described in general procedure C. The resulting residue was dissolved in

dry DCM (5 mL) and the Alloc-THP-PBD acid (0.063 g, 0.12 mmol) was added and coupled as described in general procedure B to yield a yellow foam (0.102 g, 94%). LCMS (method 1) rt = 3.42 min; *m/z* (ES+) 901 (M+1).

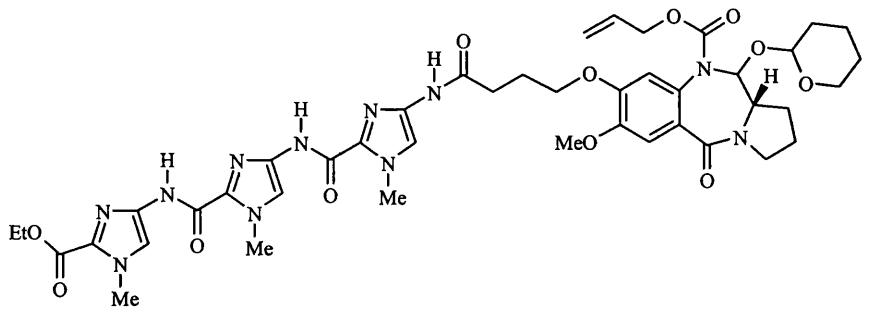

(11aS)-8-(3-{2-[2-(2-ethoxycarbonyl-1-methyl-1*H*-imidazol-4-ylcarbamoyl)-1-methyl-1*H*-imidazol-4-ylcarbamoyl]-1-methyl-1*H*-imidazol-4-ylcarbamoyl}-propoxy)-7-methoxy-5-oxo-11-(tetrahydropyran-2-yloxy)-2,3,11,11a-tetrahydro-1*H*,5*H*-pyrrolo[2,1-*c*][1,4]benzodiazepine-10-carboxylic acid allyl ester (124)

The Boc imidazole trimer (0.100 g, 0.19 mmol) was deprotected using 4M HCl in dioxane as described in general procedure C. The resulting residue was dissolved in dry DCM (5 mL) and the Alloc-THP-PBD acid (0.100 g, 0.19 mmol) was added and coupled as described in general procedure A to yield a brown foam (0.146 g, 78%). LCMS (method 1) rt = 3.48 min; *m/z* (ES+) 916 (M+1).

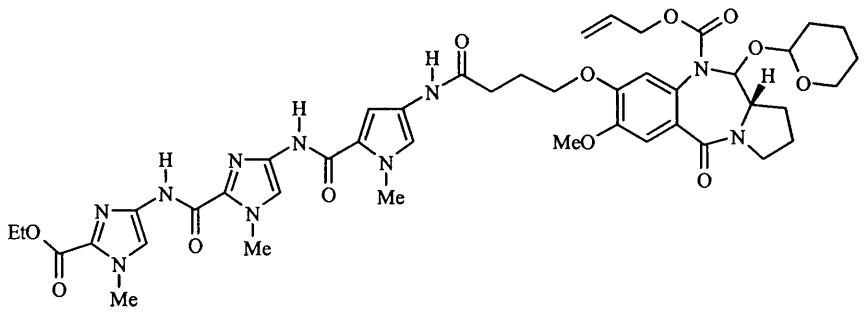

(11aS)-8-(3-{5-[2-(2-ethoxycarbonyl-1-methyl-1*H*-imidazol-4-ylcarbamoyl)-1-methyl-1*H*-imidazol-4-ylcarbamoyl]-1-methyl-1*H*-pyrrol-3-ylcarbamoyl}-propoxy)-7-methoxy-5-oxo-11-(tetrahydropyran-2-yloxy)-2,3,11,11a-tetrahydro-1*H*,5*H*-pyrrolo[2,1-*c*][1,4] benzodiazepine-10-carboxylic acid allyl ester (132)

The Boc imidazole-imidazole-pyrrole trimer (0.100 g, 0.20 mmol) was deprotected using 4M HCl in dioxane as described in general procedure C. The resulting residue was dissolved in dry DCM (5 mL) and the Alloc-THP-PBD acid (0.101 g, 0.20 mmol) was added and coupled as described in general procedure A to yield a brown foam (0.158 g, 86%). LCMS (method 1) rt = 3.22 min; *m/z* (ES+) 917 (M+1).

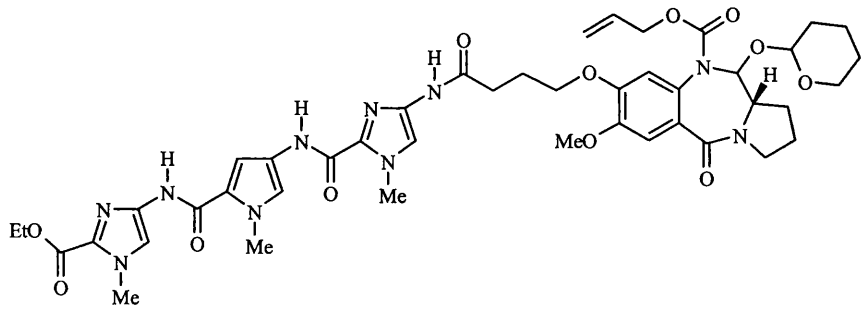

(11aS)-8-(3-{2-[5-(2-ethoxycarbonyl-1-methyl-1*H*-imidazol-4-ylcarbamoyl)-1-methyl-1*H*-pyrrol-3-ylcarbamoyl]-1-methyl-1*H*-imidazol-4-ylcarbamoyl}-propoxy)-7-methoxy-5-oxo-11-(tetrahydropyran-2-yloxy)-2,3,11,11a-tetrahydro-1*H*,5*H*-pyrrolo[2,1-*c*][1,4] benzodiazepine-10-carboxylic acid allyl ester (123)

The Boc imidazole-pyrrole-imidazole trimer (0.100 g, 0.20 mmol) was deprotected using 4M HCl in dioxane as described in general procedure C. The resulting residue was dissolved in

dry DCM (5 mL) and the Alloc-THP-PBD acid (0.101 g, 0.20 mmol) was added and coupled as described in general procedure A to yield a brown foam (0.131 g,72%). LCMS (method 1) rt = 3.46 min; *m/z* (ES+) 915 (M+1).

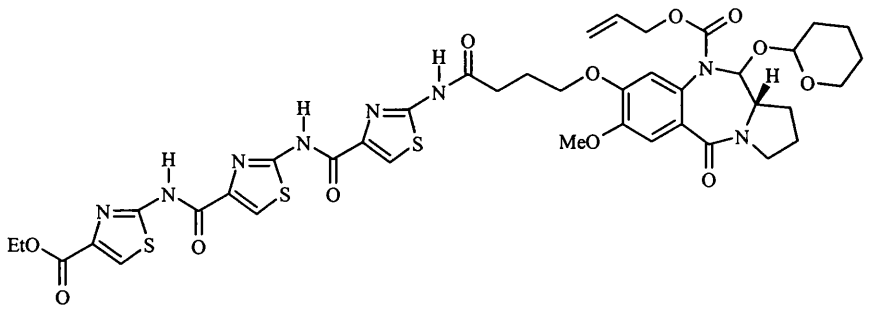

(11aS)-8-(3-{4-[4-(4-ethoxycarbonyl-thiazol-2-ylcarbamoyl)-thiazol-2-ylcarbamoyl]-thiazol-2-ylcarbamoyl}-propoxy)-7-methoxy-5-oxo-11-(tetrahydropyran-2-yloxy)-2,3,11,11a-tetrahydro-1*H*,5*H*-pyrrolo[2,1-*c*][1,4]benzodiazepine-10-carboxylic acid allyl ester (129)

The Boc thiazole trimer (0.163 g, 0.31 mmol) was deprotected using 4M HCl in dioxane as described in general procedure C. LCMS analysis showed partial Boc deprotection, therefore the mixture was treated with DCM:TFA:H_2O (50%:47.5%:2.5%) and allowed to stir for 2 hours at room temperature. The reaction mixture was concentrated *in vacuo* and DCM (20 mL) was added. The solution was washed with saturated $NaHCO_3$ solution (3 x 30 mL). The combined aqueous layers were filtered to collect the precipitated thiazole amine, which was washed with deionised water then dried under vacuum. The organic layers were combined and dried using $MgSO_4$. Concentration *in vacuo* afforded further amine which was dried under vacuum. The aqueous layer was filtered under vacuum to collect additional precipitated thiazole trimer amine. Alloc-THP-PBD acid (0.161 g, 0.31 mmol) was added to a solution of the thiazole trimer in dry DCM (5 mL) and DMF (1 mL) and coupled as described in general procedure B to yield a brown oil (0.208 g, 73%). LCMS (method 1) rt = 3.92 min; *m/z* (ES+) 925 (M+1).

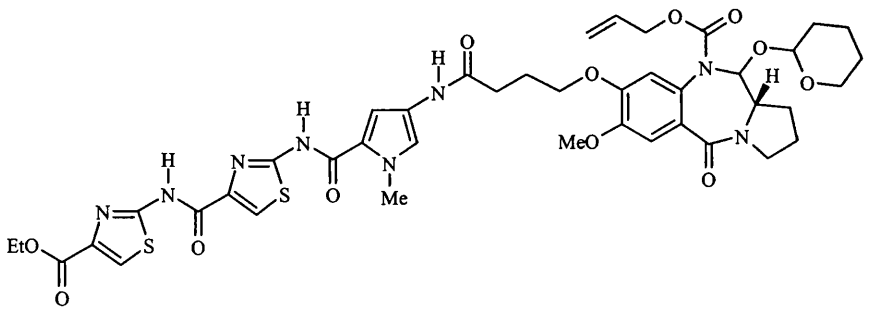

(11aS)-8-(3-{5-[4-(4-ethoxycarbonyl-thiazol-2-ylcarbamoyl)-thiazol-2-ylcarbamoyl]-1-methyl-1*H*-pyrrol-3-ylcarbamoyl}-propoxy)-7-methoxy-5-oxo-11-(tetrahydropyran-2-yloxy)-2,3,11,11a-tetrahydro-1*H*,5*H*-pyrrolo[2,1-*c*][1,4]benzodiazepine-10-carboxylic acid allyl ester (133)

The Boc thiazole-thiazole-pyrrole trimer (0.100 g, 0.19 mmol) was deprotected using 4M HCl in dioxane as described in general procedure C. The resulting residue was dissolved in dry DCM (5 mL) and the Alloc-THP-PBD acid (0.099 g, 0.19 mmol) was added and coupled as described in general procedure B to yield a brown foam (0.160 g, 91%). LCMS (method 1) rt = 3.62 min; *m/z* (ES+) 921 (M+1).

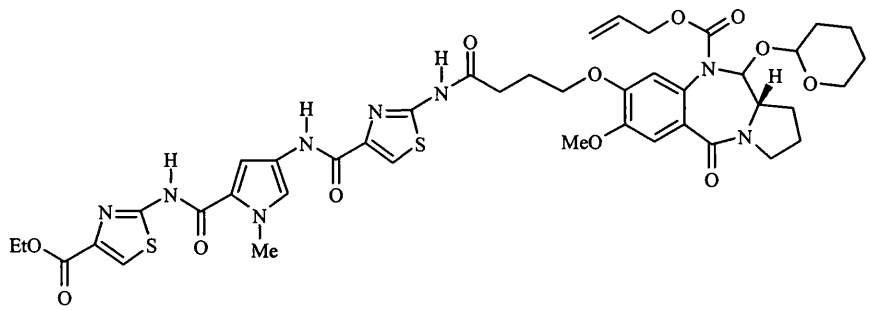

(11aS)-8-(3-{4-[5-(4-ethoxycarbonyl-thiazol-2-ylcarbamoyl)-1-methyl-1*H*-pyrrol-3-ylcarbamoyl]-thiazol-2-ylcarbamoyl}-propoxy)-7-methoxy-5-oxo-11-(tetrahydropyran-2-yloxy)-2,3,11,11a-tetrahydro-1*H*,5*H*-pyrrolo[2,1-*c*][1,4]benzodiazepine-10-carboxylic acid allyl ester (128)

The Boc thiazole-pyrrole-thiazole trimer (0.100 g, 0.19 mmol) was deprotected using 4M HCl in dioxane as described in general procedure C. The resulting residue was dissolved in dry

DCM (5 mL) and the Alloc-THP-PBD acid (0.100 g, 0.19 mmol) was added and coupled as described in general procedure B to yield a yellow foam (0.148 g, 84%). LCMS (method 1) rt = 3.65 min; *m/z* (ES+/-) 921 (M+1).

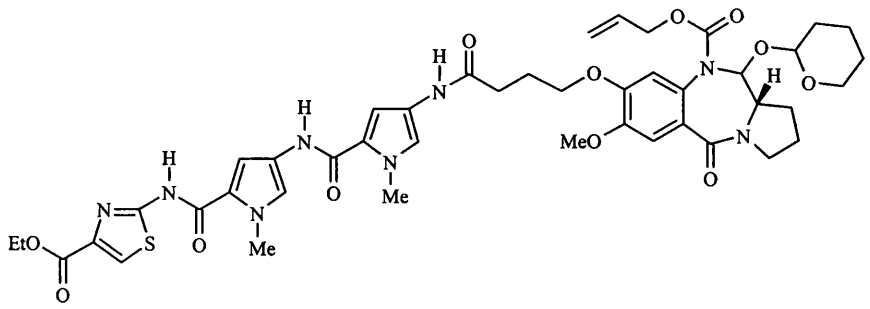

(11aS)-8-(3-{5-[5-(4-ethoxycarbonyl-thiazol-2-ylcarbamoyl)-1-methyl-1*H*-pyrrol-3-ylcarbamoyl]-1-methyl-1*H*-pyrrol-3-ylcarbamoyl}-propoxy)-7-methoxy-5-oxo-11-(tetrahydropyran-2-yloxy)-2,3,11,11a-tetrahydro-1*H*,5*H*-pyrrolo[2,1-*c*][1,4]benzodiazepine-10-carboxylic acid allyl ester (127)

The Boc thiazole-pyrrole-pyrrole trimer (0.165 g, 0.32 mmol) was deprotected using 4M HCl in dioxane as described in general procedure C. The resulting residue was dissolved in dry DCM (5 mL) and the Alloc-THP-PBD acid (0.166 g, 0.32 mmol) was added and coupled as described in general procedure B to yield an orange foam (0.225 g, 77%). LCMS (method 1) rt = 3.67 min; *m/z* (ES+) 917 (M+1).

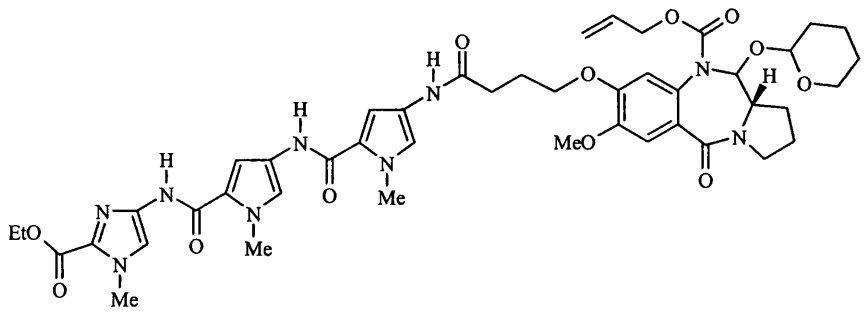

(11aS)-8-(3-{5-[5-(2-ethoxycarbonyl-1-methyl-1*H*-imidazol-4-ylcarbamoyl)-1-methyl-1*H*-pyrrol-3-ylcarbamoyl]-1-methyl-1*H*-pyrrol-3-ylcarbamoyl}-propoxy)-7-methoxy-5-oxo-11-(tetrahydropyran-2-yloxy)-2,3,11,11a-tetrahydro-1*H*,5*H*-pyrrolo[2,1-*c*][1,4]benzodiazepine-10-carboxylic acid allyl ester (122)

The Boc imidazole-pyrrole-pyrrole trimer (0.150 g, 0.29 mmol) was deprotected using 4M HCl in dioxane as described in general procedure C. The resulting residue was dissolved in dry DCM (5 mL) and the Alloc-THP-PBD acid (0.151 g, 0.29 mmol) was added and coupled as described in general procedure A to yield a brown foam (0.253 g, 95%). LCMS (method 1) rt = 3.33 min; *m/z* (ES+) 914 (M+1).

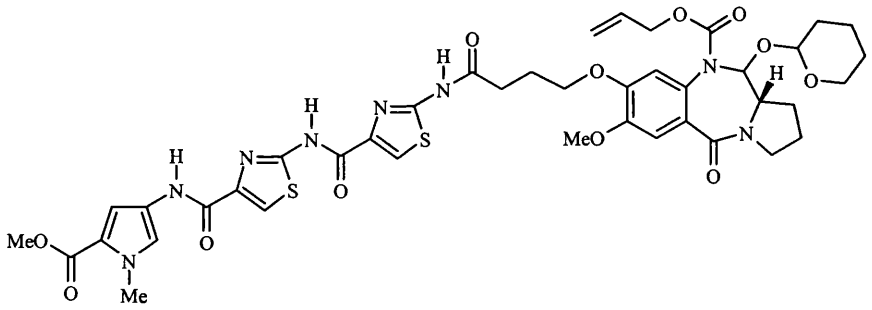

(11aS)-8-(3-{5-[4-(5-methoxycarbonyl-1-methyl-1*H*-pyrrol-3-ylcarbamoyl)-thiazol-2-ylcarbamoyl]-thiazol-2-ylcarbamoyl}-propoxy)-7-methoxy-5-oxo-11-(tetrahydropyran-2-yloxy)-2,3,11,11a-tetrahydro-1*H*,5*H*-pyrrolo[2,1-*c*][1,4]benzodiazepine-10-carboxylic acid allyl ester (126)

The Boc pyrrole-thiazole-thiazole trimer (0.163 g, 0.322 mmol) was deprotected using 4M HCl in dioxane as described in general procedure C. The resulting residue was dissolved in

dry DCM (5 mL) and the Alloc-THP-PBD acid (0.167 g, 0.32 mmol) was added and coupled as described in general procedure B to yield a yellow foam (0.146 g, 48%). LCMS (method 1) rt = 2.78min; *m/z* (ES+) 909 (M+1).

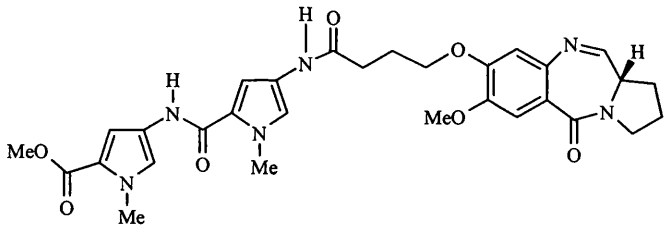

(11aS) Methyl 4-({4-[4-(7-Methoxy-5-oxo-2,3,5,11a-tetrahydro-5*H*-pyrrolo[2,1-*c*][1,4] benzodiazepine-8-yloxy)-butyrylamino]-1-methyl-1*H*-pyrrole-2-carbonyl}-amino)-1-methyl-1*H*-pyrrole-2-carboxylate (134)

The Alloc-THP-PBD-pyrrole dimer conjugate (0.130 g, 0.167 mmol) was deprotected as described in general procedure E to yield the imine product (0.035 g, 35%). ^{1}H-NMR (d_6-DMSO) δ 9.86 (1H, s, NH), 7.74 (1H, d, *J* = 4.3 Hz, H-11), 7.45 (1H, d, *J* = 1.7 Hz, Py-H), 7.33 (1H, s, H-6), 7.14 (1H, d, *J* = 1.6 Hz, Py-H), 6.90 (1H, d, *J* = 1.9 Hz, Py-H), 6.88 (1H, d, *J* = 1.8 Hz, Py-H), 6.84 (1H, s, H-9), 4.11 (1H, m, side chain H-1), 3.97 (1H, m, side chain H-1), 3.84 (6H, s, O/NCH$_3$), 3.83 (3H, s, O/NCH$_3$), 3.74 (3H, s, OCH$_3$), 3.68 (1H, m, H-11a), 3.60 (1H, m, H-3), 3.40 (1H, m, H-3), 2.45 (1H, m, side chain H-3), 2.23 (2H, m, H-1), 2.09 (2H, m, side chain H-2), 1.93 (2H, m, H-2); ^{13}C-NMR (d_6-DMSO) (100MHz) δ 168.5, 164.3, 163.6, 160.7, 158.2, 150.1, 146.7, 140.6, 122.9, 122.4, 122.0, 120.7, 119.9, 118.5, 118.2, 111.3 , 110.2, 108.3, 104.2, 67.8, 55.7, 53.4, 50.9, 46.6, 36.1, 36.0, 31.8, 28.8, 24.7, 23.5; IR (solid) ν_{max} 3300, 2948, 1703, 1596, 1582, 1448, 1437, 1252, 1197, 1100, 781 cm^{-1}; $[\alpha]^{26}_D$ +256 ° (c = 0.030, $CHCl_3$); LCMS (method 1) rt = 2.53 min; *m/z* (ES+) 591 (M+1); LCMS (method 3) rt = 9.50 min; *m/z* (ES+) 591 (M+1); LCMS (method 4) rt = 7.60 min; *m/z* (ES+) 591 (M+1); Acc. Mass $C_{30}H_{34}N_6O_7$ calc. 591.2562 found 591.2546 (M+1).

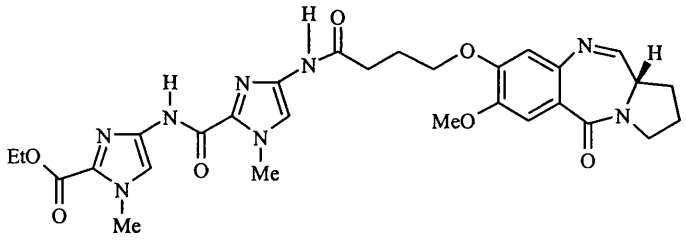

(11aS) Ethyl 4-({4-[4-(7-Methoxy-5-oxo-2,3,5,11a-tetrahydro-5*H*-pyrrolo[2,1-*c*][1,4] benzodiazepine-8-yloxy)-butyrylamino]-1-methyl-1*H*-imidazole-2-carbonyl}-amino)-1-methyl-1*H*-imidazole-2-carboxylate (138)

Palladium tetrakis[triphenylphosphine] (0.05 equiv.) and pyrrolidine (1.1 equiv.) were added to a solution of the Alloc-THP-PBD-imidazole dimer conjugate (0.060 g, 0.076 mmol) in dry DCM (5 mL). The reaction mixture was allowed to stir at room temperature for 1 hour. The solvent was removed *in vacuo* and the product was purified directly by column chromatography (silica gel, eluted with DCM 96%, MeOH 4%) to give the product as an off-white foam (0.041 g, 90%). ^{1}H-NMR (d_6-acetone) (400 MHz) δ 9.72 (s, 1H, N-H) 9.33 (s, 1H, N-H) 7.74 (d, 1H, J = 4.4 Hz, H-11) 7.59 (s, 1H, Im-H) 7.50 (s, 1H, Im-H) 7.42 (s, 1H, H-6) 6.81 (s, 1H, H-9) 4.33 (q, 2H, J = 7.1 Hz, OCH_2CH$_3$) 4.14 (m, 2H, side chain H-1) 4.07 (s, 3H, O/N-CH$_3$) 4.03 (s, 3H, O/N-CH$_3$) 3.87 (s, 3H, O/N-CH$_3$) 3.70 (m, 2H, H-11a, H-3) 3.49 (m, 1H, H-3) 2.64 (m, 2H, side chain H-3) 2.35 (m, 2H, H-1) 2.19 (m, 2H, side chain H-2) 2.09 (m, 2H, H-2) 1.35 (t, 3H, J = 7.1 Hz, OCH$_2$CH_3); LCMS (method 1) rt = 2.48 min; *m/z* (ES+) 607 (M+1); LCMS (method 3) rt = 9.27 min; *m/z* (ES+) 607 (M+1); LCMS (method 4) rt = 7.37 min; *m/z* (ES+) 607 (M+1); Acc. Mass $C_{29}H_{34}N_8O_7$ calc. 607.2623 found 607.2626 (M+1).

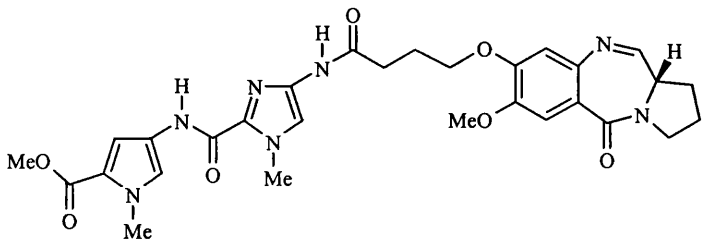

(11aS) Methyl 4-({4-[4-(7-Methoxy-5-oxo-2,3,5,11a-tetrahydro-5*H*-pyrrolo[2,1-*c*][1,4] benzodiazepine-8-yloxy)-butyrylamino]-1-methyl-1*H*-imidazole-2-carbonyl}-amino)-1-methyl-1*H*-pyrrole-2-carboxylate (135)

The Alloc-THP-PBD-imidazole-pyrrole conjugate (0.160 g, 0.21 mmol) was deprotected as described in general procedure E to yield the imine product (0.031 g, 25%). ^{1}H-NMR (d_6-acetone) (400MHz) δ 9.56 (s, 1H, N-H) 8.39 (s, 1H, N-H) 8.11 (s, 1H, Im-H) 7.51 (m, 2H, Py-H) 7.35 (s, 1H, H-6) 7.01 (d, 1H, J = 4.2 Hz, H-11) 6.81 (s, 1H, H-9) 4.08 (m, 1H, side chain H-1) 3.96 (m, 1H, side chain H-1) 3.92 (s, 3H, O/N-CH_3) 3.84 (s, 3H, O/N-CH_3) 3.77 (s, 3H, O/N-CH_3) 3.74 (m, 1H, H-11a) 3.59 (m, 2H, H-3) 2.66 (m, 2H, side chain H-3) 2.54 (m, 2H, H-1) 2.21 (m, 2H, side chain H-2) 2.09 (m, 2H, H-2); LCMS (method 1) rt = 2.53 min; *m/z* (ES+) 592 (M+1); LCMS (method 3) rt = 9.37 min; *m/z* (ES+) 592 (M+1); LCMS (method 4) rt = 7.52 min *m/z* (ES+) 592 (M+1); Acc. Mass $C_{29}H_{33}N_7O_7$ calc. 592.2514 found 592.2521 (M+1).

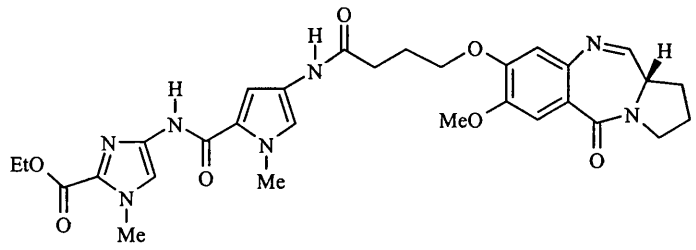

(11aS) Ethyl 4-({4-[4-(7-Methoxy-5-oxo-2,3,5,11a-tetrahydro-5*H*-pyrrolo[2,1-*c*][1,4] benzodiazepine-8-yloxy)-butyrylamino]-1-methyl-1*H*-pyrrole-2-carbonyl}-amino)-1-methyl-1*H*-imidazole-2-carboxylate (137)

The Alloc-THP-PBD-pyrrole-imidazole conjugate (0.220 g, 0.28 mmol) was deprotected as described in general procedure E to yield the imine product (0.044 g, 26%). ^{1}H-NMR (d_6-acetone) (400MHz) δ 9.25 (s, 1H, N-H) 9.21 (s, 1H, N-H) 7.74 (d, 1H, J = 4.4 Hz, H-11) 7.57 (s, 1H, Im-H) 7.41 (m, 2H, Py-H, H-6) 7.08 (d, 1H, J = 1.6 Hz, Py-H) 6.81 (s, 1H, H-9) 4.33 (q, 2H, J = 7.1 Hz, OCH_2CH$_3$) 4.14 (m, 2H, side chain H-1) 4.01 (s, 3H, O/N-CH$_3$) 3.94 (s, 3H, O/N-CH$_3$) 3.87 (s, 3H, O/N-CH$_3$) 3.69 (m, 2H, H-11a, H-3) 3.46 (m, 1H, H-3) 2.55 (m, 2H, side chain H-3) 2.36 (m, 2H, H-1) 2.17 (m, 2H, side chain H-2) 2.09 (m, 2H, H-2) 1.37 (t, 3H, J = 7.1 Hz, OCH$_2$CH_3); LCMS (method 1) rt = 2.45; *m/z* (ES+) 606 (M+1); LCMS (method 3) rt = 9.18 min; *m/z* (ES+) 606 (M+1); LCMS (method 4) rt = 7.28 min; *m/z* (ES+) 606 (M+1); Acc. Mass $C_{30}H_{35}N_7O_7$ calc. 606.2671 found 606.2690 (M+1).

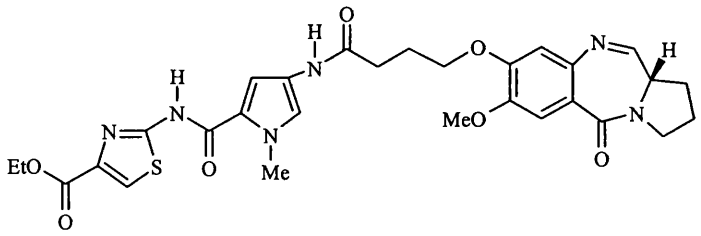

(11aS) Ethyl 2-({4-[4-(7-Methoxy-5-oxo-2,3,5,11a-tetrahydro-5*H*-pyrrolo[2,1-*c*][1,4] benzodiazepine-8-yloxy)-butyrylamino]-1-methyl-1*H*-pyrrole-2-carbonyl}-amino)-thiazole-4-carboxylate (139)

The Alloc-THP-PBD-pyrrole-thiazole conjugate (0.215 g, 0.27 mmol) was deprotected as described in general procedure E to yield the imine product (0.025 g, 15%) 1H-NMR (d_6-acetone) (400 MHz) δ 10.82 (s, 1H, N-H) 9.31 (s, 1H, N-H) 7.93 (s, 1H, Thz-H) 7.74 (d, 1H, J = 4.3 Hz, H-11) 7.54 (d, 1H, J = 1.5 Hz, Py-H) 7.41 (s, 1H, H-6) 7.32 (d, 1H, J = 1.8 Hz, Py-H) 6.81 (s, 1H, H-9) 4.32 (q, 2H, J = 7.3 Hz, OCH_2CH_3) 4.15 (m, 2H, side chain H-1) 3.99 (s, 3H, O/N-CH_3) 3.87 (s, 3H, O/N-CH_3) 3.68 (m, 2H, H-11a, H-3) 3.46 (m, 1H, H-3) 2.56 (m, 2H, side chain H-3) 2.37 (m, 2H, H-1) 2.18 (m, 2H, side chain H-2) 2.05 (m, 2H, H-2) 1.35 (t, 3H, J = 7.1 Hz, OCH_2CH_3); LCMS (method 1) rt = 2.73; *m/z* (ES+) 609 (M+1); LCMS (method 3) rt = 10.43 min; *m/z* (ES+) 609 (M+1); LCMS (method 4) rt = 8.42 min; *m/z* (ES+) 609 (M+1); Acc. Mass $C_{29}H_{32}N_6O_7S$ calc. 609.2126 found 609.2132 (M+1).

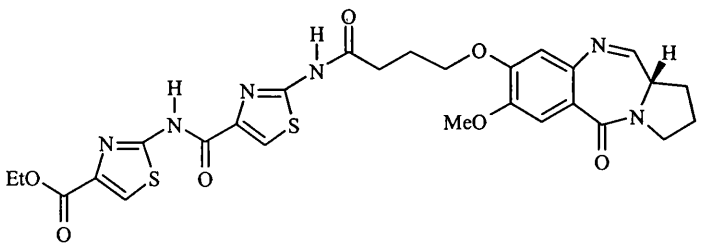

(11aS) Ethyl 2-({2-[4-(7-Methoxy-5-oxo-2,3,5,11a-tetrahydro-5*H*-pyrrolo[2,1-*c*][1,4] benzodiazepine-8-yloxy)-butyrylamino]-thiazole-4-carbonyl}-amino)-thiazole-4-carboxylate (140)

The Alloc-THP-PBD-thiazole-thiazole conjugate (0.080 g, 0.10 mmol) was deprotected as described in general procedure E to yield (0.025 g, 40%). ^{1}H-NMR (d_6-acetone) (400MHz) δ 11.57 (s, 1H, N-H) 10.71 (s, 1H, N-H) 8.11 (s, 1H, Thz-H) 8.03 (s, 1H, Thz-H) 7.75 (d, 1H, *J* = 4.4 Hz, H-11) 7.40 (s, 1H, H-6) 6.82 (s, 1H, H-9) 4.32 (q, 2H, *J* = 7.1 Hz, OC*H*$_2$CH$_3$) 4.20 (m, 2H, side chain H-1) 3.81 (s, 3H, O/N-CH$_3$) 3.69 (m, 2H, H-11a, H-3) 3.46 (m, 1H, H-3) 2.85 (m, 2H, side chain H-3) 2.36 (m, 2H, H-1) 2.27 (m, 2H, side chain H-2) 2.03 (m, 2H, H-2) 1.35 (t, 3H, *J* = 7.1 Hz, OCH$_2$C*H*$_3$); LCMS (method 1) rt = 2.78; *m/z* (ES+) 613 (M+1); LCMS (method 3) rt = 10.82 min; *m/z* (ES+) 613 (M+1); LCMS (method 4) rt = 8.77 min; *m/z* (ES+) 613 (M+1); Acc. Mass $C_{27}H_{28}N_6O_7S_2$ calc. 613.1534 found 613.1511 (M+1).

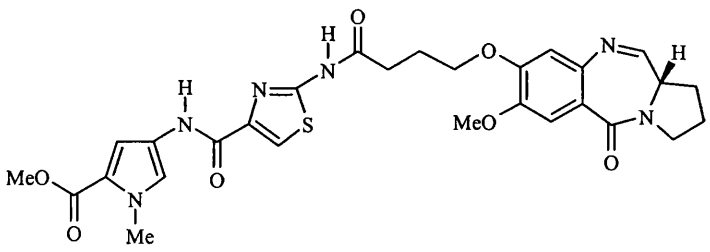

(11aS) Ethyl 4-({2-[4-(7-Methoxy-5-oxo-2,3,5,11a-tetrahydro-5*H*-pyrrolo[2,1-*c*][1,4] benzodiazepine-8-yloxy)-butyrylamino]-thiazole-4-carbonyl}-amino)-1-methyl-1*H*-pyrrole-2-carboxylate (136)

The Alloc-THP-PBD-thiazole-pyrrole conjugate (0.188 g, 0.24 mmol) was deprotected as described in general procedure E to yield (0.012 g, 8%) 1H-NMR (d_6-acetone) (400 MHz) δ 11.29 (s, 1H, N-H) 9.28 (s, 1H, N-H) 7.81 (s, 1H, Thz-H) 7.74 (d, 1H, J = 4.4 Hz, H-11) 7.53 (d, 1H, J = 1.9 Hz, Py-H) 7.40 (s, 1H, H-6) 6.96 (d, 1H, J = 2.0 Hz, Py-H) 6.81 (s, 1H, H-9) 4.19 (m, 2H, side chain H-1) 3.91 (s, 3H, O/N-CH_3) 3.87 (s, 3H, O/N-CH_3) 3.77 (s, 3H, O/N-CH_3) 3.69 (m, 1H, H-11a) 3.46 (m, 2H, H-3) 2.53 (s, 2H, side chain H-3) 2.36 (m, 2H, H-1) 2.26 (m, 2H, side chain H-2) 2.09 (s, 2H, H-2); LCMS (method 1) rt = 2.57; *m/z* (ES+) 595 (M+1); LCMS (method 3) rt = 9.68 min; *m/z* (ES+) 595 (M+1); LCMS (method 4) rt = 7.78 min; *m/z* (ES+) 595 (M+1); Acc. Mass $C_{28}H_{30}N_6O_7S$ calc. 595.1070 found 595.1957 (M+1).

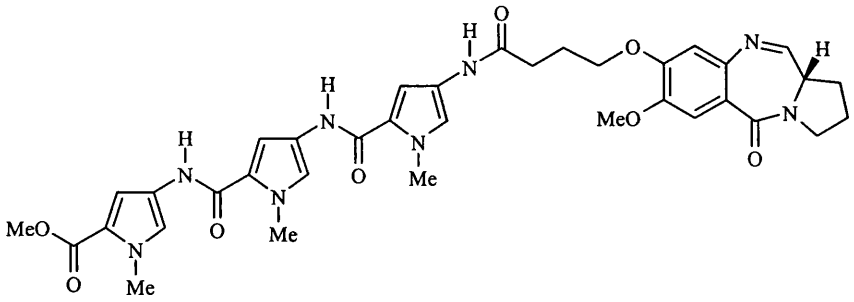

(11aS) Methyl 4-({4-[4-(7-Methoxy-5-oxo-2,3,5,11a-tetrahydro-5*H*-pyrrolo[2,1-*c*][1,4] benzodiazepine-8-yloxy)-butyrylamino]-1-methyl-1*H*-pyrrole-2-carbonyl]-amino)-1-methyl-1*H*-pyrrole-2-carbonyl]-amino}-1-methyl-1*H*-pyrrole-2-carboxylate (141)

The Alloc-THP-PBD-pyrrole trimer conjugate (0.155 g, 0.173 mmol) was deprotected as described in general procedure E to yield the imine product (0.032 g, 26%).^{1}H-NMR (d_6-DMSO) δ 9.94 (1H, s, NH), 9.92 (1H, s, NH), 9.86 (1H, s, NH), 7.76 (1H, d, J = 4.4 Hz, H-11), 7.45 (1H, d, J = 1.9 Hz, Py-H), 7.34 (1H, s, H-6), 7.24 (1H, d, J = 1.7 Hz, Py-H), 7.18 (1H, d, J = 1.7 Hz, Py-H), 7.07 (1H, d, J = 1.8 Hz, Py-H), 6.91 (1H, d, J = 1.9 Hz, Py-H), 6.89 (1H, d, J = 1.8 Hz, Py-H), 6.83 (1H, s, H-9), 4.15 (1H, m, side chain H-1), 4.05 (1H, m, side chain H-1), 3.85 (3H, s, O/NCH$_3$), 3.84 (3H, s, O/NCH$_3$), 3.84 (3H, s, O/NCH$_3$), 3.83 (3H, s, O/NCH$_3$), 3.74 (3H, s, OCH$_3$), 3.67 (1H, m, H-11a), 3.61 (1H, m, H-3), 3.40 (1H, m, H-3), 2.45 (2H, m, side chain H-3), 2.30-2.23 (2H, m, H-1), 2.03 (2H, m, side chain H-2), 1.95 (2H, m, H-2); ^{13}C-NMR (d_6-DMSO) (100MHz) δ 168.5, 164.2, 163.2, 160.8, 158.6, 158.1, 150.1, 146.9, 140.6, 123.0, 122.7, 122.3, 122.2, 122.0, 120.6, 119.8, 118.4, 118.5, 118.2, 111.3, 110.0, 108.3, 104.0, 104.0, 55.4, 53.4, 50.9, 46.4, 36.2, 36.1, 36.0, 31.9, 28.8, 24.7, 23.7; IR (solid) ν_{max} 3300, 2945, 1702, 1594, 1579, 1433, 1248, 1199, 1104, 774 cm^{-1}; $[\alpha]^{24}_{D}$ +168 ° (c = 0.06, $CHCl_3$); LCMS (method 1) rt = 2.48 min; *m/z* (ES+) 607 (M+1); LCMS (method 3) rt = 10.08 min; *m/z* (ES+) 713 (M+1); LCMS (method 4) rt = 8.23 min; *m/z* (ES+) 713 (M+1); Acc. Mass $C_{36}H_{40}N_8O_8$ calc. 713.3042 found 713.3035 (M+1).

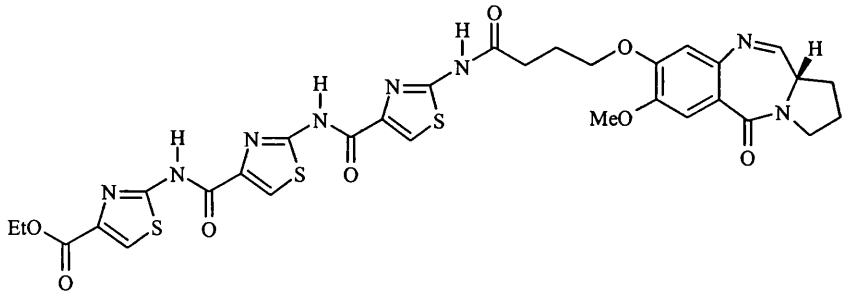

(11aS) Ethyl 4-({4-[4-(7-Methoxy-5-oxo-2,3,5,11a-tetrahydro-5*H*-pyrrolo[2,1-*c*][1,4] benzodiazepine-8-yloxy)-butyrylamino]-thiazole-4-carbonyl]-amino)-thiazole-4-carbonyl]-amino}-thiazole-4-carboxylate (151)

The Alloc-THP-PBD-thiazole-thiazole-thiazole conjugate (0.208 g, 0.23 mmol) was deprotected as described in general procedure E to yield (0.020 g, 12%). ^{1}H-NMR *(d_6*-acetone) (400MHz) δ 11.09 (s, 1H, N-H) 9.73 (s,1H, N-H) 9.57 (s, 1H, N-H) 8.12 (s, 1H, Thz-H) 8.05 (s, 1H, Thz-H) 7.72 (d, 1H, *J* = 4.4 Hz, H-11) 7.68 (s, 1H, Thz-H) 7.41 (s, 1H, H-6) 6.96 (s, 1H, H-9) 4.34 (q, 2H, *J* = 7.1 Hz, OC*H*$_2$CH$_3$) 4.08 (m, 1H, side chain H-1) 3.93 (m, 1H, side chain H-1) 3.87 (s, 3H, O/N-CH$_3$) 3.78 (m, 1H, H-11a) 3.54 (m, 1H, H-3) 3.44 (m, 1H, H-3) 2.52 (m, 2H, side chain H-3) 2.36 (m, 2H, H-1) 2.21 (m, 2H, side chain H-2) 2.09 (m, 2H, H-2) 1.36 (t, 1H, *J* = 7.1 Hz, OCH$_2$C*H*$_3$); LCMS (method 1) rt = 2.98 min; *m/z* (ES+) 739 (M+1); LCMS (method 3) rt = 12.0 min; *m/z* (ES+) 739 (M+1); LCMS (method 4) rt = 10.07 min; *m/z* (ES+) 739 (M+1) Acc. Mass $C_{31}H_{30}N_8O_8S_3$ calc. 739.1422 found 739.1443 (M+1).

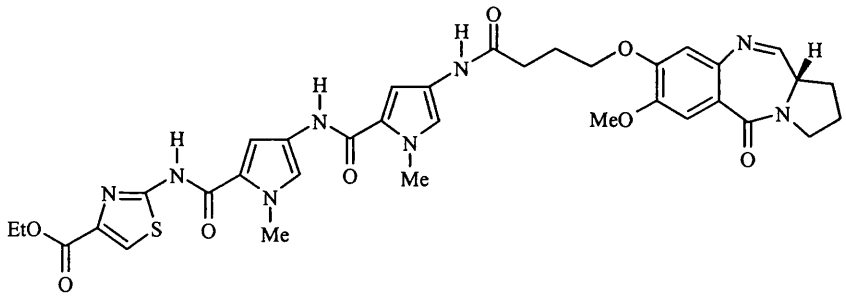

(11aS) Ethyl 4-({4-[4-(7-Methoxy-5-oxo-2,3,5,11a-tetrahydro-5*H*-pyrrolo[2,1-*c*][1,4] benzodiazepine-8-yloxy)-butyrylamino]-1-methyl-1*H*-pyrrole-2-carbonyl]-amino)-1-methyl-1*H*-pyrrole-2-carbonyl]-amino}-thiazole-4-carboxylate (149)

The Alloc-THP-PBD-pyrrole-pyrrole-thiazole conjugate (0.200 g, 0.22 mmol) was deprotected as described in general procedure E to yield the imine product (0.009 g, 6%) ^{1}H-NMR (d_6-acetone) (400MHz) δ 10.88 (s, 1H, N-H) 9.46 (s, 1H, N-H) 9.07 (s, 1H, N-H) 7.93 (s, 1H, Thz-H) 7.75 (d, 1H, J = 4.4 Hz, H-11) 7.61 (d, 1H, J = 1.6 Hz, Py-H) 7.43 (d, 2H, J = 2.3 Hz, Py-H, H-6) 7.16 (d, 1H, J = 1.7 Hz, Py-H) 6.85 (d, 1H, J = 1.8 Hz, Py-H) 6.81 (s, 1H, H-9) 4.32 (q, 2H, J = 7.1 Hz, OCH_2CH$_3$) 4.14 (m, 2H, side chain H-1) 4.02 (s, 3H, O/N-CH$_3$) 3.99 (s, 3H, O/N-CH$_3$) 3.92 (s, 3H, O/N-CH$_3$) 3.69 (m, 2H, H-11a, H-3) 3.47 (m, 1H, H-3) 2.54 (m, 2H, side chain H-3) 2.36 (m, 2H, H-1) 2.21 (m, 2H, side chain H-2) 2.09 (s, 2H, H-2) 1.36 (t, 3H, J = 7.1 Hz, OCH$_2$CH_3); LCMS (method 1) rt = 2.85 min; *m/z* (ES+) 731 (M+1); LCMS (method 3) rt = 11.05 min; *m/z* (ES+) 731 (M+1); LCMS (method 4) rt = 9.10 min; *m/z* (ES+) 731 (M+1); Acc. Mass $C_{35}H_{38}N_8O_8S$ calc. 731.2606 found 731.2603 (M+1).

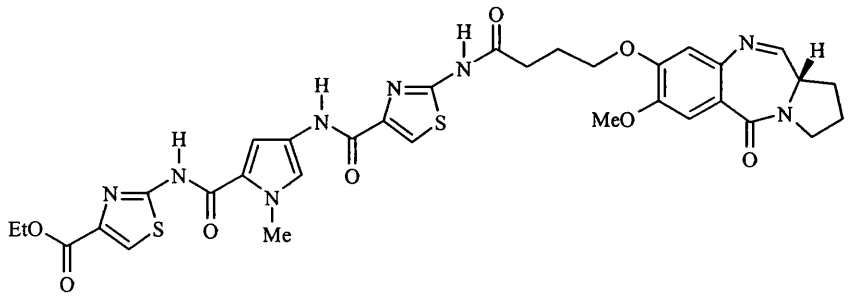

(11aS) Ethyl 4-({4-[4-(7-Methoxy-5-oxo-2,3,5,11a-tetrahydro-5*H*-pyrrolo[2,1-*c*][1,4] benzodiazepine-8-yloxy)-butyrylamino]-thiazole-4-carbonyl]-amino)-1-methyl-1*H*-pyrrole-2-carbonyl]-amino}-thiazole-4-carboxylate (150)

The Alloc-THP-PBD-thiazole-pyrrole-thiazole conjugate (0.140 g, 0.16 mmol) was deprotected as described in general procedure E to yield the imine product (0.009 g, 8%). ^{1}H-NMR (d_6-acetone) (400MHz) δ 11.28 (s, 1H, N-H) 10.95 (s, 1H, N-H) 9.30 (s, 1H, N-H) 7.95 (s, 1H, Thz-H) 7.84 (s, 1H, Thz-H) 7.75 (d, 1H, J = 4.4 Hz, H-11) 7.66 (d, 1H, J = 1.7 Hz, Py-H) 7.50 (d, 1H, J = 1.8 Hz, Py-H) 7.43 (s, 1H, H-6) 6.83 (s, 1H, H-9) 4.33 (q, 2H, J = 7.1 Hz, OCH_2CH$_3$) 4.21 (m, 2H, side chain H-1) 4.03 (s, 3H, O/N-CH$_3$) 3.87 (m, 3H, O/N-CH$_3$) 3.70 (m, 1H, H-11a) 3.58 (m, 1H, H-3) 3.50 (m, 1H, H-3) 2.53 (m, 2H, side chain H-3) 2.36 (m, 2H, H-1) 2.23 (m, 2H, side chain H-2) 2.09 (m, 2H, H-2) 1.36 (t, 3H, J = 7.1 Hz, OCH$_2$CH_3); LCMS (method 1) rt = 2.88 min; *m/z* (ES+) 735 (M+1); LCMS (method 3) rt = 11.23 min; *m/z* (ES+) 735 (M+1); LCMS (method 4) rt = 9.33 min; *m/z* (ES+) 735 (M+1) Acc. Mass $C_{33}H_{34}N_8O_8S_2$ calc. 735.2014 found 735.2026 (M+1).

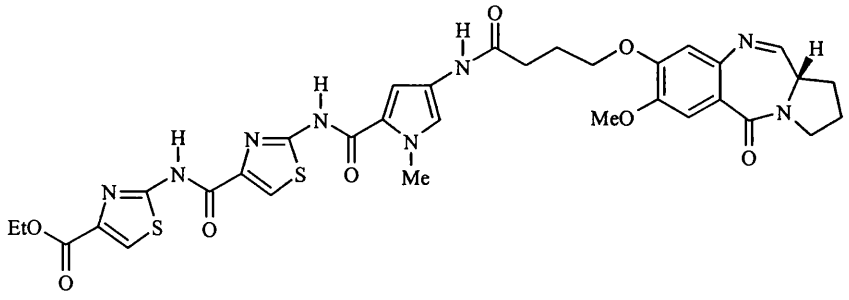

(11aS) Ethyl 4-({4-[4-(7-Methoxy-5-oxo-2,3,5,11a-tetrahydro-5*H*-pyrrolo[2,1-*c*][1,4] benzodiazepine-8-yloxy)-butyrylamino]-1-methyl-1*H*-pyrrole-2-carbonyl]-amino)-thiazole-4-carbonyl]-amino}-thiazole-4-carboxylate (155)

The Alloc-THP-PBD-pyrrole-thiazole-thiazole conjugate (0.090 g, 0.10 mmol) was deprotected as described in general procedure E to yield the imine product (0.006 g, 8%). ^{1}H-NMR (d_6-acetone) (400MHz) δ 9.28 (s, 2H, N-H) 8.23 (s, 1H, N-H) 8.09 (s, 1H, Thz-H) 8.04 (s, 1H, Thz-H) 7.75 (d, 1H, J = 4.4 Hz, H-11) 7.50 (d, 1H, J = 1.8 Hz, Py-H) 7.42 (s, 1H, H-6) 7.29 (d, 1H, J = 1.5 Hz, Py-H) 6.82 (s, 1H, H-9) 4.34 (q, 2H, J = 7.1 Hz, OCH_2CH$_3$) 4.16 (m, 2H, side chain H-1) 4.00 (s, 3H, O/N-CH$_3$) 3.88 (s, 3H, O/N-CH$_3$) 3.71 (m, 1H, H-11a) 3.59 (m, 1H, H-3) 3.46 (m, 1H, H-3) 2.56 (m, 2H, side chain H-3) 2.36 (m, 2H, H-1) 2.20 (m, 2H, side chain H-2) 2.09 (m, 2H, H-2) 1.37 (t, 3H, J = 7.1 Hz, OCH$_2$CH_3); LCMS (method 1) rt = 2.95 min; *m/z* (ES+) 735 (M+1); LCMS (method 3) rt = 11.67 min; *m/z* (ES+) 735 (M+1); LCMS (method 4) rt = 9.72 min; *m/z* (ES+) 735 (M+1) Acc. Mass $C_{33}H_{34}N_8O_8S_2$ calc. 735.2014 found 735.1989 (M+1).

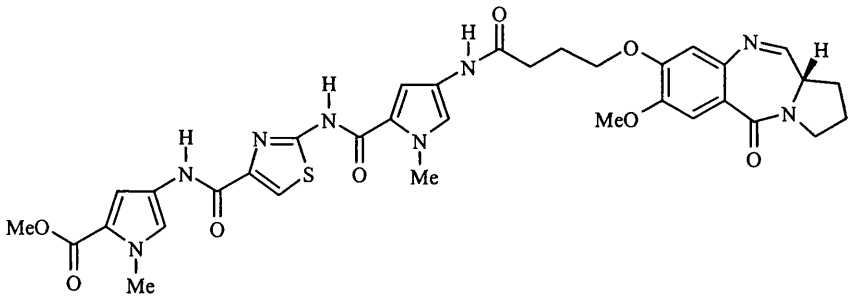

(11aS) Methyl 4-({4-[4-(7-Methoxy-5-oxo-2,3,5,11a-tetrahydro-5*H*-pyrrolo[2,1-*c*][1,4] benzodiazepine-8-yloxy)-butyrylamino]-1-methyl-1*H*-pyrrole-2-carbonyl]-amino)-thiazole-4-carbonyl]-amino}-1-methyl-1*H*-pyrrole-2-carboxylate (152)

The Alloc-THP-PBD-pyrrole-thiazole-pyrrole conjugate (0.125 g, 0.14 mmol) was deprotected as described in general procedure E to yield the imine product (0.035 g, 35%). ^{1}H-NMR (d_6-acetone) (400MHz) δ 11.07 (s, 1H, N-H) 9.25 (s, 1H, N-H) 9.23 (s, 1H, N-H) 7.81 (s, 1H, Thz-H) 7.75 (d, 1H, J = 4.4 Hz, H-11) 7.55 (d, 1H, J = 1.6 Hz, Py-H) 7.45 (d, 1H, J = 1.2 Hz, Py-H) 7.43 (s, 1H, H-6) 7.27 (d, 1H, J = 1.4 Hz, Py-H) 6.98 (d, 1H, J = 1.9 Hz, Py-H) 6.81 (s, 1H, H-9) 4.15 (m, 2H, side chain H-1) 3.98 (s, 3H, O/N-CH_3) 3.92 (s, 3H, O/N-CH_3) 3.88 (s, 3H, O/N-CH_3) 3.85 (s, 3H, O/N-CH_3) 3.68 (m, 1H, H-11a) 3.59 (m, 1H, H-3) 3.46 (m, 1H, H-3) 2.55 (m, 2H, side chain H-3) 2.36 (m, 2H, H-1) 2.18 (m, 2H, side chain H-2) 2.09 (s, 2H, H-2); LCMS (method 1) rt = 2.68 min; *m/z* (ES+) 717 (M+1); LCMS (method 3) rt =10.42 min; *m/z* (ES+) 717 (M+1); LCMS (method 4) rt = 8.62 min; *m/z* (ES+) 717 (M+1); Acc. Mass $C_{34}H_{36}N_8O_8S$ calc. 717.2449 found 717.2464 (M+1).

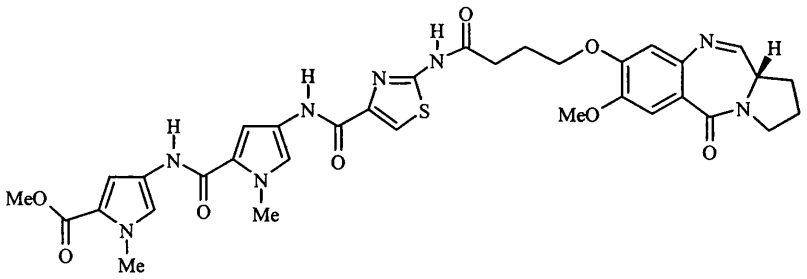

(11aS) Methyl 4-({4-[4-(7-Methoxy-5-oxo-2,3,5,11a-tetrahydro-5*H*-pyrrolo[2,1-*c*][1,4] benzodiazepine-8-yloxy)-butyrylamino]-thiazole-4-carbonyl]-amino)-1-methyl-1*H*-pyrrole-2-carbonyl]-amino}-1-methyl-1*H*-pyrrole-2-carboxylate (153)

The Alloc-THP-PBD-thiazole-pyrrole-pyrrole conjugate (0.130 g, 0.14 mmol) was deprotected as described in general procedure E to yield the imine product (0.037 g, 37%). ^{1}H-NMR (d_6-acetone) (400MHz) δ 11.19 (s, 1H, N-H) 9.34 (s, 1H, N-H) 9.13 (s, 1H, N-H) 7.81 (s, 1H, Thz-H) 7.74 (d, 1H, J = 4.4 Hz, H-11) 7.50 (d, 1H, J = 1.9 Hz, Py-H) 7.45 (s, 1H, H-6) 7.31 (d, 1H, J = 1.6 Hz, Py-H) 6.99 (d, 1H, J = 1.7 Hz, Py-H) 6.93 (d, 1H, J = 1.9 Hz, Py-H) 6.82 (s, 1H, H-9) 4.14 (m, 2H, side chain H-1) 3.94 (s, 3H, O/N-CH_3) 3.91 (s, 3H, O/N-CH_3) 3.84 (s, 3H, O/N-CH_3) 3.76 (s, 3H, O/N-CH_3) 3.68 (m, 2H, H-11a, H-3) 3.44 (m, 1H, H-3) 2.34 (m, 2H, side chain H-3) 2.27 (m, 2H, H-1) 2.21 (m, 2H, side chain H-2) 2.09 (s, 2H, H-2); LCMS (method 1) rt = 2.70 min; *m/z* (ES+) 717 (M+1); LCMS (method 3) rt = 10.32 min; *m/z* (ES+) 717 (M+1); LCMS (method 4) rt = 8.47 min; *m/z* (ES+) 717 (M+1); Acc. Mass $C_{34}H_{36}N_8O_8S$ calc. 717.2449 found 717.2441 (M+1).

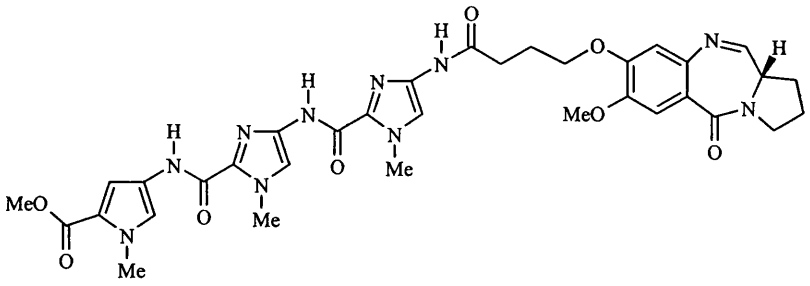

(11aS) Methyl 4-({4-[4-(7-Methoxy-5-oxo-2,3,5,11a-tetrahydro-5*H*-pyrrolo[2,1-*c*][1,4] benzodiazepine-8-yloxy)-butyrylamino]-1-methyl-1*H*-imidazole-2-carbonyl]-amino)-1-methyl-1*H*-imidazole-2-carbonyl]-amino}-1-methyl-1*H*-pyrrole-2-carboxylate (143)

The Alloc-THP-PBD-imidazole-imidazole-pyrrole conjugate (0.130 g, 0.14 mmol) was deprotected as described in general procedure E to yield the imine product (0.028 g, 28%) ^{1}H-NMR (d_6-acetone) (400MHz) δ 9.71 (s, 1H, N-H) 9.42 (s, 1H, N-H) 9.05 (s, 1H, N-H) 8.02 (s, 1H, Im-H) 7.73 (d, 1H, J = 4.4 Hz, H-11) 7.56 (s, 1H, Im-H) 7.50 (d, 1H, J = 5.0 Hz, Py-H) 7.42 (s, 1H, H-6) 7.18 (d, 1H, J = 1.2 Hz, Py-H) 6.83 (s, 1H, H-9) 4.14 (m, 2H, side chain H-1) 4.10 (s, 3H, O/N-CH_3) 4.07 (s, 3H, O/N-CH_3) 3.94 (s, 3H, O/N-CH_3) 3.92 (s, 3H, O/N-CH_3) 3.78 (s, 3H, O/N-CH_3) 3.67 (m, 1H, H-11a) 3.52 (m, 1H, H-3) 3.39 (m, 1H, H-3) 2.52 (m, 2H, side chain H-3) 2.31 (m, 2H, H-1) 2.21 (m, 2H, side chain H-2) 2.09 (s, 2H, H-2); LCMS (method 1) rt = 2.70 min; *m/z* (ES+) 715 (M+1); LCMS (method 3) rt = 10.45 min; *m/z* (ES+) 715 (M+1); LCMS (method 4) rt = 8.57 min; *m/z* (ES+) 715 (M+1); Acc. Mass $C_{34}H_{38}N_{10}O_8$ calc. 715.2974 found 715.2956 (M+1).

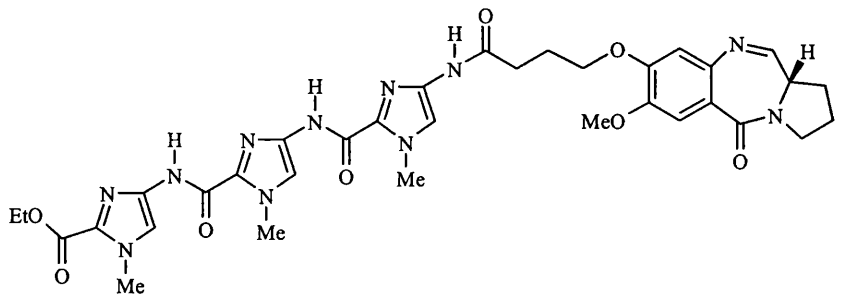

(11aS) Ethyl 4-({4-[4-(7-Methoxy-5-oxo-2,3,5,11a-tetrahydro-5*H*-pyrrolo[2,1-*c*][1,4] benzodiazepine-8-yloxy)-butyrylamino]-1-methyl-1*H*-imidazole-2-carbonyl]-amino)-1-methyl-1*H*-imidazole-2-carbonyl]-amino}-1-methyl-1*H*-imidazole-2-carboxylate (146)

The Alloc-THP-PBD-imidazole-imidazole-imidazole conjugate (0.135 g, 0.15 mmol) was deprotected as described in general procedure E to yield the imine product (0.024 g, 22%). ^{1}H-NMR (d_6-DMSO) (400MHz) δ 10.53 (m, 1H, N-H) 10.16 (s, 1H, N-H) 9.54 (s, 1H, N-H) 7.78 (d, 1H, J = 4.4 Hz, H-11) 7.71 (s, 1H, Im-H) 7.64 (s, 1H, Im-H) 7.54 (s, 1H, Im-H) 7.32 (s, 1H, H-6) 6.83 (s, 1H, H-9) 4.29 (q, 2H, J = 7.1 Hz, OCH_2CH$_3$) 4.16 (m, 2H, side chain H-1) 4.00 (s, 3H, O/N-CH$_3$) 3.98 (s, 3H, O/N-CH$_3$) 3.95 (s, 3H, O/N-CH$_3$) 3.82 (s, 3H, O/N-CH$_3$) 3.67 (m, 2H, H-11a, H-3) 3.59 (m, 1H, H-3) 2.42 (m, 2H, side chain H-3) 2.33 (m, 2H, H-1) 2.04 (m, 2H, side chain H-2) 1.93 (m, 2H, H-2) 1.31 (t, 3H, J = 7.1 Hz, OCH$_2$CH_3). LCMS (method 1) rt = 2.62 min; *m/z* (ES+) 730 (M+1); LCMS (method 3) rt =10.12 min; *m/z* (ES+) 730 (M+1); LCMS (method 4) rt = 8.28 min; *m/z* (ES+) 730 (M+1); Acc. Mass $C_{34}H_{39}N_{11}O_8$ calc. 730.3056 found 730.3070 (M+1).

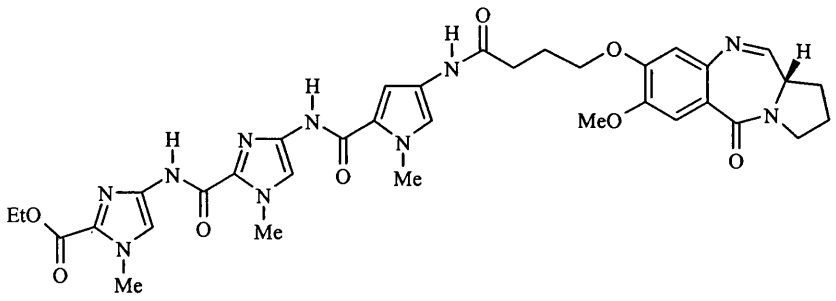

(11aS) Ethyl 4-({4-[4-(7-Methoxy-5-oxo-2,3,5,11a-tetrahydro-5*H*-pyrrolo[2,1-*c*][1,4] benzodiazepine-8-yloxy)-butyrylamino]-1-methyl-1*H*-pyrrole-2-carbonyl]-amino)-1-methyl-1*H*-imidazole-2-carbonyl]-amino}-1-methyl-1*H*-imidazole-2-carboxylate (154)

The Alloc-THP-PBD-pyrrole-imidazole-imidazole conjugate (0.145 g, 0.16 mmol) was deprotected as described in general procedure E to yield the imine product (0.016 g, 14%). ^{1}H-NMR (d_6-acetone) (400MHz) δ 9.46 (s, 1H, N-H) 9.29 (s, 1H, N-H) 9.19 (s, 1H, N-H) 7.75 (d, 1H, J = 4.4 Hz, H-11) 7.59 (s, 1H, Im-H) 7.58 (s, 1H, Im-H) 7.42 (s, 1H, H-6) 7.36 (d, 1H, J = 1.7 Hz, Py-H) 6.99 (d, 1H, J = 1.7 Hz, Py-H) 6.81 (s, 1H, H-9) 4.34 (q, 2H, J = 7.1 Hz, OCH_2CH$_3$) 4.15 (m, 2H, side chain H-1) 4.10 (s, 3H, O/N-CH$_3$) 4.04 (s, 3H, O/N-CH$_3$) 3.94 (s, 3H, O/N-CH$_3$) 3.87 (s, 3H, O/N-CH$_3$) 3.68 (m, 1H, H-11a) 3.58 (m, 1H, H-3) 3.46 (m, 1H, H-3) 2.54 (m, 2H, side chain H-3) 2.36 (m, 2H, H-1) 2.21 (m, 2H, side chain H-2) 2.09 (m, 2H, H-2) 1.36 (t, 3H, J = 7.1 Hz, OCH$_2$CH_3); LCMS (method 1) rt = 2.62 min; *m/z* (ES+) 729 (M+1); LCMS (method 3) rt = 9.98 min; *m/z* (ES+) 729 (M+1); LCMS (method 4) rt = 8.17 min; *m/z* (ES+) 729 (M+1); Acc. Mass $C_{35}H_{40}N_{10}O_8$ calc. 729.3104 found 729.3115 (M+1).

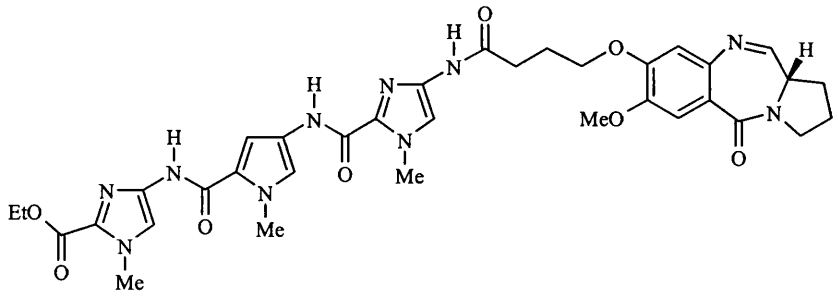

(11aS) Ethyl 4-({4-[4-(7-Methoxy-5-oxo-2,3,5,11a-tetrahydro-5*H*-pyrrolo[2,1-*c*][1,4] benzodiazepine-8-yloxy)-butyrylamino]-1-methyl-1*H*-imidazole-2-carbonyl]-amino)-1-methyl-1*H*-pyrrole-2-carbonyl]-amino}-1-methyl-1*H*-imidazole-2-carboxylate (145)

The Alloc-THP-PBD-imidazole-pyrrole-imidazole conjugate (0.120 g, 0.13 mmol) was deprotected as described in general procedure E to yield the imine product (0.026 g, 27%). ^{1}H-NMR (d_6-acetone) (400MHz) δ 9.52 (s, 1H, N-H) 9.42 (s, 1H, N-H) 9.27 (s, 1H, N-H) 7.74 (d, 1H, J = 4.4 Hz, H-11) 7.60 (s, 1H, Im-H) 7.49 (d, 1H, J = 1.7 Hz, Py-H) 7.44 (s, 1H, Im-H) 7.42 (s, 1H, H-6) 7.27 (d, 1H, J = 1.8 Hz, Py-H) 6.82 (s, 1H, H-9) 4.33 (q, 2H, J = 7.1 Hz, OCH_2CH$_3$) 4.16 (m, 1H, side chain H-1) 4.06 (m, 1H, side chain H-1) 4.02 (s, 3H, O/N-CH$_3$) 3.98 (s, 3H, O/N-CH$_3$) 3.88 (s, 3H, O/N-CH$_3$) 3.80 (s, 3H, O/N-CH$_3$) 3.69 (m, 2H, H-11a, H-3) 3.48 (m, 1H, H-3) 2.65 (m, 2H, side chain H-3) 2.35 (m, 2H, H-1) 2.18 (m, 2H, side chain H-2) 2.09 (s, 2H, H-2) 1.38 (t, 3H, J = 7.1 Hz, OCH$_2$CH_3); LCMS (method 1) rt = 2.60 min; *m/z* (ES+) 729 (M+1); LCMS (method 3) rt = 9.22 min; *m/z* (ES+) 729 (M+1); LCMS (method 4) rt = 8.12 min; *m/z* (ES+) 729 (M+1); Acc. Mass $C_{35}H_{40}N_{10}O_8$ calc. 729.3104 found 729.3075 (M+1).

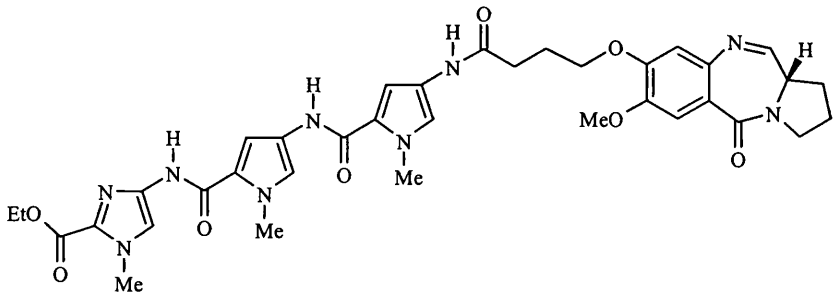

(11aS) Ethyl 4-({4-[4-(7-Methoxy-5-oxo-2,3,5,11a-tetrahydro-5*H*-pyrrolo[2,1-*c*][1,4] benzodiazepine-8-yloxy)-butyrylamino]-1-methyl-1*H*-pyrrole-2-carbonyl]-amino)-1-methyl-1*H*-pyrrole-2-carbonyl]-amino}-1-methyl-1*H*-imidazole-2-carboxylate (144)

The Alloc-THP-PBD-pyrrole-pyrrole-imidazole conjugate (0.210 g, 0.23 mmol) was deprotected as described in general procedure E to yield the imine product (0.028 g,17%). ^{1}H-NMR (d_6-acetone) (400MHz) δ 9.40 (s, 1H, N-H) 9.29 (s, 1H, N-H) 9.07 (s, 1H, N-H) 8.15 (s, 1H, Im-H) 7.74 (d, 1H, J = 4.4 Hz, H-11) 7.59 (s, 1H, H-9) 7.48 (d, 1H, J = 1.6 Hz, Py-H) 7.42 (d, 1H, J = 2.1 Hz, Py-H) 7.16 (d, 1H, J = 1.6 Hz, Py-H) 6.83 (d, 2H, J = 1.8 Hz, Py-H, H-6) 4.33 (q, 2H, J = 7.1 Hz, OCH_2CH$_3$) 4.13 (m, 2H, side chain H-1) 4.01 (s, 3H, O/N-CH$_3$) 3.96 (s, 3H, O/N-CH$_3$) 3.91 (s, 3H, O/N-CH$_3$) 3.87 (s, 3H, O/N-CH$_3$) 3.69 (m, 2H, H-11a, H-3) 3.47 (m, 1H, H-3) 2.55 (m, 2H, side chain H-3) 2.36 (m, 2H, H-1) 2.15 (m, 2H, side chain H-2) 2.09 (m, 2H, H-2) 1.37 (t, 3H, J = 7.1 Hz, OCH$_2$CH_3); LCMS (method 1) rt = 2.60 min; *m/z* (ES+) 728 (M+1); LCMS (method 3) rt = 9.80 min; *m/z* (ES+) 728 (M+1); LCMS (method 4) rt = 7.97 min; *m/z* (ES+) 728 (M+1); Acc. Mass $C_{36}H_{41}N_9O_8$ calc. 728.3151 found 728.3151 (M+1).

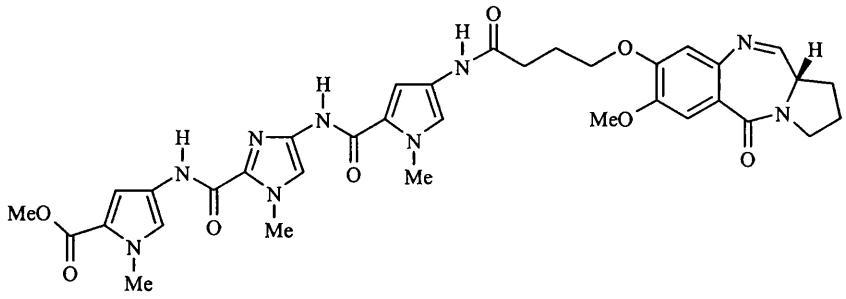

(11aS) Methyl 4-({4-[4-(7-Methoxy-5-oxo-2,3,5,11a-tetrahydro-5*H*-pyrrolo[2,1-*c*][1,4] benzodiazepine-8-yloxy)-butyrylamino]-1-methyl-1*H*-pyrrole-2-carbonyl]-amino)-1-methyl-1*H*-imidazole-2-carbonyl]-amino}-1-methyl-1*H*-pyrrole-2-carboxylate (147)

The Alloc-THP-PBD-pyrrole-imidazole-pyrrole conjugate (0.260 g, 0.29 mmol) was deprotected as described in general procedure E to yield the imine product (0.034 g, 16%). ^{1}H-NMR (d_6-acetone) (400MHz) δ 9.88 (s, 1H, N-H) 9.69 (s, 1H, N-H) 9.53 (s, 1H, N-H) 7.76 (d, 1H, J = 4.4 Hz, H-11) 7.60 (d, 1H, J = 1.1 Hz, Py-H) 7.50 (s, 1H, Im-H) 7.43 (s, 1H, H-6) 7.19 (d, 1H, J = 2.2 Hz, Py-H) 7.01 (d, 1H, J = 1.5 Hz, Py-H) 6.98 (d, 1H, J = 1.3 Hz, Py-H) 6.83 (s, 1H, H-9) 4.21 (m, 2H, side chain H-1) 4.06 (s, 3H, O/N-CH_3) 3.90 (s, 6H, O/N-CH_3) 3.88 (s, 3H, O/N-CH_3) 3.76 (s, 3H, O/N-CH_3) 3.67 (m, 2H, H-11a, H-3) 3.50 (m, 1H, H-3) 2.53 (m, 2H, side chain H-3) 2.36 (m, 2H, H-1) 2.19 (m, 2H, side chain H-2) 2.09 (s, 2H, H-2); LCMS (method 1) rt = 2.65 min; *m/z* (ES+) 714 (M+1); LCMS (method 3) rt = 10.18min; *m/z* (ES+) 714 (M+1); LCMS (method 4) rt = 8.32 min; *m/z* (ES+) 714 (M+1) Acc. Mass $C_{35}H_{39}N_9O_8$ calc. 714.2994 found 714.2999 (M+1).

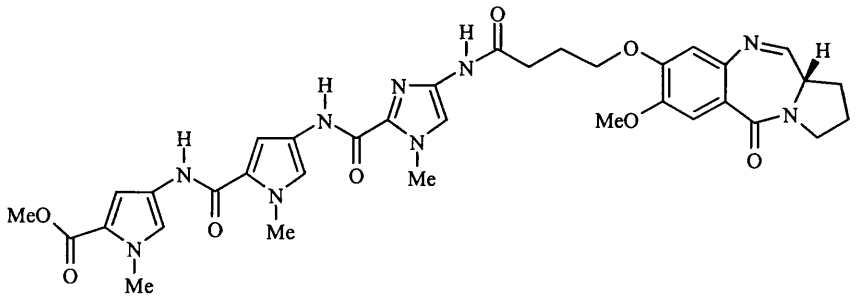

(11aS) Methyl 4-({4-[4-(7-Methoxy-5-oxo-2,3,5,11a-tetrahydro-5*H*-pyrrolo[2,1-*c*][1,4] benzodiazepine-8-yloxy)-butyrylamino]-1-methyl-1*H*-imidazole-2-carbonyl]-amino)-1-methyl-1*H*-pyrrole-2-carbonyl]-amino}-1-methyl-1*H*-pyrrole-2-carboxylate (142)

The Alloc-THP-PBD-imidazole-pyrrole-pyrrole conjugate (0.200 g, 0.22 mmol) was deprotected as described in general procedure E to yield the imine product (0.045 g, 29%). ^{1}H-NMR (d_6-acetone) (400 MHz) δ 9.38 (s, 1H, N-H) 9.37 (s,1H, N-H) 9.22 (s, 1H, N-H) 7.73 (d, 1H, J = 4.4 Hz, H-11) 7.50 (d, 1H, J = 1.9 Hz, Py-H) 7.47 (s, 1H, Im-H) 7.43 (s, 1H, H-6) 7.28 (d, 1H, J = 1.8 Hz, Py-H) 7.00 (d, 1H, J = 1.8 Hz, Py-H) 6.94 (d, 1H, J = 2.0 Hz, Py-H) 6.82 (s, 1H, H-9) 4.20 (m, 1H, side chain H-1) 4.10 (m, 1H, side chain H-1) 4.06 (s, 3H, O/N-CH_3) 4.00 (s, 3H, O/N-CH_3) 3.95 (s, 3H, O/N-CH_3) 3.91 (s, 3H, O/N-CH_3) 3.76 (s, 3H, O/N-CH_3) 3.68 (m, 2H, H-11a, H-3) 3.44 (m, 1H, H-3) 2.64 (m, 2H, side chain H-3) 2.33 (m, 2H, H-1) 2.19 (m, 2H, side chain H-2) 2.09 (s, 2H, H-2); LCMS (method 1) rt = 2.67 min; *m/z* (ES+) 714 (M+1); LCMS (method 3) rt = 10.22 min; *m/z* (ES+) 714 (M+1); LCMS (method 4) rt = 8.35 min; *m/z* (ES+) 714 (M+1). Acc. Mass $C_{35}H_{39}N_9O_8$ calc. 714.2994 found 714.3011 (M+1).

K562 Cytotoxicity Assay

K562 human chronic myeloid leukaemia cells were maintained in RPM1 1640 medium supplemented with 10% fetal calf serum and 2 mM glutamine at 37 °C in a humidified atmosphere containing 5% CO_2 and were incubated with a specified dose of drug for 1 h at 37 °C in the dark. The incubation was terminated by centrifugation (5 min, 300 *g*) and the cells were washed once with drug-free medium. Following the appropriate drug treatment, the cells were transferred to 96-well microtiter plates (10^4 cells per well, 8 wells per sample). Plates were then kept in the dark at 37 °C in a humidified atmosphere containing 5% CO_2. The assay is based on the ability of viable cells to reduce a yellow soluble tetrazolium salt, 3-(4,5-dimethylthiazol-2-yl)-2,5-diphenyl-2*H*-tetrazolium bromide (MTT, Aldrich-Sigma), to an insoluble purple formazan precipitate. Following incubation of the plates for 4 days (to allow control cells to increase in number by approximately 10 fold), 20 μL of MTT solution (5 mg/mL in phosphate-buffered saline) was added to each well and the plates further incubated for 5 h. The plates were then centrifuged for 5 minutes at 300 g and the bulk of the medium pipetted from the cell pellet leaving 10–20 μL per well. DMSO (200 μL) was added to each well and the samples agitated to ensure complete mixing. The optical density was then read at a wavelength of 550 nm on a Titertek Multiscan ELISA plate reader, and a dose-response curve was constructed. For each curve, an IC_{50} value was read as the dose required to reduce the final optical density to 50% of the control value.

NCI Cytotoxicity Assay

The human tumor cell lines of the cancer screening panel were grown in RPMI 1640 medium containing 5% fetal bovine serum and 2 mM L-glutamine. The cells were inoculated into 96 well microtiter plates in 100 µL at plating densities ranging from 5,000 to 40,000 cells/well depending on the doubling time of individual cell lines. After cell inoculation, the microtiter plates were incubated at 37° C, 5 % CO2, 95 % air and 100 % relative humidity for 24 h prior to addition of experimental drugs.

After 24 h, two plates of each cell line were fixed *in situ* with TCA, to represent a measurement of the cell population for each cell line at the time of drug addition (Tz). Experimental drugs were solubilised in dimethyl sulfoxide at 400-fold the desired final maximum test concentration and stored frozen prior to use. At the time of drug addition, an aliquot of frozen concentrate was thawed and diluted to twice the desired final maximum test concentration with complete medium containing 50 µg/ml gentamicin. Additional four, 10-fold or ½ log serial dilutions were made to provide a total of five drug concentrations plus control. Aliquots of 100 µl of these different drug dilutions were added to the appropriate microtiter wells already containing 100 µl of medium, resulting in the required final drug concentrations.

Following drug addition, the plates were incubated for an additional 48 h at 37°C, 5 % CO2, 95 % air, and 100 % relative humidity. For adherent cells, the assay was terminated by the addition of cold TCA. Cells were fixed *in situ* by the gentle addition of 50 µl of cold 50 % (w/v) TCA (final concentration, 10 % TCA) and incubated for 60 minutes at 4°C. The supernatant was discarded, and the plates were washed five times with tap water

and air dried. Sulforhodamine B (SRB) solution (100 µl) at 0.4 % (w/v) in 1 % acetic acid was added to each well, and plates were incubated for 10 minutes at room temperature. After staining, unbound dye was removed by washing five times with 1 % acetic acid and the plates were air dried. Bound stain was subsequently solubilized with 10 mM trizma base, and the absorbance was read on an automated plate reader at a wavelength of 515 nm. For suspension cells, the methodology was the same except that the assay was terminated by fixing settled cells at the bottom of the wells by gently adding 50 µl of 80 % TCA (final concentration, 16 % TCA). Using the seven absorbance measurements [time zero, (Tz), control growth, (C), and test growth in the presence of drug at the five concentration levels (Ti)], the percentage growth was calculated at each of the drug concentrations levels. Percentage growth inhibition was calculated as:

[(Ti-Tz)/(C-Tz)] x 100 for concentrations for which Ti>/=Tz or

[(Ti-Tz)/Tz] x 100 for concentrations for which Ti<Tz.

Three dose response parameters were calculated for each experimental agent. Growth inhibition of 50 % (GI50) was calculated from [(Ti-Tz)/(C-Tz)] x 100 = 50, which is the drug concentration resulting in a 50% reduction in the net protein increase (as measured by SRB staining) in control cells during the drug incubation. The drug concentration resulting in total growth inhibition (TGI) was calculated from Ti = Tz. The LC50 (concentration of drug resulting in a 50% reduction in the measured protein at the end of the drug treatment as compared to that at the beginning) indicating a net loss of cells following treatment was calculated from [(Ti-Tz)/Tz] x 100 = -50. Values were calculated for each of these three parameters if the level of activity is reached; however,

if the effect is not reached or is exceeded, the value for that parameter was expressed as greater or less than the maximum or minimum concentration tested.

Thermal Denaturation Studies

All compounds were received as powders and stored at –20 °C under anhydrous conditions prior to use. Stock ligand solutions were freshly prepared in HPLC-grade dimethylsulfoxide (DMSO) and working solutions were produced by appropriate dilution, as required.

The protocol used to determine thermal denaturation temperatures (T_m) for double-stranded calf thymus DNA and ligand-induced shifts (ΔT_m) has been described, together with the analytical procedure [A.W. McConnaughie and T.C. Jenkins, *J. Med. Chem.* **38**, 3488–3501 (1995); G.B. Jones, C.L. Davey, T.C. Jenkins, A. Kamal, G.G. Kneale, S. Neidle, G.D. Webster and D.E. Thurston, *Anti-Cancer Drug Des.* **5**, 249–264 (1990); S.J. Gregson, P.W. Howard, D.R. Gullick, A. Hamaguchi, K.E. Corcoran, N.A. Brooks, J.A. Hartley, T.C. Jenkins, S. Patel, M.J. Guille and D.E. Thurston, *J. Med. Chem.* **47**, 1161–1174 (2004)].

The PBD monomers were subjected to DNA thermal melting (denaturation) studies using calf thymus DNA (CT-DNA, type-I, highly polymerized sodium salt; 42% G+C [Sigma]) at a fixed 100 μM (in DNAp, equivalent to 50 μM in bp) concentration, quantitated using an extinction coefficient of 6600 (M phosphate)$^{-1}$ cm^{-1} at 260 nm. Solutions were prepared in pH 7.00 ± 0.01 aqueous buffer containing 10 mM NaH_2PO_4/Na_2HPO_4 and 1 mM Na_2EDTA (*all* AnalaR grade). Working solutions containing CT-DNA and the test compound (5 or 20 μM, as required) were incubated at 37.0 ± 0.1 °C for 0–72 h using a Grant GD120 water bath.

Samples were monitored at 260 nm using a Cary 4000 UV–visible spectrophotometer fitted with a Peltier heating accessory. A precision probe calibrated to ± 0.01 °C in the –10 to +120 °C range was used for temperature measurements. Heating was applied at a rate of 1 °C/min in the 50–99 °C temperature range, with optical and temperature data sampling at 100 ms intervals. A separate experiment was carried out using buffer alone, and this baseline was subtracted from each DNA melting curve before data treatment. Optical data were imported into the Origin 5 program (MicroCal Inc., Northampton, MA) for analysis. DNA helix→coil transition temperatures (T_m) were determined at the midpoint of the normalized melting profiles. Results for each compound are shown as the mean ± standard deviation from at least three determinations. Ligand-induced alterations in DNA melting behaviour (ΔT_m) are given by $\Delta T_m = T_m(\text{DNA + ligand}) - T_m(\text{DNA})$, where the T_m value determined for native CT-DNA is 67.82 ± 0.07 °C (averaged from ~110 runs). Working solutions with the candidate PBD contained ≤0.3% v/v DMSO; T_m results were corrected for the effects of DMSO co-solvent using a linear correction term determined for calibration mixtures. Other [ligand]/[DNAp] molar ratios were examined for RMH031 and RMH039 to ensure that the fixed 5:100 or 20:100 ratios used for comparative assays did not result in saturation of the host DNA duplex.

For kinetic experiments, working DNA–ligand mixtures incubated at 37 °C were evaluated after fixed time intervals of 0 h (i.e., no incubation), 4 h, 18 h and 72 h.

Footprinting Assay

DMSO (47.5 μL) and 2.5 μL of each drug (10 mM stock) were added to a 96 well plate. Five-fold serial dilutions were performed by transferring 10 μL 0.5 mM drug solution. The drug dilutions (0.5 mM, 100 μM, 20 μM, 4 μM, 0.8 μM, 160 nM, 32 nM) were 20x final concentration in drug-DNA incubations. A second incubation plate was prepared using assay buffer and drug solutions and IR-labelled DNA (10 μL) was added. The plate was gently mixed and stored in the dark at room temperature for 17 h.

DNase digestions

DNase 1 was added to each well of the drug-DNA incubation plate and after 8 mins the digestion was stopped. A vacuum manifold was used to remove all solution and the plate was blotted with tissue. Weak Tris solution (50 μL) was added to each well and the plate was allowed to stand for 3 mins, followed by gentle agitation for 10 mins. The contents of the wells were transferred to a 96 well plate and the plate was spun using a centrifuge for 1 h.

Preparation of the Sequagel-formamide solution

Formamide (10 mL) Sequagel XR concentrate, 10 x TBE and urea (42 g) were mixed together and diluted with water (100 ml).

Preparation of the gel sandwich

Gel plates (41 cm), spacers (0.25 mm0 and a 48 well comb (0.25 mm) were used to construct the gel sandwich mould. The comb area was bind-silanized (50 μL bind-silane in 10 mL EtOH).

Setting of gel

The gel solution (50 mL sequagel-formamide solution, 500 μL 10% APS and 50 μL TEMED) was prepared, poured into the gel sandwich and allowed to set for 1 h.

Loading the gel

The G+A marker sequence (1 μL) and the drug/DNA samples were loaded into the correct lanes on the gel within the LICOR equipment and the gels were allowed to run for 6 h. The gel images were saved on the LICOR, allowing the gels to be visualised.

Gel Shift Assay

Cell Lines and Culture Conditions

NIH3T3 cells (obtained from CR-UK London Research Institute) were grown in Dulbecco's MEM High Glucose (DMEM) (Autogen Bioclear) supplemented with 10% new-born calf serum (NBCS), 1% glutamine and incubated at 37^0C in 5% CO_2. HCT116 cells were also obtained from CR-UK London Research Institute and grown in RPMI medium (Bioclear) supplemented with 10% foetal calf serum (FCS), 1% glutamine and incubated at 37^0C in 5% CO_2.

Preparation of nuclear extracts.

Nuclear extracts were essentially prepared as described (Firth et al, Proc. Natl Acad Sci USA, 91:6496-6500, 1994) and all steps were performed at 4 °C in the presence of a protease inhibitor mix (Complete™, Boehringer). Briefly, cells were rinsed with ice-cold phosphate buffered saline (PBS), scraped from the surface and collected by centrifugation. The cells were washed with 5 equivolumes of hypotonic buffer containing 10mM K-Hepes pH 7.9, 1.5mM $MgCl_2$, 10mM KCl, 0.5mM dithiothreitol (DTT, Sigma). Subsequently, the cells were re-suspended in 3 equivolumes hypotonic buffer, incubated on ice for 10 min, subjected to 20 strokes of a Dounce homogenizer and the nuclei were collected by centrifugation. The nuclear pellet was re-suspended in 0.5 equivolumes low salt buffer containing 20mM K-Hepes pH7.9, 0.2mM K-EDTA, 25% glycerol, 1.5mM $MgCl_2$, 20mM KCl, 0.5mM DTT. While stirring, 0.5 equivolume high salt buffer (as low salt buffer but containing 1.4M KCl) was added and the nuclei were extracted for 30 min. Subsequently, the mixture was centrifuged for 30 min at 14,000rpm in an eppendorf

centrifuge and the supernatant was dialysed in tubing with a 12kDa cut off (Sigma) for 1 hr in a 100 times excess of dialysis buffer containing 20mM K-Hepes pH7.9, 0.2mM K-EDTA, 20% glycerol, 100mM KCl, 0.5mM DTT. The dialysed fraction was centrifuged for 30 min at 14,000rpm in an eppendorf centrifuge and the supernatant was snap frozen in an ethanol dry ice bath and stored at -80°C. The protein concentration of the nuclear extract was assayed using a BIO-RAD micro protein assay kit.

Electrophoretic mobility shift assay (EMSA).

The oligonucleotides (MWG Biotech) containing ICBs (underlined) used in EMSAs are were Topo IIα ICB1 sense: 5'-CGAGTCAGGGATTGGCTGGTCTGCTTC-3', antisense: 5'-GAAGCAGACCAGCCAAT CCCTGACTCG-3'; ICB2 sense: 5'-GGCAAGCTACGATTGGTTCTTCTGGACG-3', antisense: 5'-CGTCCAGAAGAACCAATCGTAGCTTGCC-3'; ICB3 sense: 5'-CTCCC TAACCTGATTGGTTTATTCAAAC-3', antisense: 5'-GTTTGAATAAACCAATCAGGT TAGGGAG-3' and ICB4 sense: 5'-GAGCCCTTCTCATTGGCCAGATTCCCTG-3', antisense: 5'-CAGGGAATCTGGCCAATGAGAAGGGCTC-3'. Oligonucleotides corresponding to mdr1 sense: 5'-GTGGTGAGGCTGATTGGCTGGGCAGGAA-3', antisense: 5'-TTCCTGCCCAGCCAATCAGCCTCACCA-3'; hOGG1 sense: 5'-ACCCTGA TTTCTCATTGGCGCCTCCTACCTCCTCCTCGGATTGGCTACCT-3', antisense: 5'-AGGTAGCCAATCCGAGGAGGAGGTAGGAGGCGCCAATGAGAAATCAGGGT-3'; cdc2/cdk1 sense: 5'-CGGGCTACCCGATTGGTGAATCCGGGGC-3', antisense: 5'-GCCCCGGATTCACCAATCGGGTAGCCCG-3' and cyclin B1 CCAAT box 1 sense:

5'-GACCGGCAGCCGCCAATGGGAAGGGAGTG-3', antisense: 5'-CACTCCCTTCCC ATTGGCGGCTGCCGGTC-3' and CCAAT box 2 sense: 5'-CCACGAACAGGCCAATAAGGAGGGAGCAG-3', antisense: 5'-CTGCTCCCTCCT TATTGGCCTGTTCGTGG-3' were also used for EMSA. Oligonucleotides containing mutated ICBs were used as specific competitors of similar sequence, except the wild-type ICB sequence was replaced by AAACC or GGTTT, in sense and antisense oligonucleotides, respectively. Sense and antisense oligonucleotides were annealed in an equimolar ratio. Double stranded oligonucleotides were 5' end labelled with T4 kinase (NEB) using γ-^{32}P-ATP and subsequently purified on Bio-Gel P-6 columns (BIO-RAD). EMSAs were essentially performed as described (Firth et al, Proc. Natl Acad Sci USA, 91:6496-6500, 1994). Briefly, 5µg nuclear extract in a total volume of 10µl was incubated at 4°C for 30 min in a buffer containing 20mM K-Hepes pH7.9, 1mM $MgCl_2$, 0.5mM K-EDTA, 10% glycerol, 50mM KCl, 0.5mM DTT, 0.5µg poly(dI-dC). poly(dI-dC) (Pharmacia) and 1x protease inhibitor mix (Complete™, Boehringer). For supershifts, antibodies against NF-YA (IgG fraction, Rocklands) were used and the pre-incubation on ice was extended for a total of 1.5 hr. Upon addition of approximately 0.1ng radio-labelled probe the incubation was continued for 2 hours at room temperature. In competition experiments, radiolabelled probe and competitor were added simultaneously. Subsequently, 0.5µl loading buffer (25mM Tris-Cl pH7.5, 0.02% BFB and 10% glycerol) was added and the samples were separated on a 4% poly-acrylamide gel in 0.5x TBE containing 2.5% glycerol at 4°C. After drying the gels the radioactive signal was visualized by exposing the gels to Kodak X-Omat-LS film

9 REFERENCES

Ansari, A. *Curr. Org. Chem.* **2001**, 5, 903.

Anthony, N.G., Johnson, B.F., Khalaf, A.I., Mackay, S.P., Parkinson, J.A., Suckling, C.J., Waigh, R.D. *J. Am. Chem. Soc.* **2004**, 126, 36, 11338.

Arcamore, F.A., Animati, F., Barbieri, B., Configliachhi, E., D'Alesio, R., Geroni, C., Giulani, F.C., Lazzari, E., Menozzi, M., Mogelli, N., Penco, S., Verini, M.A. *J. Med. Chem.* **1989,** 32, 774.

Bailey, C., Chaires J.B. *Bioconjug. Chem.* **1998**, 9, 5, 513.

Baker, B.F., Dervan, P.B. *J. Am. Chem. Soc.* **1989**, 111, 2700.

Baraldi, P.G., Cacciari, B., Guiotto, A., Leoni, A., Romagnoli, R., Spalluto, G., Mongelli, N., Howard, P.W., Thurston, D.E., Bianchi, N., Gambari, R. *Bioorg. Med. Chem. Lett.* **1998**, 8, 21, 3019.

Baraldi, P.G., Cacciari, B., Romagnoli, R., Spalluto, G., Leoni, A., Bianchi, N., Feriotto, C., Rutligiano, C., Mischiati, C., Gambari, R. *Nucleotides, Nucleosides and Nucleic Acids.* **2000**, 19, 1219.

Belitsky, J.M., Leslie, S.J., Arora, P.S., Beerman, T.A., Dervan, P.B. *Bioorg. Med. Chem.* **2002,** 10, 3313.

Bi, W., Wu, L., Coustry, F., de Crombrugghe, B., Maity, S.N. *J. Biol. Chem.* **1997**, 272, 26562.

Boger, D.L., Johnson, D.S. *Angew. Chem. Int. Ed. Engl.* **1996**, 35, 1438.

Boger, D.L., Fink, B.E., Hedrick, M.P. *J. Am. Chem. Soc.* **2000,** 122, 6382.

Blaskó, A., Browne, K.A., Bruice, T.C. *J. Am. Chem. Soc.* **1994**, 116, 3726.

Bonfanti, M., Caretti, G., LaValle, E., Sousa Faro, J.M.F., Faircloth, G., Mantovarni, R., D'incalci, M. *Anticancer Drug Design.* **1999,** 14, 179.

Bremer, R.E., White, S., Szewczyk, J.W., Turner, J.M., Baird, E.E., Dervan, P.B., Rees, D.C. *J. Mol. Biol.* **2000**, 295, 557.

Browne, P.M., Thurlbey, P.L. *Genomes, Molecular Biology and Drug Discovery.* Academic Press Ltd. London. **1996**

Bucher, P. *J. Mol. Biol.* **1990**, 212, 563.

Cargill, C., Bachmann, E., Zbinden, G. *J. Natl.Cancer Inst.* **1974**, 53, 481.

Chang, A.Y., Dervan, P.B. *J. Am. Chem. Soc.* **2000**, 122, 4856.

Chiang, S-Y., Burli, R.W., Benz, C.C., Gawron, L., Scott, G.K., Dervan, P.B., Beerman, T.A. *J. Biol. Chem.* **2002**, 275, 32, 24246.

Chen, H.Y., Liu, J.X., Lown, J.W. *Bioorg. Med. Chem. Lett.* **1995,** 5, 2223.

Chen, X., Ramakrishan, B., Rao, S.T., Sundaralingam, M. *Struct. Biol.* **1994**, 1, 169.

Ciucci, A., Manzini, S., Lombardi, P., Arcamore, F. *Nucl. Acids. Res.* **1996,** 24, 311.

Damayanthi, Y., Reddy, B.S.P., Lown, J.W. *J. Org. Chem.* **1999**, 64, 1, 290.

De Mico, A., Margarita, R., Parlanti, L., Vescovi, A., Piancatelli, G. *J. Org. Chem.* **1997**, 62, 6974.

Dervan, P.B. *Bioorg. Med. Chem.* **2001**, 9, 2215.

Dervan, P.B. *Science*, **1986**, 232, 464.

Dervan, P.B., Doss, R.M., Marques, M.A. *Curr. Med. Chem. Anticancer Agents.* **2005**, 5, 4, 373.

Dickinson, L.A., Gulizia, R.J., Trauger, J.W., Baird, E.E., Mosier, D.E., Gottesfeld, J.M., Dervan, P.B. *Proc. Natl. Acad. Science (USA)*, **1998**, 95, 12890.

Fagan, P., Wemmer, D.E. *J. Am. Chem. Soc.* **1992**, 114, 1080.

Fregeau, N.L., Wang, Y., Pon, R.T., Wylie, W.A., Lown, J.W. *J. Am. Chem. Soc.* **1995,** 117, 8917.

Fukuyama, T., Liu, G., Linton, S.D., Lin, S-C., Nishino, H. *Tetrahedron Lett.* **1993**, 34, 2577.

Goodsell, D. *Curr. Med. Chem.* **2001**, 8. 509.

Goodsell, D., Dickerson, R.E. *J. Med. Chem.* **1986,** 29, 727.

Graves, D.H., Pattraoni, C., Krishnan, B., Ostrander, J.M., Hurley, L.H., Krugh, T.R. *J. Biol. Chem.* **1984**, 259, 8202.

Grue, P., Grasser, A., Sehested, M., Jensen, P.B., Uhse, A., Straub, T., Ness, W., Boege, F. *J. Biol. Chem.* **1998**, 273, 33660.

Guiotto, A., Howard, P.W., Baraldi, P.G., Thurston, D.E. *Bioorg. Med. Chem. Lett.* **1998,** 8, 3017.

Hansen, M., Hurley, L. *Acc. Chem. Res.* **1996,** 29, 249.

Haq, I., Ladbury, J.E., Chowdhry ,B.Z., Jenkins, T.C. and Chaires, J.B. *J. Mol. Biol.* **1997** 271, 244.

He, G-X., Browne, K.A., Blaskó, A., Bruice, T.C. *J. Am. Chem. Soc.* **1994,** 116, 3716-.

He, G-X., Browne, K.A., Groppe, J.C., Baskó, A., Mei, H-Y., Bruice, T.C. *J. Am. Chem. Soc.* **1993,** 115, 7061.

Haq, I., Ladbury, J.E., Chowdhry ,B.Z., Jenkins, T.C. and Chaires, J.B. *J. Mol. Biol.* **1997** 271, 244.

Henderson, D., Hurley, L.H. *Nat. Med.* **1995,** 6, 525.

Hertzberg, R.P., Hecht, S.M., Reynolds, V.L., Molineaux, I.J., Hurley, L.H. *Biochemistry.* **1986,** 25, 1249.

Hurley, L.H. *J. Antibiot.* **1977,** 30, 349.

Hurley, L.H. *J. Med. Chem.* **1989,** 32, 2027.

Hurley, L.H., Draves, P.H.. *Molecular Aspects of Anti-cancer Drug-DNA Interactions.* 1. Neidle, S., Waring, M.J. (eds). Macmillan Press, London. **1993,** 89.

Hurley, L.H., Reck, T., Thurston, D.E., Langley, D.R., Holden K.G., Hertzberg, R.P., Hoover, J.R.E., Gallagher, G.Jr., Faucette, L.F., Mong, S-M., Johnson, R.K. *Chem. Res. Tox.* **1988,** 1, 258.

Hurst, H.C. *Eur J Cancer,* **1996**, 32A, 1857.

James, P.L., Merkina, E.E., Khalaf, A.I., Suckling C.J., Waigh, R.D., Brown, T., Fox, K.R. *Nucl. Acids. Res.* **2004,** 32, 11, 3410.

Jones, G.B., Davey, C.L., Jenkins, T.C., Kamal, A., Kneale, G.G., Neidle, S., Webster, G.D., Thurston, D.E. *Anti-Cancer Drug Design*. **1990**, 5, 249.

Kamal, A., Maddamsetty, V.R., Laxman, N., Ramesh, G., Reddy, G.S.K. *Curr. Med .Chem.- Anti-Cancer Agents.* **2002**, 2, 215.

Kaneko, T., Wong, H., Doyle, T.W., Rose, W.C., Bradner, W.T. *J. Med. Chem.* **1985**, 28, 388.

Kers, I., Dervan, P.B. *Bioorg. Med. Chem.*, **2002**, 10, 3339.

Khalaf, A.I., Waigh, R.D., Drummond, A.J., Pringle, B., McGroarty, I., Skellern, G.G., Suckling, C.J. *J. Med. Chem.* **2004**, 47, 2133.

Kielkopf, C.L., Baird, E.E., Dervan, P.B., Rees, D.C. *Nat. Struct. Biol.* **1998**, 5, 104.

Kim, C.G., Sheffrey, M. *J. Biol. Chem.* **1990**, 265, 13362.

Kimura, K., Saijo, M., Ui, M., Enomoto, T. *J. Biol. Chem.* **1994**, 269, 1173.

Kissinger, K.L., Dabrowiak, J.C., Lown, J.W. *Chem. Res. Toxicol.* **1990**, 3, 162.

Kissinger, K.L., Krowicki, K., Dabrowiak, J.C., Lown, J.W. *Biochemistry.* **1987**, 26, 5590.

Kohn, K.W., Glaubiger, D., Spears, C.L. *Biochem. Biophys. Acta.* **1974**, 361, 288.

Kopka, M.L. *Proc. Natl. Acad. Sci. USA*. **1985**, 82, 1376.

Kopka, M.L., Goodsell, D.S., Baikalov, I., Grzeskowiak, K., Cascio, D., Dickerson, R.E. *Biochemistry*. **1994**, 33, 13593.

Kopka, M.L., Larsen, T.A. *In Nucleic Acid targeted Drug Design*. Eds: Propst, C.L., Perun, T.J., Dekker. New York, **1992,** 302.

Krowicki, K., Lown, J.W., *J. Org. Chem.* **1987,** 52, 3493.

Kumar, R., Lown, J.W. *Oncology Research.* **2003**, 13, 4, 221.

Kumar, R., Reddy, B.S.N., Lown, J.W. *Heterocycl. Comms.* **2002**, 8, 1, 19.

Lee, M., Krowicki, K., Hatley, J.A., Pon, R.T., Lown, J.W. *J. Am. Chem. Soc.* **1988**, 110, 3641.

Lee, M., Rhodes, A.L., Wyatt, M.D., Forrow, S., Hartley, J.A. *Biochemistry.* **1993**, 32, 4237.

Lee, M., Rhodes, A.L., Wyatt, M.D., Forrow, S., Hartley, J.A. *Anti-canc. Drug Des.* **1993**, 8, 137.

Lown, J.W. *J. Mol. Recognit.* **1994**, 7, 79.

Lown, J.W., Krowicki, K. *J. Org. Chem.* **1985**, 50, 3774.

Lown, J.W., Krowicki, K., Bhat, U.G., Skorobogaty, A., Ward, B., Dabrowiak, J.C. *Biochemistry.* **1986**, 25, 7408.

Mrksich, M., Parks, M.E., Dervan.P.B. *J. Am. Chem. Soc.* **1994**, 116, 7983.

Mrksich, M., Wade, W.S., Dwyer, T.J., Geierstanger, B.H., Wemmer, D.E., Dervan, P.B. *Proc. Natl. Acad. Sci. USA.* **1992,** 89, 7586.

Murty, M.S., Sugiyama, H. *Biol. Pharm. Bull.* **2004**, 27, 468.

Nickols, N.G., Jacobs, C.S., Farkas, M.E., Dervan, P.B. *Nucl. Acid. Res.* **2007,** 35, 363.

Oyoshi, T., Kawakami, W., Narita, A., Bando, T., Sugiyama, H. *J. Am. Chem. Soc.* **2003,** 125, 4752.

Patiglou, G., Burley, S.K., *Annu. Rev. Biophys. Biomol. Struct.* **1997**, 26, 289.

Pelton , J.G., Wemmer, D.E. *J. Am. Chem. Soc.* **1990,** 112, 1393.

Petrusek, R.L., Anderson, G.L., Garner, T.F., Fannin, Q.L., Kaplan, D.J., Zimmer, S.G., Hurley, L.H. *Biochemistry.* **1981**, 20, 111.

Plouvier, B., Bailly, C., Houssin, R., Rao, K.E., Lown, J.W., Hénichart, J.P., Waring, M.J. *Nucleic Acids Res.* **1991**, 19, 5821.

Pullman, A., Pullman, B. *Q. Rev. Biophys.* **1981**, 14, 289.

Puvvada, M.S., Forrow, S.A., Hartley, J.A., Stephenson, P., Gibson, L., Jenkins, T.C., Thurston, D.E. *Biochemistry.* **1997**, 36, 2478.

Puvvada, M.S., Hartley, J.A., Jenkins, T.C., Thurston, D.E. *Nucleic Acids Res.* **1993**, 21, 3671.

Rao, K.E., Bathini, Y., Lown, J.W. *J. Org. Chem.* **1990**, 55, 728.

Rao, K.E., Zimmerman, J., Lown, J.W. *J. Org. Chem.* **1991**, 56, 786.

Satz A.L., Bruice, T.C. *Bioorg. Med. Chem.* **2002**, 10, 241.

Shadle, S.E., Bammel, B.P., Cusack, B.J., Knighton, R.A., Olson, S.J., Mushlin, P.S., Olson, R.D. *Biochem. Pharmacol.* **2002**, 60, 10, 1435.

Shinohara, K., Sasaki, S., Minoshima, M., Bando, T., Sugiyama, H. *Nucl. Acids Res.* **2006,** 34, 4, 1189.

Smellie, M., Bose, D.S., Thompson, A.S., Jenkins, T.C., Hartley, J.A., Thurston, D.E. *Biochemistry*. **2003**, 42, 8232

Sun, D., Hurley, L.H. *Chem. Biol.* **1995**, 2, 457.

Swalley, S.E., Baird, E.E., Dervan, P.B. *Chem. Eur. J.* **1997**, 3, 1600.

Swalley, S.E., Baird, E.E., Dervan, P.B. *J. Am. Chem. Soc.* **1996,** 118, 35, 8198.

Tanaka, H., Okshima, N., Hidaka, H. *Mol. Pharmacology*. **1999,** 55, 356.

Tercel, M., Stribbling, S.M., Sheppard, H., Siim, B.G., Wu, K., Pullen, S.M., Botting, K.J., Wilson, W.R., Denny, W.A. *J. Med. Chem.* **2003**, 46, 2132.

Tomasz, M. *Molecular Aspects of Anti-cancer Drug-DNA Interactions*. 1. Neidle, S., Waring, M.J. (eds). Macmillan Press, London. **1993**, 312.

Trauger, J.W., Baird, E.E., Dervan, P.B. *J. Am. Chem. Soc.* **1998**, 282, 111-115.

Trauger, J.W., Baird, E.E., Mrksich, M., Dervan, P.B. *J. Am. Chem. Soc.* **1996**, 118, 6160.

Thurston, D.E. *Br. J. Cancer.* **1999**, 80, 65

Thurston, D.E. *Molecular Aspects of Anti-cancer Drug-DNA Interactions.* 1. Neidle, S., Waring, M.J. (eds). Macmillan Press, London. **1993**, 54.

Thurston, D.E., Bose, D.S., Howard, P.W., Jenkins, T.C., Leoni, A., Baraldi, P.G., Guiotto, A., Cacciari, B., Kelland L.R., Foloppe, M.P., Rault, S. *J. Med. Chem.* **1999**, 42, 1951.

Thurston, D.E., Hurley, L.H. *CIPS.* **1983**, 8, 957.

Urbach, A.R., Dervan, P.B. *PNAS*, **2001**, 98, 8, 4343.

Venter, J.C., Adams, M.D., Myers, E.W., Li, P.W., Mural, R.J., Sutton, G.G. *Science.* **2001,** 291, 1304.

Wade, W.S., Mrksich, M., Dervan, P.B. *J. Am. Chem. Soc.* **1992,** 114, 8783.

Wade, W.S., Mrksich, M., Dervan, P.B. *Biochemistry.* **1993,** 32, 11385.

Wang, Y., Gupta, R., Huang, L., Luo, W., Lown, J.W. *Anti-cancer Drug Des.* **1996,** 11, 15.

Warren, C.L., Kratochvil, N.C., Hauschild, K.E., Foister, S., Brezinski, M.L., Dervan, P.B., Phillips, G.N.Jr., Ansari, A.Z. *Proc. Natl. Acad. Sci. U.S.A.* **2006**, 103, 4, 867.

Waring, M.J. *Annu. Rev. Biochem.* **1981**, 50,159.

Wells, G., Martin, C.R.H., Howard, P.W., Sands, Z.A., Laughton, C.A., Tiberghien A.C., Woo, C-K., Masterson, L.A., Stephenson, M.J., Hartley, J.A., Jenkins, T.C., Shnyder, S.D., Loadman, P.M., Waring M.J., Thurston, D.E. *J. Med. Chem.* **2006**, 49, 5442.

Weyermann, P., Dervan, P.B. *J. Am. Chem. Soc.* **2002,** 124, 6872.

White, S., Szewczyk, J.W., Turner, J.M., Baird, E.E., Dervan, P.B. *Nature* **1998**, 391, 468.

White, S., Turner, J.M., Szewczyk, J.W., Baird, E.E., Dervan, P.B. *J. Am. Chem. Soc.* **1999**, 121, 260.

Wyatt, M.D., Lee, M., Hartley, J.A. *Anti-cancer Drug Des.* **1997,** 12, 49.

Zhang, Y., Chen, F-X., Mehta, P., Gold, B. *Biochemistry*, **1993**, 32, 7954.

Youngquist, R.S., Dervan, P.B. *Proc. Natl. Acad. Sci. U.S.A.* **1985**, 82, 2565

Zhou, Y., Lee, A.S., *J. Natl. Cancer Inst.***1998**, 90, 381.

10 APPENDIX

National Cancer Institute Developmental Therapeutics Program

Mean Graphs

NSC : D736535 / 1	Units : Molar	SSPL : 0CCJ	EXP. ID : 0508NS15
Report Date : October 04, 2005		Test Date : August 15, 2005	

Panel/Cell Line	Log_{10}GI50	GI50	Log_{10}TGI	TGI	Log_{10}LC50	LC50
Leukemia						
CCRF-CEM	-6.80		-6.16		> -4.60	
HL-60(TB)	-6.35		> -4.60		> -4.60	
K-562	-6.28		-4.86		> -4.60	
MOLT-4	-6.37		> -4.60		> -4.60	
RPMI-8226	-6.23		-5.82		> -4.60	
Non-Small Cell Lung Cancer						
A549/ATCC	-5.86		> -4.60		> -4.60	
EKVX	-5.07		> -4.60		> -4.60	
HOP-62	-6.20		> -4.60		> -4.60	
HOP-92	-6.36		-5.92		> -4.60	
NCI-H226	-6.50		-6.16			
NCI-H23	-6.00		-5.00		> -4.60	
NCI-H322M	-5.94		-4.70		> -4.60	
NCI-H460	-6.13		> -4.60		> -4.60	
NCI-H522	-6.40		-5.94		> -4.60	
Colon Cancer						
COLO 205	-6.41		-6.10		-5.80	
HCC-2998	-5.83		-5.15		> -4.60	
HCT-116	-6.12		> -4.60		> -4.60	
HCT-15	-5.26		-4.70		> -4.60	
HT29	-6.34		-6.03			
KM12	-6.20				> -4.60	
SW-620	-6.20		> -4.60		> -4.60	
CNS Cancer						
SF-268	-6.47		-5.69		> -4.60	
SF-295	-6.08		> -4.60		> -4.60	
SF-539	-6.27		-5.60		> -4.60	
SNB-19	-6.35		> -4.60		> -4.60	
SNB-75	-6.96		-5.98		-5.02	
U251	-6.69		-5.96		> -4.60	
Melanoma						
LOX IMVI	-6.54		-6.14			
MALME-3M	-6.37		-5.98		-5.52	
M14	-6.08		-5.50		-4.88	
SK-MEL-2	-6.37		-6.07		-5.77	
SK-MEL-28	-6.30		-5.91		-5.12	
SK-MEL-5	-6.28		-5.89		> -4.60	
UACC-257	-5.96		-5.25		> -4.60	
Ovarian Cancer						
IGROV1	-6.23		-5.49		> -4.60	
OVCAR-3	-6.24		-5.81		> -4.60	
OVCAR-4	-6.47		-5.67		> -4.60	
OVCAR-5	-6.02				> -4.60	
OVCAR-8	-6.04		> -4.60		> -4.60	
SK-OV-3	-6.12		-5.19		> -4.60	
Renal Cancer						
786-0	-6.05		> -4.60		> -4.60	
A498	-6.08		-5.33		> -4.60	
ACHN	-5.98		-5.28		> -4.60	
CAKI-1	-5.87		-5.06		> -4.60	
RXF 393	-6.38		-6.05		-5.72	
TK-10	-6.01		> -4.60		> -4.60	
UO-31	-5.40		-5.04		-4.69	
Prostate Cancer						
PC-3	-6.30		-5.72		> -4.60	
DU-145	-5.98		> -4.60		> -4.60	
Breast Cancer						
MCF7	-6.46		-5.65		> -4.60	
NCI/ADR-RES	> -4.60		> -4.60		> -4.60	
MDA-MB-231/ATCC	-6.38		-5.98		> -4.60	
HS 578T	-5.98		-4.87		> -4.60	
MDA-MB-435	-6.01		> -4.60		> -4.60	
BT-549	-6.19		-5.30		> -4.60	
T-47D	-6.70		-5.98		> -4.60	
MG_MID	-6.16		-5.31		-4.71	
Delta	0.8		0.85		1.09	
Range	2.36		1.56		1.2	

+3 +2 +1 0 -1 -2 -3

Appendix 1. 60 Cell-line profile for RMH033 (Py-Im-PBD).

National Cancer Institute Developmental Therapeutics Program

Mean Graphs

NSC : D737437 / 1	Units : Molar	SSPL : 0CCJ	EXP. ID : 0509NS33
Report Date : October 25, 2005		Test Date : September 19, 2005	

Panel/Cell Line	Log_{10}GI50	Log_{10}TGI	Log_{10}LC50
Leukemia			
CCRF-CEM	< -8.30		> -4.30
HL-60(TB)	< -8.30	< -8.30	> -4.30
MOLT-4	< -8.30	< -8.30	> -4.30
RPMI-8226	-7.17	-6.53	> -4.30
Non-Small Cell Lung Cancer			
A549/ATCC	-7.38	-6.89	
EKVX	-6.66	-4.67	> -4.30
HOP-62	< -8.30	< -8.30	> -4.30
HOP-92	< -8.30	< -8.30	> -4.30
NCI-H226	-8.21		> -4.30
NCI-H322M	-7.89	-6.68	> -4.30
NCI-H460		> -4.30	> -4.30
NCI-H522	< -8.30	< -8.30	-4.92
Colon Cancer			
COLO 205	< -8.30	-7.77	-4.69
HCC-2998	< -8.30	< -8.30	-7.36
HCT-116	< -8.30		
HCT-15	-5.96	> -4.30	> -4.30
HT29	-8.22	-6.50	> -4.30
KM12	< -8.30	-7.10	-4.66
SW-620	< -8.30		> -4.30
CNS Cancer			
SF-268	> -4.30	> -4.30	> -4.30
SF-295	< -8.30	-7.52	-4.92
SF-539	< -8.30	< -8.30	-5.08
SNB-19	< -8.30	-4.96	> -4.30
SNB-75	< -8.30	< -8.30	-6.65
U251	< -8.30	-5.11	> -4.30
Melanoma			
LOX IMVI	< -8.30		-4.73
MALME-3M	< -8.30	-7.76	-5.04
SK-MEL-2	< -8.30	-5.05	> -4.30
SK-MEL-28	< -8.30	-7.78	-5.77
SK-MEL-5	< -8.30		
UACC-257	-8.13	-7.55	
UACC-62	< -8.30	< -8.30	-7.57
Ovarian Cancer			
IGROV1	-7.91		> -4.30
OVCAR-3	< -8.30	< -8.30	
OVCAR-4	-7.80	-5.22	> -4.30
OVCAR-5	-8.24		> -4.30
OVCAR-8	< -8.30	-4.99	> -4.30
SK-OV-3	-7.69	-4.81	> -4.30
Renal Cancer			
786-0	< -8.30		-4.33
A498	-7.26	-6.80	
ACHN	-6.91	-5.88	> -4.30
CAKI-1	-7.54	-6.79	-5.93
SN12C	< -8.30	-5.06	> -4.30
TK-10	< -8.30	-7.79	> -4.30
UO-31	-6.19		> -4.30
Prostate Cancer			
PC-3	< -8.30	> -4.30	> -4.30
DU-145	-8.14	-4.96	> -4.30
Breast Cancer			
MCF7	> -4.30	> -4.30	> -4.30
NCI/ADR-RES	-5.13	-4.43	> -4.30
MDA-MB-231/ATCC	< -8.30		-4.54
HS 578T	< -8.30	-4.90	> -4.30
MDA-MB-435	< -8.30	< -8.30	< -8.30
BT-549	< -8.30	-6.43	> -4.30
T-47D	< -8.30	> -4.30	> -4.30
MG_MID	-7.83	-6.44	-4.72
Delta	0.47	1.86	3.58
Range	4.0	4.0	4.0

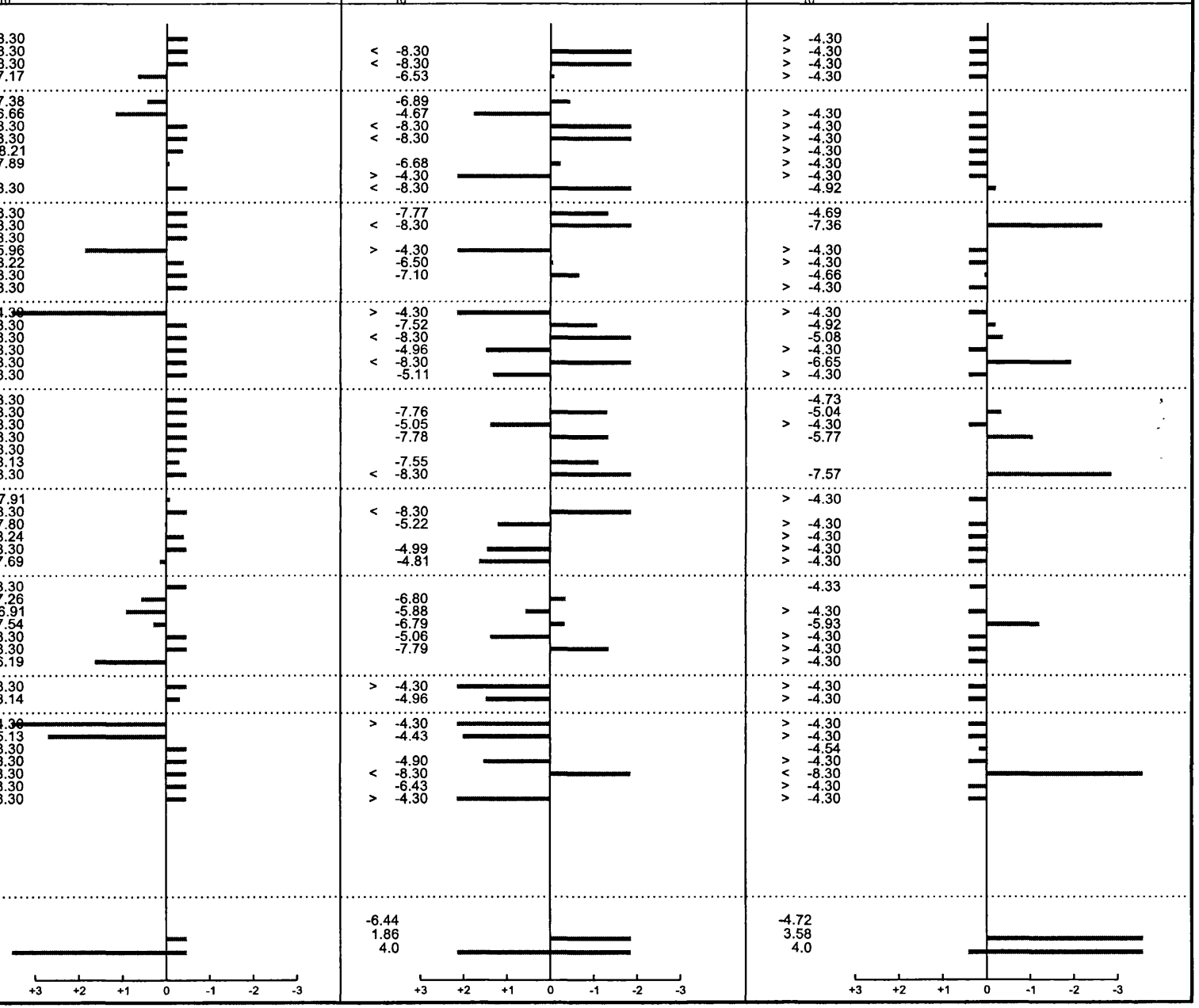

Appendix 2. 60 Cell-line profile for RMH035 (Th-Py-PBD).

National Cancer Institute Developmental Therapeutics Program

Mean Graphs

NSC : D736536 / 1	Units : Molar	SSPL : 0CCJ	EXP. ID : 0508NS15
Report Date : October 04, 2005		Test Date : August 15, 2005	

Panel/Cell Line	Log_{10}GI50	Log_{10}TGI	Log_{10}LC50
Leukemia			
CCRF-CEM	< -8.30	-7.82	
HL-60(TB)	-8.03	-6.73	> -4.30
K-562	-7.81	> -4.30	> -4.30
MOLT-4	-7.99		> -4.30
RPMI-8226	-6.95	-6.29	
Non-Small Cell Lung Cancer			
A549/ATCC	-6.13		> -4.30
EKVX	-5.75	> -4.30	> -4.30
HOP-62	-6.93	> -4.30	> -4.30
HOP-92	-7.73	-7.07	> -4.30
NCI-H226	-7.40	-6.87	
NCI-H23	-6.81	-5.43	> -4.30
NCI-H322M	-6.22	-5.53	> -4.30
NCI-H460	-6.57		> -4.30
NCI-H522	-8.13	-7.57	> -4.30
Colon Cancer			
COLO 205	-7.70	-7.14	-6.72
HCC-2998	-6.34	-5.68	> -4.30
HCT-116	-7.13		> -4.30
HCT-15	-5.72	-4.79	> -4.30
HT29	-6.73		> -4.30
KM12	-7.04		> -4.30
SW-620	-7.08	> -4.30	> -4.30
CNS Cancer			
SF-268	-7.83	-6.71	> -4.30
SF-295	-6.65	> -4.30	> -4.30
SF-539	-7.71	-6.72	> -4.30
SNB-19	-7.30		> -4.30
SNB-75	-7.20	-6.53	-5.71
U251	-7.80		> -4.30
Melanoma			
LOX IMVI	-8.08	-7.48	
MALME-3M	-6.83	-6.34	
M14	-6.63	-5.76	-4.49
SK-MEL-2	-7.09	-6.73	-6.36
SK-MEL-28	-6.73	-6.18	-4.90
SK-MEL-5	-6.88	-6.27	
UACC-257	-6.39	-5.92	
Ovarian Cancer			
IGROV1	-7.19		> -4.30
OVCAR-3	-7.15		> -4.30
OVCAR-4	-6.48	-5.77	> -4.30
OVCAR-5	-6.68	> -4.30	> -4.30
OVCAR-8	-6.60	> -4.30	> -4.30
SK-OV-3	-6.92		> -4.30
Renal Cancer			
786-0	-6.84	> -4.30	> -4.30
A498	-6.75	-5.99	> -4.30
ACHN	-6.70	-6.06	
CAKI-1	-6.24	-5.65	> -4.30
RXF 393	-7.10	-6.74	-6.38
TK-10	-6.75	> -4.30	> -4.30
UO-31	-6.07		
Prostate Cancer			
PC-3	-7.27	-6.66	> -4.30
DU-145	-6.79	> -4.30	> -4.30
Breast Cancer			
MCF7	-7.61	-6.59	> -4.30
NCI/ADR-RES	-4.88	> -4.30	> -4.30
MDA-MB-231/ATCC	-7.87	-7.06	> -4.30
HS 578T	-6.70		> -4.30
MDA-MB-435	-5.91	-5.48	-4.31
BT-549	-7.48	-5.03	> -4.30
T-47D	-8.24	-7.21	
MG_MID	-7.0	-5.84	-4.49
Delta	1.3	1.98	2.23
Range	3.42	3.52	2.42

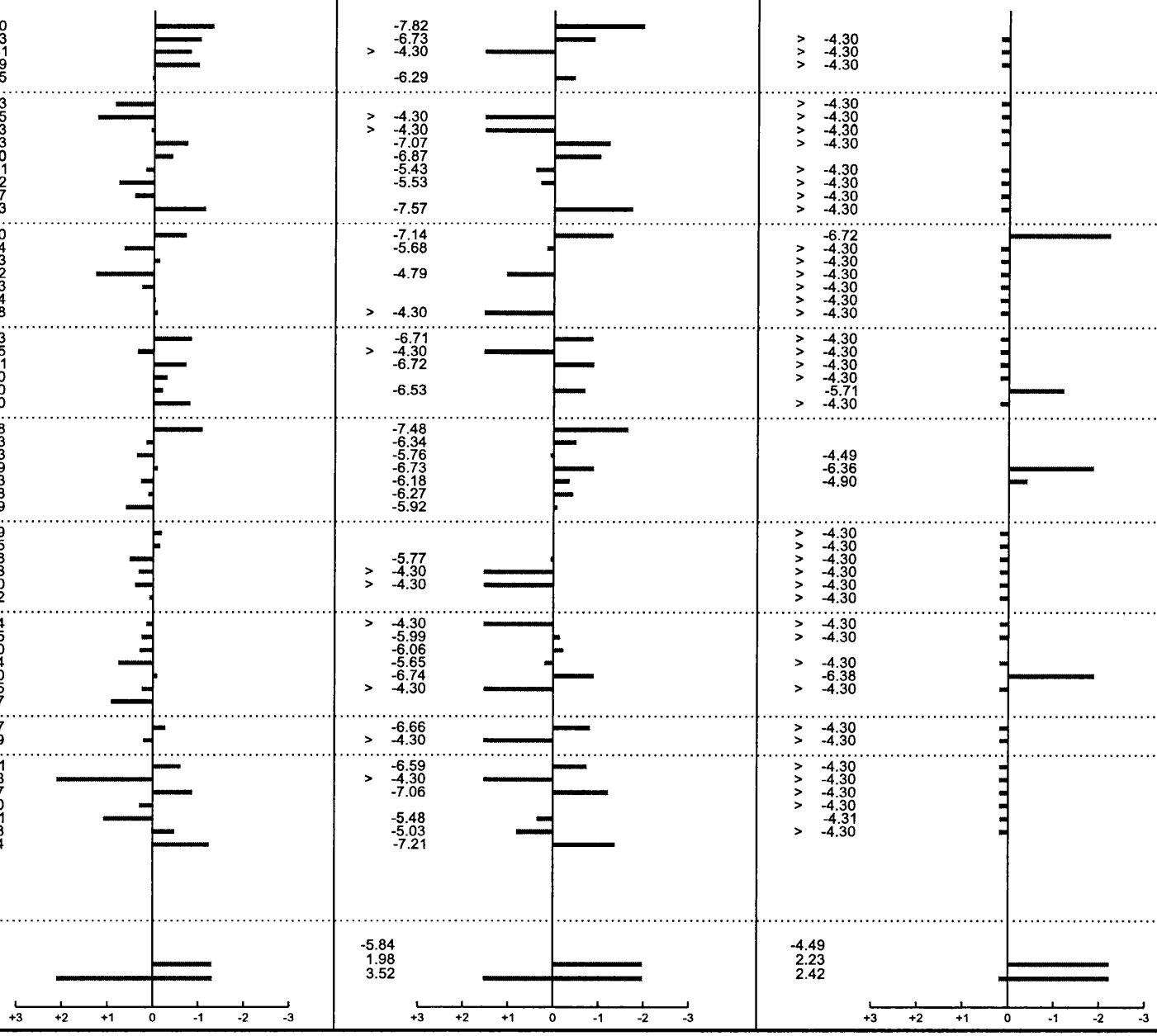

Appendix 3. 60 Cell-line profile for RMH037 (Im-Py-PBD).

National Cancer Institute Developmental Therapeutics Program

Mean Graphs

NSC : D736537 / 1 | Units : Molar | SSPL : 0CCJ | EXP. ID : 0508NS15

Report Date : October 04, 2005 | Test Date : August 15, 2005

Panel/Cell Line	Log_{10}GI50	GI50	Log_{10}TGI	TGI	Log_{10}LC50	LC50
Leukemia						
CCRF-CEM	< -8.90		< -8.90			
HL-60(TB)	< -8.90		> -4.90		> -4.90	
K-562	< -8.90		> -4.90		> -4.90	
MOLT-4	< -8.90		> -4.90		> -4.90	
RPMI-8226	< -8.90		< -8.90		-7.33	
SR	< -8.90		< -8.90		> -4.90	
Non-Small Cell Lung Cancer						
A549/ATCC	< -8.90				> -4.90	
EKVX	< -8.90		> -4.90		> -4.90	
HOP-62	< -8.90		-5.63		> -4.90	
HOP-92	< -8.90		< -8.90		> -4.90	
NCI-H226	< -8.90		< -8.90			
NCI-H23	< -8.90		< -8.90		-8.10	
NCI-H322M	< -8.90		< -8.90		> -4.90	
NCI-H460	< -8.90				> -4.90	
NCI-H522	< -8.90		< -8.90		-5.53	
Colon Cancer						
COLO 205	< -8.90		< -8.90		< -8.90	
HCC-2998	< -8.90		< -8.90			
HCT-116	< -8.90		> -4.90		> -4.90	
HCT-15	-8.71		-7.01		> -4.90	
HT29	< -8.90		< -8.90			
KM12	< -8.90				> -4.90	
SW-620	< -8.90				> -4.90	
CNS Cancer						
SF-268	< -8.90		< -8.90		> -4.90	
SF-295	< -8.90		-6.78		> -4.90	
SF-539	< -8.90				> -4.90	
SNB-19	< -8.90		-5.18		> -4.90	
SNB-75	< -8.90		< -8.90		-8.26	
U251	< -8.90		-7.75		> -4.90	
Melanoma						
LOX IMVI	< -8.90		< -8.90		> -4.90	
MALME-3M	< -8.90		< -8.90			
M14	< -8.90		< -8.90		< -8.90	
SK-MEL-2	< -8.90		< -8.90		< -8.90	
SK-MEL-28	< -8.90		< -8.90			
SK-MEL-5	< -8.90		< -8.90		< -8.90	
UACC-257	< -8.90		< -8.90		> -4.90	
Ovarian Cancer						
IGROV1	< -8.90		< -8.90			
OVCAR-3	< -8.90		< -8.90		> -4.90	
OVCAR-4	< -8.90		< -8.90			
OVCAR-5	< -8.90		> -4.90		> -4.90	
OVCAR-8	< -8.90		> -4.90		> -4.90	
SK-OV-3	< -8.90		> -4.90		> -4.90	
Renal Cancer						
786-0	< -8.90		> -4.90		> -4.90	
A498	< -8.90		< -8.90			
ACHN	< -8.90		< -8.90			
CAKI-1	< -8.90				> -4.90	
RXF 393	< -8.90		< -8.90		< -8.90	
TK-10	< -8.90		> -4.90		> -4.90	
UO-31	< -8.90		-8.86			
Prostate Cancer						
PC-3	< -8.90		-7.76		> -4.90	
DU-145	< -8.90		> -4.90		> -4.90	
Breast Cancer						
MCF7	< -8.90		-7.75		> -4.90	
NCI/ADR-RES	-7.54		> -4.90		> -4.90	
MDA-MB-231/ATCC	< -8.90		< -8.90		> -4.90	
HS 578T	< -8.90		< -8.90		> -4.90	
MDA-MB-435	< -8.90		< -8.90		< -8.90	
BT-549	< -8.90		-6.03		> -4.90	
T-47D	< -8.90		< -8.90		> -4.90	
MG_MID	-8.88		-7.62		-5.63	
Delta	0.02		1.28		3.27	
Range	1.36		4.0		4.0	

+3 +2 +1 0 -1 -2 -3

Appendix 4. 60 Cell-line profile for RMH041 (Py-Py-Im-PBD).

National Cancer Institute Developmental Therapeutics Program

Mean Graphs

NSC : D736538 / 1	Units : Molar	SSPL : 0CCJ	EXP. ID : 0508NS15
Report Date : October 04, 2005		Test Date : August 15, 2005	

Panel/Cell Line	Log_{10}GI50	GI50	Log_{10}TGI	TGI	Log_{10}LC50	LC50
Leukemia						
CCRF-CEM	< -8.90		< -8.90			
HL-60(TB)	< -8.90		> -4.90		> -4.90	
K-562	< -8.90		> -4.90		> -4.90	
MOLT-4	< -8.90		> -4.90		> -4.90	
RPMI-8226	< -8.90		-8.60		-6.83	
SR	< -8.90		< -8.90		> -4.90	
Non-Small Cell Lung Cancer						
A549/ATCC	< -8.90					
EKVX	< -8.90		> -4.90		> -4.90	
HOP-62	< -8.90				> -4.90	
HOP-92	< -8.90		< -8.90		> -4.90	
NCI-H226	< -8.90		< -8.90			
NCI-H23	< -8.90		< -8.90			
NCI-H322M	< -8.90		< -8.90		> -4.90	
NCI-H460	< -8.90		> -4.90		> -4.90	
NCI-H522	< -8.90		< -8.90		> -4.90	
Colon Cancer						
COLO 205	< -8.90		< -8.90		< -8.90	
HCC-2998	< -8.90		-8.88			
HCT-116	< -8.90					
HCT-15	-8.25		-6.97		> -4.90	
HT29	< -8.90					
KM12	< -8.90				> -4.90	
SW-620	< -8.90					
CNS Cancer						
SF-268	< -8.90		< -8.90		> -4.90	
SF-295	< -8.90		> -4.90		> -4.90	
SF-539	< -8.90				> -4.90	
SNB-19	< -8.90		> -4.90		> -4.90	
SNB-75	< -8.90		< -8.90		-7.45	
U251	< -8.90		-8.14		> -4.90	
Melanoma						
LOX IMVI	< -8.90		< -8.90		> -4.90	
MALME-3M	< -8.90		< -8.90			
M14	< -8.90		< -8.90			
SK-MEL-2	< -8.90		< -8.90		< -8.90	
SK-MEL-28	< -8.90		< -8.90			
SK-MEL-5	< -8.90		< -8.90			
UACC-257	< -8.90		< -8.90			
Ovarian Cancer						
IGROV1	< -8.90					
OVCAR-3	< -8.90				> -4.90	
OVCAR-4	-8.60		-8.21		> -4.90	
OVCAR-5	< -8.90		> -4.90		> -4.90	
OVCAR-8	< -8.90		> -4.90		> -4.90	
SK-OV-3	< -8.90				> -4.90	
Renal Cancer						
786-0	< -8.90				> -4.90	
A498	< -8.90		< -8.90			
ACHN	< -8.90		< -8.90			
CAKI-1	< -8.90		< -8.90		> -4.90	
RXF 393	< -8.90		< -8.90		< -8.90	
TK-10	< -8.90		> -4.90		> -4.90	
UO-31	< -8.90		-8.47		> -4.90	
Prostate Cancer						
PC-3	< -8.90		-7.51		> -4.90	
DU-145	< -8.90		> -4.90		> -4.90	
Breast Cancer						
MCF7	< -8.90				> -4.90	
NCI/ADR-RES	-7.31		> -4.90		> -4.90	
MDA-MB-231/ATCC	< -8.90		< -8.90		> -4.90	
HS 578T	< -8.90		-5.90		> -4.90	
MDA-MB-435	< -8.90		< -8.90		-7.31	
BT-549	< -8.90		> -4.90		> -4.90	
T-47D	< -8.90				> -4.90	
MG_MID	-8.86		-7.53		-5.36	
Delta	0.04		1.37		3.54	
Range	1.59		4.0		4.0	

+3 +2 +1 0 -1 -2 -3

Appendix 5. 60 Cell-line profile for RMH043 (Py-Py-Th-PBD).

National Cancer Institute Developmental Therapeutics Program

Mean Graphs

NSC : D736539 / 1	Units : Molar	SSPL : 0CCJ	EXP. ID : 0508NS15
Report Date : October 04, 2005		Test Date : August 15, 2005	

Panel/Cell Line	Log_{10}GI50	GI50	Log_{10}TGI	TGI	Log_{10}LC50	LC50
Leukemia						
CCRF-CEM	< -8.60		< -8.60			
HL-60(TB)	< -8.60		> -4.60		> -4.60	
K-562	< -8.60		> -4.60		> -4.60	
MOLT-4	< -8.60		> -4.60		> -4.60	
RPMI-8226	< -8.60		-8.19			
SR	< -8.60		< -8.60		> -4.60	
Non-Small Cell Lung Cancer						
A549/ATCC	< -8.60				> -4.60	
EKVX	-8.04		> -4.60		> -4.60	
HOP-62	< -8.60				> -4.60	
HOP-92	< -8.60		< -8.60		> -4.60	
NCI-H226	< -8.60		< -8.60			
NCI-H23	< -8.60		< -8.60		-6.74	
NCI-H322M	< -8.60		< -8.60		> -4.60	
NCI-H460	< -8.60				> -4.60	
NCI-H522	< -8.60		< -8.60		> -4.60	
Colon Cancer						
COLO 205	< -8.60		< -8.60		< -8.60	
HCC-2998	< -8.60		-8.28			
HCT-116	< -8.60					
HCT-15	-7.36		-6.38		> -4.60	
HT29	< -8.60		< -8.60			
KM12	< -8.60		< -8.60		> -4.60	
SW-620	< -8.60		< -8.60		> -4.60	
CNS Cancer						
SF-268	< -8.60		< -8.60		> -4.60	
SF-295	< -8.60		-5.71		> -4.60	
SF-539	< -8.60		< -8.60		> -4.60	
SNB-19	< -8.60				> -4.60	
SNB-75	< -8.60		< -8.60		-7.15	
U251	< -8.60		-7.41		> -4.60	
Melanoma						
LOX IMVI	< -8.60		< -8.60		> -4.60	
MALME-3M	< -8.60		< -8.60			
M14	< -8.60		-8.22		-5.90	
SK-MEL-2	< -8.60		< -8.60		-7.87	
SK-MEL-28	< -8.60		< -8.60		-8.42	
SK-MEL-5	< -8.60		< -8.60		-8.31	
UACC-257	< -8.60		-8.48			
Ovarian Cancer						
IGROV1	< -8.60		< -8.60			
OVCAR-3	< -8.60				> -4.60	
OVCAR-4	< -8.60		-8.41		> -4.60	
OVCAR-5	< -8.60				> -4.60	
OVCAR-8	< -8.60		> -4.60		> -4.60	
SK-OV-3	< -8.60		< -8.60		> -4.60	
Renal Cancer						
786-0	< -8.60					
A498	< -8.60		< -8.60			
ACHN	< -8.60		-8.48			
CAKI-1	< -8.60				> -4.60	
RXF 393	< -8.60		< -8.60		< -8.60	
TK-10	< -8.60				> -4.60	
UO-31	-8.50		-7.49			
Prostate Cancer						
PC-3	< -8.60		-6.77		> -4.60	
DU-145	< -8.60		> -4.60		> -4.60	
Breast Cancer						
MCF7	< -8.60		-7.17		> -4.60	
NCI/ADR-RES	-6.60		> -4.60		> -4.60	
MDA-MB-231/ATCC	< -8.60		< -8.60		> -4.60	
HS 578T	< -8.60		-7.78		> -4.60	
MDA-MB-435	< -8.60		< -8.60			
BT-549	< -8.60		-7.24		> -4.60	
T-47D	< -8.60		< -8.60		> -4.60	
MG_MID	-8.53		-7.7		-5.18	
Delta	0.07		0.9		3.42	
Range	2.0		4.0		4.0	

+3 +2 +1 0 -1 -2 -3

Appendix 6. 60 Cell-line profile for RMH045 (Py-Im-Py-PBD).

National Cancer Institute Developmental Therapeutics Program

Mean Graphs

NSC : D736540 / 1	Units : Molar	SSPL : 0CCJ	EXP. ID : 0508NS15
Report Date : October 04, 2005		Test Date : August 15, 2005	

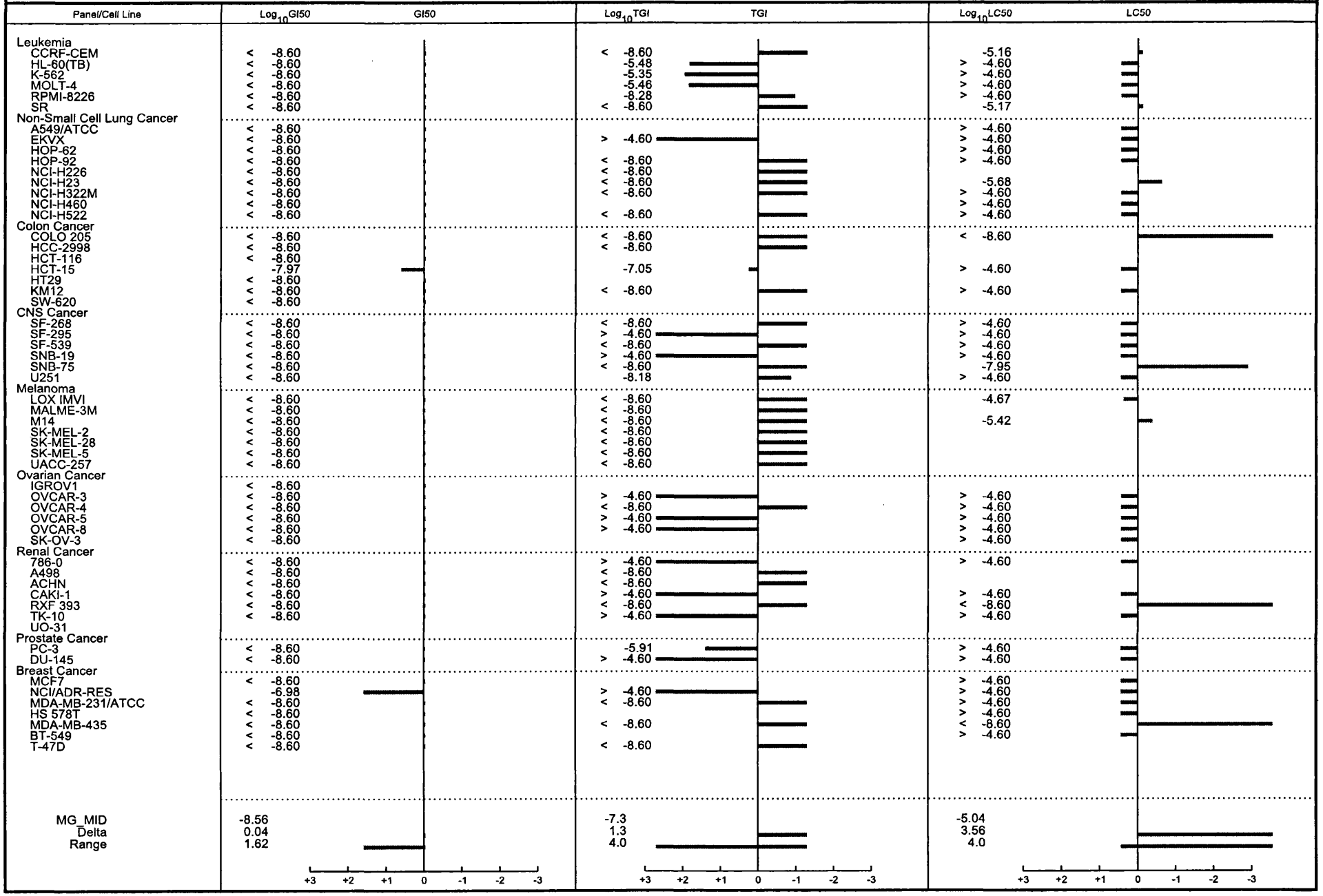

Appendix 7. 60 Cell-line profile for RMH047 (Py-Th-Py-PBD).

National Cancer Institute Developmental Therapeutics Program

Mean Graphs

NSC : D736541 / 1	Units : Molar	SSPL : 0CCJ	EXP. ID : 0508NS15
Report Date : October 04, 2005		Test Date : August 15, 2005	

Panel/Cell Line	Log_{10}GI50	GI50	Log_{10}TGI	TGI	Log_{10}LC50	LC50
Leukemia						
HL-60(TB)	< -8.60		> -4.60		> -4.60	
K-562	< -8.60		-5.60		> -4.60	
MOLT-4	< -8.60		> -4.60		> -4.60	
RPMI-8226	-8.33		-7.56		-6.65	
SR	< -8.60		< -8.60		> -4.60	
Non-Small Cell Lung Cancer						
A549/ATCC	-8.20		-6.14		> -4.60	
EKVX	-7.31				> -4.60	
HOP-62	< -8.60				> -4.60	
HOP-92	< -8.60		< -8.60		> -4.60	
NCI-H226	< -8.60		-8.28			
NCI-H23	< -8.60		-7.23		> -4.60	
NCI-H322M	-8.38		-7.86		> -4.60	
NCI-H460	-8.41				> -4.60	
NCI-H522	< -8.60		< -8.60		-5.80	
Colon Cancer						
COLO 205	< -8.60		< -8.60		< -8.60	
HCC-2998	-8.51		-7.23		-5.34	
HCT-116	< -8.60					
HCT-15	-6.80		-5.78		> -4.60	
HT29	< -8.60		-8.29			
KM12	< -8.60		-8.22		> -4.60	
SW-620	< -8.60		-8.34		> -4.60	
CNS Cancer						
SF-268	< -8.60		-8.05		> -4.60	
SF-295	< -8.60		-7.82		> -4.60	
SF-539	< -8.60		-8.57		-4.71	
SNB-19	< -8.60		-7.47		> -4.60	
SNB-75	< -8.60		< -8.60		-7.17	
U251	< -8.60				-4.96	
Melanoma						
LOX IMVI	< -8.60		< -8.60		-5.30	
MALME-3M	< -8.60		-8.18		-4.94	
M14	< -8.60		-8.12		-7.36	
SK-MEL-2	< -8.60		-8.30		-7.13	
SK-MEL-28	< -8.60		-8.42		-7.79	
SK-MEL-5	< -8.60		-8.21			
UACC-257	-8.45		-7.92		> -4.60	
Ovarian Cancer						
IGROV1	< -8.60		-8.16			
OVCAR-3	< -8.60				> -4.60	
OVCAR-4	-8.25		-7.71		> -4.60	
OVCAR-5	-8.55				> -4.60	
OVCAR-8	< -8.60		> -4.60		> -4.60	
SK-OV-3	< -8.60				> -4.60	
Renal Cancer						
786-0	< -8.60				> -4.60	
A498	-8.46		-7.78		> -4.60	
ACHN	-8.17		-7.33			
CAKI-1	-7.94		-7.14		> -4.60	
RXF 393	< -8.60		-8.52		-7.92	
TK-10	-8.23		> -4.60		> -4.60	
UO-31	-7.42		-7.11			
Prostate Cancer						
PC-3	< -8.60		-7.29		> -4.60	
DU-145	< -8.60		> -4.60		> -4.60	
Breast Cancer						
MCF7	< -8.60		-7.44		-5.00	
NCI/ADR-RES	-6.27		> -4.60		> -4.60	
MDA-MB-231/ATCC	< -8.60		-8.16		> -4.60	
HS 578T	< -8.60		-6.77		> -4.60	
MDA-MB-435	< -8.60		< -8.60		-7.99	
BT-549	< -8.60		-7.85		> -4.60	
T-47D	< -8.60		< -8.60		> -4.60	
MG_MID	-8.42		-7.43		-5.17	
Delta	0.18		1.17		3.43	
Range	2.33		4.0		4.0	

+3 +2 +1 0 -1 -2 -3

Appendix 8. 60 Cell-line profile for RMH049 (Py-Im-Im-PBD).

National Cancer Institute Developmental Therapeutics Program

Mean Graphs

NSC : D736542 / 1	Units : Molar	SSPL : 0CCJ	EXP. ID : 0508NS15
Report Date : October 04, 2005		Test Date : August 15, 2005	

Panel/Cell Line	Log_{10}GI50	GI50	Log_{10}TGI	TGI	Log_{10}LC50	LC50
Leukemia						
HL-60(TB)	-7.46		> -4.60		> -4.60	
K-562	-7.42		> -4.60		> -4.60	
MOLT-4	-7.53		> -4.60		> -4.60	
RPMI-8226	-6.84		-6.19		> -4.60	
SR	-8.21		-7.30		> -4.60	
Non-Small Cell Lung Cancer						
A549/ATCC	-6.40				> -4.60	
EKVX	-6.00		> -4.60		> -4.60	
HOP-62	-7.28				> -4.60	
HOP-92	-7.44		-6.94		> -4.60	
NCI-H226	-7.42		-6.93		> -4.60	
NCI-H23	-6.90		-5.78		> -4.60	
NCI-H322M	-6.57		-5.86		> -4.60	
NCI-H460	-6.80		> -4.60		> -4.60	
NCI-H522	-7.68		-6.98		> -4.60	
Colon Cancer						
COLO 205	-7.44		-7.15		-6.86	
HCC-2998	-6.74				> -4.60	
HCT-116	-7.28					
HCT-15	-5.64		-4.65		> -4.60	
HT29	-7.03				> -4.60	
KM12	-7.22				> -4.60	
SW-620	-7.33				> -4.60	
CNS Cancer						
SF-268	-7.30		-6.39		> -4.60	
SF-295	-7.04				> -4.60	
SF-539	-7.70		-6.86		> -4.60	
SNB-19	-7.34		> -4.60		> -4.60	
SNB-75	-7.26		-6.75		-5.90	
U251	-7.84				> -4.60	
Melanoma						
LOX IMVI	-7.47		-6.99		> -4.60	
MALME-3M	-7.11		-6.64		> -4.60	
M14	-6.89		-6.34		-5.85	
SK-MEL-2	-7.23		-6.86		-5.51	
SK-MEL-28	-7.19		-6.85		-5.81	
SK-MEL-5	-7.10				> -4.60	
UACC-257	-6.86		-6.28			
Ovarian Cancer						
IGROV1	-7.36		-6.80		> -4.60	
OVCAR-3	-7.10				> -4.60	
OVCAR-4	-6.19		-5.69		> -4.60	
OVCAR-5	-7.23				> -4.60	
OVCAR-8	-6.88		> -4.60		> -4.60	
SK-OV-3	-7.08				> -4.60	
Renal Cancer						
786-0	-7.02		> -4.60		> -4.60	
A498	-7.01				> -4.60	
ACHN	-6.53		-6.11			
CAKI-1	-6.41				> -4.60	
RXF 393	-7.41		-7.02		-6.63	
TK-10	-6.44		> -4.60		> -4.60	
UO-31	-6.29		-5.96			
Prostate Cancer						
PC-3	-7.27		-6.61		> -4.60	
DU-145	-6.87		> -4.60		> -4.60	
Breast Cancer						
MCF7	-7.26		> -4.60		> -4.60	
NCI/ADR-RES	-5.13		> -4.60		> -4.60	
MDA-MB-231/ATCC	-7.34		-6.87		> -4.60	
HS 578T	-6.86		> -4.60		> -4.60	
MDA-MB-435	-7.35		-7.03		-6.71	
BT-549	-7.32		> -4.60		> -4.60	
T-47D	-7.85		-7.10		> -4.60	
MG_MID	-7.06		-5.89		-4.81	
Delta	1.15		1.41		2.05	
Range	3.08		2.7		2.26	

+3 +2 +1 0 -1 -2 -3

Appendix 9. 60 Cell-line profile for RMH051 (Im-Im-Im-PBD).

Appendix 10. 60 Cell-line profile for RMH053 (Im-Im-Py-PBD).

National Cancer Institute Developmental Therapeutics Program

Mean Graphs

NSC : D736543 / 1	Units : Molar	SSPL : 0CCJ	EXP. ID : 0508NS15
Report Date : October 04, 2005		Test Date : August 15, 2005	

Panel/Cell Line	Log_{10}GI50	GI50	Log_{10}TGI	TGI	Log_{10}LC50	LC50
Leukemia						
HL-60(TB)	< -8.60		> -4.60		> -4.60	
K-562	-8.33		> -4.60		> -4.60	
MOLT-4	-8.51		> -4.60		> -4.60	
RPMI-8226	-7.57		-7.03		> -4.60	
SR	< -8.60		-7.80		> -4.60	
Non-Small Cell Lung Cancer						
A549/ATCC	-7.51					
EKVX	-6.87		> -4.60		> -4.60	
HOP-62	-8.05				> -4.60	
HOP-92	-8.07		-7.16		> -4.60	
NCI-H226	-8.53		-7.56			
NCI-H23	-8.31		-7.31		-6.31	
NCI-H322M	-7.36				> -4.60	
NCI-H460	-8.06		-7.21			
NCI-H522	-8.40		-7.74		-5.60	
Colon Cancer						
COLO 205	-7.82		-7.30		-6.90	
HCC-2998	-7.42		-7.12			
HCT-116	-7.84				> -4.60	
HCT-15	-6.46		-5.86		> -4.60	
HT29	-7.73		-7.29			
KM12	-7.44		-6.97		> -4.60	
SW-620	-7.94				> -4.60	
CNS Cancer						
SF-268	-8.45		-7.21		> -4.60	
SF-295	-7.72		-5.75		> -4.60	
SF-539	-8.45		-6.96		> -4.60	
SNB-19	< -8.60		> -4.60		> -4.60	
SNB-75	< < -8.60		-8.54		-6.78	
U251	< -8.60		-8.35			
Melanoma						
LOX IMVI	-8.59		-7.79		> -4.60	
MALME-3M	-7.90		-7.30			
M14	-7.61		-7.15		-6.69	
SK-MEL-2	-7.86		-7.30		-6.83	
SK-MEL-28	-7.65		-7.18		-6.75	
SK-MEL-5	-7.59		-7.25			
UACC-257	-7.45		-7.08			
Ovarian Cancer						
IGROV1	-8.24		-7.38			
OVCAR-3	-7.93				> -4.60	
OVCAR-4	-7.26		-6.82		> -4.60	
OVCAR-5	-7.85		> -4.60		> -4.60	
OVCAR-8	-7.50		> -4.60		> -4.60	
SK-OV-3	-7.88		-5.03		> -4.60	
Renal Cancer						
786-0	-8.01		> -4.60		> -4.60	
A498	-7.58		-7.13			
ACHN	-7.99		-7.26			
CAKI-1	-7.52		-6.66		> -4.60	
RXF 393	-8.01		-7.33		-6.90	
TK-10	-7.12		> -4.60		> -4.60	
UO-31	-7.14		-6.66			
Prostate Cancer						
PC-3	-7.84		-6.40		> -4.60	
DU-145	-7.68		> -4.60		> -4.60	
Breast Cancer						
MCF7	-8.42		-7.35		> -4.60	
NCI/ADR-RES	-5.85		-4.64		> -4.60	
MDA-MB-231/ATCC	-8.02		-7.03		> -4.60	
HS 578T	-7.34		-6.68		> -4.60	
MDA-MB-435	-8.21		-7.47		-6.62	
BT-549	-8.07		-6.65		> -4.60	
T-47D	< -8.60		-7.34		> -4.60	
MG_MID	-7.87		-6.56		-5.02	
Delta	0.73		1.98		1.88	
Range	2.75		3.94		2.3	

+3 +2 +1 0 -1 -2 -3

National Cancer Institute Developmental Therapeutics Program

Mean Graphs

NSC : D736544 / 1	Units : Molar	SSPL : 0CCJ	EXP. ID : 0508NS15
Report Date : October 04, 2005		Test Date : August 15, 2005	

Panel/Cell Line	Log_{10}GI50	GI50	Log_{10}TGI	TGI	Log_{10}LC50	LC50
Leukemia						
HL-60(TB)	< -8.60		> -4.60		> -4.60	
K-562	< -8.60		-5.55		> -4.60	
MOLT-4	< -8.60		> -4.60		> -4.60	
RPMI-8226	-8.20		-7.27		> -4.60	
SR	< -8.60		< -8.60		> -4.60	
Non-Small Cell Lung Cancer						
A549/ATCC	-8.07				> -4.60	
EKVX	-7.06		> -4.60		> -4.60	
HOP-62	< -8.60				> -4.60	
HOP-92	< -8.60		< -8.60		> -4.60	
NCI-H226	< -8.60		-8.31			
NCI-H23	< -8.60		-8.14		> -4.60	
NCI-H322M	-8.18		-7.02		> -4.60	
NCI-H460	-8.50				> -4.60	
NCI-H522	< -8.60		< -8.60			
Colon Cancer						
COLO 205	< -8.60		-8.45		-8.01	
HCC-2998	-8.29		-7.47			
HCT-116	< -8.60					
HCT-15	-6.60		> -4.60		> -4.60	
HT29	-8.52		-7.96			
KM12	< -8.60				> -4.60	
SW-620	< -8.60		> -4.60		> -4.60	
CNS Cancer						
SF-268	< -8.60		-8.01		> -4.60	
SF-295	< -8.60		> -4.60		> -4.60	
SF-539	< -8.60		-8.25		> -4.60	
SNB-19	< -8.60		> -4.60		> -4.60	
SNB-75	< -8.60		< -8.60		-7.18	
U251	< -8.60					
Melanoma						
LOX IMVI	< -8.60		< -8.60		> -4.60	
MALME-3M	< -8.60		-8.15			
M14	-8.49		-7.40			
SK-MEL-2	< -8.60		-8.36		-7.84	
SK-MEL-28	< -8.60		-8.29		-7.84	
SK-MEL-5	-8.56					
UACC-257	-8.33		-7.60			
Ovarian Cancer						
IGROV1	< -8.60		-8.25			
OVCAR-3	< -8.60				> -4.60	
OVCAR-4	-7.91		-7.10		> -4.60	
OVCAR-5	-8.49				> -4.60	
OVCAR-8	< -8.60		> -4.60		> -4.60	
SK-OV-3	< -8.60		> -4.60		> -4.60	
Renal Cancer						
786-0	< -8.60				> -4.60	
A498	-8.29		-7.46		> -4.60	
ACHN	-8.47		-7.45			
CAKI-1	-7.64				> -4.60	
RXF 393	< -8.60		-8.20			
TK-10	-8.03		> -4.60		> -4.60	
UO-31	-7.51		-7.11			
Prostate Cancer						
PC-3	< -8.60		-6.56		> -4.60	
DU-145	< -8.60		> -4.60		> -4.60	
Breast Cancer						
MCF7	< -8.60				> -4.60	
NCI/ADR-RES	-6.15		> -4.60		> -4.60	
MDA-MB-231/ATCC	< -8.60		-8.25		> -4.60	
HS 578T	-8.28		> -4.60		> -4.60	
MDA-MB-435	< -8.60		-8.07			
BT-549	< -8.60				> -4.60	
T-47D	< -8.60				> -4.60	
MG_MID	-8.38		-6.85		-4.91	
Delta	0.22		1.75		3.1	
Range	2.45		4.0		3.41	

+3 +2 +1 0 -1 -2 -3

Appendix 11. 60 Cell-line profile for RMH055 (Im-Py-Im-PBD).

Appendix 12. 60 Cell-line profile for RMH057 (Im-Py-Py-PBD).

National Cancer Institute Developmental Therapeutics Program
Mean Graphs

NSC : D736545 / 1 | Units : Molar | SSPL : 0CCJ | EXP. ID : 0508NS15

Report Date : October 04, 2005 | Test Date : August 15, 2005

Panel/Cell Line	Log_{10}GI50	GI50	Log_{10}TGI	TGI	Log_{10}LC50	LC50
Leukemia						
CCRF-CEM	< -8.60		< -8.60			
HL-60(TB)	< -8.60		> -4.60		> -4.60	
K-562	< -8.60		> -4.60		> -4.60	
MOLT-4	< -8.60		> -4.60		> -4.60	
RPMI-8226	< -8.60		< -8.60		> -4.60	
SR	< -8.60		< -8.60		> -4.60	
Non-Small Cell Lung Cancer						
A549/ATCC	< -8.60					
EKVX	-8.15		> -4.60		> -4.60	
HOP-62	< -8.60				> -4.60	
HOP-92	< -8.60		< -8.60		> -4.60	
NCI-H226	< -8.60		< -8.60			
NCI-H23	< -8.60		< -8.60		-7.30	
NCI-H322M	< -8.60		< -8.60		> -4.60	
NCI-H460	< -8.60		< -8.60		> -4.60	
NCI-H522	< -8.60		< -8.60		-6.13	
Colon Cancer						
COLO 205	< -8.60		< -8.60		-8.55	
HCC-2998	< -8.60		-8.55			
HCT-116	< -8.60					
HCT-15	-8.23		-6.88		> -4.60	
HT29	< -8.60		< -8.60			
KM12	< -8.60		-6.32		> -4.60	
SW-620	< -8.60				> -4.60	
CNS Cancer						
SF-268	< -8.60		< -8.60		> -4.60	
SF-295	< -8.60		-5.26		> -4.60	
SF-539	< -8.60		-8.31		-4.70	
SNB-19	< -8.60		> -4.60		> -4.60	
SNB-75	< -8.60		< -8.60		-7.28	
U251	< -8.60		< -8.60		> -4.60	
Melanoma						
LOX IMVI	< -8.60		< -8.60		> -4.60	
MALME-3M	< -8.60		< -8.60		-8.09	
M14	< -8.60		-8.00		-5.18	
SK-MEL-2	< -8.60		< -8.60		< -8.60	
SK-MEL-28	< -8.60		< -8.60		-8.41	
SK-MEL-5	< -8.60		< -8.60			
UACC-257	< -8.60		< -8.60			
Ovarian Cancer						
IGROV1	< -8.60		< -8.60			
OVCAR-3	< -8.60		-7.53		> -4.60	
OVCAR-4	-8.56		-7.63		> -4.60	
OVCAR-5	< -8.60		-5.71		> -4.60	
OVCAR-8	< -8.60		> -4.60		> -4.60	
SK-OV-3	< -8.60				> -4.60	
Renal Cancer						
786-0	< -8.60				> -4.60	
A498	< -8.60		< -8.60			
ACHN	< -8.60		< -8.60			
CAKI-1	< -8.60		< -8.60		> -4.60	
RXF 393	< -8.60		< -8.60		< -8.60	
TK-10	< -8.60				> -4.60	
UO-31	< -8.60		< -8.60			
Prostate Cancer						
PC-3	< -8.60		-6.33		> -4.60	
DU-145	< -8.60		> -4.60		> -4.60	
Breast Cancer						
MCF7	< -8.60		-6.82		> -4.60	
NCI/ADR-RES	-7.01		-5.50		> -4.60	
MDA-MB-231/ATCC	< -8.60		< -8.60		> -4.60	
HS 578T	< -8.60		-6.13		> -4.60	
MDA-MB-435	< -8.60		< -8.60		-6.59	
BT-549	< -8.60		-7.25		> -4.60	
T-47D	< -8.60		< -8.60		> -4.60	
MG_MID	-8.56		-7.56		-5.24	
Delta	0.04		1.04		3.36	
Range	1.59		4.0		4.0	

+3 +2 +1 0 -1 -2 -3

National Cancer Institute Developmental Therapeutics Program

Mean Graphs

NSC : D736547 / 1 | Units : Molar | SSPL : 0CCJ | EXP. ID : 0508NS15

Report Date : October 04, 2005 | Test Date : August 15, 2005

Panel/Cell Line	Log_{10}GI50	GI50	Log_{10}TGI	TGI	Log_{10}LC50	LC50
Leukemia						
CCRF-CEM	< -8.60		-7.86			
HL-60(TB)	-7.46		> -4.60		> -4.60	
K-562	-7.09		> -4.60		> -4.60	
MOLT-4	-7.48		> -4.60		> -4.60	
RPMI-8226	-6.42		-6.00		-5.25	
SR	-7.67		-6.96		> -4.60	
Non-Small Cell Lung Cancer						
A549/ATCC	-6.03		-5.42		-4.77	
EKVX	-4.94		> -4.60		> -4.60	
HOP-62	-6.90		> -4.60		> -4.60	
HOP-92	-6.85		-5.94		> -4.60	
NCI-H226	-6.55		-6.21		-5.87	
NCI-H23	-6.55		-5.90		> -4.60	
NCI-H322M	-6.23		-5.83		> -4.60	
NCI-H460	-6.43		-6.01		> -4.60	
NCI-H522	-7.37		-6.78		-5.38	
Colon Cancer						
COLO 205	-6.81		-6.32		-5.95	
HCC-2998	-6.37		-5.90		> -4.60	
HCT-116	-6.69				> -4.60	
HCT-15	-4.66		> -4.60		> -4.60	
HT29	-6.48		-6.19			
KM12	-6.46		-6.02		> -4.60	
SW-620	-6.58		-5.42		> -4.60	
CNS Cancer						
SF-268	-6.92		-5.99		> -4.60	
SF-295	-6.23		> -4.60		> -4.60	
SF-539	-6.96		-5.83		> -4.60	
SNB-19	-7.06		-5.70		> -4.60	
SNB-75	-7.24		-6.66		-5.64	
U251	-7.48		-7.02		> -4.60	
Melanoma						
LOX IMVI	-7.18		-6.47		> -4.60	
MALME-3M	-6.83		-6.26		-5.83	
M14	-6.24		-5.61		-4.70	
SK-MEL-2	-6.67		-6.24			
SK-MEL-28	-6.48		-6.13		-5.79	
SK-MEL-5	-6.43		-6.09		-5.75	
UACC-257	-6.32		-6.01			
Ovarian Cancer						
IGROV1	-6.75		-6.25			
OVCAR-3	-7.14		-6.35		> -4.60	
OVCAR-4	-6.27		-5.84		> -4.60	
OVCAR-5	-6.01				> -4.60	
OVCAR-8	-6.31		> -4.60		> -4.60	
SK-OV-3	-6.20		-5.73		> -4.60	
Renal Cancer						
786-0	-6.22		> -4.60		> -4.60	
A498	-6.20		-5.69		> -4.60	
ACHN	-5.63		> -4.60		> -4.60	
CAKI-1	-5.21		> -4.60		> -4.60	
RXF 393	-6.94		-6.51		-6.00	
TK-10	-6.02		> -4.60		> -4.60	
UO-31	-4.99		> -4.60		> -4.60	
Prostate Cancer						
PC-3	-6.76		-5.37		> -4.60	
DU-145	-6.15		> -4.60		> -4.60	
Breast Cancer						
MCF7	-7.22				> -4.60	
NCI/ADR-RES	> -4.60		> -4.60		> -4.60	
MDA-MB-231/ATCC	-7.06		-6.08		> -4.60	
HS 578T	-6.45		-5.23		> -4.60	
MDA-MB-435	-6.49		-6.07			
BT-549	-6.94		-5.86		> -4.60	
T-47D	-7.18		-6.61		> -4.60	
MG_MID	-6.55		-5.69		-4.8	
Delta	2.05		2.17		1.2	
Range	4.0		3.26		1.4	

+3 +2 +1 0 -1 -2 -3

Appendix 13. 60 Cell-line profile for RMH059 (Th-Th-Th-PBD).

National Cancer Institute Developmental Therapeutics Program

Mean Graphs

NSC : D736827 / 1	Units : Molar	SSPL : 0CCJ	EXP. ID : 0510NS60
Report Date : January 10, 2006		Test Date : October 24, 2005	

Panel/Cell Line	Log_{10}GI50	GI50	Log_{10}TGI	TGI	Log_{10}LC50	LC50
Leukemia						
CCRF-CEM	< -8.90		< -8.90			
HL-60(TB)			<< -4.90		> -4.90	
K-562	< -8.90		<< -4.90		>> -4.90	
MOLT-4	< -8.90		-8.13		> -4.90	
RPMI-8226	-8.45		-7.66		-6.93	
SR	< -8.90		< -8.90		> -4.90	
Non-Small Cell Lung Cancer						
A549/ATCC	-8.89				> -4.90	
EKVX	-8.23		>> -4.90		>> -4.90	
HOP-62	< -8.90		< -8.90		-5.77	
HOP-92	<< -8.90		-8.68		-5.42	
NCI-H226	<< -8.90		-8.73			
NCI-H23	< -8.90		< -8.90		-8.13	
NCI-H322M	-8.75		-8.24		> -4.90	
NCI-H460	<< -8.90		-5.86		-5.08	
NCI-H522	< -8.90		< -8.90		-6.45	
Colon Cancer						
COLO 205	< -8.90		-8.69			
HCC-2998	<< -8.90		-8.60		-8.14	
HCT-116	< -8.90				-5.33	
HCT-15	-7.50		> -4.90		> -4.90	
HT29	<< -8.90		-5.90		-4.93	
KM12	<< -8.90		-8.31		-5.53	
SW-620	< -8.90		> -4.90		> -4.90	
CNS Cancer						
SF-268	< -8.90		-5.79		>> -4.90	
SF-295	<< -8.90		-8.06		>> -4.90	
SF-539	<< -8.90		-7.84		-5.09	
SNB-19	< -8.90		-5.72		> -4.90	
SNB-75	<< -8.90		-8.83		-7.32	
U251	< -8.90					
Melanoma						
LOX IMVI	< -8.90				-5.29	
MALME-3M	<< -8.90		< -8.90			
M14	< -8.90		-8.77		-8.09	
SK-MEL-2	-8.79		-8.42		-8.06	
SK-MEL-28	< -8.90		-8.54		-7.53	
SK-MEL-5	-8.90					
UACC-257	-8.86		-8.36		-5.36	
UACC-62	< -8.90		< -8.90		-8.77	
Ovarian Cancer						
IGROV1	< -8.90					
OVCAR-3	< -8.90		-8.70		-5.01	
OVCAR-4	-8.85		-8.14		> -4.90	
OVCAR-5	<< -8.90				>> -4.90	
OVCAR-8	< -8.90		< -8.90		>> -4.90	
SK-OV-3	-8.54		-7.84		> -4.90	
Renal Cancer						
786-0	< -8.90				-5.34	
A498	-8.56		-7.58		-4.99	
ACHN	<< -8.90				> -4.90	
CAKI-1	<< -8.90		-7.19		>> -4.90	
RXF 393	<< -8.90		< -8.90			
SN12C	< -8.90		< -8.90		-5.67	
TK-10	-8.47				> -4.90	
UO-31	-7.85		-7.49			
Prostate Cancer						
PC-3	< -8.90		-7.45		> -4.90	
DU-145	< -8.90		-5.75		-4.94	
Breast Cancer						
MCF7	< -8.90		-6.99		-5.08	
NCI/ADR-RES	-6.93		-6.19		> -4.90	
MDA-MB-231/ATCC	< -8.90		-5.81		-5.08	
HS 578T	<< -8.90		> -4.90		> -4.90	
MDA-MB-435	<< -8.90		< -8.90		-8.01	
BT-549	<< -8.90		-6.18		> -4.90	
T-47D	< -8.90		-8.73		>> -4.90	
MG_MID	-8.78		-7.56		-5.58	
Delta	0.12		1.34		3.19	
Range	1.97		4.0		3.87	

+3 +2 +1 0 -1 -2 -3

Appendix 14. 60 Cell-line profile for RMH061 (Th-Py-Th-PBD).

National Cancer Institute Developmental Therapeutics Program

Mean Graphs

NSC : D736548 / 1	Units : Molar	SSPL : 0CCJ	EXP. ID : 0508NS15
Report Date : October 04, 2005		Test Date : August 15, 2005	

Panel/Cell Line	Log_{10}GI50	GI50	Log_{10}TGI	TGI	Log_{10}LC50	LC50
Leukemia						
CCRF-CEM	< -8.60		< -8.60		> -4.60	
HL-60(TB)	< -8.60		> -4.60		> -4.60	
K-562	< -8.60		> -4.60		> -4.60	
MOLT-4	< -8.60		> -4.60		> -4.60	
RPMI-8226	< -8.60		-8.09		> -4.60	
SR	< -8.60		< -8.60		> -4.60	
Non-Small Cell Lung Cancer						
A549/ATCC	< -8.60					
EKVX	-8.45		> -4.60		> -4.60	
HOP-62	< -8.60				> -4.60	
HOP-92	< -8.60		< -8.60		> -4.60	
NCI-H226	< -8.60		< -8.60			
NCI-H23	< -8.60		< -8.60			
NCI-H322M	< -8.60		< -8.60		> -4.60	
NCI-H460	< -8.60				> -4.60	
NCI-H522	< -8.60		< -8.60		> -4.60	
Colon Cancer						
COLO 205	< -8.60		< -8.60		< -8.60	
HCC-2998	< -8.60		-8.51			
HCT-116	< -8.60					
HCT-15	-7.37				> -4.60	
HT29	< -8.60					
KM12	< -8.60		< -8.60		> -4.60	
SW-620	< -8.60				> -4.60	
CNS Cancer						
SF-268	< -8.60		< -8.60		> -4.60	
SF-295	< -8.60		> -4.60		> -4.60	
SF-539	< -8.60		< -8.60		> -4.60	
SNB-19	< -8.60				> -4.60	
SNB-75	< -8.60		< -8.60		-7.67	
U251	< -8.60		-8.28		> -4.60	
Melanoma						
LOX IMVI	< -8.60		< -8.60		> -4.60	
MALME-3M	< -8.60		< -8.60			
M14	< -8.60		-8.50			
SK-MEL-2	< -8.60		< -8.60			
SK-MEL-28	< -8.60		< -8.60		< -8.60	
SK-MEL-5	< -8.60					
UACC-257	< -8.60		< -8.60			
Ovarian Cancer						
IGROV1	< -8.60		< -8.60			
OVCAR-3	< -8.60				> -4.60	
OVCAR-4	< -8.60		-8.38		> -4.60	
OVCAR-5	< -8.60				> -4.60	
OVCAR-8	< -8.60		> -4.60		> -4.60	
SK-OV-3	< -8.60				> -4.60	
Renal Cancer						
786-0	< -8.60		> -4.60		> -4.60	
A498	< -8.60		-8.60			
ACHN	< -8.60		< -8.60			
CAKI-1	< -8.60		-7.85		> -4.60	
RXF 393	< -8.60		< -8.60		< -8.60	
TK-10	< -8.60				> -4.60	
UO-31	< -8.60		-7.95			
Prostate Cancer						
PC-3	< -8.60		-7.29		> -4.60	
DU-145	< -8.60		> -4.60		> -4.60	
Breast Cancer						
MCF7	< -8.60				> -4.60	
NCI/ADR-RES	-6.23		> -4.60		> -4.60	
MDA-MB-231/ATCC	< -8.60		< -8.60		> -4.60	
HS 578T	< -8.60		> -4.60		> -4.60	
MDA-MB-435	< -8.60		< -8.60		-7.85	
BT-549	< -8.60				> -4.60	
T-47D	< -8.60		< -8.60		> -4.60	
MG_MID	-8.54		-7.56		-5.05	
Delta	0.06		1.04		3.55	
Range	2.37		4.0		4.0	

+3 +2 +1 0 -1 -2 -3

Appendix 15. 60 Cell-line profile for RMH063 (Th-Py-Py-PBD).

National Cancer Institute Developmental Therapeutics Program

Mean Graphs

NSC : D736546 / 1	Units : Molar	SSPL : 0CCJ	EXP. ID : 0508NS15
Report Date : October 04, 2005		Test Date : August 15, 2005	

Panel/Cell Line	Log_{10}GI50	GI50	Log_{10}TGI	TGI	Log_{10}LC50	LC50
Leukemia						
CCRF-CEM	< -8.60		< -8.60		> -4.60	
HL-60(TB)	< -8.60		> -4.60		> -4.60	
K-562	< -8.60		> -4.60		> -4.60	
MOLT-4	< -8.60		> -4.60		> -4.60	
RPMI-8226	-7.11		-6.27		> -4.60	
SR	< -8.60		-8.48		> -4.60	
Non-Small Cell Lung Cancer						
A549/ATCC	-6.44				> -4.60	
EKVX	-5.92		> -4.60		> -4.60	
HOP-62	-7.56				> -4.60	
HOP-92	-8.19		-7.14		> -4.60	
NCI-H226	-7.60		-7.01		> -4.60	
NCI-H23	-7.34		-6.52			
NCI-H322M	-6.50		-5.83		> -4.60	
NCI-H460	-6.91				> -4.60	
NCI-H522	< -8.60		-8.30		-5.46	
Colon Cancer						
COLO 205	-8.44		-7.61		-7.08	
HCC-2998	-7.13		-6.36		-5.81	
HCT-116	-7.40				> -4.60	
HCT-15	-5.62		-4.76		> -4.60	
HT29	-7.13				> -4.60	
KM12	-7.28		> -4.60		> -4.60	
SW-620	-7.39		> -4.60		> -4.60	
CNS Cancer						
SF-268	< -8.60		-6.74		> -4.60	
SF-295	-6.99		> -4.60		> -4.60	
SF-539	< -8.60		-6.97		> -4.60	
SNB-19	-8.06		> -4.60		> -4.60	
SNB-75	< -8.60		-7.45		-6.17	
U251	< -8.60		-8.21			
Melanoma						
LOX IMVI	< -8.60		-7.58			
MALME-3M	-7.28		-6.68		> -4.60	
M14	-6.92		-6.18		> -4.60	
SK-MEL-2	-7.49		-7.10		-6.72	
SK-MEL-28	-7.19		-6.72		-5.43	
SK-MEL-5	-7.08					
UACC-257	-6.81		-6.14		> -4.60	
Ovarian Cancer						
IGROV1	-7.53		-6.75			
OVCAR-3	-7.16		> -4.60		> -4.60	
OVCAR-4	-6.41		-5.84		> -4.60	
OVCAR-5	-7.28					
OVCAR-8	-7.03		> -4.60		> -4.60	
SK-OV-3	-7.25				> -4.60	
Renal Cancer						
786-0	-7.17		> -4.60		> -4.60	
A498	-6.97		-6.22		> -4.60	
ACHN	-6.59		-6.14			
CAKI-1	-6.38		-5.77		> -4.60	
RXF 393	-7.44		-7.01		-6.50	
TK-10	-6.98		> -4.60		> -4.60	
UO-31	-6.32		-5.90		> -4.60	
Prostate Cancer						
PC-3	-7.47		-5.43		> -4.60	
DU-145	-6.95		> -4.60		> -4.60	
Breast Cancer						
MCF7	-8.52		> -4.60		> -4.60	
NCI/ADR-RES	-5.30		> -4.60		> -4.60	
MDA-MB-231/ATCC	-8.15		-7.06		> -4.60	
HS 578T	-6.99		> -4.60		> -4.60	
MDA-MB-435	-7.39		-7.00		-6.61	
BT-549	-8.16		> -4.60		> -4.60	
T-47D	< -8.60		-7.51			
MG_MID	-7.45		-6.03		-4.87	
Delta	1.15		2.57		2.21	
Range	3.3		4.0		2.48	

+3 +2 +1 0 -1 -2 -3

Appendix 16. 60 Cell-line profile for RMH067 (Im-Im-PBD).

National Cancer Institute Developmental Therapeutics Program

Mean Graphs

NSC : D737438 / 1	Units : Molar	SSPL : 0CCJ	EXP. ID : 0509NS33
Report Date : October 25, 2005		Test Date : September 19, 2005	

Panel/Cell Line	Log_{10}GI50	GI50	Log_{10}TGI	TGI	Log_{10}LC50	LC50
Leukemia						
CCRF-CEM	< -8.43		-8.36		-5.77	
HL-60(TB)	-8.15		-7.59		-5.84	
MOLT-4	-8.17		-7.58		> -4.43	
RPMI-8226	-7.37		-6.24		-5.72	
Non-Small Cell Lung Cancer						
A549/ATCC	-6.40		-5.97		-5.53	
EKVX	-6.05		-4.62		> -4.43	
HOP-62	-7.64		-6.71		-4.95	
HOP-92	-7.74		-6.89		-4.80	
NCI-H226	-6.97		-5.51		> -4.43	
NCI-H322M	-6.77		-5.81		> -4.43	
NCI-H460	< > -4.43		> -4.43		> -4.43	
NCI-H522	< -8.43		-7.58		-5.18	
Colon Cancer						
COLO 205	-7.75		-7.04		-6.46	
HCC-2998	-7.67		-7.14		-6.53	
HCT-116	-7.58		-6.67		-4.88	
HCT-15	-5.41		> -4.43		> -4.43	
HT29	-6.93		-6.26		> -4.43	
KM12	-7.27		-6.29		-4.98	
SW-620	-7.37		-5.42		> -4.43	
CNS Cancer						
SF-268	-6.21		> -4.43		> -4.43	
SF-295	-7.14		-6.29		-5.01	
SF-539	-7.89		-6.77		-4.86	
SNB-19	-7.65		-5.11		> -4.43	
SNB-75	-7.77		-6.81		-5.84	
U251	-8.26		-5.00		> -4.43	
Melanoma						
LOX IMVI	-8.00		-6.96		-4.82	
MALME-3M	-7.37		-6.86		-4.91	
SK-MEL-2	-7.11		-6.34		-4.48	
SK-MEL-28	-7.15		-6.72		-5.69	
SK-MEL-5	-7.10		-6.58		-5.13	
UACC-257	-7.09		-6.66		-5.89	
UACC-62	-7.36		-6.91		-6.46	
Ovarian Cancer						
IGROV1	-6.88		-5.75		> -4.43	
OVCAR-3	-8.05		-7.58		> -4.43	
OVCAR-4	-7.09		-5.48		-4.47	
OVCAR-5	-7.07				> -4.43	
OVCAR-8	-7.14		-5.39		> -4.43	
SK-OV-3	-7.07		-6.51		> -4.43	
Renal Cancer						
786-0	-7.05		-6.00		-4.73	
A498	-6.38		-5.97			
ACHN	-6.14		-5.72		> -4.43	
CAKI-1	-7.18		-6.45		-5.74	
SN12C	-7.07		-5.37		> -4.43	
TK-10	-7.40		-6.73		> -4.43	
UO-31	-5.77		> -4.43		> -4.43	
Prostate Cancer						
PC-3	-7.52		-6.28		-4.80	
DU-145	-6.97		-5.60		-4.94	
Breast Cancer						
MCF7	> -4.43		> -4.43		> -4.43	
NCI/ADR-RES	-5.02		> -4.43		> -4.43	
MDA-MB-231/ATCC	-7.91		-6.86		-4.69	
HS 578T	-7.12		> -4.43		> -4.43	
MDA-MB-435	-7.85		-7.15		-6.52	
BT-549	-8.06		-6.08		> -4.43	
T-47D	-8.09		> -4.43		> -4.43	
MG_MID	-7.15		-6.09		-4.91	
Delta	1.28		2.27		1.62	
Range	4.0		3.93		2.1	

+3 +2 +1 0 -1 -2 -3

Appendix 17. 60 Cell-line profile for RMH071 (Th-Th-PBD).

National Cancer Institute Developmental Therapeutics Program

Mean Graphs

NSC : D737439 / 1	Units : Molar	SSPL : 0CCJ	EXP. ID : 0509NS33
Report Date : October 25, 2005		Test Date : September 19, 2005	

Panel/Cell Line	Log_{10}GI50	GI50	Log_{10}TGI	TGI	Log_{10}LC50	LC50
Leukemia						
CCRF-CEM	< -8.60		< -8.60		> -4.60	
HL-60(TB)	< -8.60		< -8.60		> -4.60	
MOLT-4	< -8.60		< -8.60		> -4.60	
RPMI-8226	< -8.60		-8.11		-5.35	
Non-Small Cell Lung Cancer						
A549/ATCC	< -8.60		-8.24			
EKVX	-8.03		> -4.60		> -4.60	
HOP-62	< -8.60				> -4.60	
HOP-92	< -8.60		< -8.60		> -4.60	
NCI-H226	< -8.60				> -4.60	
NCI-H322M	< -8.60		-8.36		> -4.60	
NCI-H460	< -8.60		> -4.60		> -4.60	
NCI-H522	< -8.60		< -8.60		> -4.60	
Colon Cancer						
COLO 205	< -8.60		< -8.60		-6.39	
HCC-2998	< -8.60		< -8.60		< -8.60	
HCT-116	< -8.60				> -4.60	
HCT-15	-7.26		> -4.60		> -4.60	
HT29	< -8.60				> -4.60	
KM12	< -8.60		< -8.60		> -4.60	
SW-620	< -8.60		> -4.60		> -4.60	
CNS Cancer						
SF-268	< -8.60		> -4.60		> -4.60	
SF-295	< -8.60		-8.05		> -4.60	
SF-539	< -8.60		< -8.60		> -4.60	
SNB-19	< -8.60		> -4.60		> -4.60	
SNB-75	< -8.60		< -8.60		-7.55	
U251	< -8.60		> -4.60		> -4.60	
Melanoma						
LOX IMVI	< -8.60		< -8.60		> -4.60	
MALME-3M	< -8.60		< -8.60			
SK-MEL-2	< -8.60		> -4.60		> -4.60	
SK-MEL-28	< -8.60		< -8.60			
SK-MEL-5	< -8.60					
UACC-257	< -8.60		< -8.60			
UACC-62	< -8.60		< -8.60		-8.29	
Ovarian Cancer						
IGROV1	< -8.60				> -4.60	
OVCAR-3	< -8.60		< -8.60		> -4.60	
OVCAR-4	< -8.60				> -4.60	
OVCAR-5	< -8.60				> -4.60	
OVCAR-8	< -8.60		> -4.60		> -4.60	
SK-OV-3	< -8.60		< -8.60		> -4.60	
Renal Cancer						
786-0	< -8.60				> -4.60	
A498	< -8.60		-8.23		> -4.60	
ACHN	< -8.60				> -4.60	
RXF 393	< -8.60		< -8.60		< -8.60	
SN12C	< -8.60		> -4.60		> -4.60	
TK-10	< -8.60		< -8.60		> -4.60	
UO-31	-7.73					
Prostate Cancer						
PC-3	< -8.60		-5.49		> -4.60	
DU-145	< -8.60		> -4.60		> -4.60	
Breast Cancer						
MCF7	< -8.60		> -4.60		> -4.60	
NCI/ADR-RES	-6.42		-5.71		> -4.60	
MDA-MB-231/ATCC	< -8.60				> -4.60	
HS 578T	< -8.60		-5.27		> -4.60	
MDA-MB-435	< -8.60		< -8.60		< -8.60	
BT-549	< -8.60		-5.73		> -4.60	
T-47D	< -8.60		> -4.60		> -4.60	
MG_MID	-8.51		-7.02		-5.04	
Delta	0.09		1.58		3.56	
Range	2.18		4.0		4.0	

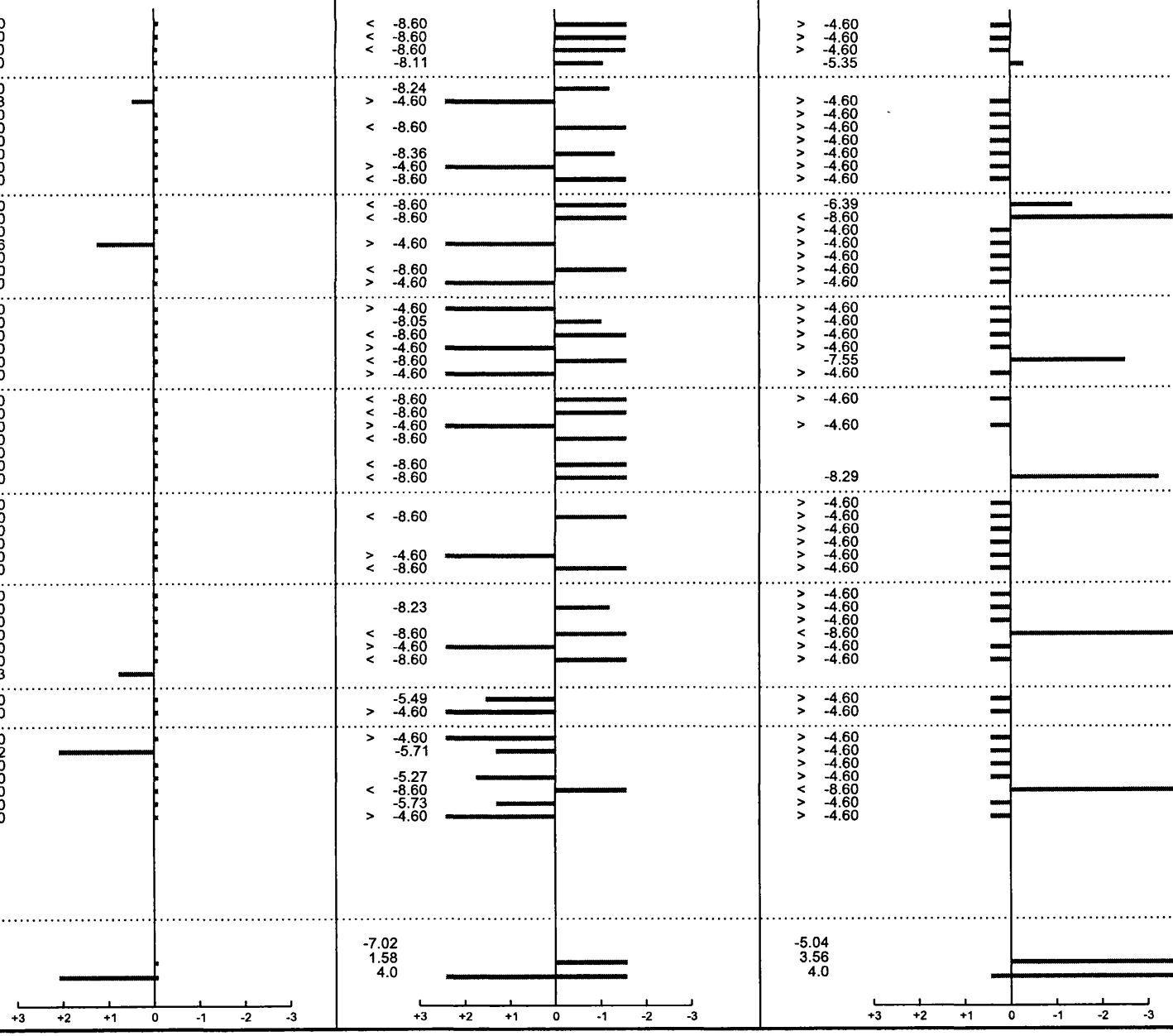

Appendix 18. 60 Cell-line profile for RMH073 (Py-Th-PBD).